INVESTIGATING THE ENDOPLASMIC RETICULUM UNFOLDED PROTEIN RESPONSE AND ITS ROLE IN SLEEP

Atreyi Chakrabarty

St Cross College, University of Oxford

Department of Pharmacology

A thesis submitted to the University of Oxford for the degree of

Doctor of Philosophy

Trinity Term 2023

To my parents,

Sutapa and Gautam Chakrabarty,

for everything you have given me.

ABSTRACT

Proteostasis involves regulating the synthesis, folding and quality control of proteins in the cell, and is essential for all cells in our body, including neurons in our brain. Errors in protein folding are dealt with by quality control mechanisms in the cell. One such mechanism is the Unfolded Protein Response (UPR), which is elicited by the accumulation of unfolded proteins in the endoplasmic reticulum (ER) under conditions of ER stress. The UPR is an adaptive process involved in maintaining proteostasis under normal physiological conditions, however, sustained or severe activation of the UPR can lead to cell death and has been implicated in pathological conditions. One process that has been linked with ER stress is sleep deprivation, which has been reported to increase levels of UPR activation in the cerebral cortex. Sleep deprivation is also associated with an increase in cortical slow wave activity (SWA) during subsequent non-REM sleep, reflecting increased sleep intensity. However, the effect of sleep deprivation upon the UPR has not been thoroughly characterised across different regions or cell types within cortex. Moreover, the potential role of the UPR in modulating cortical activity is not well understood. In this thesis, I aimed to investigate the interactions between the UPR and sleep in mice by addressing three central objectives.

Firstly, I investigate whether different regions and cell populations within cortex undergo different degrees of UPR activation as a function of their sleep-wake history. Tissue-wide molecular biological assays and cell-specific quantitative immunohistochemical analyses are used to measure UPR levels across different regions and cell types in mouse cerebral cortex after a period of sleep deprivation. Sleep deprivation elicited a small but consistent upregulation of the UPR in the frontal region of cortex. Specifically, neuronal cells were identified to contribute to the sleep deprivation effect. However, inhibitory neurons did not display a sleep deprivation-induced UPR, suggesting that the UPR is a heterogenous process within cortex.

Secondly, I examine the effects of the UPR triggered by ER stress on local cortical activity patterns during wake and sleep. Continuous electrophysiological recordings are performed during sleep and wake in freely-moving mice following pharmacological induction of the UPR in a local region of cortex. While no differences were observed in global sleep, changes were observed in neural activity patterns, including a consistent localised decrease in SWA magnitude during sleep. However, the outcomes indicated that the pharmacological approach results in severe activation of the UPR, which may not accurately reflect the physiological UPR that occurs with sleep deprivation.

Thirdly, I investigate whether it is possible to develop a novel fluorescent reporter of a cell's global UPR, which is optimised for the quantification of low levels of UPR and has improved kinetics. The resulting reporter, named sensor of UPR activity (sUPRa), showed substantial changes in fluorescence in response to a variety of UPR-activating stimuli. sUPRa reflected the temporal dynamics of UPR initiation and dissipation after drug treatment. Finally, sUPRa was leveraged to reveal the sleep deprivation-induced UPR in a subset of mouse cortical neurons. These properties validate the reporter as a useful tool for monitoring the dynamics of physiological UPR in individual neurons across the sleep-wake cycle, with the potential to genetically arget cell populations.

Together, this thesis suggests that the UPR is a heterogeneous process in cortex and highlights the need for more refined tools to monitor and manipulate the physiological UPR. Providing the field with an improved fluorescent reporter of UPR activation represents one step towards better understanding the relationship between UPR activation and sleep.

ACKNOWLEDGEMENTS

First and foremost, I express my deepest gratitude to my supervisors, Professor Colin Akerman and Professor Vladyslav Vyazovskiy. Colin, thank you for everything you have done for me as a supervisor and mentor, from the very first email even before I arrived in Oxford, to the rotation project and finally throughout the DPhil journey. Thank you for your constant support and patience, and for always having your office door open for troubleshooting chats. I truly admire the attention to detail, meticulous feedback, and guiding drive that you have provided throughout the project. Vlad, thank you for giving me the opportunity to be a part of this exciting and collaborative project. Your enthusiasm and insight have been a source of inspiration for cultivating my interest in sleep. Thank you for your endless encouragement and support throughout the project. I am immensely grateful to have had the opportunity to work with you both and learn from you, as a scientist and as a person.

I would like to thank Dr Sarah Newey for being my third supervisor in the lab, taking me under her wing and sharing her knowledge of molecular biology and general life. Equally, I would like to thank Dr Jose Prius Mengual for being my constant companion and friend throughout the project, from long chats in the soldering room to walks in Uni Park. I am grateful to all my other colleagues and friends in the Akerman lab, Gemma, Alexios, Hannah, Richard, Matt, Paul, Kashif, Anne, Alex Mathy, for creating such a stimulating environment to do research in. The rigorous discussions during lab meetings, the willingness to stop and help at any time, the lunchtime trips to ATS, and of course the stealing of Christmas presents, have all made my experience one to be cherished. I would also like to thank members of the Vyazovskiy group, Sian, Elise, Ben, Christian, Lewis, Laura, for being nothing but welcoming to me, and for being excellent conference buddies. Thank you for your generosity in helping with time-consuming experiments, and for the eclectic music playlists during surgeries. I am incredibly grateful for the friendships I have gained.

I would like to thank Professor Esther Becker and Professor Gail Preston for all their work for the DTP, and for being a source of support and guidance. To all the friendly staff at Pharmacology, the BSB and the DTP for making things run smoothly and always lending a helping hand. I would like to thank St Cross College and the Doctoral Training Program for the opportunity to meet so many wonderful people.

I am grateful for the constant love and support of my close friends over the last few years, and through the difficult pandemic times. Vashti, thank you for always being here. To Pippa, Victor, Tom for the endless belly laughs and deep chats. Ben and Nikki for being the best housemates and keeping me sane. Jeevan, Natasha, Sparshita, you made Oxford feel like home.

A huge thank you goes to my family. To Amma and Baba, I am here because of your unconditional love and support and your unwavering belief in me. You have taught me the value of hard work, resilience and compassion, which have stood me in good stead throughout this DPhil and far beyond. I am grateful for my grandparents' love and blessings, I wish they could all be here to see this.

And last but not least, to Jeeven, I want to express how grateful I am for having you by my side all along, and especially during the most intense part of this journey. For your countless midnight lifts to the lab, your free proofreading service for this thesis, and for sharing in my tears and excitement. Thank you for keeping me grounded and providing perspective when I have most needed it. You are my rock. I could not have done this without you.

Statement of Originality and Collaborations

I declare that this thesis has not been submitted for any qualification other than the degree of Doctor of Philosophy at the University of Oxford. The work presented in this thesis is my own and I clearly acknowledge where others have made contributions.

In **Chapter 2**, electrophysiological data in **Figure 2.1** was collected by Dr Lukas Krone. The RT-PCR experiment presented in **Figure 2.3** was conducted by Dr Lewis Taylor and Dr Jose Prus Mengual, and primers were designed by Dr Sarah Newey. I am grateful for their permission to include some of their data in my thesis. Part of the western blot data in **Figure 2.3** was contributed by Maisha Maliha Promi, who was an MSc student working under the supervision of myself and Dr Sarah Newey. Immunohistochemical protocols used in **Chapter 2** were developed with the help of Dr Anna Hoerder-Suabedissen. Passive infrared recordings for a subset of mice used in immunohistochemistry were supervised by Prof Stuart Peirson and Dr Eric Tam. Mouse colonies were managed by Dr Kashif Mahfooz and Gemma Gothard.

For the experiments in **Chapter 3**, my initial implantation surgeries and electrophysiological experiments were kindly supervised by Dr Jose Prius Mengual, who also implanted an animal for the pilot Tunicamycin infusion study presented in **Figure 3.6**. I learned to perform craniotomies and durotomies under the supervision of Dr Richard Burman. Dr Hannah Alfonsa kindly taught me how to perform *in vivo* drug infusions in freely-moving mice. Elise Meijer, Sian Wilcox and Dr Jose Prius Mengual all assisted with *in vivo* drug infusions on the experimental days. The RT-PCR experiment presented in **Figure 3.6** was conducted by Dr Sarah Newey.

The UPR reporter construct in **Chapter 4** was developed under the close guidance of Dr Sarah Newey. Initial tissue culture experiments were supervised by Dr Sarah Newey. Pilot studies and experimental repeats for characterising the reporter at different stages of its development were conducted by MSc students under my and Dr Sarah Newey's supervision: Daniella Munro, Maisha Maliha Promi and Belinda Agbetiameh.

Dr Kashif Mahfooz and Gemma Gothard generously performed the *in utero* electroporation surgeries used in **Chapter 5**. Alexios Vourvoukelis supervised my initial viral injection surgeries. Dr Sarah Newey supervised the initial experiments using organotypic brain slices. Finally, I am grateful for those who helped with the 12-hour sleep deprivation experiment: Alexios Vourvoukelis, Gemma Gothard, Sian Wilcox, Christian Harding, Linus Milinski, Vanda Reiss, and Ritika Mukherji.

TABLE OF CONTENTS

ABBREVIATIONS

ANOVA	analysis of variance
AAV	adeno-associated virus
ADP	adenosine diphosphate
AMPA	α-amino-3-hydroxy-5-methyl-4-isoxazolepropionic acid
AP	antero-posterior
ATF4	activating transcription factor-4
ATF6	activating transcription factor-6
ATP	adenosine triphosphate
AZC	L-Azetidine-2-carboxylic acid
BACE	β-secretase
Bak	BCL-2 homologous antagonist killer
Bax	BCL-2 associated X protein
BCL-2	B-cell lymphoma-2 protein
BiP	binding immunoglobulin protein
bp	base pairs
bZIP	basic leucine zipper
cAMP	cyclic adenosine monophosphate
CHOP	CCAAT-enhancer binding protein (C/EBP) homologous protein
CICR	calcium-induced calcium release
CLB	cell lysis buffer
CRE	cAMP response element
DAPI	4',6-diamadino-2-phenylindole
DIV	days *in vitro*
DMEM	Dulbecco's Modified Eagle's Medium
DMSO	dimethylsulfoxide
EDTA	ethylenediaminetetraacetic acid
EEG	electroencephalogram
EF1α	elongation factor-1α
EGFP	enhanced GFP
eIF2α	eukaryotic translation initiation factor-2α
EMG	electromyogram
ER	endoplasmic reticulum
ERAD	ER-associated degradation
ERAI	ER stress-activated indicator
ERSE	ER stress response element
FOV	field of view
FRAP	fluorescence recovery after photobleaching
FRET	fluorescence resonance energy transfer
GABA	γ-aminobutyric acid
GADD34	growth arrest and DNA damage-inducible protein 34
GAPDH	glyceraldehyde 3-phosphate dehydrogenase
GFAP	glial fibrillary acidic protein
GFP	green fluorescent protein
Grp78	glucose-regulated protein 78 kDa
Grp94	glucose-regulated protein 94 kDa
GTP	guanosine triphosphate
Hsp70	heat shock protein 70
IRE1	inositol-requiring enzyme 1
ISH	*in situ* hybridisation
IUE	*in utero* electroporation
IVC	individually ventilated cage
JNK	c-Jun N-terminal kinase

KDEL	Lys-Asp-Glu-Leu (amino acid sequence)
LFP	local field potential
LTC	light/time-controlled
LTP	long-term potentiation
mAb	monoclonal antibody
ML	medio-lateral
mNG	mNeonGreen
mRNA	messenger RNA
mSc	mScarlet
nEF	short EF1α promoter
NGS	normal goat serum
NMDA	N-methyl-D-aspartate
NREM	non-rapid eye movement
ODC	ornithine decarboxylase
ORF	open reading frame
pAb	polyclonal antibody
PBS	phosphate buffered saline
PCR	polymerase chain reaction
PDI	protein disulphide isomerase
PDL	poly-D-lysine
PERK	protein kinase RNA like ER kinase
PEST	proline-glutamate-serine-threonine (amino acid sequence)
PFA	paraformaldehyde
PIR	passive infrared recording
PV	parvalbumin
REM	rapid eye movement
RFP	red fluorescent protein
RIDD	IRE1-dependent decay
RPL19	ribosomal protein L19
RNA	ribonucleic acid
RT-PCR	reverse transcription PCR
S1P and S2P	Site-1 and site-2 proteases
scRNA-seq	single cell RNA sequencing
SD	sleep deprivation
SDS-PAGE	Sodium dodecyl-sulfate polyacrylamide gel electrophoresis
SEKDEL	Ser-Glu-Lys-Asp-Glu-Leu (amino acid sequence)
SERCA	sarco/endoplasmic reticulum calcium ATPase
SHY	synaptic homeostasis hypothesis
SPOTlight	Selective Phospho-eIF2α ORF Tracking light
SST	somatostatin
SWA	slow wave activity
sXBP1	spliced XBP1
TBS	tris buffered saline
Thaps	Thapsigargin
tRNA	transfer RNA
TUN	Tunicamycin
uORF	upstream ORF
UPR	unfolded protein response
VEH	vehicle
WPRE	woodchuck hepatitis virus post-transcriptional regulatory element
XBP1	X-box binding protein 1
ZT	Zeitgeber time

Chapter 1 Introduction

Contents

We experience the restorative power of sleep every night, as we fall asleep, tired, and wake up more refreshed. Like eating or drinking, the drive to sleep seems to fulfil a fundamental need. However, unlike eating or drinking, sleeping is the only major biological process whose biological functions are not clear. Hobson famously declared that "sleep is of the brain, by the brain and for the brain" (Hobson, 2005). However, even after decades of research in behaviour and neurophysiology, the fundamental purpose of sleep for the brain remains unknown.

One of the most fundamental processes carried out by any cell in our body, including neurons in our brain, is the maintenance of protein synthesis, trafficking and turnover, together known as protein homeostasis. Proteins are the functional units of cells, and errors in protein folding can cause cells to come under stress, malfunction and ultimately die. Sleep loss is associated with a stress response to the accumulation of unfolded proteins in the endoplasmic reticulum (ER) in the cerebral cortex (Naidoo et al., 2005). Moreover, insufficient or disrupted sleep is a risk factor for neurodegenerative conditions that are caused by impaired protein homeostasis (Lim et al., 2013; Wulff et al., 2010). Therefore, research into the fundamental properties of sleep and sleep loss is of significant importance. In this thesis, I specifically investigate the unfolded protein response (UPR), which is a complex protective process mounted by cells in response to or in preparation for high protein burdens in the ER, and its relationship to sleep.

In this chapter, I will first provide a background of key concepts to understand the UPR and its fundamental roles, with a particular focus on neurons and the brain. Next I will introduce the principles of measuring sleep, the key electrophysiological and molecular correlates of sleep loss, and some of the current hypotheses around the function of sleep. In the last section, I will provide a summary of the specific gaps in knowledge that the rest of the thesis aims to address, and outline the specific approaches taken to address these aims.

1.1 The role of the ER in protein homeostasis

1.1.1 The neuronal ER

The majority of proteins that are secreted, expressed on cell membranes, involved in exosomes or endosomes are folded and assembled in the endoplasmic reticulum (ER), and account for over 30% of the human proteome (Uhlen et al., 2010; Uhlén et al., 2015). The ER plays a crucial role in maintaining proteostasis within a cell, regulating the overall pace of protein production and the accuracy of protein structure. Therefore, ER proteostasis is vital for all aspects of brain function, all the way from development, to the intricate modulation of neuronal connections necessary for information processing, to the maintenance of cell health throughout the ageing process (Malhotra & Kaufman, 2007; Martínez et al., 2018; Naidoo & Brown, 2012).

The regulation of proteostasis is of great importance in neurons, as the *de novo* production of proteins is essential for efficient neuronal activity. The ER network in these polarised cells is extensive, spanning from the cell body or soma to the axon and dendrites (Sree et al., 2021), and has been famously termed "a neuron-within-a-neuron" (Berridge, 1998)(**Figure 1.1**). In the

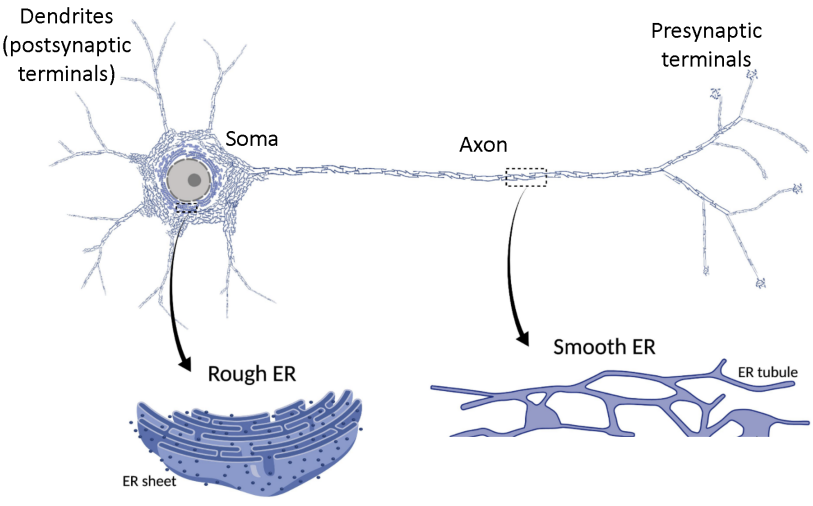

Figure 1.1 Endoplasmic reticulum (ER) distribution in neuronal cells.

ER network (blue) is continuously distributed throughout the neuron. The soma consists largely of parallel ER sheets associated with ribosomes (dark blue dots). The dendrites, considered to be the primary post-synaptic site, and the axon terminals, considered to be the primary presynaptic site, contain ER tubules, also mostly associated with ribosomes. The axon contains a network of interconnected tubules of smooth ER. Figure modified from Öztürk et al. (2020).

neuronal soma, the ER appears as a complex network of interconnected cisternae and tubules. ER sheets and tubules studded with ribosomes, known as the rough ER, are predominant in the neuronal soma and dendrites, whereas the axon segment consists of predominantly smooth ER tubules (Broadwell & Cataldo, 1983; Öztürk et al., 2020; Wu et al., 2017). The rough ER is involved in the synthesis and transport of newly translated proteins, while the smooth ER lacks ribosomal attachments and is primarily involved in lipid, steroid and carbohydrate synthesis (Csala et al., 2006; Voeltz et al., 2002).

The vast ER network and ribosomal protein translation machinery facilitates local protein production, including at the synapse. Messenger ribonucleic acid (mRNA) produced in the soma is transported to the axon terminals and dendrites, where translation can be initiated both pre-synaptically and post-synaptically (Hafner et al., 2018). The cycling of synaptic vesicles, receptor-mediated signalling, ion transport and the physical stability of the synapse, all rely upon ER proteostasis (Ashery et al., 2014). Furthermore, the synthesis of new synaptic proteins can increase as a function of a neuron's activity-dependent history, through synaptic plasticity mechanisms (Cajigas et al., 2010; Ehlers, 2003; Lüscher et al., 2000).

Neurons in the brain have a huge degree of heterogeneity in terms of their morphology, gene expression and functionality (Masland, 2004). In the cerebral cortex alone, there are at least 133 transcriptomically distinct cell types that are distributed into layers and functionally distinct regions (Tasic et al., 2018). The precise roles of the ER are also highly variable by cell type. However, a common feature of all neurons is their lack of capacity to regenerate, which makes proteostasis essential for maintaining cell viability. Failure in proteostasis has been implicated in neurodegenerative disorders, such as Alzheimer's disease (Gerakis & Hetz, 2018; Hetz & Saxena, 2017; Roussel et al., 2013). Therefore, under physiological conditions, the ER environment is tightly controlled to maintain the correct folding and processing of proteins in a cell-specific manner.

1.1.2 The ER environment

The ER lumen harbours a unique environment optimised for the folding of nascent polypeptides into their functional native structures. After translation, transmembrane and secretory proteins enter the ER lumen, where they are modified with N-linked glycans, stabilised by disulphide bonds, folded into secondary and tertiary structures and assembled into multimeric complexes (Walter and Ron, 2011). Unfolded or misfolded proteins are retained in the ER lumen, while only proteins in their native conformation reach their destination (Ellgaard and Helenius, 2003). Since proteins that are secreted to or interact with the extracellular space are folded in the ER, the luminal environment of the ER mimics the extracellular space, with its high calcium concentration and oxidising conditions, complemented with a set of molecular chaperones and folding enzymes (Halperin et al., 2014).

Chaperones are proteins that assist in the folding of nascent unfolded or incorrectly folded proteins into their native state, and are an integral part of the quality control system in the ER. There are various types of molecular chaperones found in the ER, including the heat shock family of proteins, lectins and protein disulphide isomerases (PDIs). The best characterised ER-resident chaperone is BiP (binding immunoglobulin protein), also known as Grp78 (glucose-regulated protein 78 kDa). BiP was first identified as one of two proteins that were upregulated in fibroblast cells under glucose deprivation, the second protein being Grp94 (Shiu et al., 1977). BiP was also independently identified in B lymphocyte cells, where it was found to preferentially bind to immunoglobulin chains, garnering the name BiP (Haas & Wabl, 1983). Further characterisation revealed that BiP is part of the Hsp70 heat shock protein family, which are found in normal unstressed cells and induced by a variety of stress stimuli (Munro & Pelham, 1986). BiP and other molecular chaperones interact with structural elements of unfolded proteins with high affinity and can limit undesirable conformational combinations, whilst favouring particular folding pathways (Gidalevitz et al., 2013). PDIs are also important for stabilising intermediate folded states and

dictating correct folding pathways by aiding the formation of disulphide bonds, which relies on the high oxidative potential of the ER lumen (Creighton, 1997).

The ER lumen also maintains a high calcium concentration to preserve protein folding success. The ER is a major intracellular calcium store, with a total concentration of 1-3 mM and a free calcium concentration ranging from 1 to 400 µM (Halperin et al., 2014). The high calcium concentration in the ER is actively maintained by the ATP-dependent sarco/endoplasmic reticulum calcium (SERCA) pump (Krebs et al., 2015). Calcium can directly influence protein folding by binding to amino acid side chains. However, changes in calcium levels can also indirectly impact protein folding through the modulation of interactions between chaperones and unfolded proteins. Several chaperones, including BiP, Grp94, calreticulin, Erp72 and the PDIs bind to calcium, and their folding activity depends on calcium levels (Gidalevitz et al., 2013). As the primary intracellular calcium store, the ER can also respond to metabolic needs of the cell through rapid changes in free luminal calcium levels, which can influence protein folding in the ER lumen (Krebs et al., 2015).

In addition, proper folding in the ER lumen requires the maintenance of high levels of ATP and carbohydrates. ATP in the ER is necessary to maintain calcium stores, redox homeostasis and chaperone function, including BiP (Halperin et al., 2014). BiP associates with its unfolded protein substrate, or "client", in the ER lumen in an ATP-bound conformation, and is locked onto its client protein upon hydrolysis of ATP to ADP (Gething & Sambrook, 1992). For BiP to "reopen" and dissociate from its client, the ADP needs to be released. It is thought that DnaJ (Hsp40) and BAP, an ER nucleotide exchange factor, regulate this cycle of ATP/ADP binding and unbinding from BiP that allows BiP to bind and release its client proteins (Y. Ma & Hendershot, 2004). On the other hand, carbohydrates play several roles in the processing of glycoproteins through glycosylation. Due to their hydrophilic nature, addition of carbohydrate groups to proteins increases the solubility of the glycoprotein and prevents the back-translocation through the ER membrane once the glycoproteins are transported out of the ER (Gidalevitz et al., 2013). Apart from these roles, carbohydrates also

affect protein folding, although in ways that are not well-understood. In many cases, under-glycosylated proteins are prone to aggregation and are retained in the ER (Martayan et al., 2008; Parham, 1996). Since the correct folding and maturation of proteins is essential, ER quality control systems are crucial for balancing the level of unfolded protein burden within the lumen (ER load) with the ER folding capacity.

1.2 Quality control in the ER

1.2.1 The Unfolded Protein Response (UPR)

To maintain ER homeostasis, quality control systems are in place to ensure that only properly folded proteins exit the ER and are translocated to the Golgi apparatus or final cellular destinations. Unfolded or misfolded proteins are retained in the ER to enable more contact time with protein folding chaperones, thereby increasing the likelihood of proteins being correctly folded. Meanwhile, persistently misfolded proteins are directed toward degradation pathways through ER-associated degradation (ERAD) (Christianson & Carvalho, 2022).

The processes involved in protein folding in the ER are highly sensitive to changes in the ER luminal environment. Various environmental challenges, such as calcium depletion, redox imbalance, or glucose deprivation, can cause an accumulation of unfolded or misfolded proteins in the ER lumen, increasing the ER load (Ellgaard & Helenius, 2003). In neurons, the generation of action potentials result in calcium fluxes, which can trigger calcium-induced calcium release (CICR) from the ER calcium store (Bardo et al., 2006). Consequently, such disruptions of the calcium concentration in the neuronal ER may result in a build-up of unfolded proteins in the ER lumen (Bahar et al., 2016; Krebs et al., 2015; Michalak et al., 2002). In addition to environmental fluctuations, elevated protein synthesis and trafficking through the ER may also increase ER load. For example, the synthesis and trafficking of new synaptic proteins that mediate synaptic activity or plasticity, such as AMPA and NMDA receptors (W. Lu & Roche, 2012; Mu et al., 2003; Pick & Ziff, 2018), ion channels (D. Ma et al., 2001) and synaptic vesicle proteins (Chanaday & Kavalali, 2022),

may act to increase ER load. When ER load surpasses the ER's folding capacity, it leads to the onset of ER stress (Malhotra & Kaufman, 2007). Under conditions of ER stress, an orchestrated set of signalling pathways known as the unfolded protein response (UPR) serves as an adaptive mechanism to restore ER function (P. Walter & Ron, 2011).

The UPR is an evolutionarily conserved process across unicellular and multicellular organisms (Hollien, 2013). However, the mammalian UPR is considerably more complex than in budding yeast. The mammalian UPR consists of three signalling arms, transduced by three ER transmembrane protein sensors: inositol- requiring protein-1 (IRE1), activating transcription factor-6 (ATF6) and protein kinase R-like ER kinase (PERK) (Hetz, 2012). These proteins have domains in the ER lumen for ER stress detection and integration, and cytosolic domains for activation of downstream effectors and signalling pathways. In unstressed conditions, the ER luminal domain of each of these three sensor proteins are bound to BiP, one of the most abundant molecular chaperones in the ER, which keeps the proteins in an inactive state (Gething & Sambrook, 1992; Gidalevitz et al., 2013; Y. Ma & Hendershot, 2001; Pincus et al., 2010). At the onset of ER stress, BiP dissociates from the three sensors to preferentially bind to unfolded proteins in the ER lumen, which results in the activation of discrete signalling pathways via the cytosolic domains of the three sensor proteins (Bertolotti et al., 2000; Hetz, 2012; Read & Schröder, 2021). Together, these signalling pathways result in reduced protein translation, upregulation of chaperones for protein folding, and ERAD by the proteasome (P. Walter & Ron, 2011). A strong or sustained induction of the UPR that fails to effectively restore ER proteostasis can result in programmed cell death (Hetz, 2012; Iurlaro & Muñoz-Pinedo, 2016; Kim et al., 2006).

1.2.2 Molecular pathways of the UPR

Upon BiP dissociation, IRE1 undergoes oligomerisation and autophosphorylation, which results in the activation of its endoribonuclease (RNAse) activity (Korennykh et al., 2009). The RNAse activity triggers two main pathways through which IRE1 exerts its effects (**Figure 1.2**). The first

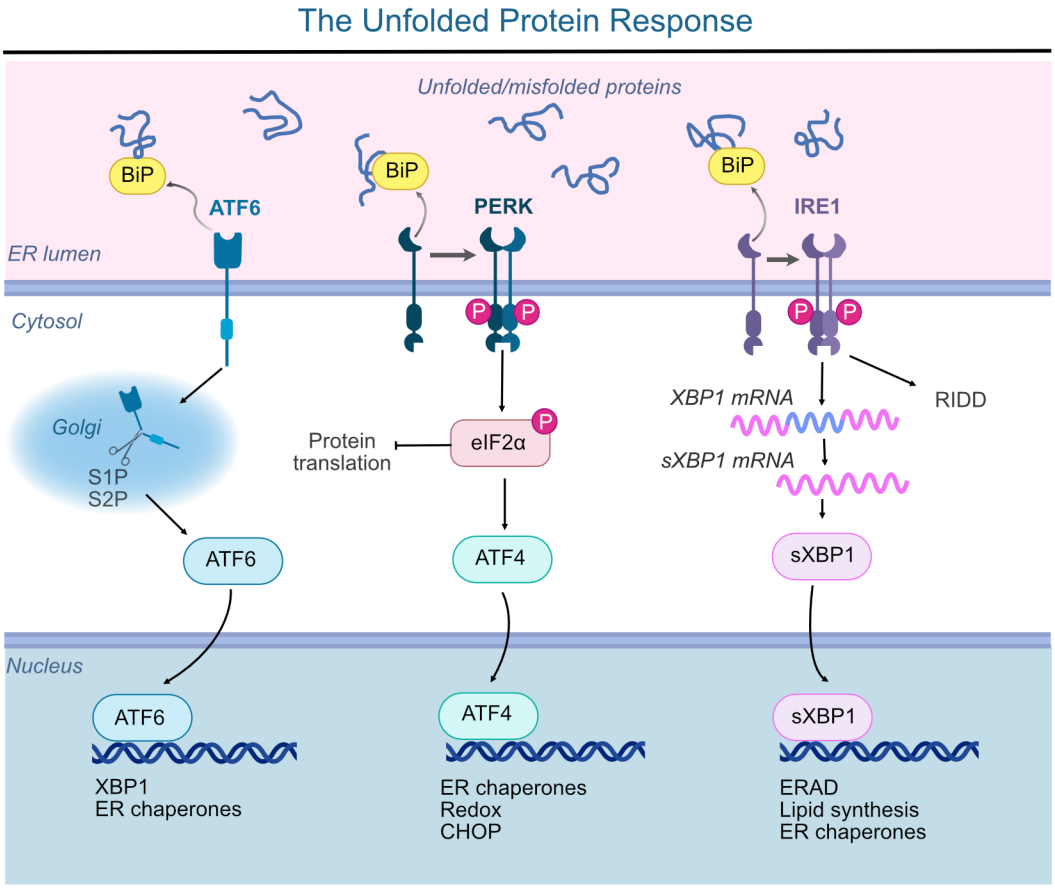

Figure 1.2 The signalling pathways of the mammalian unfolded protein response (UPR).

Under conditions of acute ER stress, BiP is recruited to preferentially bind to accumulating unfolded proteins in the ER lumen thereby dissociating from the three UPR stress sensor proteins: ATF6, PERK and IRE1. This results in distinct signalling cascades downstream of each sensor. Figure modified from Walter and Ron (2011).

pathway involves the site-specific splicing of a 26-nucleotide intron from the mRNA of a transcription factor called X-box binding protein-1 (XBP1). The splicing event results in the expression of the active form of XBP1, spliced XBP1 (sXBP1), by creating a translational frameshift to produce a larger form of XBP1 containing a transcriptional activator domain (Malhotra & Kaufman, 2007). sXBP1 plays a role in enhancing protein folding by increasing the production of ER chaperones, including BiP (Acosta-Alvear et al., 2007; P. Walter & Ron, 2011). Additionally, sXBP1 promotes the upregulation of UPR target genes that are responsible for the degradation of misfolded proteins through ERAD (Acosta-Alvear et al., 2018). The second role of IRE1's RNAse activity is the cleavage of specific mRNAs and microRNAs, a process known as IRE1-dependent

decay (RIDD) (Hollien et al., 2009; Hollien & Weissman, 2006). This activity serves as a mechanism to reduce the amount of protein translation, thereby alleviating the protein folding burden on the ER.

Like IRE1, PERK is also activated through the process of oligomerisation and trans-autophosphorylation. When BiP detaches from the luminal domain of PERK, it exposes the cytosolic kinase domain of PERK. Consequently, this domain phosphorylates a protein called eukaryotic translation initiation factor 2 on the alpha subunit (eIF2α) (**Figure 1.2**). The phosphorylation of eIF2α leads to attenuation of protein translation, thereby reducing the influx of newly synthesised proteins into the stressed ER (Harding et al., 2002). Phosphorylated eIF2α (p-eIF2α) inhibits the guanine nucleotide exchange factor, eIF2B, which is responsible for cycling the eukaryotic translation initiation factor 2 (eIF2) complex to its active GTP-bound state to form a ternary complex with transfer RNA (tRNA). The ternary complex is required for recognition of the AUG translation initiation codon, therefore lower levels of the ternary complex result in lower levels of translation initiation (Harding et al., 1999). While p-eIF2α inhibits general protein translation, it is required for the selective translation of several mRNAs that encode for key UPR effectors, such as the activating transcription factor 4 (ATF4), through alternative open reading frames (ORF) (Harding et al., 1999; Read & Schröder, 2021). ATF4 plays a role in feedback mechanisms to restore protein homeostasis through the transcriptional activation of BiP, to increase the ER's folding capacity, and increased production of growth arrest and DNA damage-inducible protein 34 (GADD34), which dephosphorylates p-eIF2α (Kohno, 2010; Malhotra & Kaufman, 2007). ATF4 also regulates the expression of genes related to redox balance, amino acid metabolism and autophagy (Ameri & Harris, 2008; Schröder & Kaufman, 2005).

The ATF6 signalling pathway of the mammalian UPR is distinct from both the IRE1 and PERK pathways (**Figure 1.2**). Following dissociation from BiP, ATF6 translocates to the Golgi apparatus, where it undergoes sequential site-specific cleavage by proteases known as site-1 and site-2

proteases (S1P and S2P)(Haze et al., 1999). This cleavage process results in the release of a fragment called ATF6p50, which functions as an active basic leucine zipper transcription (bZIP) factor (Haze et al., 1999; Shen et al., 2002; Y. Wang et al., 2000). Activated ATF6 promotes the transcription of important genes to restore protein homeostasis, including BiP and other chaperones and foldases, as well as ERAD components. ATF6 also upregulates the expression of XBP1 (Yoshida et al., 2001). ATF6 and sXBP1 then work in concert to upregulate several other components of the UPR (Yamamoto et al., 2007).

Several studies have suggested that the activity of each of these three arms of the UPR is highly dependent on the context, intensity and duration of the ER stress stimulus. The three UPR arms exhibit distinct sensitivities and kinetics to specific stress inducers (DuRose et al., 2006; Yoshida et al., 2003). For example, reducing agents may cause faster IRE1 activation than calcium dysregulation, while both stimuli result in the same PERK activation kinetics (DuRose et al., 2006). Meanwhile, certain conditions may result in the activation of specific arms of the UPR, such as selective ATF6 activation in response to ER membrane protein load (Maiuolo et al., 2011). Moreover, the UPR sensors may be activated by specific misfolded or unfolded proteins rather than by general ER stress (Hetz, 2012). The signalling arms also show different rates of attenuation after removal of the ER stress stimulus or during prolonged ER stress (Hetz, 2012). These findings together indicate that the UPR stress-sensing process is highly sophisticated, with tremendous combinatorial complexity.

If the UPR is unable to restore ER proteostasis due to prolonged or severe conditions of ER stress, this typically leads to the triggering of apoptosis. Exactly how the balance between pro-survival and pro-apoptotic signalling is determined remains poorly understood. However, several mechanisms have been found to contribute to the generation of apoptotic signals in the ER. One of the most significant ER stress-induced apoptotic pathways is mediated by CCAAT-enhancer binding protein (C/EBP) homologous protein (CHOP) (Zinszner et al., 1998). CHOP is a bZIP transcription

factor induced downstream of the ATF6 and PERK pathways. One of its functions is to promote downregulation of the anti-apoptotic B cell lymphoma-2 protein (BCL-2), while upregulating other cell death mediators that activate the mitochondrial apoptosis pathway (Hetz, 2012; Oyadomari & Mori, 2004). Additionally, activated IRE1 promotes apoptosis by activating the c-Jun N-terminal Kinase (JNK) signalling pathway (J. H. Lin et al., 2007). Further downstream events, such as Bak/Bax regulated calcium release from the ER and activation of Caspases, also contribute to ER stress-mediated apoptotic signalling (Hetz, 2012). UPR signalling is therefore involved in complex cell fate decisions for cells under stress, which can have significant implications for its role in disease.

1.2.3 The UPR in normal physiology

The UPR is able to effectively regulate physiological processes and accommodate the diverse functions of the ER by discerning various activation stimuli and initiating appropriate responses. The varied activation mechanisms of the UPR stress sensors by physiological stimuli are far more intricate than previously recognised. Several studies support a more anticipatory role of the UPR in maintaining normal physiology, by preparing for distinct cellular states that are likely to burden the ER (Rutkowski & Hegde, 2010; Shapiro et al., 2016). An anticipatory UPR was first observed in differentiating B lymphocyte cells following antigen exposure, before the increased production of antibodies (Anken et al., 2003; Gass et al., 2002). Since then, endocrine stimuli such as oestrogen and epidermal growth factor have also been identified to activate an anticipatory UPR independent of ER stress (Andruska et al., 2015; Shapiro et al., 2016; Yu et al., 2016). Moreover, low-level activation of the UPR, specifically the IRE1 arm, is observed to have a diurnal rhythm controlled by the circadian clock in the liver, where it regulates lipid metabolism (Cretenet et al., 2010). Since nutritional inputs and metabolism are both predicable and typically diurnal, an anticipatory UPR is entirely appropriate to prepare the ER for increased activity. Such anticipatory responses are primarily found in dividing or secretory cells before massive protein synthesis for differentiation or secretion, which may arguably be less relevant in post-mitotic cells like neurons.

In the brain, the UPR shows a sleep-wake dependent alteration. Specifically, the upregulation of BiP after prolonged wakefulness has been observed in the brains of several species such as mice (Mackiewicz et al., 2007; Maret et al., 2007; Naidoo et al., 2005), fruit flies (Cirelli et al., 2005; Naidoo et al., 2007a; Shaw et al., 2000), rats (Cirelli et al., 2004; Terao et al., 2006) and white-crowned sparrows (Jones et al., 2008). Sleep is a fundamental physiological process that has been demonstrated in every animal studied to date, and its relationship with the UPR has begun to be elucidated, however, fundamental questions remain. It is not clear what the role of the physiological UPR is in sleep-wake functions: whether it is reactive to ER stress or a protective anticipatory mechanism. There is also a lack of understanding of the kinetics of UPR activation, modulation and attenuation as a function of sleep deprivation and sleep, and the activity of individual arms of the UPR is not clear. Moreover, how UPR activity varies among diverse regions and cell types within the brain is not well studied. Understanding cell-specific UPR may be important to understanding the function of the UPR in sleep and other physiological conditions, as well as its potential roles in pathological conditions.

1.2.4 The UPR in pathophysiology

The UPR has been more broadly studied in the context of pathophysiology and disease. The failure to maintain protein homeostasis and the initiation of UPR-mediated cell death have been linked to numerous metabolic (Nedeltcheva & Scheer, 2014; Scheuner & Kaufman, 2008) and neurodegenerative diseases (Ashraf et al., 2014; Hetz & Saxena, 2017). It is known that the pathological aggregation of proteins contributes to the aetiology of Alzheimer's disease, Parkinson's disease, and Huntington's disease among others. Although the aggregation of proteins associated with these diseases are primarily cytosolic, research has shown that these aggregates may exacerbate ER stress vulnerability by altering the ER environment or directly interacting with components of the UPR (Abisambra et al., 2013; Hetz & Saxena, 2017; Katayama et al., 1999; Uddin et al., 2020). Furthermore, BiP activity has been reported to be downregulated in certain neurodegenerative models, which limits the adaptive effects of the UPR in the ER (Hetz & Saxena,

2017; Zhao et al., 2005). Prolonged ER stress leads to persistent activation of the PERK/p-eIF2α arm of the UPR, resulting in impaired protein translation, which contributes to a decline in synaptic function and ultimately neuronal loss (Halliday et al., 2017; Moreno et al., 2012). Animal models of neurodegeneration with genetic manipulations of the IRE1 arm of the UPR have also shown significant modifications in disease progression (Duran-Aniotz et al., 2017). Given the widespread dysregulation of the UPR and consequent cell death, there are ongoing efforts to develop therapeutic approaches to target the excessive activation of the UPR in pathological conditions (Gonzalez-Teuber et al., 2019; Halliday et al., 2017; Hetz, 2021; Hetz et al., 2019). In addition to elevated UPR activation, neurodegenerative disorders are also linked to disturbances in neuronal activity and disrupted sleep (Kastanenka et al., 2019; Y. F. Lee et al., 2020). Interestingly, sleep abnormalities have been found to be predictive of the development of neurodegenerative diseases (Lazar et al., 2015; Lim et al., 2013; Ngo et al., 2020; Winer et al., 2019). Therefore, it is important to further uncover the interactions between UPR activation and sleep in order to elucidate potential mechanisms regulating the onset and progression of neurodegenerative diseases.

1.3 Sleep and sleep homeostasis

1.3.1 Defining sleep

Sleep can be behaviourally defined as the reversible reduction in responsiveness, reflected in an increased arousal threshold, typically accompanied by immobility and a characteristic body posture (Cirelli & Tononi, 2008). Defined in this way, sleep is found to be an evolutionarily conserved phenomenon in all animals studied to date (Anafi et al., 2019). Sleep has been most widely studied in mammals and birds, but it is also observed in other organisms such as zebrafish (Yokogawa et al., 2007), fruit flies (*Drosophila melanogaster*)(Shaw et al., 2000) and roundworms (Caenorhabditis elegans)(Raizen et al., 2008). The widespread occurrence of sleep justifies the use of animal models in understanding human sleep.

In animals that have a developed cerebral cortex, the behavioural features of sleep and wake are accompanied by characteristic brain activity patterns. These can be measured using

electrodes on the skull to record an electroencephalogram (EEG) or electrodes implanted into the extracellular space of the brain to record local field potentials (LFP). The LFP reflects the summed signal of excitatory and inhibitory potentials from a large number of neurons near the recording site, as well as some volume-conducted signals from distant locations. The scalp EEG is a spatiotemporally smoothed version of the LFP, integrating neural signals across a wider surface area (Buzsáki et al., 2012). Wakefulness can be characterised by low amplitude, high frequency EEG and LFP signals, which are accompanied by irregular muscle activity that can be recorded using an electromyogram (EMG)(**Figure 1.3**). Non-rapid eye movement (NREM) sleep is characterised by a reduced EMG signal and the presence of a prominent high-amplitude and slow oscillation in the delta frequency range (0.5 – 4 Hz), also called slow wave activity (SWA), and bursts of spindle activity in the sigma range (10 – 15 Hz) (Adamantidis et al., 2019). NREM sleep alternates cyclically with periods of rapid eye movement (REM) sleep, which is so called due to the presence of rhythmic saccadic eye movements with closed eyelids (Aserinsky & Kleitman, 1953). During REM sleep, the EEG and LFP signals exhibit a consistent theta activity (6 – 9 Hz) pattern, which is accompanied by a further loss of EMG signal due to the general muscle atonia that occurs during this sleep stage (D. Liu & Dan, 2019)(**Figure 1.3**).

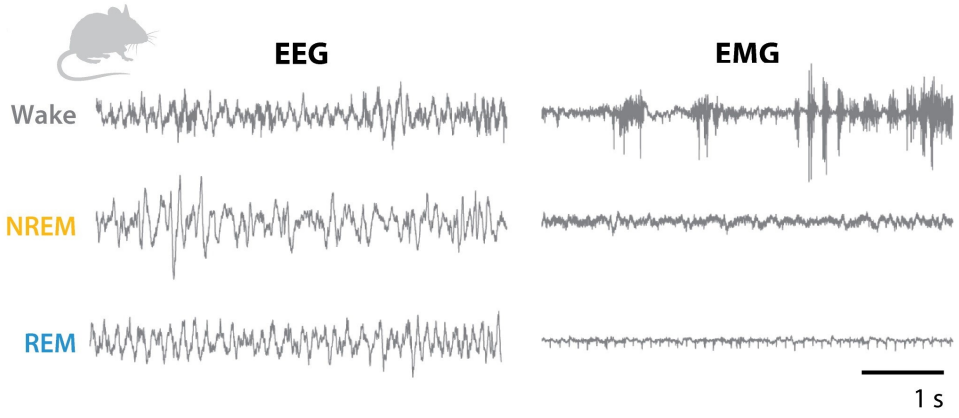

Figure 1.3 Electrophysiological recordings of sleep and wake in mouse.

Example electroencephalogram (EEG) and electromyogram (EMG) signals from mice demonstrate distinct brain and muscle activity patterns during wake, non-rapid eye movement (NREM) and rapid eye movement (REM) sleep. Figure adapted from Liu & Dan (2019).

The timing of sleep and wake states varies by species, but is relatively stable among individuals of the same species and from one day to another. Rodents play a crucial role as a model organism in researching the neuronal mechanisms of sleep, but they display significant distinctions in sleep patterns compared to humans. Notably, laboratory mice, being nocturnal, are primary active during the night and display polyphasic sleep patterns, where they have multiple sleep episodes interspersed with periods of wakefulness primarily during the daytime (Le Bon et al., 2007). One of the most significant factors influencing the timing of sleep is an organism's endogenous circadian clock (Mistlberger, 2005). Circadian rhythms allow animals to adaptively coordinate their behaviour and physiological processes based on predictable daily patterns in their environment. Specifically, circadian rhythms strongly influence the timing of wakefulness and sleep phases in accordance with the Earth's daily light-dark cycle. The regulation of sleep by circadian rhythms relies on the presence of physiological oscillatory mechanisms with a 24-hour period. Such mechanisms exist at the molecular level and involve highly conserved gene expression processes (Bell-Pedersen et al., 2005).

1.3.2 Sleep homeostasis, slow wave activity and the individual neuron

In addition to the circadian contribution to sleep timing, another fundamental process determines the relative quantity and intensity of sleep. This corresponds to the accumulation of "sleep pressure" or "sleep drive", which increases the need to sleep as a function of time spent awake. This process is evident following prolonged wakefulness or sleep deprivation, for example, when animals respond with a compensatory increase in sleep duration (Benington, 2000; Carskadon & Dement, 1979). The compensation in sleep duration is accompanied by an increase in sleep intensity, which is best reflected in the EEG by increased levels of slow wave activity (SWA) during NREM sleep (Borbély et al., 1981, 1984). The initial level of SWA is determined by the duration of prior waking, while the decline of SWA during sleep reflects the discharge of sleep pressure (Tobler & Borbély, 1986; V. V. Vyazovskiy et al., 2007)(**Figure 1.4**).

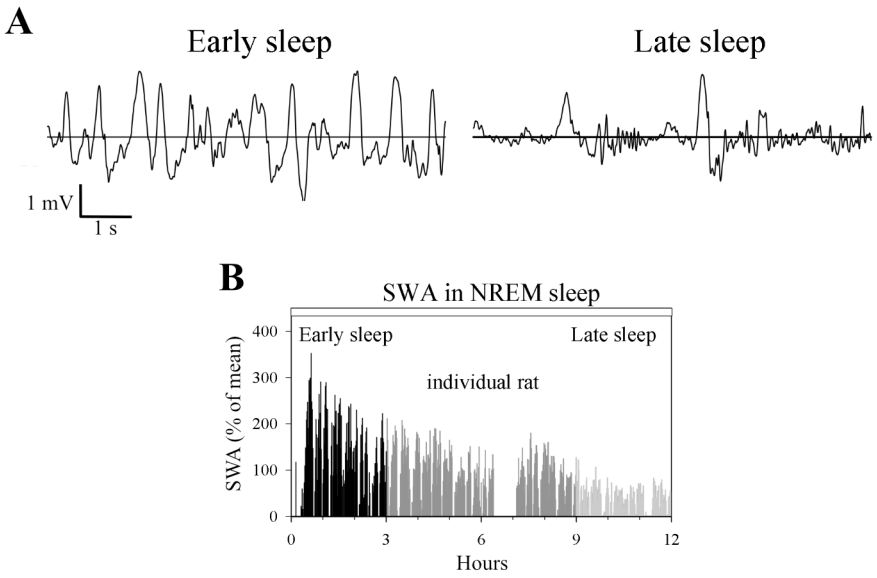

Figure 1.4 Slow wave activity, a marker of sleep pressure, is high during early NREM sleep and reduces during late sleep.

(A) Representative local field potentials (LFP) during early NREM and late NREM sleep. **(B)** NREM sleep slow wave activity (0.5 – 4 Hz) power profile during the light period in 1 minute intervals from a representative rat. Figure adapted from Vyazovskiy et al. (2007).

Cortical SWA, reflects the synchronised fluctuations between depolarisation (UP state) and hyperpolarisation (DOWN state) of membrane potentials in individual neurons of the neocortex, and the corresponding synchronised ON and OFF periods of neuronal firing (Chauvette et al., 2010; Poulet & Petersen, 2008; Steriade et al., 2001; V. V. Vyazovskiy & Harris, 2013)(**Figure 1.5**). These slow oscillations have been proposed to be the "default" network activity in the cortex. This is because slow oscillations manifest when the cortex is disconnected from its inputs either functionally, during NREM sleep or anaesthesia, or anatomically, such as in cortical slices *in vitro* (Chauvette et al., 2011; Sanchez-Vives & McCormick, 2000) or after brain lesions (Gloor et al., 1977). This cortical SWA relies on recurrent cortico-cortical activity and activity-dependent inhibition (Amzica & Steriade, 1995; Mattia & Sanchez-Vives, 2012).

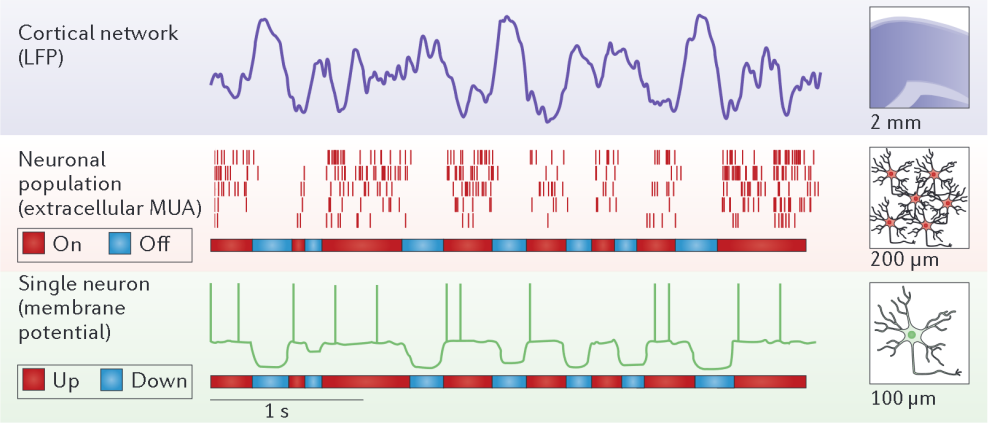

Figure 1.5 Slow wave activity during NREM sleep at the network and neuronal level.

(Top row) A trace of the local field potential (LFP) recorded from within the cortex of a rat during NREM sleep. **(Middle row)** A raster plot of the corresponding neuronal spiking activity of 5 individual neurons. **(Bottom row)** A schematic representation of the membrane potential expected in an individual neuron within this network. During slow wave activity, the LFP waves are associated with generalised population silence (OFF period), alternating with periods of raised spiking activity (ON periods). OFF periods are associated with a prominent membrane hyperpolarisation (DOWN state), which alternates with periods of depolarisation (UP state) when spiking tendency increases. Figure adapted from Vyazovskiy and Harris (2013).

During natural NREM sleep, slow waves propagate throughout the brain. Mechanistically, the synchronisation of SWA across the cortex relies on thalamocortical loops, which drives cortical activity in the characteristic delta frequency range (0.5 – 4 Hz)(Steriade et al., 1993; Timofeev & Steriade, 1996). Moreover, the activity of different excitatory and inhibitory neuronal cell types in the cortex has been found to regulate UP and DOWN states during cortical SWA. In addition to principal excitatory (pyramidal) neurons, parvalbumin (PV) and somatostatin (SST) expressing inhibitory interneurons have been shown to preferentially fire during the UP state of the cortical slow oscillation, and optogenetic activation of these inhibitory neuronal types can trigger the transition into a DOWN state (Funk et al., 2017; Zucca et al., 2017). In terms of cortical laminae, UP states have been shown to be initiated by excitatory pyramidal neurons in layer 5 (L5) of the cortex (Beltramo et al., 2013; Sanchez-Vives & McCormick, 2000), while feedforward projections from layer 2/3 (L2/3) to L5 contribute to SWA propagation (Wester & Contreras, 2012).

While network interactions drive synchronous slow waves across the cortex, the frequency, amplitude and spatial coordination of slow waves are influenced by sleep homeostatic process, and these changes are reflected in the underlying neuronal activity. When sleep pressure is high, such as following sleep deprivation, SWA increases, and the periods of neuronal inactivity (OFF periods) become longer in duration and occur across larger spatial areas. Conversely, as sleep progresses, there is a reduction in SWA, accompanied by shorter OFF periods and decreased synchrony between brain regions (Nir et al., 2011; V. V. Vyazovskiy et al., 2009). The intrinsic cellular properties of individual cortical neurons determine their propensity to enter ON/OFF periods (V. V. Vyazovskiy & Harris, 2013). Therefore, there must be a cellular mechanism that changes as a function of wakefulness and tracks the accumulation of sleep pressure. This mechanism may then enable the translation of sleep pressure into specific neuronal dynamics, which in turn contributes to the homeostatic regulation of SWA.

Importantly, SWA has been found to show regional heterogeneity across the cortex (Nir & de Lecea, 2023) and vary in a use-dependent manner (Krueger & Obäl Jr., 1993). This also supports the idea of a localised, cellular mechanism that tracks waking activity of neurons and translates this into sleep pressure. SWA has been consistently found to have an antero-posterior gradient across the cortex, with the highest SWA over the frontal cortical derivation of the EEG (Huber et al., 2000; Nir et al., 2011; Werth et al., 1996). The homeostatic rebound in SWA amplitude following sleep deprivation and its discharge during recovery sleep has also been found to be most prominent in the frontal cortex (Cajochen et al., 1999; Schwierin et al., 1999; Zavada et al., 2009). Additionally, the magnitude of NREM SWA varies by cortical layer, with L5 exhibiting the greatest levels of SWA (Krone et al., 2021). The regional modulation of SWA is also use-dependent. In humans, unilateral arm immobilisation during wakefulness was shown to result in a local decrease in SWA during subsequent NREM sleep in the contralateral hemisphere (Huber et al., 2006). In addition, in rats, unilateral whisker stimulation during wakefulness results in a local increase in the contralateral hemisphere SWA during subsequent sleep (V. Vyazovskiy et al., 2000). Slow waves, or neuronal OFF

periods, have also been observed to occur in local regions of the cortex during wakefulness under conditions of high sleep pressure, despite the rest of the cortex displaying a characteristic waking EEG profile (V. V. Vyazovskiy et al., 2011). These findings suggest that the homeostatic mechanisms of sleep are not only regulated at the global organism level, but also in local cortical regions, and perhaps also at the individual neuron level. While the topography of electrophysiological correlates of sleep and sleep pressure have been extensively studied, the spatial patterns of the molecular correlates of sleep pressure have been less explored.

1.3.3 Sleep and the UPR

Sleep is an evolutionarily conserved phenomenon, even if its global function and regulation may vary among different species (Rechtschaffen, 1998). However, it seems likely that there are fundamental cellular functions underlying the need to sleep that are shared among invertebrates and mammals. This is because the mechanisms of intercellular and intracellular signalling, including membrane receptors, ion channels and transcription factors are largely conserved across species, despite significant differences in the anatomy and complexity of brain circuits (Cirelli, 2006). The function of sleep is intertwined with its homeostatic regulation. Therefore, as sleep deprivation prevents sleep from fulfilling its function, it also provides a useful framework for studying the underlying mechanisms of sleep drive. It is assumed that subsequent alterations in gene and protein expression is a result of changing the homeostatic drive to sleep.

One influential hypothesis proposes that sleep functions to restore key cellular elements of macromolecule biosynthesis (Mackiewicz et al., 2007, 2008; Mignot, 2008). This theory is based on the observation that key components involved in macromolecule synthesis, such as protein production, are downregulated in the brain with extended wakefulness (Zimmerman et al., 2006), and upregulated during sleep (Mackiewicz et al., 2007). Slow wave sleep (NREM) is also associated with higher rates of protein synthesis in the brain compared to wake or REM sleep (Nakanishi et al., 1997; Ramm & Smith, 1990). On the contrary, sleep deprivation is associated with an inhibition of

protein synthesis, and subsequently detrimental effects on neuronal plasticity and cognition (Lyons et al., 2023a). The restorative hypothesis proposes that sleep, perhaps slow wave sleep in particular, functions to restore cellular stresses in order to relieve the inhibition of protein synthesis.

The UPR has a bidirectional relationship with protein synthesis. Increased rates of protein synthesis and trafficking through the ER requires the UPR's quality control mechanisms, while the UPR then functions as part of a negative feedback loop to slow down protein synthesis. Extended wakefulness is accompanied by increased expression of molecular chaperones and the adaptive UPR, which might underlie reduced rates of protein synthesis during this vigilance state (Naidoo et al., 2005; Terao et al., 2003). Specifically, the upregulation of BiP after prolonged wakefulness has been observed in the brains of all species that have been studied (Cirelli et al., 2004, 2005; Jones et al., 2008; Mackiewicz et al., 2007; Maret et al., 2007; Naidoo et al., 2005, 2007a; Shaw et al., 2000; Terao et al., 2006). In mouse cortex, BiP upregulation was accompanied by BiP dissociation from PERK, an increase in activated PERK and p-EIF2α, and a reduction in actively translating ribosomes, indicating an attenuation of protein translation (Naidoo et al., 2005). PERK pathway activity has also been found to be sleep-inducing in *Drosophila* (Ly et al., 2020). Chronic sleep fragmentation has also been shown to induce all three arms of the UPR in mice (Hakim et al., 2015). These experimental observations have been assimilated as a hypothesis, which proposes that the wakefulness-induced UPR may serve a prophylactic restorative purpose to protect neurons from ER overload and irreversible damage (V. V. Vyazovskiy & Harris, 2013). Therefore, subsequent sleep may act to provide neurons with periods of rest and cellular maintenance, during which protein synthesis can be resumed (Mackiewicz et al., 2007).

Within this hypothesis, it has been proposed that intense neuronal activity during wakefulness could lead to cellular stresses, including an accumulation of unfolded proteins in the ER, which may increase an individual neuron's propensity to undergo OFF periods (V. V. Vyazovskiy & Harris, 2013). This cellular process could underlie the increase in SWA associated with high sleep

pressure. In turn, the OFF periods can be seen as providing the neuron with a period of "rest" to undergo basic cellular maintenance to prepare for intense synaptic activity in a prophylactic manner. This hypothesis is supported by the observation that cortical induction of stress response genes, including molecular chaperones downstream of the UPR, is a molecular correlate of sleep deprivation (Cirelli et al., 2004; Naidoo et al., 2005; Terao et al., 2003, 2006). Moreover, enforced activation of the UPR's PERK pathway during sleep deprivation using Salubrinal results in a greater rebound in SWA levels during recovery sleep in rats (Methippara et al., 2012), suggesting that UPR activation may directly impact SWA. Therefore, slow wave sleep may serve a function to restore protein homeostasis in neurons following the suppression of protein synthesis as a result of the UPR during wakefulness. However, it is not known whether SWA is upregulated by ER stress, via an increase in unfolded protein burden, or whether it is regulated by the UPR signalling pathways independent of upstream ER stress.

The aforementioned changes are correlates of sleep deprivation and may not necessarily indicate a cause-and-effect relationship with sleep regulation. To identify cellular functions that cause the homeostatic increase in sleep intensity following sleep deprivation, it is necessary to manipulate those functions and observe a causative alteration in the homeostatic sleep response. In addition, if the cellular function is manipulated in the opposite direction, it should also lead to an opposite effect on the homeostatic sleep response.

It has been shown that genetic manipulation of BiP levels in *Drosophila* alters the amount of recovery sleep following sleep deprivation (Naidoo et al., 2007a). Systemic overexpression of BiP increases the homeostatic response of recovery sleep following sleep deprivation, whereas expressing a dominant-negative form of BiP decreases recovery sleep following sleep deprivation, without changing the amounts of baseline sleep or wakefulness. The bidirectional manipulation of BiP has opposing effects on recovery sleep, which suggests that BiP may play a causative role in the regulation of *Drosophila* recovery sleep following sleep deprivation. However, it is not clear whether

physiological levels of BiP also have a causative effect on sleep regulation in mammals. BiP levels increase proportionally to the duration of sleep deprivation in mouse cortex (Naidoo et al., 2005). However, while BiP levels are reduced over the course of recovery sleep, they still remain higher than baseline conditions after 24 hours of recovery (Naidoo et al., 2005, 2007a; Terao et al., 2003). This demonstrates that BiP remains upregulated in the cortex long after the homeostatic sleep response has subsided, suggesting that the level of endogenously expressed BiP may not be directly related to regulating sleep.

Since BiP levels also determine or reflect UPR levels, the UPR has been further dissected to specifically investigate the role of the PERK pathway in sleep regulation using *Drosophila* as a model organism. PERK activation occurs after prolonged wakefulness (Ly et al., 2020; Naidoo et al., 2005) and manipulating PERK activity and expression levels also alters sleep in *Drosophila* and zebrafish (Ly et al., 2020). Systemic pharmacological and genetic inhibition of PERK in *Drosophila* resulted in reduced sleep amounts, as did the specific knockdown of PERK in *Drosophila* brain neurons. Meanwhile, neuronal overexpression of PERK increased sleep amounts. The effects of PERK manipulation on sleep regulation mirror the effects of BiP manipulation in *Drosophila,* however, whether the two are causally linked has not yet been shown. Furthermore, there is a lack of understanding of the dynamics of PERK activation as well as the activity of the ATF6 and IRE1 arms of the UPR and their relationship with the dynamics of sleep homeostasis.

While there have been efforts to elucidate the UPR's role in modulating sleep at the global level, there is a lack of evidence for the relationship between the UPR and sleep pressure in local regions of the cortex. In 1993, Krueger proposed the idea that sleep is "quantal" in nature and that global sleep arises from the coordination of sleep in local networks, which are driven by sleep-regulating substances at the molecular level (Krueger & Obäl Jr., 1993). The cortex is a highly heterogenous region of the brain, displaying region- and cell type-specific differences in function and, therefore, are likely to have vastly different regulation of basal physiology by processes such

as the UPR. Whether the correlation between the tissue-wide increase in UPR and global sleep pressure also hold at the local and cellular level in the cortex remains to be determined.

1.3.4 Other theories of sleep function

Since protein homeostasis and the UPR is vital for numerous other biological processes, they may also relate to other theories about the functions of sleep in the brain. The synaptic homeostasis hypothesis (SHY) proposes that sleep functions to restore synaptic strengths in the brain, which have undergone potentiation during waking activity (Tononi & Cirelli, 2003). This is supported by the finding that spontaneous wakefulness is associated with the widespread induction of genes related to long-term potentiation (LTP) (Cirelli et al., 2004; Cirelli & Tononi, 2000b). Moreover, spontaneous and extended wakefulness was accompanied by a higher contact area between cortical axons and dendritic spines, which is a measure of structural potentiation (Bellesi & de Vivo, 2020). Within this framework, the potentiation of synaptic strength during waking activity becomes energetically unsustainable, and sleep provides the opportunity to downscale synaptic connections back to some baseline level. This hypothesis is also supported by the observed upregulation of the UPR in the brain during wakefulness and sleep deprivation. Wakefulness is associated with the upregulation of genes involved in synaptic plasticity and glutamatergic neurotransmission, which, if translated into proteins, require processing through the ER (Cirelli et al., 2004). Therefore, it could be that during waking activity, a high proportion of protein synthesis requires ER processing, which cumulatively results in a mild physiological UPR. During subsequent sleep, which is associated with synaptic downscaling, neurons may rely less upon ER proteostasis, thereby reducing the UPR levels.

An older theory, the energy restoration hypothesis of sleep, proposes that sleep serves to restore energy substrates that have been depleted during wakefulness (Benington & Craig Heller, 1995). This idea is supported by positron emission tomography studies in humans showing that brain glucose consumption is higher during wake compared to slow wave sleep (Buchsbaum et al.,

1989; Heiss et al., 1985; Kennedy et al., 1982). In the brain, regional increases in glucose and oxygen metabolism also correlate with synaptic activity levels and metabolic need (Fellows et al., 1992; Hawkins et al., 1983; Logothetis et al., 2001). Moreover, glycogen - the major energy source for neurons to produce ATP - decreases during waking periods (Karnovsky et al., 1983), which results in increased adenosine levels in the extracellular space and subsequent manifestations of sleep pressure (Benington et al., 1995). In addition, there are structural changes within cellular sub-compartments that indicate an increase in cellular metabolic needs. The ER relies on mitochondria to deliver ATP, and ER-mitochondria interactions were found to be increased during sleep deprivation, which may be a response to increased ATP demand in the ER during periods of wakefulness (Aboufares El Alaoui et al., 2023). In the energy restoration framework, NREM sleep is claimed to be the most important for the restorative effects of sleep, since it correlates with the lowest rates of glucose utilisation in the brain (Braun et al., 1997). Quiescent periods of neuronal silence (OFF periods) may reduce the brain's energetic demand for glucose and glycogen, thereby replenishing the energy stores (Benington & Craig Heller, 1995). This theory can also be related to the observed increase in UPR levels during wakefulness. Glucose depletion is known to inhibit glycosylation of proteins in the ER and induce expression of the glucose-regulated protein family of chaperones, including BiP/Grp78 (Shiu et al., 1977). Likewise, transient local shortages in cerebral metabolic supply may result in fluctuations in ATP levels, which can disrupt the ER environment and activate the UPR (Gomez et al., 2008).

The UPR can therefore be seen as correlating not just with wakefulness, but also a multitude of other wake-related biological processes. The functions of sleep are likely to be manifold, as are the functions of the physiological UPR. Therefore, there is a need for improved characterisation of the UPR within the brain, specifically in individual cells, during sleep and wakefulness. This will provide a deeper understanding of its involvement in the fundamental physiological processes of sleep.

1.4 Project aims and objectives

In the four experimental chapters of this thesis, my aim is to investigate and enhance our understanding of the relationship between the physiological UPR and sleep. In this section, I will provide an overview of the main research problems that this thesis addresses, building upon gaps in our knowledge mentioned in the earlier sections. Additionally, I will outline how I approach the three key objectives of my DPhil project:

1. Investigate whether sleep deprivation results in a heterogeneous activation of the UPR across cortical regions and cell types.
2. Investigate whether local ER stress induction in the cortex results in altered sleep and associated changes in neural activity patterns.
3. Develop a molecular genetic tool to effectively quantify the overall UPR in the nervous system for future applications.

The first key question I chose to address is whether the activation of the UPR is heterogenous across the cortex in a sleep-wake dependent manner. As different cortical regions and cell types serve distinct functions, they may also differ in their UPR activation during sleep deprivation. The electrophysiological correlates of sleep deprivation have been characterised both spatially and in a cell type-specific manner. Both before and after sleep deprivation, the intensity of SWA varies across cortical regions, most prominently along the antero-posterior axis, highlighting potential local differences in homeostatic sleep pressure (Huber et al., 2000). The relative activity of specific cell types during different vigilance states has also been characterised (Niethard et al., 2016; Ushimaru & Kawaguchi, 2015; Zucca et al., 2017). To the best of my knowledge, there has not yet been a systematic evaluation of the regional differences in UPR across the antero-posterior axis of the cortex. In addition, most evidence for the sleep deprivation-induced upregulation of the UPR is based on tissue-wide biochemical assays, which does not retain cell type information. Brain tissue consists of a variety of cell types, such as neurons, glia, vascular, and immune cells. Therefore, it remains to be determined whether neurons in particular contribute to sleep deprivation effects on the UPR, and whether neuronal subpopulations differ in their response. Therefore, in Chapter 2, I

aimed to better characterise the UPR under conditions of sleep deprivation, which poses a physiological challenge to protein homeostasis.

Within **Chapter 2**, I first aim to confirm the characteristic increase in SWA and BiP levels in mouse frontal cortex following a paradigm of sleep deprivation using novel objects exposure. Second, I characterise the UPR across different antero-posterior regions of cortex using bulk tissue strategies of western blotting and reverse transcription polymerase chain reaction (RT-PCR). Third, I develop an immunohistochemistry pipeline to quantify the somatic UPR in individual cells, specifically in neuronal cells in the cortex. Fourth and last, I explore whether there are differences in UPR activation with sleep deprivation in specific neuronal subpopulations.

The second key question I address in this thesis is whether ER stress induction in the cortex alters sleep and its associated electrophysiological patterns of brain ctivity. It has been proposed that under physiological conditions, SWA during sleep may be acting to restore neuronal stresses as a prophylactic mechanism to prevent irreversible damage and prepare for increased demands during waking activity (V. V. Vyazovskiy & Harris, 2013). However, there has not yet been compelling evidence to directly link ER stress and the UPR as underlying the need to sleep. Although manipulating a component of the UPR, p-eIF2α activation, has been found to alter global sleep and SWA in mice (Methippara et al., 2012), the role of the UPR in regulating local SWA and other activity patterns in the cortex is not known. Therefore, in Chapter 3, I aim to explore whether local ER stress induction in the cortex leads to altered sleep or modulation of cortical activity patterns.

Within **Chapter 3**, I first aim to establish a pharmacological approach to induce mild ER stress and UPR activation in a localised region of mouse cortex. I combine intracortical drug infusions with continuous electrophysiological recordings to monitor the effects of local UPR activation across sleep and wake in freely behaving mice. Second, I aim to establish the effects of local UPR activation on global sleep-wake architecture. Third, I explore the effects of local UPR activation on local neural activity patterns, including SWA. Fourth, I aim to explore whether the

electrophysiological effects of local UPR activation are local or global. Lastly, I characterise the properties of local cortical slow waves following UPR activation.

The third key problem I address in this thesis is the lack of tools for long-term monitoring of the physiological UPR in individual neurons. There is a lack of understanding of the temporal dynamics of UPR activation during wakefulness or sleep deprivation and its deactivation during subsequent sleep. Older studies that have attempted to address this have used single-timepoint bulk tissue analyses to measure UPR levels at different timepoints of sleep deprivation and following recovery from sleep deprivation (Naidoo et al., 2005; Terao et al., 2003). A different approach is needed to monitor UPR activation and recovery dynamics in individual neurons to be able to better investigate the bidirectional relationship between sleep and the UPR in neuronal protein homeostasis. Furthermore, newer, more sensitive tools are required for the detection of low levels of the UPR in physiological conditions. Therefore, I aim to develop a novel genetic fluorescent reporter to capture all three arms of the UPR with high sensitivity, and provide a temporal readout of UPR activation and recovery with cellular resolution. Furthermore, I aim to characterise the reporter's expression in neuronal systems to establish its usefulness for detecting physiological UPR activation as a result of sleep deprivation.

Within **Chapter 4**, I first aim to design and optimise a transcriptional reporter based on the BiP promoter that is capable of providing a quantifiable readout of low levels of UPR activation in individual cells. Next, I characterise the reporter's performance in terms of sensitivity and temporal readout of experimentally induced UPR compared to previously developed reporters of specific arms of the UPR. Finally, I characterise the reporter's ability to respond to a variety of ER stress stimuli. In **Chapter 5**, I aim to optimise the reporter's expression in neuronal tissue using different delivery methods. Next, I characterise the reporter's response to experimentally induced UPR *in vitro* using cultured brain slices. Finally, I examine the reporter's response in a specific neuronal subpopulation to physiologically activated UPR following sleep deprivation.

Each experimental chapter will include a brief introduction, the experimental methods used for procedures within the chapter, the research findings and a discussion of the results. The final chapter of the thesis will provide an overall summary of the findings, followed by a broader discussion of the implications of this work, and recommendations for future research.

Chapter 2 Sleep deprivation elevates UPR levels in mouse cortex in a region and cell type-specific manner

Contents

2.1 Introduction

Animal studies have revealed that cortical induction of stress response genes, including molecular chaperones downstream of the unfolded protein response (UPR), is a robust molecular correlate of sleep deprivation (Cirelli et al., 2004; Naidoo et al., 2005; Terao et al., 2003, 2006). Meanwhile, the increase in cortical slow wave activity (SWA) is a robust electrophysiological correlate of sleep deprivation and accumulated sleep pressure (Borbély et al., 1981, 1984; V. V. Vyazovskiy et al., 2007). However, there is a lack of understanding about how heterogenous the effects of sleep deprivation are across the brain and the cerebral cortex.

Both at baseline and after sleep deprivation, the intensity of SWA displays topographical variations across the cortex, with the highest SWA power observed in the anterior pole and the lowest in the posterior pole (Cajochen et al., 1999; Huber et al., 2000; Schwierin et al., 1999; Werth et al., 1996; Zavada et al., 2009). Indeed, the homeostatic regulation of SWA represents a local phenomenon as much as a global one (Bernardi et al., 2018; Huber et al., 2006; Krueger et al., 2019; Siclari & Tononi, 2017; Thomas et al., 2020). These observations, combined with the findings that the UPR is consistently upregulated in the frontal areas of the cortex after sleep deprivation, have led to the hypothesis that regional and cell-specific differences at the molecular level may underlie the local regulation of homeostatic SWA (V. V. Vyazovskiy & Harris, 2013). In particular, neurons may vary in their propensity to enter into OFF-periods depending on their susceptibility to cellular stress or as a prophylactic mechanism for cellular “rest”.

The cerebral cortex is characterised by substantial heterogeneity, both in terms of spatially defined regions and transcriptionally defined cell types (Ng et al., 2009; Tasic et al., 2018). It consists of a well-defined laminar cytoarchitecture, where each layer plays distinct roles in network activity and information processing (Bos et al., 2016; Fiáth et al., 2016; S. Zhang et al., 2016). As cortical regions and circuits differ in their functional roles, they may also differ in their response to sleep deprivation. Few studies to date have systematically addressed the regional differences in UPR

activation with sleep deprivation. In a microarray study, Terao et al. (2003) found differences in sleep deprivation-induced BiP upregulation in dorsal and lateral areas of the cortex. With technological advances in spatial transcriptomics, more recent studies have attempted to map the transcriptional profile of regions across the whole mouse brain, reporting cortical layer-specific transcriptional changes following sleep deprivation (Vanrobaeys et al., 2023). While these methods provide a wealth of data that can be used to identify regional effects of sleep deprivation on the UPR, they do not provide information at cellular resolution.

Advances in high throughput single cell RNA sequencing (scRNA-seq) allows for the transcriptional profiling of individual cells across the brain. Several datasets exist where cells collected from the brain have been profiled and clustered into transcriptionally distinct cellular subtypes (Jha et al., 2022; Paul et al., 2017; Tasic et al., 2018). With the vast breadth of transcripts that can be identified using scRNA-seq, these datasets can be mined to identify cell type differences in levels of UPR transcripts specifically. However, scRNA-seq data does not provide information about the spatial locations of the cells, which would instead need a technique combining spatial transcriptomics with scRNA-seq (Longo et al., 2021).

Alternative methods, such as *in situ* hybridisation (ISH), can provide insight into the effects of sleep deprivation on the expression levels of genes of interest in individual cells within spatially intact brain tissue. Thompson et al. (2010) mapped the transcriptional changes of select genes, including UPR-related genes, with sleep deprivation in sagittal sections across the entire mouse brain using ISH, reporting differential gene expression in an area-, layer- and cell type-specific manner. BiP transcript (also known as *Hspa5*) showed regional variations in its expression pattern, although this was not quantified. While information about transcript levels in the brain provides part of the picture of how cells respond to sleep deprivation, it may not correlate with the level of functional proteins that are expressed (Y. Liu et al., 2016a; Noya et al., 2019). To date, there have only been a handful of proteomic studies on sleep deprivation (Basheer et al., 2005; Cirelli et al.,

2009; Jha et al., 2022; Ren et al., 2016), and it remains a challenge to assess the proteome in a region- and cell type-specific manner. More traditional methods like immunohistochemistry are still immensely useful in evaluating protein expression levels in the beginning stages of addressing a research question. Immunohistochemistry offers the potential for multi-channel imaging of spatially preserved brain structures, to quantify the protein of interest in cell subpopulations using cell-specific markers.

The UPR is a sophisticated and adaptable process that operates at the cellular level, and aims to preserve proteostasis in response to, or in anticipation of, the increasing metabolic demands of individual cells (Rutkowski & Hegde, 2010). Therefore, it is likely that the UPR varies across functionally distinct cell types in the brain, including neuronal, glial, vascular and immune cells. It is not surprising that synaptic function of neuronal cell types has been linked to the UPR, given its reliance upon the activity-dependent production and turnover of multiple protein components (Martínez et al., 2018). The cycling of synaptic vesicles, receptor-mediated signalling, ion transport and the physical stability of the synapse, all rely upon ER proteostasis (Ashery et al., 2014). Pharmacologically increasing levels of neuronal activity can trigger the UPR, possibly via action potential-mediated elevations in intracellular $Ca2^{+}$ (Bahar et al., 2016; Jin et al., 2014; Kezuka et al., 2016; Yan et al., 2015). Although it is well-known that neuronal subpopulations exhibit variations in their synaptic activity and firing patterns, it remains unclear how they differ in their expression of the UPR, both at baseline and with sleep deprivation.

AIMS

In this chapter, I first empirically confirm the electrophysiological and UPR effects of acute sleep deprivation using novel object introduction (V. V. Vyazovskiy et al., 2002), since there are known to be variable physiological effects of different sleep deprivation paradigms (Havekes et al., 2012). Then, I go on to explore regional and cell type differences in baseline and sleep deprivation-induced UPR levels in mouse cortex.

More specifically, I aimed to:

1. Attempt to replicate findings from previous studies on the effect of sleep deprivation on SWA and BiP protein levels in mouse frontal cortex.
2. Investigate whether the upregulation of BiP levels after sleep deprivation differs between cortical regions.
3. Identify whether the overall neuronal population exhibits an increase in BiP levels after sleep deprivation.
4. Explore whether there is heterogeneity in BiP levels in cortical neuronal subpopulations at baseline and with sleep deprivation.

2.2 Methods

2.2.1 Animals for protein and RNA expression experiments

Sleep deprivation experiments were performed for subsequent analysis of protein and RNA expression levels in the mouse brain. All mice used in this chapter were males aged 9-10 weeks at the time of experiments. One batch of twenty C57BL/6J wild-type mice was used for western blot analyses (n=10 control, n=10 sleep deprivation). A batch of twelve C57BL/6J mice were used for RT-PCR analyses (n=4 control, n=7 sleep deprivation). A batch of twenty C57BL/6J wild-type mice was used for quantitative immunohistochemistry (n=10 control, n=10 sleep deprivation). In order to quantify immunohistochemical signals within somatostatin (SST) interneurons, I used a batch of eight transgenic mice (n=4 control, n=4 sleep deprivation) from the SST-ires-Cre;Ai9 line (hereon referred to as SST-Ai9), which was already established and maintained in the Akerman lab. SST-ires-Cre;Ai9 is a SST interneuron reporter line, where the Ai9 *loxP-STOP-loxP-TdTomato* reporter expresses tdTomato in the presence of Cre recombinase in SST-expressing neurons (Taniguchi et al., 2011). To make this recombinant line, a SST Cre driver line (SST-IRES-Cre:*Sst*$^{tm2.1(cre)Zjh}$/J; RRID:IMSR_JAX:013044, The Jackson Laboratory, USA)(Călin et al., 2023) was crossed with the Ai9 reporter line (B6;129S6-Gt(ROSA)26Sor$^{tm9(CAG-tdTomato)Hze}$/J; RRID:IMSR_JAX:007909, The Jackson Laboratory)(Madisen et al., 2010). The SST-Ai9 reporter mice were used because SST antibody markers failed to produce a uniform cytosolic signal, which is required within my quantitative immunohistochemistry pipeline to obtain cell masks from cell somas. All C57BL/6J wild-type mice were purchased from Charles River and SST-Ai9 mice were bred in-house in the Oxford Biomedical Sciences. Mice used for sleep deprivation experiments were singly housed under a 12-hour light/12-hour dark cycle. All mice were bred, housed and used in accordance with the UK Animals (Scientific Procedures) Act (1986).

2.2.2 Animals for electrophysiological recordings

Electrophysiological data presented in this chapter were obtained from one representative wild-type male C57BL/6J mouse (**Figure 2.1** C,D) and five Cre-negative mice from a 'cortical SNAP25-

ablated' mouse line (**Figure 2.1** B), Ai14;Snap25fl/fl (Krone et al., 2021), and were collected by Dr Lukas Krone from the Vyazovskiy lab. Standard procedures for conducting electrophysiological recordings, data acquisition and vigilance state scoring were followed, as detailed in the Chapter 3 **Methods** section. In this chapter, electroencephalograms (EEG) were recorded from frontal and occipital derivations in mice. The electrode screws were implanted at the following coordinates relative to bregma: [AP: +2.0 mm, ML: +2.0 mm] for the frontal derivation, and [AP: -3.5 mm, ML: +2.5 mm] for the occipital derivation.

2.2.3 Sleep deprivation and passive infrared monitoring

Following at least 3 days of habituation to housing conditions, sleep deprivation (SD) was performed for 6 hours starting at light onset as described in Vyazovskiy et al. (2002). Mouse behaviour and locomotion were constantly monitored, and upon signs of sleepiness the experimenter provided the animal with novel objects, such as cotton tips, tissue paper, polystyrene blocks and wood blocks to encourage exploratory behaviour. A subset of undisturbed control animals (used for immunohistochemistry) were monitored using a passive infrared recording (PIR) system (Brown et al., 2016) to ensure they had slept during the same time period. For these recordings, mice were singly housed in light/time-controlled (LTC) chambers, in which the light-dark cycle can be set using a timer switch. Each mouse cage was placed under a PIR motion detector that continuously recorded infrared emission from the mice in 100 ms intervals. Individual activity readings were pooled into 10 second epochs. All bouts of inactivity >40 seconds were scored as sleep, since previous work has validated this to be a reliable readout of behaviourally defined sleep (Brown et al., 2016). All control animals were confirmed to have spent more than 85% of the 6-hour period sleeping.

2.2.4 Cell culture and drug treatment

Media and culture materials were purchased from ThermoFisher Scientific, UK (including: Gibco, Invitrogen and Life Technologies) unless otherwise stated. NIH3T3 mouse fibroblast cells, isolated from a mouse NIH/Swiss embryo, were maintained at 37 °C and 5% CO_2 in Dulbecco's

modified Eagle medium (DMEM) with high glucose and pyruvate, supplemented with GlutaMAX and 10% bovine serum, and passaged at 90-95% confluence.

In preparation for immunofluorescence experiments, 13 mm glass coverslips were placed in 24-well plates, incubated with 0.1 mg/ml poly-D-lysine (PDL, in dH_2O) for 1 hour at 37 °C, then washed and air-dried. For experiments, NIH3T3 cells were trypsinised using 0.05% Trypsin-ethylenediaminetetraacetic acid (EDTA) and seeded onto the coverslips at a density of $1x10^6$ cells. In preparation for western blot experiments, NIH3T3 cells were seeded directly onto 6-well plates coated with PDL. The media was changed and the cells were left overnight before further treatment. Tunicamycin was prepared as a 5 mg/ml stock in dimethyl sulfoxide (DMSO) and further diluted in cell culture media. Final concentrations of Tunicamycin and incubation times are indicated where relevant.

2.2.5 Quantitative immunofluorescence of cultured fibroblasts

For immunofluorescence measurements, cells treated with Tunicamycin were pre-fixed in 2% paraformaldehyde (PFA) in 0.1 M phosphate buffered saline (PBS) for 10 minutes, followed by fixation in 4% PFA in PBS for another 10 minutes. Fixed cells were first incubated in 10% goat serum, 0.3% TritonX-100 for 1 hour at room temperature before being incubated with primary antibodies (summarised in **Table 2.1**) diluted in 5% goat serum in 0.15% TritonX-100 for 1 hour at room temperature. After washing in 0.3% TritonX-100, the cells were then incubated with Alexa Fluor-conjugated IgG secondary antibodies diluted in 5% goat serum in 0.15% TritonX-100 for 1 hour at room temperature. After further washes, the cells were stained with 4',6-diamadino-2-phenylindole (DAPI, 1:10,000 in PBS) for 5 minutes. Following a final wash, coverslips were mounted onto glass microscope slides using Prolong Diamond Antifade mountant (Invitrogen, Thermo Fisher Scientific, UK).

Fixed NIH3T3 cells on coverslips were imaged using an Olympus System Fluorescence Microscope Model BX40, and imaged using a Hamamatsu ORCA-ER camera and HCImage Live

software, with Auto Hi-Lo and Contrast settings turned off. Imaging parameters including exposure times were adjusted per fluorescent construct to avoid saturation, and kept constant per experiment.

For quantification of UPR-related antibody immunofluorescence, NIH3T3 cells were identified from images using the recently released Python package, `Cellpose` (Stringer et al., 2020). Segmentation "masks" generated by `Cellpose` were applied on the UPR antibody fluorescence channel to obtain a sum fluorescence value for each cell. An averaged background fluorescence value, which was obtained for each image by averaging all the pixels that were excluded from the cell masks, was subtracted from each cell. A threshold was applied such that cells with a background-subtracted fluorescence of zero or less were not included.

UPR protein	***Primary antibody***
BiP + GRP94	KDEL 10C3 mouse mAb (Enzo Life Sciences, ADI-SPA-827)
BiP	BiP rabbit mAb (Abcam 108615)
CHOP	CHOP (L63F7) mouse mAb (Cell Signalling Technology, #2895)
p-PERK	Phospho-PERK (Thre980) (16F8) rabbit mAb (Cell Signalling Technology, #3179)
sXBP1	XBP1 rabbit pAb (Abcam 198999)

Table 2.1 Commercially available antibody candidates for detecting UPR-related proteins.

2.2.6 Western blotting

Fibroblast sample preparation

Fibroblasts on 6-well plates treated with Tunicamycin were placed on ice and washed with ice-cold sterile PBS. Next, 100-300 µl of 1x cell lysis buffer (CLB, Cell Signalling Technology, USA) containing 1x Roche cOmplete Mini protease inhibitor cocktail (Merck, Germany) was added to wells for 15 minutes, followed by scraping and transferring detached cells to a fresh 1.5 ml tube. Cells were then homogenized using a micro-pestle and QIAshredder (Qiagen, USA) prior to centrifugation at 16,000 g for 2 minutes at 4 °C. The supernatants were transferred into a fresh 1.5 ml tube.

Mouse brain tissue sample preparation

At Zeitgeber time (ZT) 6, rested and sleep-deprived mice were rapidly anaesthetised with 4% isoflurane with an O_2 flow rate of 4 L/min in an induction chamber, and decapitated. Rested and sleep deprived mice were sacrificed in a counter-balanced manner (one rested animal sacrificed followed by one sleep deprived animal). The frontal, somatosensory and visual cortices were rapidly dissected from the brain, collected in foil pouches and immediately flash frozen in liquid nitrogen. The tissue was then stored at -80 °C until use.

Tissue samples were homogenised in chilled 1x CLB supplemented with 0.1% sodium dodecyl sulphate (SDS) and 1% Halt™ protease and phosphatase inhibitor (Thermo Fisher Scientific, UK), sonicated, vortexed and incubated on ice for 30 minutes. Samples were then centrifuged at 16,000 g for 10 minutes at 4 °C. The supernatants were transferred into a fresh 1.5 ml tube.

SDS-PAGE

For all samples, protein concentrations were determined using the Pierce™ BCA protein assay kit (Thermo Fisher Scientific, UK) according to manufacturer's instructions, using a series of bovine serum albumin standards of known concentration to generate a standard curve. Samples were normalised to 1 µg/µl by diluting in 1x CLB and 4x sample loading buffer (125 mM Tris, pH 6.8, 4% SDS, 50% glycerol, 0.2% w/v Orange G, LI-COR Biosciences, USA).

Protein samples were treated with 5% v/v 2-mercaptoethanol (Thermo Fisher Scientific, UK), after which they were heated for 5 minutes at 95 °C. 25 µg of each protein sample was loaded per lane of a 10% SDS polyacrylamide gel, and 10 µl of Precision Plus protein standard (Bio-Rad Laboratories, USA) was loaded to provide protein standard markers. Protein samples were then separated by electrophoresis in running buffer (25 mM Tris, 192 mM glycine, 0.1% SDS, pH 8.3) at 150 V for approximately 1.5 hours. Separated proteins were transferred from the gels to nitrocellulose membranes (Schleicher and Schuell from SigmaAldrich) at 85 V for 1 hour in transfer buffer (25 mM Tris base, 192 mM glycine, 20% v/v methanol, pH 8.3), after which the membranes were dried for 10 minutes at 37 °C. Membranes were blocked for 1 hour at room temperature (RT)

in Intercept blocking buffer (LICOR Biosciences, USA), after which they were incubated overnight at 4 °C with primary antibodies, diluted in Intercept blocking buffer containing 0.2% Tween 20. Fibroblast samples were prepared on separate membranes to be incubated with candidate UPR antibodies (**Table 2.1**). Brain tissue samples were incubated with the anti-KDEL mouse monoclonal antibody, KDEL 10C3, which detects BiP (**Table 2.1**). Blots were then washed 4x for 5 minutes with Tris-buffered saline containing 0.1% Tween 20 (TBS-T) prior to incubating with secondary antibodies. For fibroblast samples, IR Dye 680 or IR Dye 800 conjugated goat anti-mouse or anti-rabbit secondary antibodies (LICOR Biosciences, USA) were diluted 1:20000 in blocking reagent containing 0.2%v/v Tween 20. For brain tissue samples, the goat anti-mouse IR dye 800CW (LICOR Biosciences, USA) was diluted 1:20000 in LICOR Intercept blocking buffer containing 0.2% Tween 20. Membranes were incubated with secondary antibodies for 1 hour at room temperature. Membranes were again washed 5x with TBS-T followed by 1x TBS wash and imaged on an Odyssey Classic imaging system (LICOR Biosciences, USA). For normalization of the signal, blots were re-probed with a mouse anti-β-actin antibody (clone AC-15, Sigma-Aldrich, USA) for 1 hour at room temperature as described above. Blots were washed and incubated for 1 hour at RT with the secondary antibody goat anti-mouse IR dye 680RD (LICOR Biosciences, USA) diluted to 1:20000 as described above. Blots were washed again and reimaged.

For brain tissue samples, the detected BiP bands were quantified using Image Studio Lite Version 5.2 and graphs were plotted using GraphPad Prism version 9.2.0. β-actin was used as an internal loading control for all protein samples. To confirm that β-actin levels were unaffected by sleep deprivation, western blots were incubated with Revert 700 Total Protein Stain and imaged on the Odyssey scanner to obtain the total protein signal. The β-actin signal normalised to the total protein signal showed no difference between sleep deprived and control mice (data not shown; n=8; p=0.27, paired *t* test).

2.2.7 RNA extraction and RT-PCR

For RNA analyses, rested and sleep-deprived mice were sacrificed by cervical dislocation at Zeitgeber time (ZT) 4. Brains were rapidly removed and placed into a brain matrix (Kent Scientific). Skin graft blades (Swann-Morton) were placed were placed 1 mm apart and 1 mm thick coronal brain slices were dissected. Tissue punches were taken from the frontal cortex, somatosensory cortex and the visual cortex using a sample corer (1 mm internal diameter, Fine Science Tools GmBH), flash frozen on dry ice and stored at -80 °C until use.

While I was involved in sleep deprivation and tissue collection procedures, the RT-PCR experiments and analyses were conducted by Dr Lewis Taylor and Dr Jose Prius Mengual, collaborators on this project. For tissue RNA extraction, the tissue was firstly mechanically disrupted in 100 µl of Trizol. The sample was then made up to 500 µl using Trizol, after which 100 µl chloroform was added and then thoroughly mixed. Following a 5-minute incubation at room temperature, the sample was centrifuged for 15 minutes at 15,000 g, 4 °C. The clear top layer was then carefully collected, mixed with an equal volume of 70% ethanol and RNA was extracted using the RNeasy Plus Mini Kit (Qiagen, USA) following the manufacturer's instructions. RNA concentration and quality was determined using a NanoDrop ND-1000 spectrophotometer and cDNA synthesized using the qScript cDNA synthesis kit. RT-PCR was then conducted using the Quantifast SYBR Green PCR Kit and a StepOnePlus thermal cycler (Applied Biosystems, USA) with the following thermal profile: 95 °C for 5 minutes and then 40 cycles of 95 °C for 10 seconds, 60 °C for 30 seconds and 72 °C for 12 seconds. Quantification of transcript levels was conducted using the relative standard curve method, for comparing within a gene, or the $2^{-\Delta Ct}$ method for comparison across genes. Expression was normalised to the average of two reference housekeeping genes, GAPDH and RPL19. Primers used for this analysis are provided in **Table 2.2** and were designed by Dr Sarah Newey, from the Akerman lab.

Gene name	*Primer sequences*
BiP	**Forward** CCTGCGTCGGTGTGTTCAAG
	Reverse AAGGGTCATTCCAAGTGCG
sXBP1	**Forward** TACGGGAGAAAACTCACGGC
	Reverse GCACCTGCTGCGGACTCA
ATF4	**Forward** TAAGTTGTGTGCTCGGGTGT
	Reverse AACACTGCTGCTGGATTTCG
GAPDH	**Forward** TGCACCACCAACTGCTTAG
	Reverse GATGCAGGGATGATGTTC
RPL19	**Forward** ATGCCAACTCCCGTCAGCAG
	Reverse TCATCCTTCTCATCCAGGTCACC

Table 2.2 Primers used for RT-PCR to measure levels of UPR related transcripts.

2.2.8 Immunohistochemistry

Following the 6-hour SD period, rested and sleep-deprived mice were injected with pentobarbital and transcardially perfused with PBS followed by 4% PFA solution before tissue collection in a counter-balanced design. Coronal sections (50 μm) were cut from the left hemisphere of each perfusion-fixed brain using a vibrating microtome (Leica VT1000S), and stored in PBS with 0.05% sodium azide in 20-well plates until use. For immunohistochemistry, fixed sections were incubated in PBS with 5% normal goat serum (NGS) and 0.5% TritonX-100, for 2 hours at room temperature. Sections were incubated for 24-72 hours at 4 °C with primary antibodies (**Table 2.3**) diluted in 2.5% NGS and 0.25% TritonX-100. Sections were then washed and incubated with Alexa Fluor conjugated secondary antibodies (**Table 2.3**) diluted in 2.5% NGS and 0.25% TritonX-100 for 2 hours at room temperature or overnight at 4 °C. After further washes in PBS, the sections were mounted onto glass microscope slides using VectaShield mounting medium (Vector Laboratories, USA), under a rectangular coverslip. Slides were left to dry overnight before the coverslip was sealed with clear nail varnish.

Primary AB	*Catalogue no. and supplier*	*Dilution*	*Secondary AB*	*Catalogue no. and supplier*	*Dilution*
Mouse anti-KDEL (IgG2a)	KDEL 10C3 mouse mAb (Enzo Life Sciences, ADI-SPA-827)	1:250	Goat anti-mouse al488 IgG2a	Life Technologies, A21131	1:500
Guinea pig anti-PV	Synaptic Systems, 195004	1:2000	Goat anti-guinea pig al594	Life Technologies, A11076	1:500
Mouse anti-NeuN (IgG1)	Millipore, MAB377	1:500	Goat anti-mouse al647 IgG1	Life Technologies, A21240	1:500

Table 2.3 Summary of the primary and secondary antibodies and their respective dilutions used for brain immunohistochemistry.

2.2.9 Confocal imaging and image analysis

Fluorescence images from fixed mouse brain slices were captured with a LSM 710 confocal microscope using ZEN software. Z-stack images were taken from the middle ~5 µm of each section at intervals of ~0.5 µm. Exposure times were carefully adjusted such that the fluorescence signals were not saturated, and kept constant across all slices. Other settings such as pinhole aperture, optical zoom, laser intensity and dwell time were also kept constant in each experiment. Tile scan images were taken from a segment of the cortex, spanning all cortical layers.

Neurons in brain sections were identified on the pan-neuronal nuclear marker, NeuN, channel using a recently released Python package, `Cellpose` (Stringer et al., 2020). Segmentation "masks" generated by `Cellpose` were applied on the BiP antibody measurement channel to obtain a mean fluorescence value for each cell, using a custom-written script. A mean nearest background value surrounding the cell masks was subtracted. Parvalbumin-positive (PV+) cells were segmented on the PV antibody channel, and a neighbouring NeuN-positive, PV-negative (PV-) cell within ~25 µm was selected for calculating BiP ratios (PV+:PV-). Similarly, somatostatin-positive (SST+) cells were segmented and a neighbouring SST- cell was selected for calculating SST+:SST- ratios of BiP fluorescence.

2.2.10 Statistical analysis

All data were assessed for normality using the Shapiro Wilk test, following which the appropriate parametric or non-parametric statistical tests were applied. Statistical analyses were performed using the `Scipy` and `Statsmodels` packages in Python. For comparing immunofluorescence across cortical layers, repeated measures 2-way ANOVAs were conducted using GraphPad Prism (version 9.5.1), with within-subject factors. All graphs were generated using `Matplotlib` and `Seaborn` packages in Python. Asterisks represent significant p-values following statistical tests (*p<0.05, **p<0.01 and ***p<0.001). The statistical tests and p-values are detailed in the appropriate figure legends.

2.3 Results

2.3.1 Slow wave activity during NREM sleep varies regionally across the cortex

Slow wave activity (SWA) is a characteristic feature of the electroencephalogram (EEG) during NREM sleep. SWA serves as a reliable indicator of homeostatic sleep pressure, reflecting prior sleep-wake history. Notably, power in the delta range (0.5 – 4 Hz), which encompasses SWA, is highest during NREM compared with wake or REM sleep (**Figure 2.1**A). SWA in the cerebral cortex exhibits a homeostatic response, which manifests as an increase in power in the delta frequency

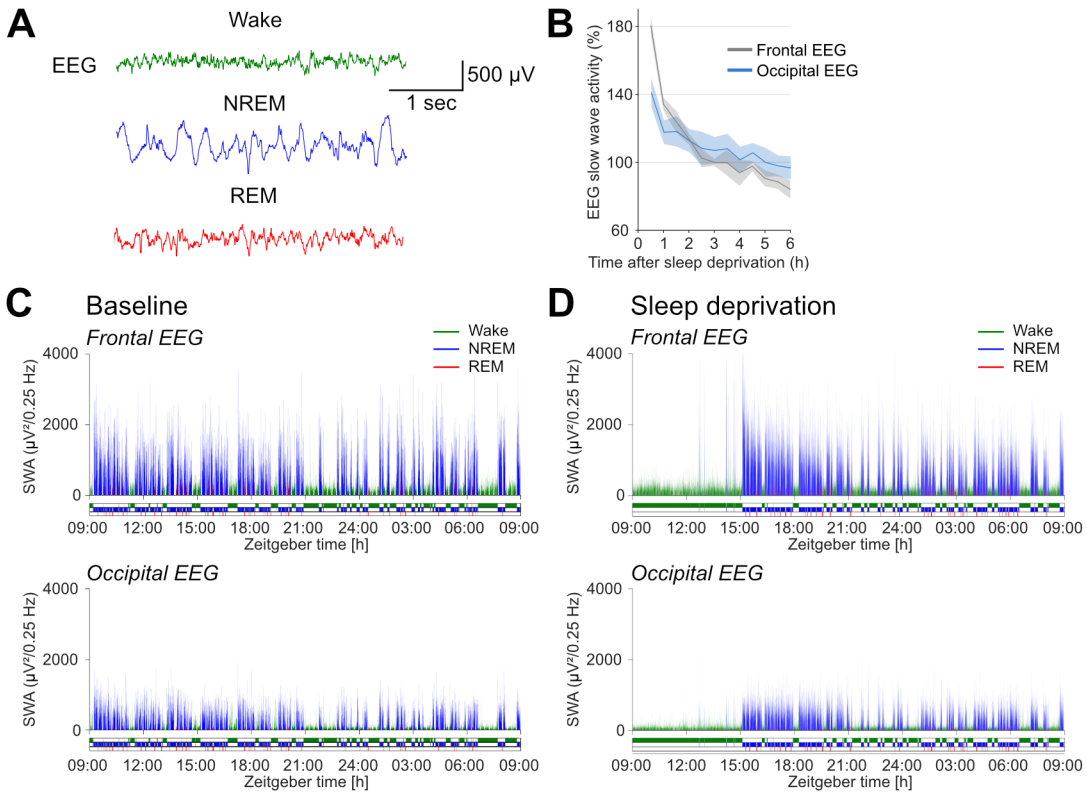

Figure 2.1 Slow wave activity, a marker of NREM sleep and homeostatic sleep pressure, is most pronounced in the frontal cortex.

(A) Example signals from the frontal cortex EEG from a representative mouse. **(B)** Time course of SWA (0.5 – 4 Hz) in frontal and occipital EEGs during NREM sleep after 6 hours of sleep deprivation relative to baseline average. Data represented as mean ± SEM from n=5 animals. **(C)** Hypnogram and SWA power density (in 4 second epochs) from the frontal and occipital EEG of one representative mouse during a 24-hour baseline recording. The light period was from 09:00 until 21:00, and the dark period was from 21:00 until 09:00. **(D)** Hypnogram and EEG SWA power density from the same representative mouse on sleep deprivation day, with a 6-hour sleep deprivation period from 09:00 until 15:00. NREM epochs immediately after sleep deprivation showed a marked increase in SWA power in the frontal EEG, followed by a discharge during subsequent hours. Data in '**B**', '**C**' and '**D**' were collected and provided by Dr Lukas Krone.

range following periods of sleep deprivation. However, this homeostatic rebound varies across different cortical regions, with the anterior frontal cortex exhibiting a greater increase in SWA than posterior occipital cortex following sleep deprivation (Huber et al., 2000).

While earlier studies investigating the frontal predominance of SWA employed gentle handing as the method of sleep deprivation, I first confirmed that a 6-hour period of sleep deprivation achieved through novel object introduction yielded the same frontal predominance of SWA (**Figure 2.1**B). The frontal EEG showed a greater SWA rebound and a faster recovery following sleep deprivation compared to occipital EEG, which was remarkably consistent across all individual animals. Moreover, continuous 24-hour traces of SWA from a representative animal illustrated regional variation in SWA even at baseline conditions, with higher SWA power observed in the frontal EEG relative to the occipital EEG (**Figure 2.1**C). Following 6 hours of sleep deprivation using novel objects, the same animal showed a substantial enhancement of SWA power during subsequent NREM sleep, which was most obvious in the frontal EEG compared to the occipital EEG (**Figure 2.1**D). Hence, these data confirm that frontal cortex exhibits a greater increase in SWA than posterior occipital cortex following sleep deprivation achieved through novel object introduction.

2.3.2 Validating a method to detect global UPR activation

In order to identify tools that would be useful for detecting UPR activation, I initially used an immortalised mouse embryonic fibroblast cell line, NIH3T3, and subjected cells to ER stress in culture. Treatment with pharmacological inducers of ER stress such as Tunicamycin (TUN), an N-linked glycosylation inhibitor that disrupts protein folding in the ER (Heifetz et al., 1979), have been widely used to elicit and study the UPR. Therefore, I treated the cells with TUN for 24 hours to elicit a global UPR (Abdullahi et al., 2017; Heifetz et al., 1979), after which the cells were either fixed for immunolabelling or lysed for western blotting.

To identify commercially available antibodies capable of detecting various UPR-related proteins, I tested a number of antibodies and scored them based on two criteria (**Table 2.4**). Firstly,

the antibody had to show a significant increase in immunofluorescence signal upon UPR activation. Secondly, the antibody had to detect upregulated protein expression of the correct molecular mass by western blotting. An antibody was considered to have successfully detected the UPR component if it met both of these criteria.

UPR protein	*Antibody (Supplier and Catalogue Number)*	*Tunicamycin-induced immunofluorescence*	*Tunicamycin-induced correct band on western blot*
BiP + Grp94	KDEL 10C3 mouse mAb (Enzo Life Sciences, ADI-SPA-827)	**Yes**	**Yes**
BiP	BiP rabbit mAb (Abcam, 108615)	**No**	**No**
CHOP	CHOP (L63F7) mouse mAb (Cell Signalling Technology, #2895)	**Yes**	**Yes**
p-PERK	Phospho-PERK (Thre980) (16F8) rabbit mAb (Cell Signalling Technology, #3179)	**No**	**No**
sXBP1	XBP1 rabbit pAb (Abcam, 198999)	**Yes**	**No**

Table 2.4 Summary of commercially available antibodies and their effectiveness in detecting UPR components, as well as the specificity of protein detection.

To visualise levels of BiP, I tested two antibodies: first, a monoclonal antibody (mAb) known as KDEL, raised against the C-terminal ER retention sequence motif 'SEKDEL' (amino acids 649-654 of rat BiP) and known to detect BiP as well as the related chaperone Grp94, which is also upregulated by the UPR (Munro & Pelham, 1986; P. Walter & Ron, 2011); second, a rabbit mAb generated against the BiP C-terminus, which theoretically should specifically detect BiP. I also evaluated a rabbit polyclonal antibody (pAb) against spliced XBP1 (sXBP1), as well as a rabbit mAb against phosphorylated PERK (p-PERK) to detect activation of the IRE1 and PERK pathways of the UPR, respectively. A mAb against CHOP was tested for indications of pro-apoptotic signalling downstream of the PERK pathway (Zinszner et al., 1998).

The antibodies were first tested by immunolabelling cultured mouse fibroblast cells that had been treated either with DMSO vehicle (VEH, 1:1000) or 2 µg/ml Tunicamycin (TUN) for 24 hours (**Figure 2.2**A). Even though cells intrinsically express BiP protein under baseline (non-stress) conditions, quantification of the cellular immunofluorescence signal revealed that KDEL displayed the largest fold-increase (3.9-fold) in response to TUN-induced UPR. CHOP displayed the second

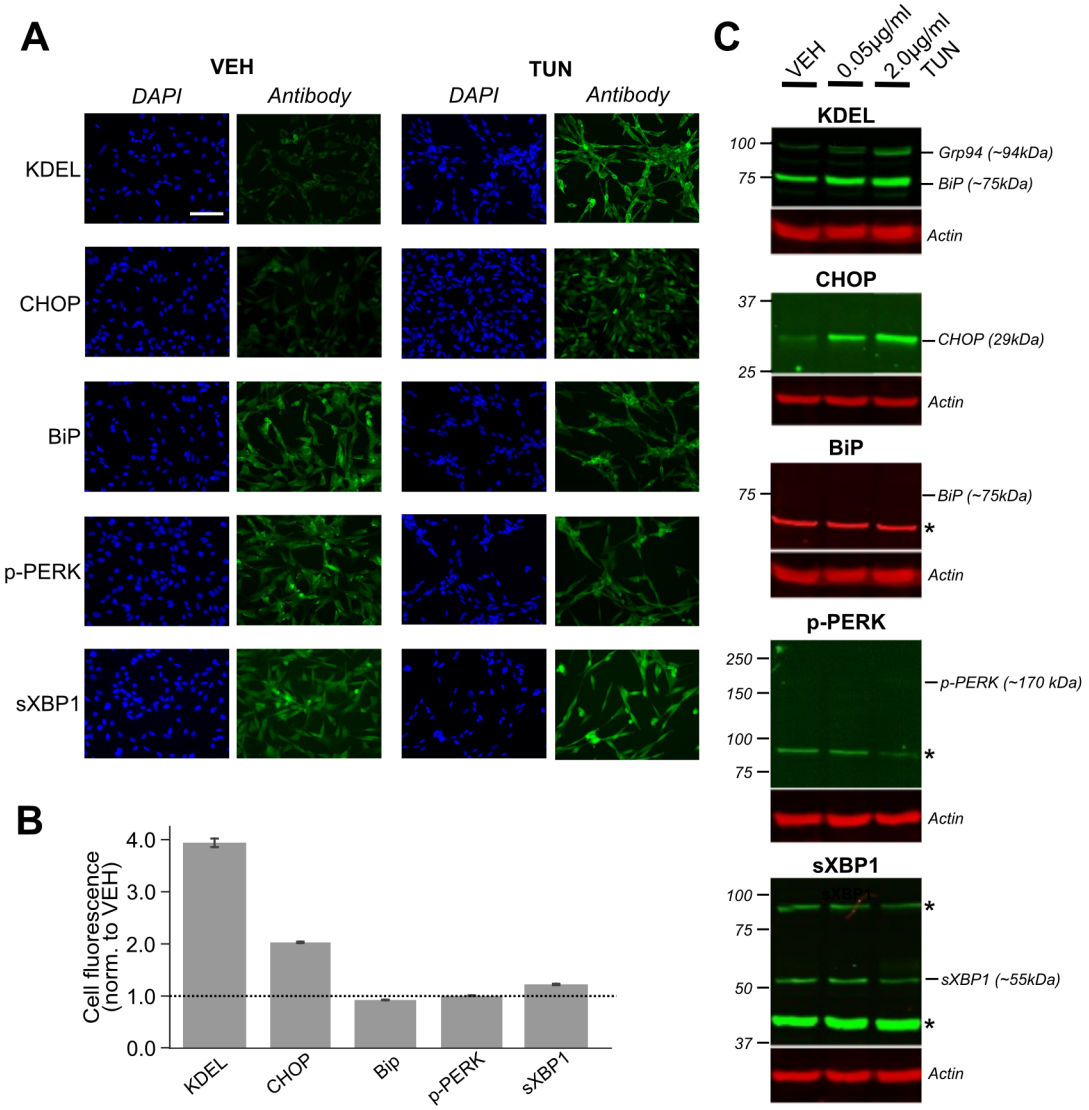

Figure 2.2 An antibody against the ER chaperone, BiP, displays a robust response to Tunicamycin-induced UPR.

(A) NIH3T3 fibroblast cells were treated with 2 µg/ml Tunicamycin (TUN), an ER stress inducer, or 1:1000 DMSO vehicle (VEH) for 24 hours, immunolabelled with five candidate UPR antibodies (KDEL, CHOP, BiP, p-PERK, spliced XBP1) and stained with DAPI. Scalebar: 100 µm. **(B)** Quantification of the KDEL and CHOP cellular immunofluorescence signals showed the largest fold-increase in fluorescence levels with TUN (normalised to VEH control). **(C)** Representative western blots showing protein bands detected by each antibody with VEH, 0.05 µg/ml or 2 µg/ml TUN, and actin loading control. KDEL and CHOP antibodies detect proteins at the expected molecular weight and show an increase in BiP and CHOP protein levels, respectively, with TUN compared to VEH. The anti-KDEL antibody primarily detects BiP protein, and to Grp94 to a lesser extent, both of which are ER-resident chaperones that respond to ER stress. Asterisk (*) next to western blot images denote non-specific bands. BiP and p-PERK antibodies do not display a band at the expected molecular weight, whereas sXBP1 detects multiple non-specific protein bands and the band at 55 kDa is not upregulated as expected. Numbers on the left of blots represent molecular mass standard marker (in kDa).

largest response (2.1-fold; **Figure 2.2**B) to TUN relative to VEH. The other antibodies failed to show a robust immunofluorescence response to TUN relative to VEH. Next, western blots were performed on NIH3T3 cell lysates that had been treated with either VEH, 0.05 µg/ml or 2 µg/ml TUN for 24 hours (**Figure 2.2**C). The results revealed that a number of the antibodies (BiP, p-PERK, and sXBP1) do not detect a TUN-upregulated protein band of the correct size. These findings are summarised in **Table 2.4** and establish that the KDEL antibody represents the best candidate for specifically and sensitively detecting UPR activation. Hereon in the thesis, I will refer to KDEL fluorescence as 'BiP fluorescence', since it primarily provides a readout of BiP protein levels. This exercise demonstrates the importance of independently verifying the specificity of commercial antibodies rather than solely relying on company datasheets.

2.3.3 Sleep deprivation elevates UPR levels in mouse cortex in a region-specific manner

Previously, microarray studies have reported that sleep deprivation or extended periods of wakefulness can elevate the levels of UPR-related transcripts in the rodent cerebral cortex (Cirelli et al., 2004; Mackiewicz et al., 2007; Terao et al., 2003, 2006). Additionally, protein level of the major ER chaperone, BiP, has been shown to be robustly and consistently upregulated in mouse frontal cortex as a function of sleep deprivation duration (Naidoo et al., 2005). The cerebral cortex is thought to play a key role in mediating the homeostatic response to prolonged wakefulness, as reflected in increased levels of SWA, with the anterior frontal cortex region exhibiting greater SWA than posterior occipital cortex (**Figure 2.1**). Therefore, I aimed to investigate potential variations in UPR levels across different regions of the cortex in response to sleep deprivation. To do this, mice were either sleep deprived by introduction of novel objects or allowed to sleep undisturbed, after which they were sacrificed and tissue was collected from the frontal (anterior), somatosensory (medial) and visual (posterior) cortical regions of the brains for western blotting and RT-PCR analysis (**Figure 2.3**A).

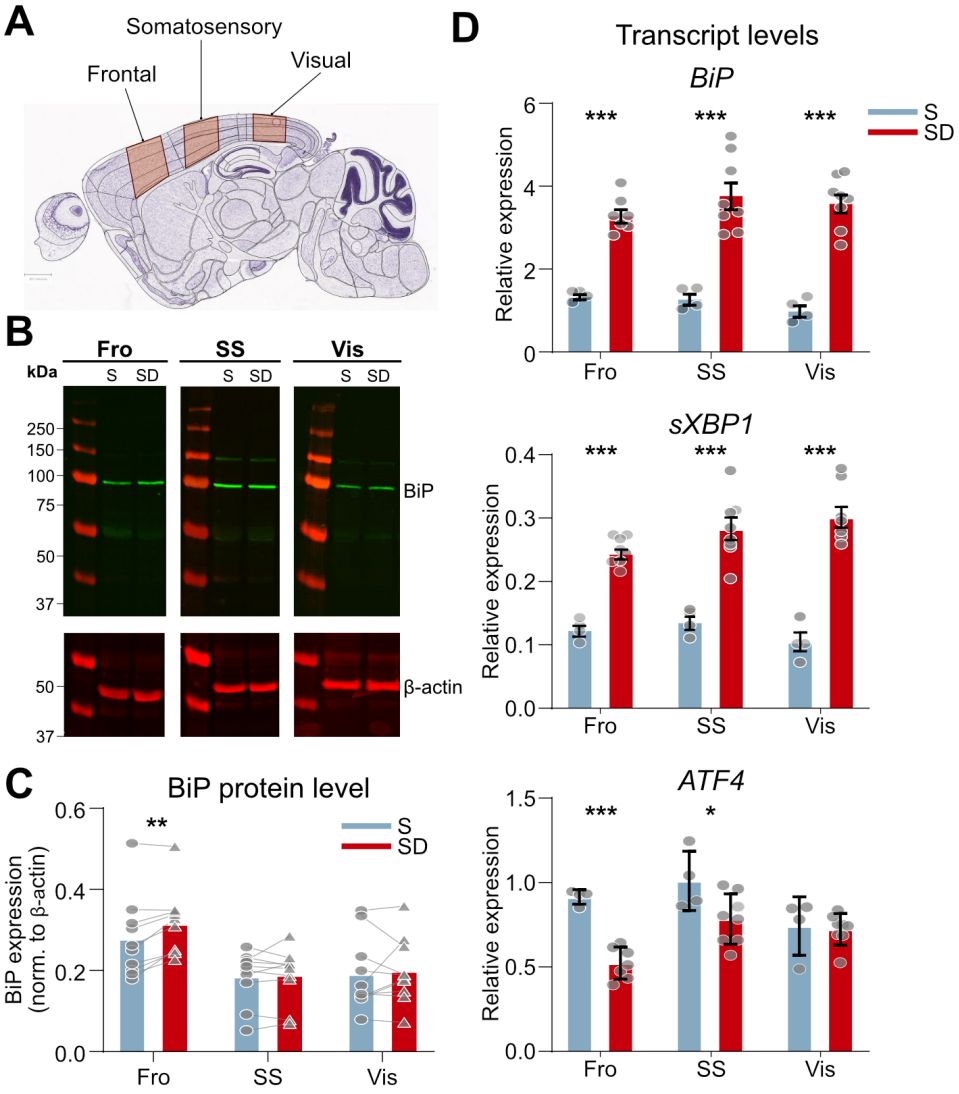

Figure 2.3 Sleep deprivation results in an activation of the UPR in mouse cortex in a region-specific manner.

(A) Schematic showing the regions of tissue from the mouse brain that were collected and processed for western blotting and RT-PCR: the frontal, somatosensory and visual cortices. **(B)** Representative western blots, probed with anti-KDEL antibody (green channel), illustrating BiP protein bands at ~75 kDa and β-actin as a loading control (red channel, ~42 kDa) in frontal (Fro), somatosensory (SS) and visual (Vis) cortex tissue samples from rested control (S) or sleep deprived (SD) mice. **C)** The level of BiP protein was quantified by analysing fluorescence intensity of the protein bands from the western blots. BiP protein levels were different across cortical region and sleep history (n=10; Region: p=0.0334, Sleep history: p=0.0493, Interaction: p=0.1415; repeated measures 2-way ANOVA). Specifically, samples from the frontal cortex in SD mice showed a 16% increase in BiP protein levels compared to corresponding samples from control S mice, that were matched for the time-point of tissue collection (n=10; p=0.0077, Sidak's multiple comparisons test). However, there was no difference between S and SD samples from the somatosensory or visual cortices (n=10; p=0.9807 and p=0.9654 respectively, Sidak's multiple comparisons tests).

Legend continued on next page……

Legend continued from previous page……..

(D) Cortical samples from a separate batch of S (n=4) and SD (n=7) mice were collected for RT-PCR, to measure the expression levels of UPR-related transcripts relative to the housekeeping genes, GAPDH and RPL19. BiP transcript levels varied with sleep history, but not cortical region ($p<0.001$ and $p=0.6012$ respectively, 2-way ANOVA). Samples across all cortical regions from SD mice had a higher level of BiP mRNA compared to S mice ($p<0.001$, Sidak's multiple comparisons tests). The level of sXBP1 mRNA also varied with sleep history, but not cortical region ($p<0.001$ and $p=0.2976$ respectively, 2-way ANOVA). ATF4 mRNA levels showed a difference across cortical regions and sleep history (Region: $p<0.0044$; Sleep history: $p<0.001$; Interaction: $p=0.0079$, 2-way ANOVA). Frontal and somatosensory cortex samples showed a decrease in ATF4 transcript in SD compared to S mice ($p<0.001$ and $p=0.0197$ respectively, Sidak's multiple comparisons tests). Meanwhile, there was no difference in ATF4 transcript levels in the visual cortex of SD and S mice ($p=0.9922$, Sidak's multiple comparisons test). Asterisks in '**C**' and '**D**' depict significant difference between S and SD conditions from individual regions. Data in '**D**' was provided by Dr Lewis Taylor.

BiP is a common target downstream of all three arms of the UPR, and can be used to provide a readout of global UPR activation when the contribution of the individual arms is unknown. Therefore, I used the anti-KDEL antibody, which is a sensitive marker of BiP (section **2.3.2**), to examine BiP protein level as a proxy for UPR levels in cortical tissue. Cortical tissue samples were collected for western blotting from a batch of ten control animals that were sleep deprived for 6 hours from light onset, and a batch of ten control animals that were allowed to sleep undisturbed during the same time period. Protein samples from the cortical tissue, matched for the timepoint of tissue collection, were separated on SDS-PAGE gels and probed with the anti-KDEL antibody to detect BiP, which was normalised to levels of β-actin (**Figure 2.3**B). I found that sleep deprivation resulted in a small but significant increase in BiP expression in mouse frontal cortex relative to control (16.02% ± 4.12), but the somatosensory and visual cortices did not show a detectable BiP upregulation with sleep deprivation. However, there was an overall effect of sleep deprivation across all cortical regions, and overall BiP levels also varied across the regions (**Figure 2.3**C).

Alongside translational changes at the protein level, the UPR also involves large-scale transcriptional changes. Therefore, cortical tissue samples were collected for measurement of UPR transcript levels from a separate batch of seven animals that had been sleep deprived for 4 hours from light onset, and four control animals that were allowed to sleep undisturbed during the same

time period. Sleep deprivation resulted in a robust increase in BiP transcript levels compared to controls in all three cortical regions (frontal: 2.42-fold, somatosensory: 2.91-fold, visual: 3.53-fold) and there was no difference in overall BiP transcript levels between cortical regions (**Figure 2.3**D top). The BiP transcript level provides a measure of activation by all UPR arms, the ATF6, IRE1 and PERK arms, but does not provide information about the activity levels of the individual arms. Therefore, to dissect the contribution of the arms, mRNA levels of the transcription factors sXBP1 (a readout of the IRE1 arm) and ATF4 (a readout of the PERK arm) were also examined. sXBP1 transcript levels were upregulated with sleep deprivation relative to control across all cortical regions (frontal: 1.97-fold, somatosensory: 2.06-fold, visual: 2.88-fold)(**Figure 2.3**D middle). Contrastingly, ATF4 transcript levels were downregulated with sleep deprivation in the frontal and somatosensory cortices (frontal: 0.57-fold, somatosensory: 0.78-fold), but not altered in the visual cortex. Taken together, these results suggest that the effects of sleep deprivation on UPR levels in the cerebral cortex are region-specific.

2.3.4 A quantitative immunohistochemistry pipeline for assessing UPR levels in mouse cortex at cellular resolution

Given that sleep deprivation related activation of the UPR in mouse cortical tissue varies in a region-specific manner, it is also possible that the effects vary in a cell type-specific manner. Therefore, the next objective was to dissect which cell types in the cortex were contributing to the effect of sleep deprivation on the UPR. To do this, I developed a quantitative immunofluorescence-based method for measuring UPR levels in different cell populations in mouse cortex (**Figure 2.4**). The KDEL antibody validated in section **2.3.2** was selected as a marker of global UPR activation based on its robust detection of BiP. An anti-NeuN antibody, which recognises the DNA-binding neuron-specific protein, NeuN, was used to identify the neuronal cell type population in mouse cortex. A second marker was used to further distinguish neuronal subtypes, such as an antibody against parvalbumin (PV), used to identify fast-spiking GABAergic PV interneurons (**Figure 2.4**A).

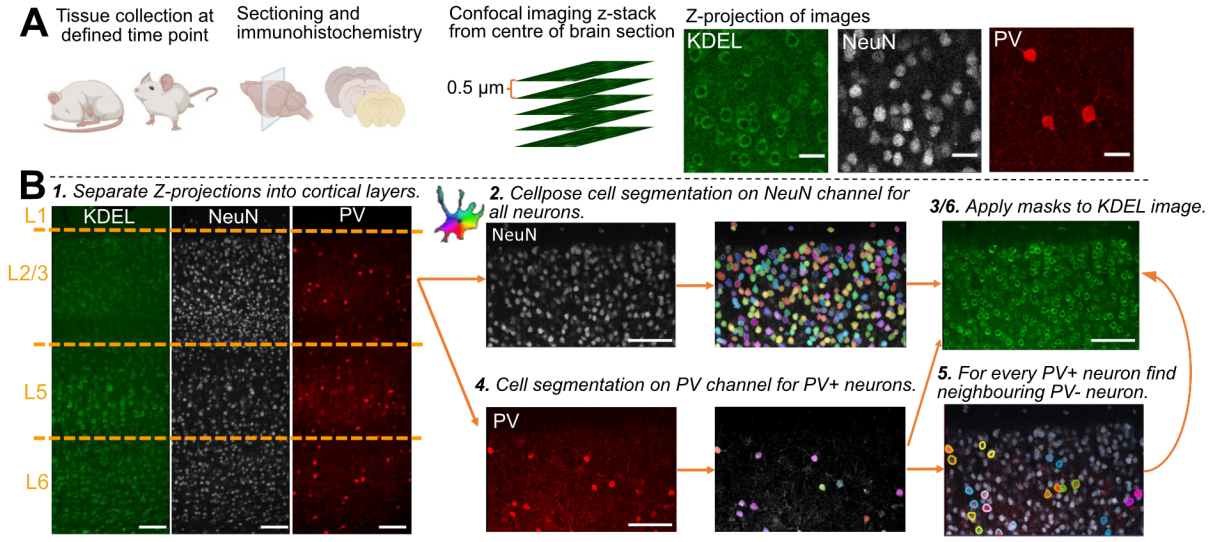

Figure 2.4 A quantitative immunofluorescence pipeline allows cell-specific measurements of BiP protein levels in mouse cortex.

(A) Sleep deprived and rested control mice were transcardially perfused and fixed, after which the brains were sliced to obtain 50 µm-thick coronal sections. For each mouse, sections were chosen from the same brain region (frontal or somatosensory cortex), to be stained with antibodies against BiP (KDEL antibody), a pan-neuronal marker (NeuN) and a cell-type specific marker (for example, PV, a subset of GABAergic interneurons). Z-stack of images was obtained from the central 5 µm of each 50 µm-thick section, and later summed z-projections were calculated for each antibody channel. Scale bar: 25 µm. **(B)** To quantify BiP fluorescence, images were initially divided into cortical layers (depicted by orange dashed lines in step 1) and cells were segmented using a Python image processing package, 'Cellpose', on the NeuN channel to detect the majority of neurons. These masks were then applied to the BiP channel to measure each neuron's mean BiP fluorescence. To investigate cell type-specific effects, the cell subset marker (e.g. PV) channel was also used to generate cell masks. For each PV+ interneuron, a neighbouring PV- neuron was detected from the NeuN masks (colour-coded pairs). These paired masks could then be applied to the BiP channel to obtain a PV+:PV- ratio, to compare a neuronal subpopulation to a general neuronal population within the same brain sections. Scale bars: 100 µm.

Confocal images were captured in tiles and stitched together to provide coverage of all cortical layers. Neuronal populations could then also be distinguished according to cortical layers (**Figure 2.4**B), which are associated with unique cell types that exhibit distinct activity patterns *in vivo* (Fiáth et al., 2016; Krone et al., 2021; S. Zhang et al., 2016). An automated cell-segmentation Python package, `Cellpose`, was then used to define "masks" for individual NeuN-positive (NeuN+) neurons. These masks were then applied to the BiP fluorescence channel, to quantify mean BiP levels per neuron. If a second cell type marker was also present, such as for PV-expressing interneurons, the NeuN masks could also be used to identify PV-negative (PV-) and PV-positive (PV+) subpopulations. By comparing these subpopulations, there was the opportunity to measure

differences in BiP levels between the neuronal subtype and the general NeuN population (**Figure 2.4**B).

2.3.5 Sleep deprivation results in activation of the UPR in neurons of the mouse frontal cortex

One of the physiological effects of sleep deprivation is to initiate an upregulation of the UPR in mouse cerebral cortex in a region-specific manner. The cortex is composed of various cell types, including neurons, glia, vascular and immune cells. However, it remains unclear whether the sleep deprivation-induced increase in UPR levels is displayed by neurons, which are the primary electrically active cells in the brain that generate sleep slow wave activity and brain oscillations. The quantitative immunofluorescence pipeline provides an opportunity to characterise physiologically relevant changes in UPR levels in specific cortical cell types. To examine whether cortical neurons in particular exhibit differences in their UPR under baseline conditions and following a period of sleep deprivation, mice were either kept awake for 6 hours, starting from light onset, or allowed to sleep undisturbed. At the end of the 6 hour period, animals were sacrificed, perfusion-fixed and their brains processed for quantitative immunofluorescence (**Figure 2.4**).

Neurons in fixed brain slices from the frontal cortex were identified with the anti-NeuN antibody, and their BiP fluorescence was quantified (**Figure 2.5**A, first panel). At the individual cell level, NeuN+ neurons from sleep deprived mice (SD) displayed a greater BiP fluorescence compared to slept controls (S), as demonstrated by the right-shift in their cumulative probability distributions, with a 16% increase in the median value (**Figure 2.5**A, second panel). This was consistent with the 16% increase observed in BiP protein level in frontal cortical tissue with western blotting (**Figure 2.3**C). The median BiP fluorescence of cells grouped by brain slice and animal also showed a ~16% increase with SD compared to S (**Figure 2.5**A, third and fourth panels).

Next, NeuN+ neurons were examined in brain slices of the somatosensory cortex, which did not previously show an increase in UPR levels in response to sleep deprivation at the tissue level

(section **2.3.3**). Likewise, quantification of BiP fluorescence in NeuN+ neurons from both S and SD mice indicated no discernible difference at the level of individual cells, slices or animals (**Figure 2.5**B).

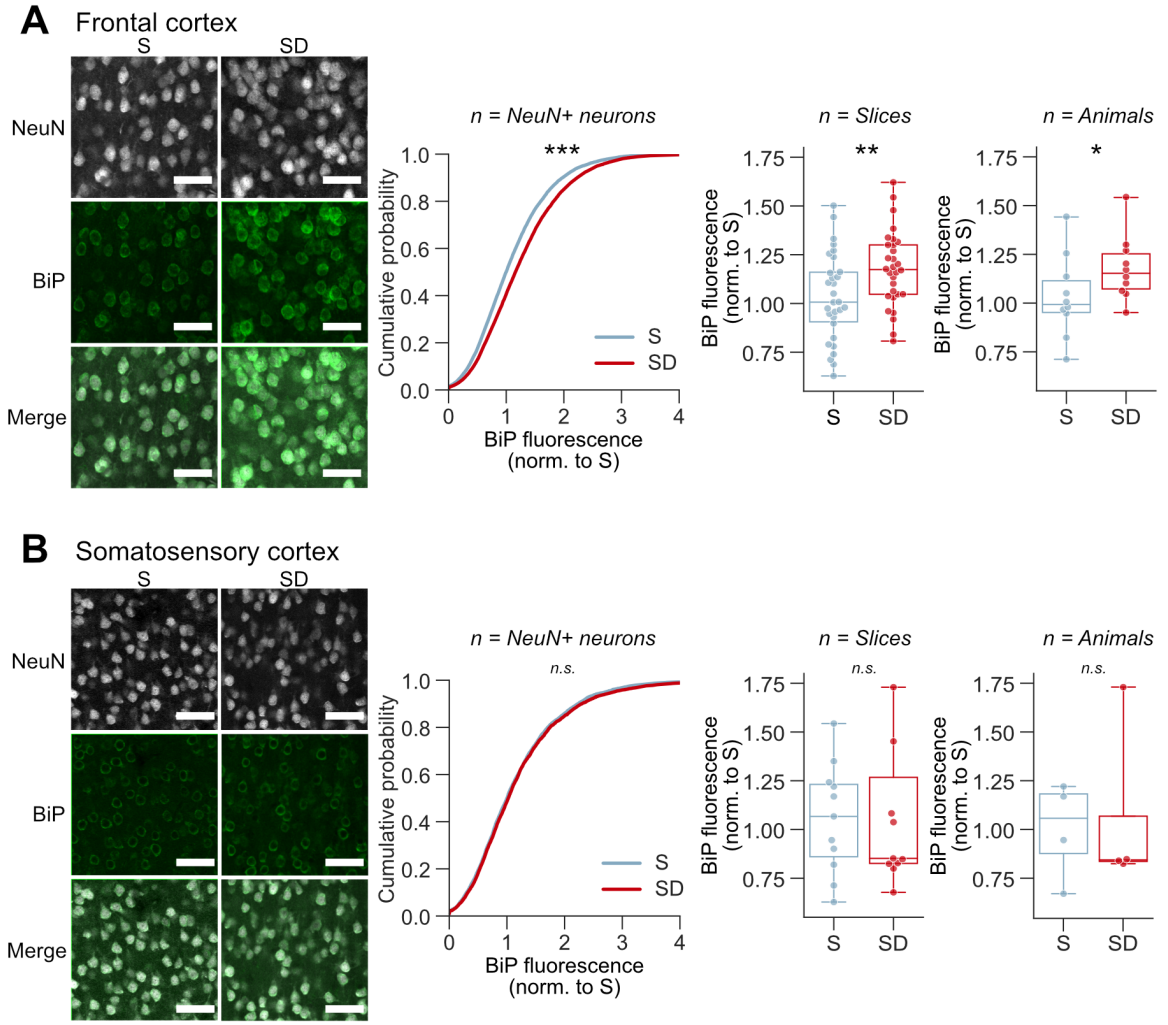

Figure 2.5 Sleep deprivation results in an increase in BiP protein levels in neurons of the frontal cortex but not the somatosensory cortex.

(A) Immunofluorescence of BiP in NeuN+ neurons of the frontal cortex from sleep deprived (SD) and rested control (S) mice. The cumulative probability distribution of BiP fluorescence (normalised to control) in SD brains was biased towards higher values compared to S brains (n=11040 neurons; p<0.001, Kolmogorov Smirnov test). Neurons grouped by brain slice (n=30, 3 slices per animal) and by animal (n=10) also show a significant increase in BiP fluorescence in SD brains compared to S brains (p=0.0066 and p=0.0378 respectively, Mann Whitney U tests). **(B)** Immunofluorescence of BiP in NeuN+ neurons of the somatosensory cortex from sleep deprived (SD) and rested control (S) mice. There was no difference in the cumulative probability distribution of BiP fluorescence between SD and S brains (n=4400 neurons; p=0.2794, Kolmogorov Smirnov test). Neurons grouped by brain slice (n=12, 3 slices per animal) and by animal (n=4) also showed no difference between SD and S brains (p=0.4478 and p=0.4426 respectively, Mann Whitney U test). Scalebars: 50 µm.

2.3.6 Interneuron cell types do not show an increase in UPR levels with sleep deprivation

Specific subclasses of GABAergic inhibitory interneurons are easily identifiable and their functional properties are well-characterised in the literature (DeFelipe et al., 2013; Tremblay et al., 2016). In particular, PV+ fast-spiking interneurons and somatostatin-positive (SST+) interneurons are two of the biggest subclasses of inhibitory interneurons in the mouse brain and have been implicated in the regulation of UP and DOWN states of cortical networks corresponding to slow waves (Funk et al., 2017; Neske & Connors, 2016; Rodarie et al., 2021; Tossell et al., 2020; Zucca et al., 2017). Therefore, I wanted to investigate whether these inhibitory subpopulations exhibit differences in their baseline UPR level compared to other neurons, and whether their UPR is affected by sleep deprivation.

PV+ interneurons represent an interesting population in terms of the UPR, as these neurons are known to have one of the highest energy expenditures in the brain, which may be associated with different UPR levels (Kann, 2016). To examine whether cortical PV+ interneurons exhibit differences in their UPR compared to PV-negative neurons (PV-) under baseline conditions, fixed brain slices from the frontal cortex were immunolabelled with anti-PV and anti-NeuN antibodies (**Figure 2.6**A). The BiP fluorescence of every PV+ interneuron was measured as a ratio of the BiP fluorescence of a neighbouring PV-, NeuN+ neuron. The ratio of excitatory to inhibitory neurons in the mouse cortex is ~7:1 (Alreja et al., 2022; Rodarie et al., 2021), and therefore, neighbouring PV- neurons were highly likely to be excitatory pyramidal neurons. Interestingly, I found that the BiP fluorescence level in PV+ interneurons was 91% of neighbouring PV- neurons (**Figure 2.6**B), indicating cell type-specific differences in endogenous levels of the UPR.

SST+ interneurons represent another interesting neuronal population in terms of the UPR as they produce the secreted neuropeptide, somatostatin, which is processed in the ER (Goodman et al., 1983) and have been shown to be vulnerable to behavioural stress (Tomoda et al., 2022). The antibody-based method for identifying SST+ interneurons yielded an irregular, punctate expression

pattern, making it unsuitable for use with the automated cell detection pipeline. As a result, I utilised a SST reporter mouse line, SST-Ai9, which enabled the detection of tdTomato expression in SST+ interneurons. Frontal cortex brain sections from SST-Ai9 mice were immunolabelled with anti-NeuN, to detect SST-negative (SST-) neurons, and anti-KDEL to measure BiP levels (**Figure 2.6**C). The BiP fluorescence of every SST+ interneuron was measured as a ratio of the BiP fluorescence of a neighbouring SST-, NeuN+ neuron. The BiP fluorescence level in SST+ interneurons was 89% of neighbouring SST- neurons (**Figure 2.6**D), similar to PV+ neurons, suggesting that the inhibitory interneuron population may display lower levels of baseline UPR compared to neighbouring putative excitatory pyramidal neurons.

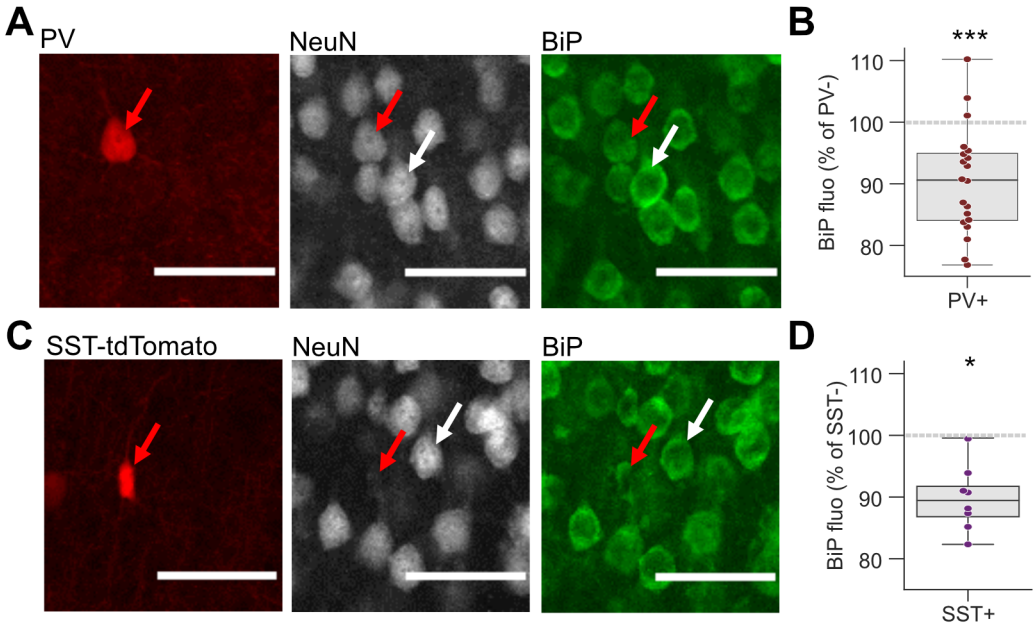

Figure 2.6 Interneuron subtypes have varying levels of BiP expression compared to the general neuronal population.

(A) Brain sections from wild-type adult mice were immunolabelled with antibodies against PV (parvalbumin) and NeuN to identify PV+ interneurons and the general NeuN+ neuronal population. Each identified PV+ interneuron was paired with a nearest neighbour PV-, NeuN+ neuron (within 25 µm maximum). **(B)** The median BiP fluorescence in PV+ interneurons (grouped by animal) was 91% of the BiP fluorescence in neighbouring PV- neurons (n=20 animals, $p<0.001$, Wilcoxon rank-sum test). Scalebars: 50 µm. **(C)** Brain sections from transgenic adult mice (SST-Ai9), expressing tdTomato in SST+ interneurons, were immunolabelled to detect BiP levels and identify NeuN+ neurons. Each identified SST+ interneuron was paired with a nearest neighbour SST-, NeuN+ neuron. **(D)** The median BiP fluorescence in SST+ interneurons (grouped by animal) was 89% of the BiP fluorescence in neighbouring SST- neurons (n=8 animals, $p=0.0117$, Wilcoxon rank-sum test). Scalebars: 50 µm.

Given that PV+ and SST+ interneurons exhibited a lower level of BiP relative to other neurons, I next explored whether these interneuron subtypes respond to sleep deprivation similarly to the general NeuN+ population. Mice were either sleep deprived for 6 hours or allowed to sleep undisturbed. PV+ interneurons from sleep deprived (SD) mice displayed a slightly greater BiP fluorescence compared to slept controls (S), with a 8% increase in the median value (**Figure 2.7**A, second panel). However, there was no detectable difference in BiP fluorescence of PV+ interneurons grouped by brain slice or animal with SD compared to S (**Figure 2.7**A, third and fourth panels). Meanwhile, for SST+ interneurons, there was no difference in BiP fluorescence between SD and S mice at the level of individual neurons, slices or animals (**Figure 2.7**B). These results suggest that interneurons are less prone to exhibit a sleep deprivation-induced UPR compared to other neurons.

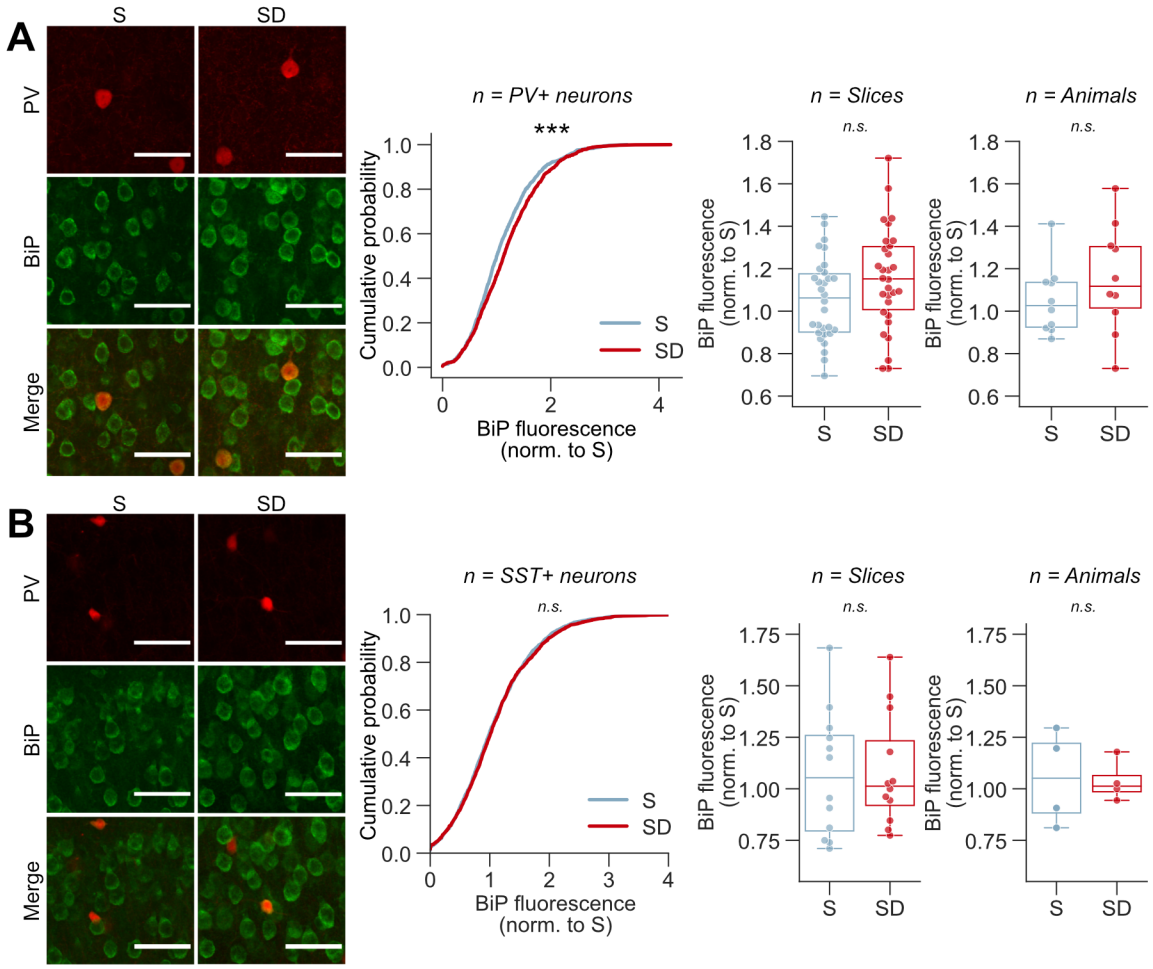

Figure 2.7 The effects of sleep deprivation on BiP protein levels in PV+ and SST+ interneurons of the frontal cortex.

(A) Immunofluorescence of BiP in PV+ interneurons of the frontal cortex from sleep deprived (SD) and rested control (S) mouse brains. The cumulative probability distribution of PV+ interneurons' BiP fluorescence in SD brains (normalised to S) was biased towards higher values compared to S brains (n~1150 cells; p<0.001, Kolmogorov Smirnov test). However, neurons grouped by brain slice (n=30 slices, 3 slices per animal) and by animal (n=10) failed to show a significant difference in BiP fluorescence between SD and S brains (p=0.056 and p=0.1537 respectively, Mann Whitney U test). **(B)** Immunofluorescence of BiP in SST+ interneurons of the frontal cortex from S and SD mouse brains. There was no difference in the cumulative probability distribution of SST+ interneurons' BiP fluorescence between SD and S brains (n~1300 cells; p=0.6032, Kolmogorov Smirnov test). Neurons grouped by brain slice (n=30 slices, 3 slices per animal) and by animal (n=10) also showed no difference between SD and S brains (p=0.3754 and p=0.4426 respectively, Mann Whitney U test). Scalebars: 50 µm.

2.3.7 BiP level in cortical neurons varies across layers and as a function of sleep-wake history

The cerebral cortex consists of a well-defined laminar cytoarchitecture, where each layer plays distinct roles in network activity and information processing (Bos et al., 2016; Fiáth et al., 2016; S. Zhang et al., 2016). Therefore, I wanted to investigate whether neurons across cortical layers exhibit differences in their baseline UPR level, and whether their UPR is affected differently by sleep deprivation. NeuN+, PV+ and SST+ neurons were identified in fixed brain slices from the frontal cortex of sleep deprived and control mice. For each brain slice, a tile scan image was taken of the entire slice from one hemisphere and matched to its corresponding Allen Brain Atlas image to identify cortical layers 2/3, 5 and 6 (L2/3, L5 and L6 respectively) using the NeuN channel (**Figure 2.8**A). BiP fluorescence was then measured in NeuN+, PV+ and SST+ neurons across L2/3, L5 and L6 (**Figure 2.8**B,C).

I found that BiP levels in the general NeuN+ neuronal population as well as the PV+ and SST+ interneuron subpopulations varied as a function of cortical layer (Layer effect: $p<0.05$, repeated measures 2-way ANOVA, see stats in **Figure 2.8**). For NeuN+ neurons, L5 BiP levels were greater than both L2/3 (n=10 animals; $p<0.001$, Sidak's multiple comparisons test) and L6 ($p=0.0021$, Sidak's multiple comparisons test)(**Figure 2.8**D). L2/3 BiP levels did not differ from L6 ($p=0.8794$, Sidak's multiple comparisons test). NeuN+ neurons showed an overall increase in BiP levels in the SD group compared to S group, but upon post-hoc multiple comparisons tests, there were no significant differences detected between S and SD at each layer. For PV+ interneurons, BiP levels were significantly different between each layer (n=10 animals; L2/3 vs L5: $p=0.0037$; L2/3 vs L6: $p<0.001$; L5 vs L6: $p=0.0038$, Sidak's multiple comparisons test)(**Figure 2.8**E). Moreover, BiP levels in PV+ neurons showed greater variance in the SD group compared to the S group across all layers, and a trend suggesting higher BiP levels in L2/3 and L6 in the SD group compared to S. However, PV+ interneurons did not show a significant effect of SD. In contrast, BiP levels in SST+

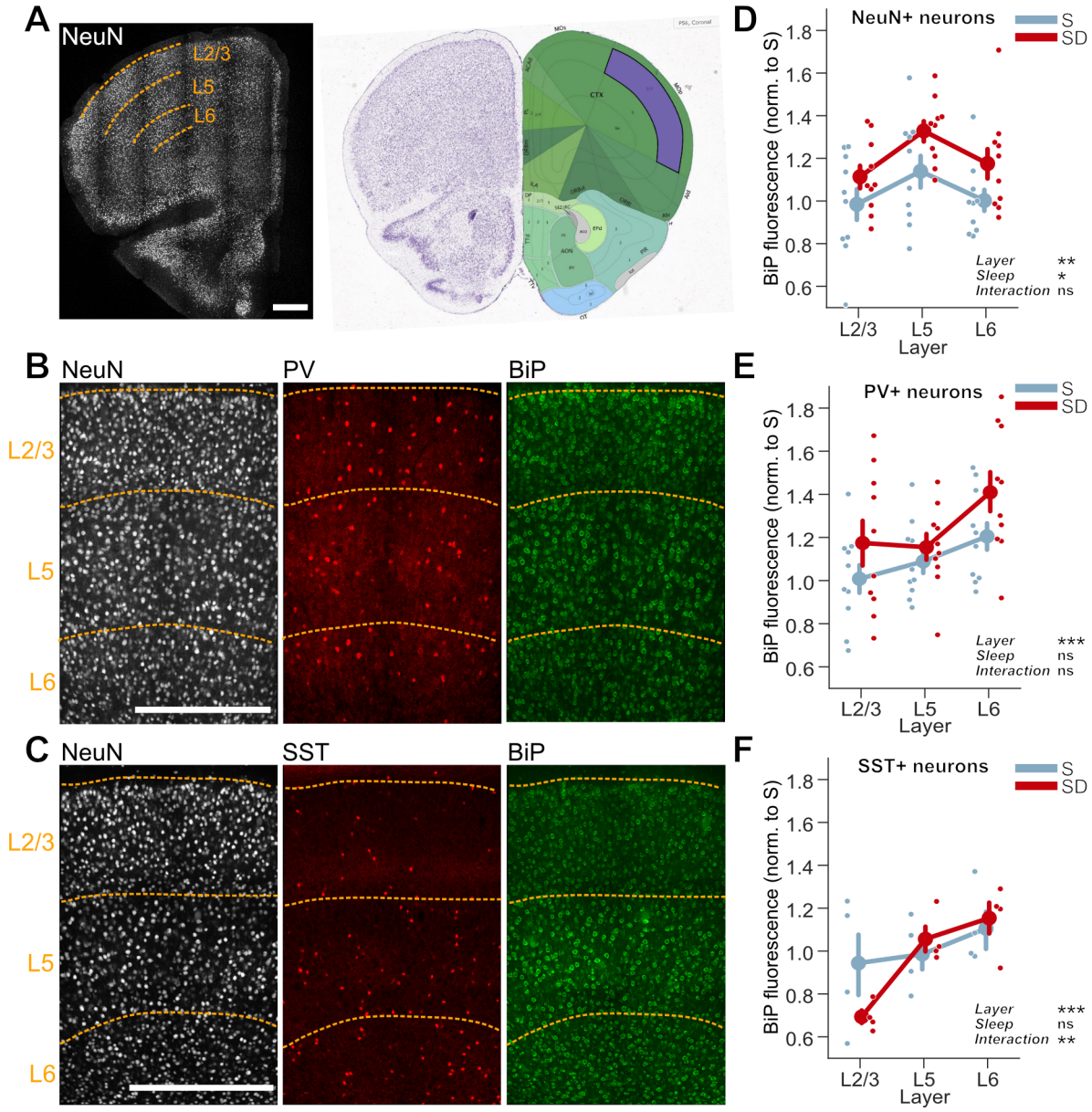

Figure 2.8 BiP protein levels in neurons across cortical layers in the frontal cortex.

(A) Confocal images were taken of frontal cortex sections (left image) from rested control (S) and sleep deprived (SD) mice, and cortical layers were identified on the NeuN channel according to the Allen Brain Atlas of the corresponding coronal section (right image). **(B)** In addition to NeuN, brain sections were immunolabelled with an anti-PV antibody to identify PV+ interneurons across the layers, and anti-KDEL to measure BiP levels. **(C)** Brain sections form SST-Ai9 mice, expressing tdTomato in SST+ interneurons, were also immunolabelled with anti-KDEL to detect BiP levels. **(D)** BiP fluorescence in all NeuN+ neurons varied across layers and with sleep condition, but there was no interaction between layer and sleep condition (n=10 animals; Layer: p=0.0011, Sleep: p=0.0489, Interaction: p=0.8308, repeated measures 2-way ANOVA). **(E)** BiP fluorescence in PV+ neurons varied across layers but not with sleep condition (n=10 animals; Layer: p<0.001, Sleep: p=0.1151, Interaction: p=0.3046, repeated measures 2-way ANOVA). **(F)** BiP fluorescence in SST+ interneurons also varied across layers, and although there was no overall effect of sleep condition, there was an interaction between layer and sleep condition (n=4 animals; Layer: p<0.001, Sleep: p=0.7264, Interaction: p=0.0074, repeated measures 2-way ANOVA). Data represented as mean +- SEM, with individual points representing animals. All scale bars: 500 µm.

interneurons varied as a function of cortical layer differently in the S and SD groups (**Figure 2.8**F). In the SD group there were significant differences between L2/3 BiP levels compared to L5 and L6 ($n=4$; $p<0.001$ for both, Sidak's multiple comparisons test). However, in the S group, there were no differences in BiP levels between layers. None of the layers showed significant differences between S and SD. Therefore, these results suggest that although there are differences in BiP levels between cortical layers in a cell type-specific manner, there are no detectable differences in the response to SD across the layers.

2.4 Discussion

The aim of this chapter was to replicate previous findings of the effects of sleep deprivation on UPR levels in mouse cortex, and further explore potential heterogeneity in the effects across cortical regions and cell types. To address these aims, it was first necessary to confirm that the sleep deprivation paradigm resulted in the characteristic increase in the level of SWA during subsequent sleep. Indeed, SWA was found to increase following sleep deprivation using novel object introduction, and was most prominent in the frontal EEG compared to the occipital EEG, which is consistent with existing literature (Huber et al., 2000). Once this was established, I identified an anti-KDEL antibody as being able to provide a readout of BiP protein levels, which I subsequently used to examine the influence of sleep deprivation on mouse cortex. Measurements of BiP protein and transcript levels, as well as sXBP1 transcript level, showed an upregulation in the frontal cortex following sleep deprivation, consistent with previous findings (Mackiewicz et al., 2007; Maret et al., 2007; Naidoo et al., 2005; Terao et al., 2003). Moreover, BiP protein levels showed regional differences, with a sleep deprivation-induced upregulation not observed in somatosensory or visual cortical tissue. Surprisingly, ATF4 transcript levels were found to decrease in frontal and somatosensory cortex following sleep deprivation. These measurements of bulk tissue expression levels were combined with immunohistochemistry to measure BiP protein levels at cellular resolution, specifically in cortical neurons. Neurons exhibited a similar upregulation in BiP expression in a region-specific manner, as observed at the tissue level. Furthermore, neuronal subtypes across cortical layers were found to show variations in their baseline BiP expression levels, and the PV+ and SST+ inhibitory interneuron populations did not exhibit a detectable sleep deprivation-induced UPR upregulation. These results provide novel insight into the heterogeneity of UPR levels across the cerebral cortex.

At the beginning of this work, it was necessary to establish whether the effects of sleep deprivation described in earlier studies can be replicated using the chosen sleep deprivation

paradigm of introducing novel objects (V. V. Vyazovskiy et al., 2002). Previous studies investigating the impact of sleep deprivation on UPR-related proteins or transcripts have employed 'gentle handling' to keep animals awake (Elliott et al., 2014). However, this method of forced sleep deprivation is likely to exert different effects compared to the more naturalistic exploratory behaviour evoked by the introduction of novel objects (Colavito et al., 2013; Havekes et al., 2012). Using western blots, Naidoo et al. (2005) reported a ~40% greater BiP protein level in the frontal cortex of 10 weeks-old C57BL/6J male mice after 6 hours of sleep deprivation with gentle handling compared to equivalent sleep. This is a bigger effect than the 16% increase in BiP protein that was found in this chapter, in the frontal cortex of 9-10 weeks-old C57BL/6J male mice. This discrepancy could be attributed to the sleep deprivation technique used. Gentle handing of mice elevates serum corticosterone levels (Longordo et al., 2011), while novel object introduction does not (Kopp et al., 2006), suggesting that they affect physiological stress differently. Naidoo et al. (2005) found no increase in BiP protein levels with gentle handing during the animals' natural waking time, which suggests that the sleep deprivation effect was not attributable to gentle handling alone. However, in that study, gentle handling was used to stimulate the animals upon any signs of inactivity, which may have reduced the amount of time spent in quiet wakefulness, and therefore limit intrusions of microsleeps or local sleep. On the contrary, sleep deprivation using novel objects is seen as a milder insult, allowing animals to behave spontaneously including spending time in quiet wakefulness, which was judged by the mice having eyes open and a waking posture. Therefore, the lower induction of BiP seen in this chapter compared to previous findings may reflect the milder form of sleep deprivation used.

BiP protein was found to be specifically increased in the frontal cortex following sleep deprivation, but not in the somatosensory or visual cortices, whereas BiP mRNA level increased across all three cortical regions. Protein and mRNA expression dynamics in response to stress are known to be variable, and the level of mRNA does not necessarily correspond to protein expression (Cheng et al., 2016; Y. Liu et al., 2016b). This observation may reflect varying temporal patterns in

the activation of the UPR within the cortex. The discrepancy between mRNA and protein levels could be attributed to insufficient time for translation processes to occur in the somatosensory or visual cortices after transcriptional changes had already occurred. It has also been shown that BiP is regulated post-transcriptionally, whereby increased BiP mRNA levels do not translate to increased BiP protein synthesis in unstressed cells (Gülow et al., 2002). Therefore, the observed lack of effect at the protein level could reflect a genuine lack of ER stress, and therefore, UPR activity. To the best of my knowledge, this was the first time that BiP levels in different antero-posterior regions of the cortex have been investigated with sleep deprivation. Terao et al. (2003) had previously measured the number of BiP-positive cells in the "lateral" and "dorsal" regions of an unnamed cortical area in mice, and found both regions to exhibit an increase in BiP levels following 6 hours of sleep deprivation with gentle handling. However, they did find a region-specific effect of continued BiP upregulation after recovery sleep in the lateral cortex only. Therefore, it is evident that the cerebral cortex exhibits heterogenous effects as a function of sleep-wake history.

BiP is a reliable marker of the global UPR, since transcription factors downstream of all the UPR arms drive BiP promoter activity (A. S. Lee, 2005; Luo et al., 2003a; Yoshida et al., 1998, 2001). However, the activity of each individual UPR arm during sleep deprivation is poorly understood. To gain a better understanding, I probed the transcript levels of sXBP1, upregulated by IRE1 activation, and ATF4, upregulated by PERK activation. sXBP1 RNA levels in cortical tissue showed an increase upon sleep deprivation, which is consistent with previous findings (Mackiewicz et al., 2007). However, ATF4 transcript levels were found to decrease with sleep deprivation using the primers described, especially in the frontal cortex. Sleep deprivation has previously been shown to increase levels of p-PERK and p-eIF2α levels in mouse cortex (Naidoo et al., 2005, 2008), suggesting that PERK is activated after 6 hours of sleep deprivation with gentle handling. ATF4 is mostly regulated at the translational level downstream of PERK, as p-EIF2α acts on an upstream open reading frame (uORF) of ATF4 to increase its translation (Wortel et al., 2017). Therefore, the level of transcriptional upregulation of ATF4 may not be a reliable marker of PERK activation. However, to rule out technical

issues, the RT-PCR could be repeated using different ATF4 primer sets to confirm the observation. Since it was challenging to identify good antibodies against p-PERK and sXBP1, I was not able to measure the activation of the IRE1 and PERK pathways at the protein level. Activation of ATF6 results in its cleavage into the active short-form of the transcription factor protein (ATF6α), therefore, the detection of ATF6 activation requires an antibody against ATF6α. Since ATF6 is the least studied arm of the UPR, there is a shortage of tools to be able to measure its activity. However, ATF6α (Haze et al., 1999; Yoshida et al., 1998) is a major activator of BiP transcription, therefore, measurement of BiP is likely to capture ATF6 activity (Haze et al., 1999; Yoshida et al., 1998).

Given that BiP showed a sleep-deprivation induced upregulation at both the RNA and protein level, and the fact that it serves as a good proxy for global UPR activation, I decided to focus on investigating BiP protein levels in a cell-specific manner. Neurons are a major cell type in the brain that are likely to be impacted by sleep deprivation. Immunohistochemistry offered a useful technique for visualising BiP in a neuron-specific manner in intact tissue with preserved spatial information. A global neuronal marker, NeuN, was used to identify neurons in the cortex. NeuN+ neurons in the frontal cortex, but not the somatosensory cortex, were found to display an increased level of BiP expression with sleep deprivation, consistent with the results obtained from frontal cortical tissue by western blotting. This suggests that neuronal UPR may be the major contributor of the effect seen in frontal cortex at the tissue level. Although I did not measure BiP levels in non-neuronal cell types, the “background” measure around neuronal cell masks provided an indirect indicator of non-neuronal cell type BiP expression, which did not show a difference between sleep deprivation and the slept control condition (data not shown). A recent study investigating cortical cell type-specific proteomics following sleep deprivation found that protein expression is affected more strongly in cortical neurons compared to astrocytes, including proteins involved in processing in the ER (Jha et al., 2022). The study also found brain region-specific differences in the altered transcriptional profile of neurons in brainstem, hypothalamus and cortex, although they did not investigate different areas within the cortex. Therefore, for the first time, the immunohistochemical

analyses in this chapter offer direct evidence of BiP levels being upregulated following sleep deprivation specifically in neuronal populations in a cortical region-specific manner.

To gain further insights into the implications of sleep deprivation on neuronal subpopulations, immunohistochemistry was used to quantify BiP expression in PV+ and SST+ interneurons from the frontal cortex. These two neuronal subtypes have been implicated in the regulation of homeostatic sleep SWA in the cortex, which make them an interesting set of neurons to investigate (Funk et al., 2017; Neske, 2016; Neske & Connors, 2016; Niethard et al., 2016; Tossell et al., 2020; Ushimaru & Kawaguchi, 2015; Zucca et al., 2017). I found that both the interneuron subtypes expressed lower levels of BiP compared to the general NeuN+ population at baseline, and that they did not show a significant response to sleep deprivation. This is in line with previous findings that the impact of sleep deprivation on the translational profile of interneurons is less pronounced compared to excitatory neurons (Puentes-Mestril et al., 2021). Furthermore, the cortical network excitation-inhibition balance shifts in a vigilance state-specific manner, with highest inhibitory activity during REM sleep, and lowest during wake (Niethard et al., 2016). Therefore, the lower susceptibility of interneurons to sleep deprivation-induced BiP upregulation may reflect their lower activity levels compared to excitatory neurons.

Neurons show functional diversity across cortical layers (Adesnik & Naka, 2018; Gao et al., 2022; Kawaguchi, 2017; S. Zhang et al., 2016), with different layers giving rise to distinct network activity patterns (Bos et al., 2016; Csercsa et al., 2010; Fiáth et al., 2016). Cortical layers also differ in their transcriptional response to sleep deprivation (Vanrobaeys et al., 2023). However, little is known about how the UPR varies across different layers. To address this question, BiP expression was quantified in L2/3, L5 and L6 of the frontal cortex, in Neun+, PV+ and SST+ neuronal populations. Interestingly, each cell type showed varying BiP expression as a function of layer, while NeuN+ neurons also exhibited an overall effect of sleep deprivation. SST+ interneurons displayed an interaction of effects between layer and sleep deprivation, suggesting that different layers may

respond differently to sleep deprivation. However, the NeuN+ neurons and PV+ interneurons did not display an interaction of effects between layer and sleep deprivation, suggesting that all layers respond similarly to sleep deprivation. There were non-significant trends indicating that L5 NeuN+ neurons, the majority of which are excitatory neurons, displayed a higher level of BiP expression compared to other layers, and the greatest BiP upregulation with sleep deprivation. Meanwhile, L5 PV+ interneurons displayed the smallest upregulation of BiP with sleep deprivation. L5 neurons in the frontal cortex have been implicated in the homeostatic response of SWA after sleep deprivation (Krone et al., 2021). In particular, excitatory neurons in L5 are important for the generation of low frequency network activity (Beltramo et al., 2013). Therefore, future work could investigate whether the higher level of UPR in L5 is linked to its role in homeostatic sleep SWA.

In summary, findings from this chapter confirm the effect of sleep deprivation on elevating SWA and UPR levels in mouse cerebral cortex. They also provide additional evidence for the heterogeneity of UPR levels across regions, cell types and layers of the cortex. Considering the relatively modest UPR activation observed in response to sleep deprivation using novel objects, future investigations could employ alternative paradigms that amplify the impact of sleep deprivation, such as longer periods of sleep deprivation. Such approaches may facilitate the identification of smaller effects in specific cortical regions and cell types that did not exhibit a significant response in the current study. Subsequent studies could provide valuable insights by examining the underlying factors contributing to the observed regional and cell type-specific effects on UPR levels observed in this chapter. Moreover, it would be intriguing to explore the potential connections between the regional and cell type-specific differences in UPR levels and the local mechanisms governing sleep homeostasis and SWA.

Chapter 3 Investigating the effects of UPR activation on cortical activity during wake and sleep

Contents

3.1 Introduction

Sleep is an evolutionarily conserved phenomenon, with many cellular and molecular features shared across species. Yet, despite decades of research, it has proven difficult to agree on whether sleep has a core, fundamental function. The homeostatic regulation of sleep implies that it is important for restoring neuronal function to a set-point from which they deviate during waking. It has been proposed that the increased synaptic and neural activity associated with wakefulness (Cirelli & Tononi, 2000a; Tononi & Cirelli, 2006; V. V. Vyazovskiy et al., 2009) may increase cellular demands and elicit stress responses, such as the unfolded protein response (UPR)(Saito et al., 2018; V. V. Vyazovskiy & Harris, 2013). In **Chapter 2**, I demonstrated that increasing sleep pressure with sleep deprivation resulted in elevated levels of UPR in the brain. This is corroborated by previous evidence suggesting that sleep deprivation contributes to an upregulation of ER stress response genes in *Drosophila* (Naidoo et al., 2007a; Shaw et al., 2000), mouse (Mackiewicz et al., 2007; Maret et al., 2007; Naidoo et al., 2005) and rat (Cirelli et al., 2004; Terao et al., 2003, 2006) brains. Thus, in physiological conditions, sleep may be acting, more fundamentally, to restore neuronal ER stress to a set-point as a prophylactic mechanism to prevent irreversible damage (V. V. Vyazovskiy & Harris, 2013). Neuronal cellular stress has been shown to contribute to increased sleep in *C. Elegans* and *Drosophila* (A. J. Hill et al., 2014; V. M. Hill et al., 2018). However, there has not yet been compelling evidence to directly link ER stress and the UPR as underlying the need to sleep in mammals.

The homeostatic process of sleep need is reflected most prominently in cortical slow wave activity (SWA; EEG or LFP spectral power between 0.5 – 4 Hz), which increases proportionally with the duration of prior wakefulness and dissipates during sleep (Borbély et al., 2016; Tobler & Borbély, 1986). The brain is generally more metabolically and electrically active during wakefulness (Buchsbaum et al., 1989; DiNuzzo & Nedergaard, 2017; Karnovsky et al., 1983; V. V. Vyazovskiy et al., 2009; Watson et al., 2016). High levels of neural activity and synaptic changes can place greater demands on neuronal protein synthesis pathways in the ER, which are required to provide receptors

and synaptic vesicle components (Martínez et al., 2018). SWA occurs in cortical networks upon the synchronised slow oscillation in the membrane potential of millions of neurons, which results in ON and OFF periods of cortical neuronal firing (Chauvette et al., 2011; Steriade et al., 2001). While network interactions drive synchronous slow waves across the cortex, intrinsic cellular properties of individual cortical neurons are likely to determine their propensity to enter ON/OFF periods, resulting in the local regulation of SWA (Krueger et al., 2019; Nir & de Lecea, 2023; Siclari & Tononi, 2017). Local differences in SWA are observed across brain regions in a use-dependent manner (Huber et al., 2006), and local slow waves can occur during wakefulness (Nir et al., 2017; V. V. Vyazovskiy et al., 2011). In Chapter 2, I found that sleep deprivation results in elevated levels of UPR specifically in the frontal cortex (Chapter 2, section **2.3.3**), which is also associated with the highest level of SWA (Chapter 2, section **2.3.1**). However, whether the UPR caused by sleep deprivation in turn represents the mechanism of increased SWA during subsequent sleep remains unknown.

There is growing evidence implicating the UPR in the regulation of sleep. Manipulating the PERK pathway has been shown to result in changes in sleep durations in zebrafish and *Drosophila* (Ly et al., 2020). Moreover, the effects of PERK pathway activity on sleep and SWA have also been examined in rats using intracerebroventricular infusions of Salubrinal (Methippara et al., 2009, 2012). PERK activation results in the phosphorylation of eIF2α, leading to a global translational block and reduction in protein synthesis. Salubrinal blocks the dephosphorylation of eIF2α by phosphatases, thereby maintaining eIF2α in an activated state downstream of PERK pathway activation. Administration of Salubrinal in rats during sleep deprivation was reported to increase NREM sleep duration and briefly elevate SWA spectral power during the recovery period. However, when Salubrinal was administered during recovery sleep, it significantly decreased SWA (Methippara et al., 2009, 2012). While this study highlights some of the effects of the global translational block elicited downstream of PERK activation, the PERK pathway is part of the integrated stress response and may not exclusively reflect UPR activity per se (Costa-Mattioli & Walter, 2020). Moreover, Salubrinal targets the PERK pathway downstream of PERK activation

rather than an upstream manipulation to activate the UPR as a result of increased ER load. The intracerebroventricular infusions used in this study to administer Salubrinal into the cerebrospinal fluid produced a global effect on the brain. Therefore, the effects of UPR activation as a result of ER stress on local SWA remains unexplored.

In order to investigate the role of the UPR in the local regulation of cortical activity patterns, it is necessary to induce ER stress in a local region of the cortex and compare the local and global effects of the manipulation on the LFP and surface EEG, respectively. Since little is known about the effects of the UPR on neural activity patterns, there is also a need to explore the broader effects of the UPR on physiologically relevant activity patterns during different vigilance states. For example, NREM sleep is dominated by slow waves in the delta frequency band (0.5 – 4 Hz)(Sirota & Buzsaki, 2005), and sleep spindles in the sigma frequency band (12 – 15 Hz). Spindles are burst-like signals, arising from thalamocortical circuits, which are considered to be important for memory consolidation (Fernandez & Lüthi, 2020). REM sleep is predominantly characterised by strong theta activity (6 – 9 Hz), originating from the hippocampus (Girardeau & Lopes-dos-Santos, 2021). During wake, power in the lower theta band is a marker of sleep pressure, and is often evident in quiet waking during sleep deprivation (Finelli et al., 2000; V. V. Vyazovskiy & Tobler, 2005). In contrast, high frequency gamma activity (30 – 100 Hz) during wakefulness, arising from local cortical mechanisms, is associated with attentiveness, sensory perception and movement (Gross & Gotman, 1999; Maloney et al., 1997). Each of these oscillatory patterns of cortical activity are associated with specific global behavioural states, for example SWA is closely associated with NREM sleep. Therefore, to establish whether a local activation of the UPR results in a local and/or global effect, it is also necessary to measure the behavioural phenotype, for example the proportion of time the animal spends in NREM sleep.

AIMS

The aim of this chapter was to investigate whether local cortical UPR may contribute to sleep regulation and the local regulation of SWA. To do this, I activated the UPR pharmacologically in a local cortical region by intracortical administration of Tunicamycin, an N-glycosylation inhibitor that results in the accumulation of unfolded proteins in the ER (Heifetz et al., 1979). The visual cortex was selected as the region of manipulation since it shows low levels of endogenous UPR levels (Chapter 2 **Figure 2.3**C), thereby the percentage increase in UPR activation is likely to be higher compared to the frontal cortex. Alongside drug infusions, I recorded LFP signals from the infusion site to measure cortical activity over multiple days to monitor the effects of UPR activation. I also recorded LFPs from the contralateral hemisphere and EEG from the frontal cortex, to obtain a measure of global network responses.

Specifically, I aimed to:

1. Establish a method to induce an UPR in cortical tissue using intracortical Tunicamycin infusions.
2. Determine the effects of local Tunicamycin-induced UPR on sleep-wake architecture at the behavioural level.
3. Investigate the effects of UPR activation on neural activity patterns, SWA in particular, during sleep and wake.
4. Examine whether local manipulation of UPR levels in cortex results in changes to local or global SWA.
5. Investigate the effects of UPR activation on slow waves during NREM sleep.

3.2 Methods

3.2.1 Animals and animal husbandry

The experiment described in this chapter was performed on a batch of eight 8-10 weeks-old male C57BL6/6J wild-type mice purchased from Charles River. Animals were singly housed under a 12-hour light/12-hour dark cycle. Ambient room temperature was maintained at 22 ± 2 °C and humidity at 50 ± 20%.

3.2.2 Preparation of implantation devices

For chronic recordings of EEG, LFP and EMG activity combined with drug infusions, I constructed custom headstage devices for each mouse (**Figure 3.1**A). The headstage comprised of two stainless steel bone tapping screws (Fine Science Tools), to record EEG, and two stainless steel wires, to record EMG, connected to an 8-pin surface mount connector (8415-SM, Pinnacle Technologies Inc., USA). To record LFP activity alongside local intracortical drug infusions, custom-designed cannulas (26 gauge, cut to 4.8 mm below pedestal) were coupled to two polyimide-insulated tungsten wires (C315G, Plastics One Inc., USA) cut at specified lengths to span the cortical layers (-0.1 mm and 0.2 mm projection relative to cannula end). The cannula-electrode devices were then connected to the same 8-pin surface mount connector. Connections were sealed and insulated using dental acrylic cement (Simplex Rapid, Associated Dental Products Ltd., UK), and tested for conductivity.

3.2.3 Pre-operative procedures

First, mice were anaesthetised with 4% isoflurane at an oxygen flow rate of ~2 L/min in an induction chamber until they no longer exhibited a righting or pedal reflex. Mice were then transferred to a heat mat, where anaesthesia was maintained using ~2% isoflurane at an oxygen flow rate of 1.5 L/min through a nose mask. Next, the fur on the head and neck was carefully shaved, and analgesics were administered subcutaneously (Metacam, meloxicam 5 mg/kg and Vetergesic, buprenorphine 0.1 mg/kg). Mice were then transferred to a stereotactic frame (David Kopf Instruments, USA) and the head was secured into a stable position. Body temperature was

monitored using a rectal probe, and maintained at 35-36 °C using a heat mat and added insulation. Anaesthetic depth was monitored closely throughout the procedure by measuring respiration rate, and isoflurane concentration was adjusted to maintain a rate of 40-80 breaths per minute. Viscotears Liquid Gel (Alcon Laboratories Ltd., UK) was applied to the animal's eyes to keep them hydrated. Finally, the skin at the implantation site was cleaned with povidone-iodine and ethanol. All subsequent procedures were carried out under aseptic conditions.

3.2.4 Implantation of recording device

The skull was exposed with a midline incision and the skin was retracted using bulldog clips. To enhance the attachment of the implant (**Figure 3.1**A) to the skull, connective tissue was carefully removed from the skull surface, the bone was scraped with a scalpel blade and treated with phosphoric acid etching gel (Henry Schein, USA) for 2 minutes before being rinsed with saline. The position of lambda and bregma were measured using the stereotactic frame, and if necessary the head position was adjusted to ensure a level dorsoventral plane (lambda and bregma within ± 0.3 mm). Implantation coordinates relative to bregma were marked onto the skull using a stereotactic arm (**Table 3.1**).

	Antero-posterior	**Medio-lateral**
Frontal EEG	+ 2	+ 2
Occipital cannula-electrode	- 2.5	± 2.7

Table 3.1 Standard coordinates relative to bregma used for implantation of EEG screws and custom cannula-electrode devices.

Using a surgical microscope, craniotomies were performed with a 0.5 mm diameter drill burr (Fine Science Tools). The exposed dura was kept moist with saline. The EEG screws were carefully implanted in the skull over the frontal left cortex and the cerebellum and fixed with SuperBond dental cement (Prestige Dental Products Ltd., UK). Before implanting the cannula-electrode devices bilaterally, durotomies were performed to reduce the resistance of intracortical implantation of the cannulas. The dura was gently pierced and resected using a 30 gauge needle tip to expose the cortex. The cannula-electrode devices were mounted onto the stereotactic arm with a 10-degree tilt to be perpendicular to the cortical surface at the site of implantation. They were

then slowly lowered 0.5 mm radially into the cortex relative to the pial surface. Immediately after insertion, the implantation site was sealed with a silicone elastomer (Kwik-Sil, World Precision Instruments Inc., USA). The cannula shaft was then secured onto the skull with dental cement. Next, the two stainless steel EMG wires were inserted bilaterally into the nuchal muscles. Finally, the complete implant and wires were secured with dental cement and the neck incision was sutured if necessary.

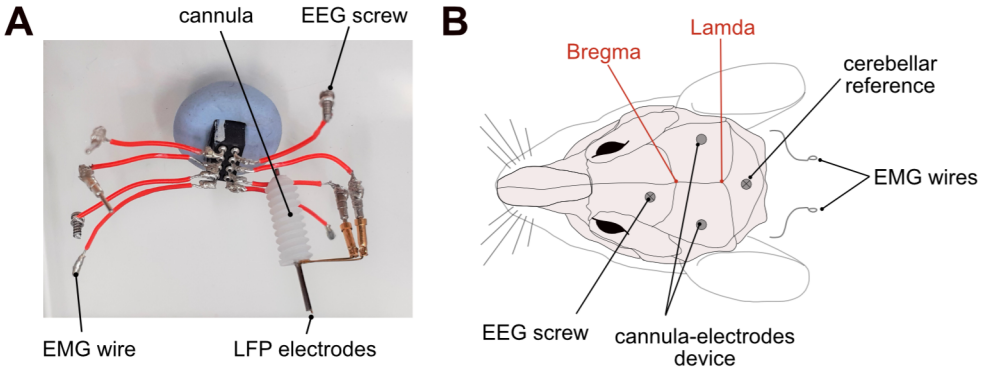

Figure 3.1 Mice were implanted with a custom-built headstage for continuous electrophysiological recordings and intracortical drug infusions.

(A) Custom-built headstages consisted of stainless steel screws for recording EEG, electrodes for recording LFP coupled with a cannula for local drug delivery, and soldered wires for recording EMG. **(B)** Head position and coordinates for the screws and electrodes were determined in relation to the skull suture joints, bregma and lambda. Implantation surgeries were stereotactically guided.

3.2.5 Post-operative procedures

Following the surgical procedure, saline was administered subcutaneously to compensate for fluid loss during the surgery (5 ml/kg per hour of surgery) and animals were recovered from anaesthesia in a recovery chamber maintained at 26 °C for ~30 minutes. After this, animals were transferred to freshly prepared individually ventilated cages (IVC) with soft bedding to be singly housed, and were given Metacam in a strawberry jelly for at least three days after surgery. Animals were scored on their body weight, provoked behaviour, spontaneous behaviour and grimace daily until the mice had recovered to baseline health for three consecutive days. Usually, the mice recovered fully within one week post-surgery. When they were fully recovered, mice were rehoused in individual custom-made Plexiglass cages (20.3 x 32 x 35 cm), which were placed inside ventilated,

sound-attenuated and light-controlled Faraday chambers for electrophysiological recordings (Campden Instruments, UK). Animals had access to food pellets and water *ad libitum*. A camera was mounted in each chamber to be able to monitor the animals continuously without disturbing the chambers. To prepare animals for the experimental procedures, they were habituated to the new housing conditions and to handling and restraining for one week. During this time, the dummy cannula obdurator in each implanted cannula was removed and replaced daily to prevent blockage. The implanted headstages were connected to the electrophysiology recording equipment using custom-made cables, such that mice retained full range of motion and free activity. Mice were allowed to habituate to the tethered conditions for at least three days before recordings began.

3.2.6 Data acquisition

Electrophysiological recordings were performed using the 128 Channel Neurophysiology Recording System (Tucker-Davis Technologies Inc., USA), acquired using the recording software Synapse (Tucker-Davis Technologies Inc., USA) and stored on a local computer for offline analysis. EEG and LFP signals were referenced against the cerebellar EEG, while an EMG signal was obtained as the differential of the two EMG wires. All signals were amplified (PZ5 NeuroDigitizer preamplifier, Tucker-Davis Technologies Inc., USA) and raw signals were stored with a sampling rate of 305 Hz. EEG and LFP signals were filtered between 0 and 30 Hz, and EMG signals between 10 and 100 Hz for visualisation purposes.

3.2.7 *In vivo* drug infusions experimental design

Following habituation in the recording chambers, continuous recordings were started in blocks of 24 hours from light onset. Initially, a 24-hour baseline recording was performed, during which animals were not disturbed. The next day, animals were allowed to sleep undisturbed during the light period. Drug infusions were administered in the last 1 hour of the light period, when endogenous ER stress levels were expected to be low due to prior sleep (Cirelli & Tononi, 2000b; Terao et al., 2003). To increase the chances of successful infusions and obtain high quality signals at the intended infusion site, animals were implanted with cannula-electrode devices bilaterally. I

initially selected the hemisphere with the best LFP signal quality as the infusion site and used the contralateral hemisphere as the non-infusion site for assessing local and non-local drug effects. On the first day of infusion, animals were randomly assigned to receive either drug or vehicle in one hemisphere. After a six-day interval, the second infusion was administered. The day before the second infusion was used as the new baseline for all days subsequent to the second infusion. The experimental timeline is illustrated in **Figure 3.2**A.

Stock solutions of Tunicamycin (Tocris Bioscience, UK), an N-glycosylation inhibitor and inducer of ER stress, were prepared in sterile dimethyl sulfoxide (DMSO, Tocris Bioscience, UK) at a concentration of 40 mg/ml and aliquoted and stored at -80 °C. On the day of the infusions, Tunicamycin stocks were diluted in sterile PBS to reach a final concentration of 0.1 mg/ml. To encourage complete solubility of Tunicamycin stocks in PBS, the pH of the diluted solution was adjusted to pH 8.0 using sterile NaOH, and vortexed until no precipitates were visible upon

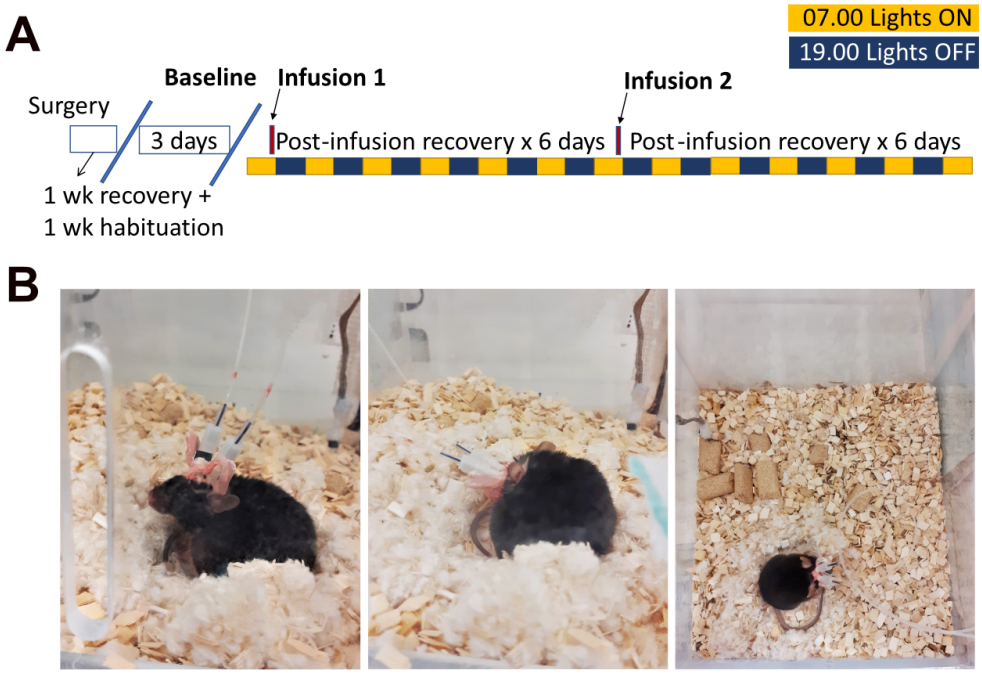

Figure 3.2 Drug infusion experimental design.

(A) Timeline of experiment from surgery to drug infusion and recovery. Electrophysiological recordings were performed in 24-hour blocks from light onset, with an undisturbed 24-hour baseline before each infusion. **(B)** During the infusions, an internal cannula with tubing was connected to the implanted guide cannula on the headstage. Mice were returned to their cages and showed normal spontaneous behaviour.

centrifugation. To prepare the vehicle solution, DMSO stocks were diluted at an equivalent ratio (0.25%) in sterile PBS.

The infusion protocol was adapted from the method presented in Alfonsa et al. (2023). Tubing and internal cannulas for infusions (PlasticsOne, USA) were flushed with 70% ethanol and sterile saline. Each infusion solution was loaded into heavy-walled polyethylene tubing (PE50 C313CT, PlasticsOne, USA), which was connected to an internal cannula (C315I, PlasticsOne, USA). An air bubble was loaded into the tubing before connecting it to a 5 µl Hamilton syringe (26 gauge) and the movement of the bubble was monitored during infusions to confirm successful drug delivery. Mice were gently restrained, by briefly covering their eyes to evoke temporary freezing behaviour, to remove the dummy cannula, insert the internal cannula into the implanted cannula, and secure it to the cannula pedestal with a captive collar (PlasticsOne, USA). The internal cannulas were custom-made to have a projection of 0.2 mm from the base of the implanted guide cannula to effectively delivery the infusion solution into the cortical tissue. Mice were returned to their home cages and were able to move freely (**Figure 3.2**B). Infusions were performed using infuse/withdraw pumps (Nanomite pump heads, Biochrom Ltd., UK), which were programmed to deliver a 1 µl volume of infusion solution at a rate of 70 nl/min with a HAPC 4-syringe pump controller (Biochrom Ltd., UK). This infusion volume was deemed suitable to produce a local diffusion of Tunicamycin (mol. wt. 845) within a ~1.6 mm radius, based on dye infusion studies with Evans blue (mol. wt. 961)(Myers, 1966). The progression of the infusion was monitored by tracking the movement of the air bubble in the tubing. After completing the infusion, the tubing was kept connected to the implanted cannulas for at least 10 minutes to allow the solution to diffuse through the tissue and minimise backflow during disconnection. Four mice received infusions simultaneously using this pump setup, and infusions for all eight mice were completed within an hour. To further assess the infusion success, the internal cannula was disconnected from the implanted cannula and carefully checked for backflow of fluid, after which the dummy cannula was replaced. If an infusion was not successful due to cannula blockage, determined by either no

movement of the air bubble in the tubing or significant backflow from the implanted cannula, the infusion was attempted again in the opposite hemisphere at the same time the following day. For the second infusion 6 days later, I used the hemisphere that had a successful first infusion. In this cohort, all animals received successful first and second infusions at the same site.

3.2.8 Histology and immunohistochemistry

At the end of experiments, animals were given a lethal dose of pentobarbital (Euthatal, 100 µl per 20 g body weight) and immediately perfused with 0.1 M PBS followed by 4% PFA / 4% sucrose solution for tissue fixation. After the implant attached to the skull was removed and the brain was carefully dissected out, the brains were kept in PFA at 4 °C for a further 24 hours to ensure a thorough fix. After this, brains were transferred to 0.05% sodium azide in PBS (PBSA) for longer term storage.

To assess the effects of Tunicamycin on the brains and to check implantation positions, the brains were processed for histological imaging. First, 50 µm-thick coronal brain sections were prepared using a vibrating microtome (Leica VT1000S). Sections were then immunostained with primary antibodies (**Table 3.2**) to detect ER stress markers and cell types (see Chapter 2 **Methods** section **2.2.8**). Next, sections were stained with 4',6-diamidino-2-phenylindole (DAPI). Finally, sections were imaged using an Olympus BX40 epifluorescent microscope for visualisation.

Primary AB	Catalogue no. and supplier	Dilution	Secondary AB	Catalogue no. and supplier	Dilution
Mouse anti-KDEL (IgG2a)	KDEL 10C3 mouse mAb (Enzo Life Sciences, ADI-SPA-827)	1:300	Goat anti-mouse al488 IgG2a	Life Technologies, A21131	1:500
Mouse anti-CHOP (IgG2a)	CHOP (L63F7),Cell Signalling Technology, #2895	1:300	Goat anti-mouse al594 IgG2a	Life Technologies, A11076	1:500
Mouse anti-NeuN (IgG1)	Millipore, MAB377	1:500	Goat anti-mouse al647 IgG1	Life Technologies, A21240	1:500
Mouse anti-GFAP (IgG1)	Millipore, MAB360	1:500	Goat anti-mouse al647 IgG1	Life Technologies, A21240	1:500
Rabbit anti-active Caspase3	BD Pharmingen, 559565	1:300	Goat anti-rabbit al568	Life Technologies, A11036	1:500

Table 3.2 Primary antibodies used for histological assessment of brains that received intracortical Tunicamycin infusions.

3.2.9 Electrophysiology data processing

EEG, LFP and EMG signals were resampled at 256 Hz using MATLAB's `resample` function. Before signal analysis, EEG and LFP signals were filtered between 0.1 – 120 Hz, while EMG signals were filtered between 10 – 120 Hz. A notch filter was applied to attenuate 50 Hz line noise in all signals. The spectral properties of the continuous signals were analysed in 4-second epochs. First, each 4-second epoch of EEG and LFP signals was multiplied by a Hann window in order to reduce edge artefacts. Then, power spectral densities were calculated for each 4-second epoch using MATLAB's `pwelch` function with no window overlap. Power spectral densities represent the distribution of power (or energy) in a signal across different frequencies. This allows us to determine the frequency components that are most significant in each epoch's signal, which enables us to identify vigilance states and measure effects on network activity.

3.2.10 Vigilance state scoring

Resampled recording files were converted to the European Data Format (EDF) to perform vigilance state scoring. I chose to use automated vigilance state scoring for all of my data, to minimise human error and biases, while dramatically increasing the efficiency of the process. Data were pre-processed using Python scripts (**https://github.com/paulbrodersen/somnotate.git**) for automated scoring by computing the spectrograms of the EEG, LFP and EMG traces as previously described (Alfonsa et al., 2023). Spectral power in the 0 – 0.5 Hz frequency range was removed because it was most affected by movement artefacts and signal drift (**Figure 3.3**A). Spectral power between 45 – 55 Hz were also removed, since this range was affected by mains electrical noise. Spectral power above 90 Hz was removed because frequencies above 90 Hz were not used to characterise vigilance states. The frontal EEG, the occipital LFP channel that exhibited the highest signal stability, and EMG were used for scoring vigilance states. Vigilance states were scored automatically in 4-second epochs using `Somnotate` (Brodersen et al., 2021), which uses a hidden Markov model to compute the probability of each state based on: (1) the frequency distribution in the given sample and (2) the likelihood of states in previous timepoints. Probability distributions

were estimated based on training data that I had manually scored using the SleepSign for Animals software (Kissei Comtec Co. Ltd., Japan) with criteria as described previously (McKillop et al., 2018a).

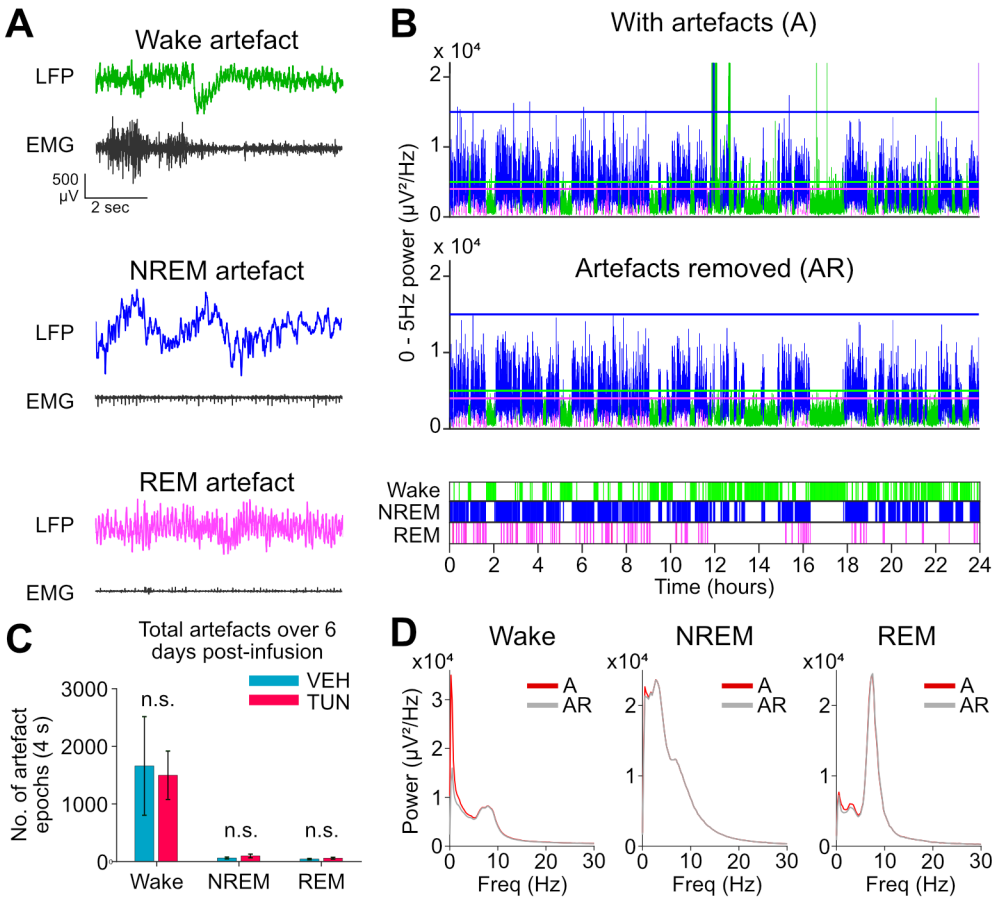

Figure 3.3 Artefact thresholding after automated vigilance state scoring.

(A) Example LFP traces showing wake, NREM and REM artefacts, which appear as large, slow oscillations that deviate from the baseline signal. **(B)** LFP spectral power in the 0 – 5 Hz frequency range before removing artefacts (top) and after removing artefacts (middle) from an example 24-hour recording. Horizontal lines represent the artefact threshold selected for each vigilance state. Automatic vigilance state scoring is shown in the hypnogram (bottom). **(C)** There were no differences in the number of artefact epochs over a period of 6 days post-infusion with vehicle (VEH) or Tunicamycin (TUN)(n=8 animals; p>0.05, paired *t* tests). **(D)** Power spectra of the 24-hour recording shown in '**B**' during wake, NREM and REM before and after artefact removal. Wake spectra were most affected by artefacts.

Epochs were classified as "wake" when there were low amplitude and high frequency EEG and LFP signals with a high level of EMG activity. Epochs were classified as "NREM" when there was a dominance of low frequencies at high amplitude, especially in the frontal EEG, and a low level of EMG activity. In turn, epochs were classified as "REM" when there was a dominance of theta (6 – 9

Hz) activity, especially in the occipital LFP, and low EMG activity. Short intrusions of wakefulness lasting up to 4 epochs (16 seconds) during NREM or REM sleep were classified as "movement" and did not contribute to the overall amount of wakefulness. Since Somnotate did not classify artefactual epochs, signals were post-processed to threshold for signal artefacts. Since movement-related artefacts were high power and low frequency (**Figure 3.3**A), in the range of 0.5 – 5 Hz, artefact thresholds were determined for each signal for each animal individually based on the 0.5 – 5 Hz power in their corresponding baseline signal (**Figure 3.3**B top). I confirmed that the treatment condition had no effect on the number of artefacts per vigilance state (**Figure 3.3**C). After removing artefactual epochs, power spectral densities were almost identical across vigilance states scored automatically by Somnotate and manually using SleepSign (**Figure 3.4**). Automated and manual scoring showed a high degree of correspondence, with a 91 ± 0.9% match for wake, 94 ± 0.7% match for NREM and 98 ± 0.2% match for REM epochs (n=16 24-hour recordings).

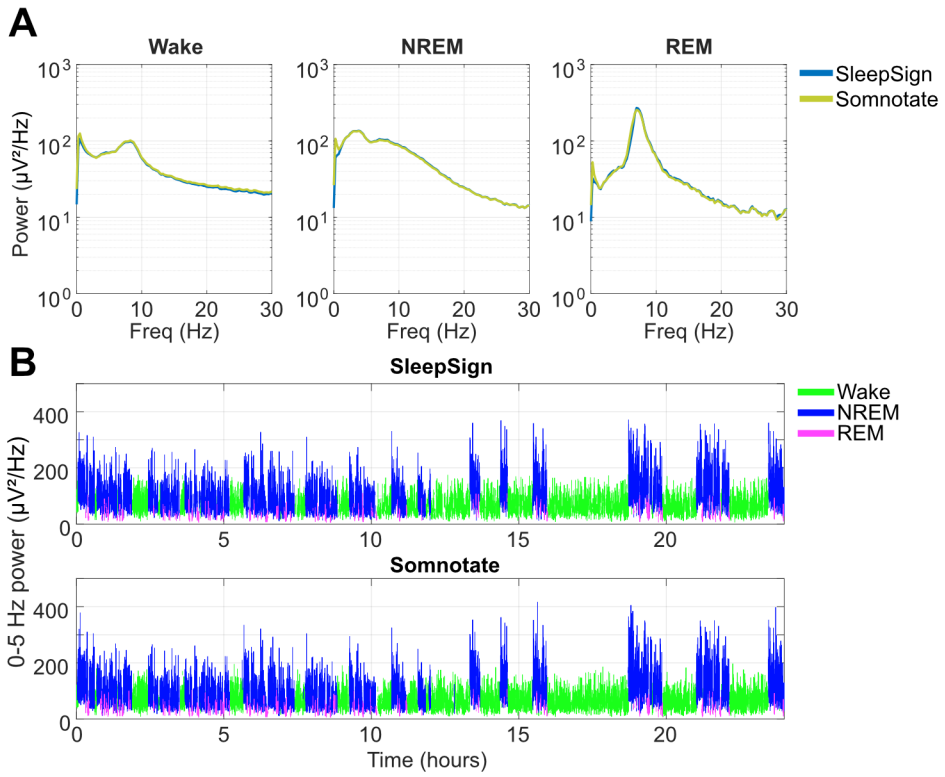

Figure 3.4 Automated and manual vigilance state scoring show a high degree of correspondence.

(A) LFP power spectra in wake, NREM and REM states from a representative 24-hour recording after scoring either manually using SleepSign, or automatically using Somnotate. The two scoring methods showed very similar frequency profiles. **(B)** Power in the 0 – 5 Hz artefact range, in the same 24-hour recording used in '**A**', was also very similar after manual and automated scoring and artefact removal.

3.2.11 Slow wave detection

To detect slow waves in the LFPs, the signal was first bandpass filtered between 0.5 – 4 Hz (with stopband frequencies 0.3 and 8 Hz) using a Chebyshev Type II filter function in MATLAB (`filtfilt`). Slow waves were defined as positive deflections in between two consecutive negative deflections below the zero-crossing (V. V. Vyazovskiy et al., 2007). All detected slow waves were subjected to an amplitude threshold, which was determined individually per animal, such that the top 25th percentile of bona fide large slow waves were retained for subsequent analyses.

3.2.12 Statistical analysis

All statistical tests in this chapter were performed using MATLAB. Averages are reported as mean ± SEM and asterisks represent significant p-values (*p<0.05, **p<0.01 and ***p<0.001). Paired samples *t* tests were conducted for comparisons between treatment conditions within the same animals. Repeated measures ANOVAs were conducted with within-subject factors. Where appropriate, bar charts showing means per treatment condition are presented alongside individual data points per animal. For EEG/LFP spectral analysis, post-hoc paired *t* tests were conducted per frequency bin, only if the repeated measures ANOVA showed a significant interaction effect. *T* tests' outcomes were not corrected since correction for multiple comparisons consisting of 118 spectral bins was deemed to be too conservative and reduce statistical power (Achermann & Borbély, 1998). Statistical tests and p-values are detailed in the appropriate figure legends.

3.3 Results

3.3.1 Sleep and wake states displayed distinct electrophysiological characteristics

The vigilance states of animals can be determined using recordings of brain and muscle activity. As expected, wakefulness was distinguished by low amplitude, high frequency EEG and LFP signals, accompanied by irregular high amplitude EMG signal, reflecting voluntary muscle activity

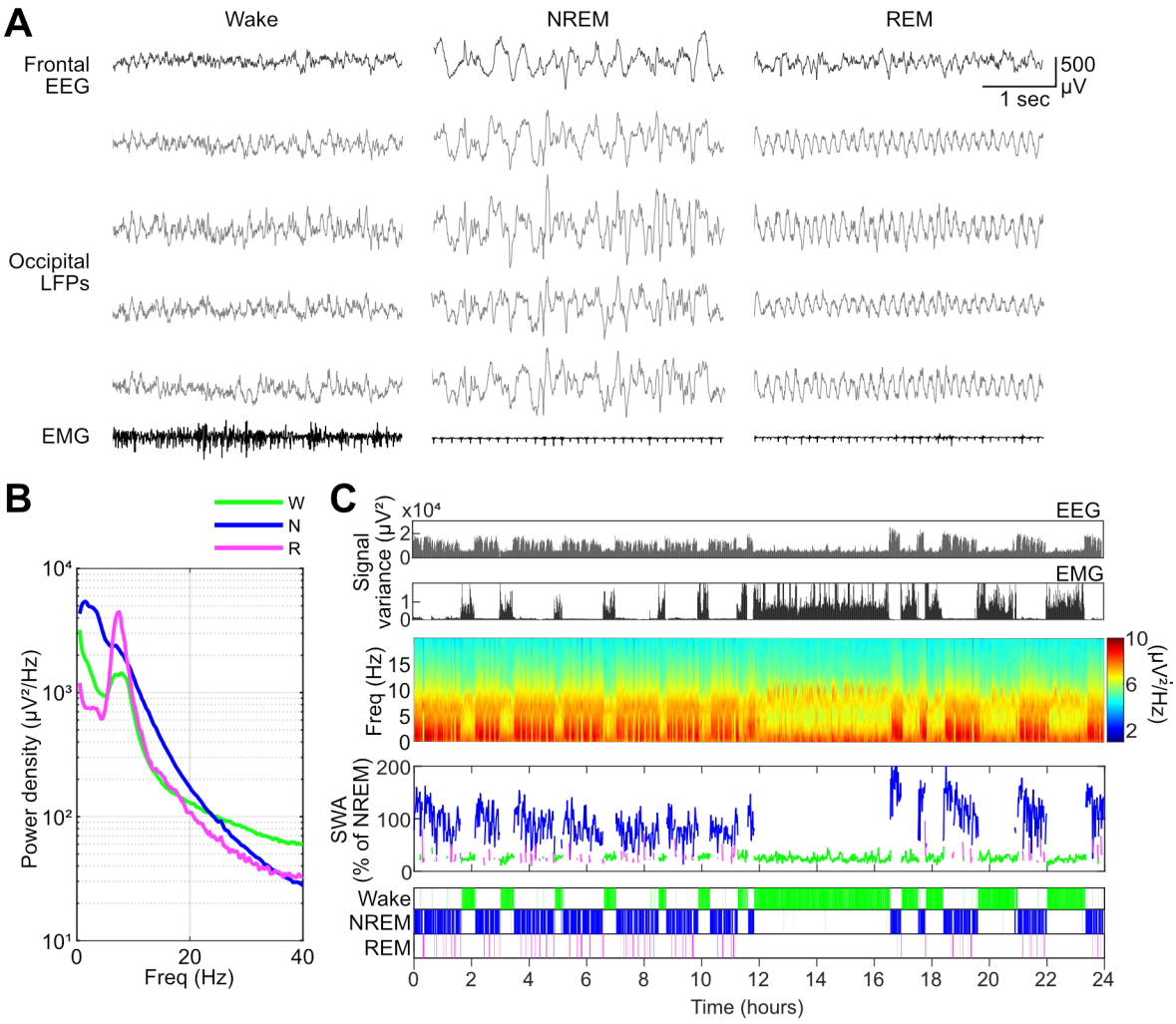

Figure 3.5 Electrophysiological characteristics during wake and sleep.

(A) Example signals from a frontal electroencephalogram (EEG), four occipital local field potentials (LFP) and an electromyogram (EMG) during representative epochs of wake, NREM and REM sleep. **(B)** Average spectral power density in an occipital LFP during wake, NREM and REM epochs over a 24-hour recording. **(C)** Variance profiles of the EEG and EMG signal (top); spectrogram showing colour-scale of power in different frequency components of the EEG signal over time (middle); profile of slow wave activity (0.5 - 4 Hz) from the frontal EEG during wake (green), NREM (blue) and REM (pink); hypnogram showing scored vigilance states in each 4-second epoch. All panels are derived from an example 24-hour recording.

(**Figure 3.5**A left). NREM sleep was characterised by the presence of high-amplitude slow waves in the EEG and LFP, and the EMG showed regular low amplitude spikes indicating a visible heartbeat rhythm (**Figure 3.5**A middle). During REM sleep, the EEG and LFP signals exhibited a consistent theta activity (6 – 9 Hz) pattern (**Figure 3.5**A right). This was either accompanied by muscle atonia, indicated by a flat EMG with visible heart beats, or infrequent muscle twitches during phasic REM sleep.

In this dataset, the EEG and LFP from all animals displayed greater average spectral power in the slow wave activity (SWA) range (0.5 – 4 Hz) during epochs scored as NREM compared to those scored as wake or REM (**Figure 3.5**B). Continuous 24-hour recordings reveal distinct patterns of signal variance during sleep and wake, with the high amplitude oscillations during NREM contributing the increase in EEG variance during sleep, when EMG variance is at its lowest (**Figure 3.5**C, first panel). A spectrogram reveals the distinct pattern of EEG signal frequencies emerging over time across wake and sleep (**Figure 3.5**C, second panel). The power in the SWA range, also known as delta power, shows a distinct increase during periods of NREM sleep compared to wake and REM sleep (**Figure 3.5**C, third panel). All recordings in this chapter's dataset were examined to meet these characteristic criteria before proceeding with Tunicamycin infusions.

3.3.2 Evidence that Tunicamycin treatment of brain tissue activates the UPR

Tunicamycin (TUN) is a widely used inducer of ER stress, which I have shown to activate the UPR in mouse fibroblast cells in the previous chapter (Chapter 2 **Figure 2.2**). It was necessary to confirm the extent of UPR activation in mouse brain tissue using TUN. This was first checked in an *in vitro* experimental model, using TUN treatment of mouse hippocampal organotypic brain slices (description of methods to prepare organotypic slice cultures is provided in Chapter 5 **Methods** section **5.2.1**). The drug- and vehicle-treated brain slices were then processed to detect XBP1 splicing, downstream of IRE1 activation, using RT-PCR. Incubation of brain slices with a low dose of TUN (5 µg/ml) for 6 hours or 24 hours produced a robust increase in sXBP1 compared to the equivalent incubation with DMSO vehicle (**Figure 3.6**A). This confirmed that TUN treatment can

successfully activate the UPR in brain tissue. However, drug action, dilution and clearance are likely to be very different in the brain *in vivo* compared to in culture conditions. Therefore, it was also important to assess UPR activation in the mouse brain following *in vivo* drug delivery. In a pilot study, a cohort of 2 animals were bilaterally implanted with drug infusion cannulas and allowed to recover post-surgery. Once fully recovered and habituated to handling, each mouse received a 0.1 mg/ml TUN infusion in one hemisphere and a 1:400 DMSO VEH infusion in the opposite hemisphere. The chosen concentration of TUN has been reported to induce robust BiP upregulation in the brain by 24 hours (C.-M. Chen et al., 2012), but is also relatively low compared to concentrations used by other studies (Cóppola-Segovia et al., 2017; Ozcan et al., 2009; Tong et al., 2017a; Y. Wang et al., 2018). The concentration of DMSO used has been shown to be innocuous and could therefore be safely used as a vehicle (Hanslick et al., 2009; C. Zhang et al., 2017).

Since the effects of TUN lasted for at least 24 hours in culture, mouse brains were collected 24 hours post-infusion. Brains were then sectioned and immunostained with antibodies against NeuN, KDEL and Caspase3 to detect numbers of viable neuronal cells, levels of BiP as a marker of UPR activation, and levels of apoptotic activity, respectively (**Figure 3.6**B). In the hemisphere treated with TUN, there was an increase in BiP expression in cells around the cannula implantation site, which extended down towards the hippocampus. Notably, there was a cluster of high BiP-expressing cells adjacent to the infusion site, which were not NeuN+ and hence may have been reactive astrocytes or microglia that had accumulated in high density at the implantation site. However, when BiP immunofluorescence was quantified in NeuN+ cells, no difference was observed between the TUN-treated and VEH-treated hemispheres (data not shown). A small degree of Caspase3 activation was observed in the TUN-treated hemisphere in a restricted location at the infusion site, which corresponded to lower numbers of NeuN+ neurons, but there was no widespread pattern of neuronal loss compared to the VEH-treated hemisphere. In all, these observations suggested that TUN induces a mild local activation of the UPR in cortex without significant apoptosis by 24 hours post-infusion.

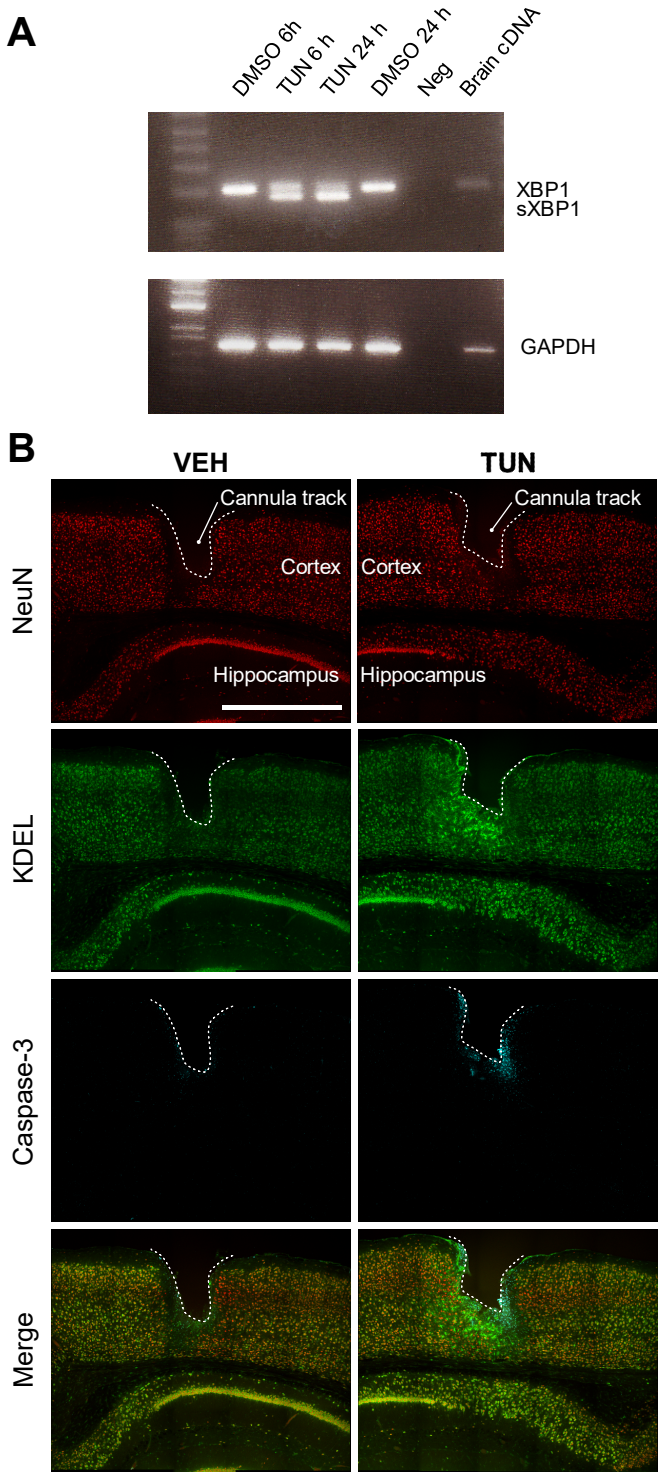

Figure 3.6 Tunicamycin induces the UPR in brain tissue.

(A) RT-PCR gel of hippocampal organotypic brain slices treated with either DMSO vehicle or 5 µg/ml TUN for 6 or 24 hours, a negative control, or control brain cDNA. Slices treated with TUN showed robust expression of spliced XBP1 (sXBP1), indicating activation of the IRE1 arm of the UPR. This data was collected and provided by Dr Sarah Newey. **(B)** Adult mice were implanted with cannulas in the neocortex, for infusion of either VEH (1:400 DMSO in PBS) or TUN (0.1 mg/ml). Brains were collected 24 hours post-infusion and sections were immunostained with NeuN, KDEL and Caspase3 to visualise neuronal viability, BiP expression and apoptotic signalling respectively. TUN infusion resulted in a visible increase in KDEL immunofluorescence, without widespread Caspase-3 expression or loss of NeuN, indicating a mild induction of the UPR by 24 hours post-infusion.

3.3.3 Five days after Tunicamycin infusion, some animals showed a collapse in LFP signal power

Due to the lack of available information about the duration of effects of TUN on the brain, electrophysiological recordings were conducted for a total of 15 days, with a recovery period of 6 days between drug and vehicle infusions. This allowed for the monitoring of long-term effects of TUN beyond the initial 24-hour period. I observed that half of the experimental cohort (4 animals)

showed a distinct decrease in broadband LFP power at the infusion site 5 days after TUN treatment (**Figure 3.7**). This decrease occurred across all vigilance states, suggesting that it was likely to be a generalised pathophysiological effect of compromised tissue health. However, between 1 and 4 days post-infusion, LFP power remained normal in these animals, indicating that the effects of TUN during this time frame were not pathological. As there was a distinct subgroup of animals that displayed a drop in LFP power, all subsequent analyses will be conducted on the entire cohort, as well as separately on the two subgroups (4 animals with no drop in LFP power and 4 animals with a drop in LFP power after 5 days).

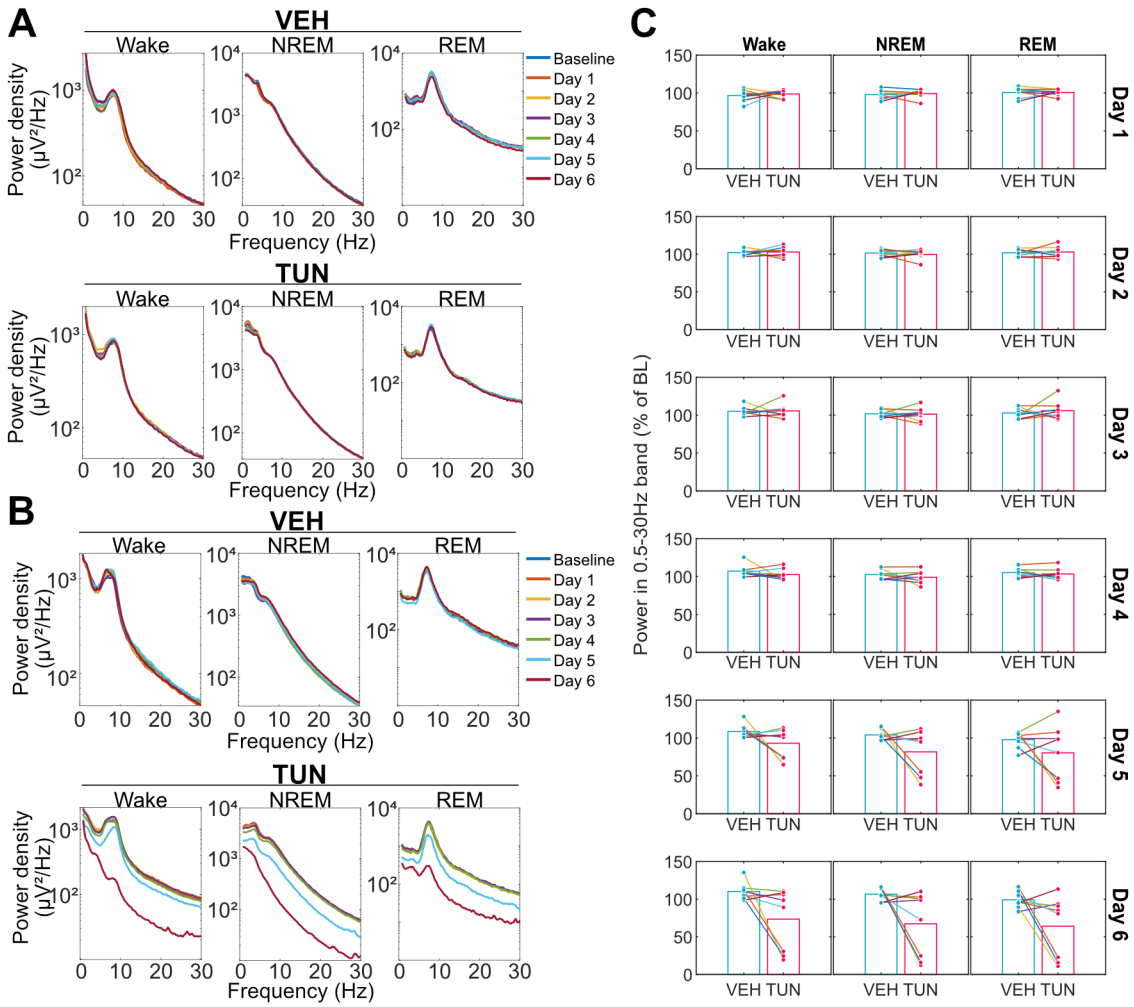

Figure 3.7 Tunicamycin infusion results in a loss of signal power in some animals.

(A) Example LFP spectral power density on baseline day and each 24-hour day following vehicle (VEH) or Tunicamycin (TUN) infusion in an animal that did not show a loss of LFP power following TUN. **(B)** Example LFP spectral power density in an animal that did show a loss of LFP power following TUN **(C)** Mean power in the boradband frequency range, 0.5-30 Hz, relative to 24-hour baseline (BL) on days 1-6 post-infusion with VEH or TUN during wake, NREM and REM. There was inter-individual variability in overall signal power over time after infusion, but no significant difference between VEH and TUN were detected ($p>0.05$, paired *t* tests).

3.3.4 Local Tunicamycin infusion did not alter sleep-wake architecture

Firstly, my aim was to investigate if the local intracortical TUN infusions had an impact on the global vigilance state patterns of the mice. To achieve this, I calculated the time course of wake, NREM or REM sleep in 2-hour intervals. I then compared the vigilance state patterns from 0 – 144 hours (6 days) after VEH and TUN infusions. The UPR in the cortex is heightened during natural wakefulness and reduced during sleep (Cirelli et al., 2004). Therefore, in order to prevent any potential restoration of TUN-induced UPR activation through sleep immediately after drug infusion, the infusions were administered just before the animals' natural waking period. In cell culture experiments, I discovered that a brief 2-hour TUN treatment activated the UPR within 6 hours after treatment washout (see Chapter 4, section **4.3.4**). Consequently, the timing of the infusions in this experiment was also aimed at allowing sufficient time for TUN to activate the UPR by the time of the next sleep episode.

The experimental cohort showed an expected periodicity in the occurrence of vigilance states across days, reflecting the well-known propensity of laboratory mice to sleep predominantly during the light period, and stay awake during the dark phase (**Figure 3.8**). At the onset of lights-OFF, animals gradually awoke, and the time spent asleep in either NREM or REM states decreased. As sleep pressure increased during wakefulness in the dark period, animals spent more time in NREM interspersed with REM. Following the naps, animals spent more time awake again until the end of the dark period, resulting in the characteristic dip in wakefulness and a peak in NREM seen during lights-OFF (**Figure 3.8**). At lights-ON, animals began nesting and preparing for sleep, leading to a sharp increase in NREM and a decrease in wake times.

The sleep-wake architecture was highly consistent across all animals of the experimental cohort, and there was no observed difference between VEH and TUN conditions (**Figure 3.8**A). Since half of the experimental group exhibited a drop in LFP power by 5 days after TUN infusion while the other half did not, I investigated how the sleep-wake architecture was impacted in these two

distinct subgroups. Interestingly, neither subgroup demonstrated a noticeable variation in sleep-wake architecture as a function of treatment condition throughout the 6-day period after VEH and TUN infusions (**Figure 3.8**B, C). These data suggest that the local TUN infusions did not exert a global effect on sleep phenotype.

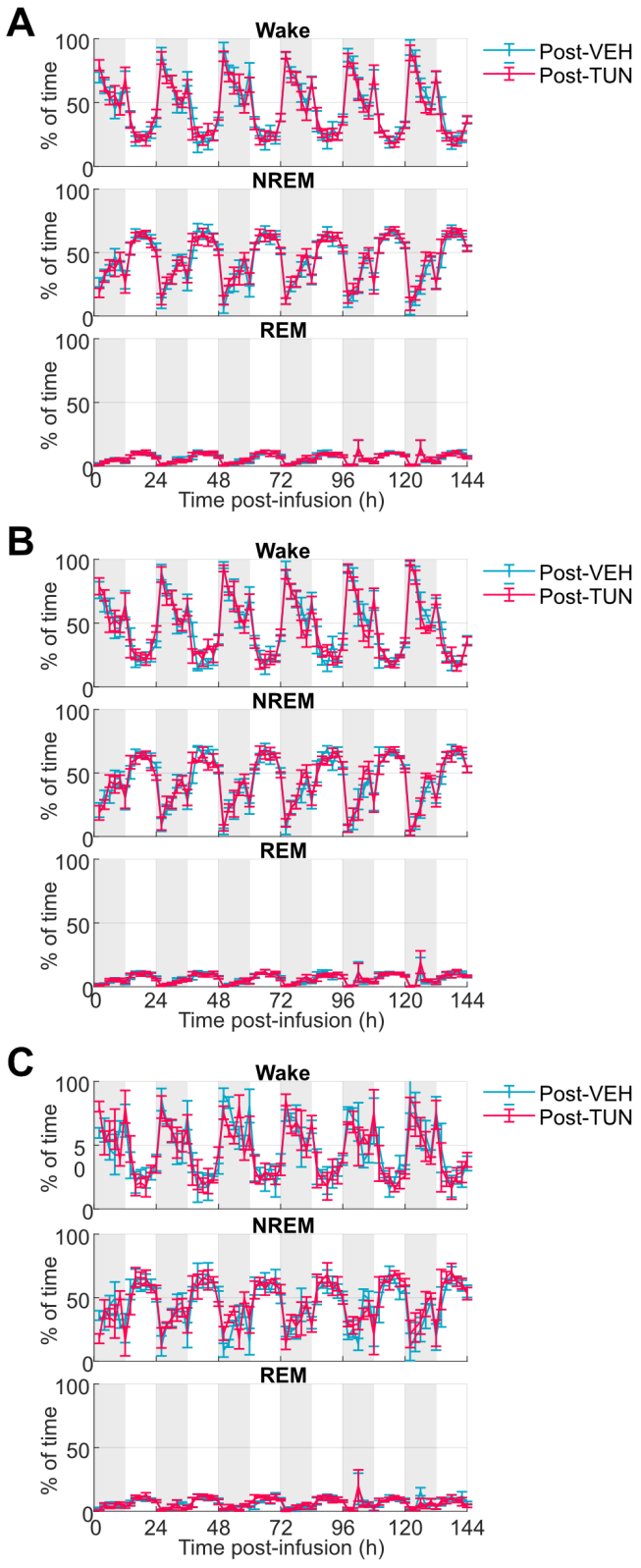

Figure 3.8 Local cortical UPR induction does not alter sleep-wake architecture.

(A) Percentage of recording time spent in wake, NREM or REM in 2-hour intervals over 6 days following infusion with either VEH or TUN (n=8; repeated measures 2-way ANOVA, Treatment: $p>0.05$, Time: $p<0.001$, Interaction: $p>0.05$). **(B)** Sleep-wake architecture of animals that did not show a drop in LFP signal following TUN infusion (n=4; repeated measures 2-way ANOVA, Treatment: $p>0.05$, Time: $p<0.001$, Interaction: $p>0.05$). **(C)** Sleep-wake architecture of animals that showed a drop in LFP signal at day 5 following TUN infusion (n=4; repeated measures 2-way ANOVA, Treatment: $p>0.05$, Time: $p<0.001$, Interaction: $p>0.05$). Grey shaded background in all graphs represent the lights-off period.

3.3.5 LFP spectral power changes occurred over several days following Tunicamycin infusion

Although local cortical TUN infusion did not produce any observable effects on the global sleep phenotype, the next step was to investigate whether there were any electrophysiological effects on the local infusion site LFP and the global frontal EEG signals. To address this, I conducted spectral analysis to compare the power spectra of the signals on baseline day and subsequent days following VEH or TUN infusion in 24-hour intervals. Each animal received VEH and TUN infusions with an interval of 6 days, therefore, each TUN infusion was compared to control VEH infusion in the same animal. This accounted for variability in signal quality across animals by providing an internal control. For this and all subsequent analyses, the baseline day for each animal was the 24-hour recording on the day before infusion with either VEH or TUN. This analysis aimed to identify any signal frequencies that showed differences following VEH or TUN infusion.

For the first four days post-infusion, even though there were significant interactions between drug treatment and frequency, no pair-wise differences in the LFP spectral power were observed at any frequencies between VEH and TUN treatments at the infusion site. However, on day 5 post-TUN, there was a selective decrease in the low delta frequency range during NREM, specifically within 0.5 – 1.75 Hz, relative to post-VEH (**Figure 3.9**A). On day 6 post-TUN, there was a further decrease in specific low frequencies during NREM, wake and REM relative to post-VEH (NREM: 1 - 3.5 Hz; wake: 0.75 – 3.25 Hz; REM: 0.5 Hz, 1.5 – 2 Hz and 5.25 – 5.5 Hz). These differences in the power spectra were only observed locally at the infusion site, but not in the frontal EEG, which arguably represents a more global signal (**Figure 3.9**B). Absolute spectral power, as shown in **Figure 3.9**, is not truly comparable between VEH and TUN. This is due to variations in the spectra on the corresponding baseline days, caused by changes in the composition of implantation site, drifts in signal quality, and effects of prior drug infusion over time. This is evident in the significant interaction effect of treatment x frequency in the infusion site LFP on baseline day. Therefore, the spectra per day post-VEH and post-TUN must be normalised to their own baseline day spectra.

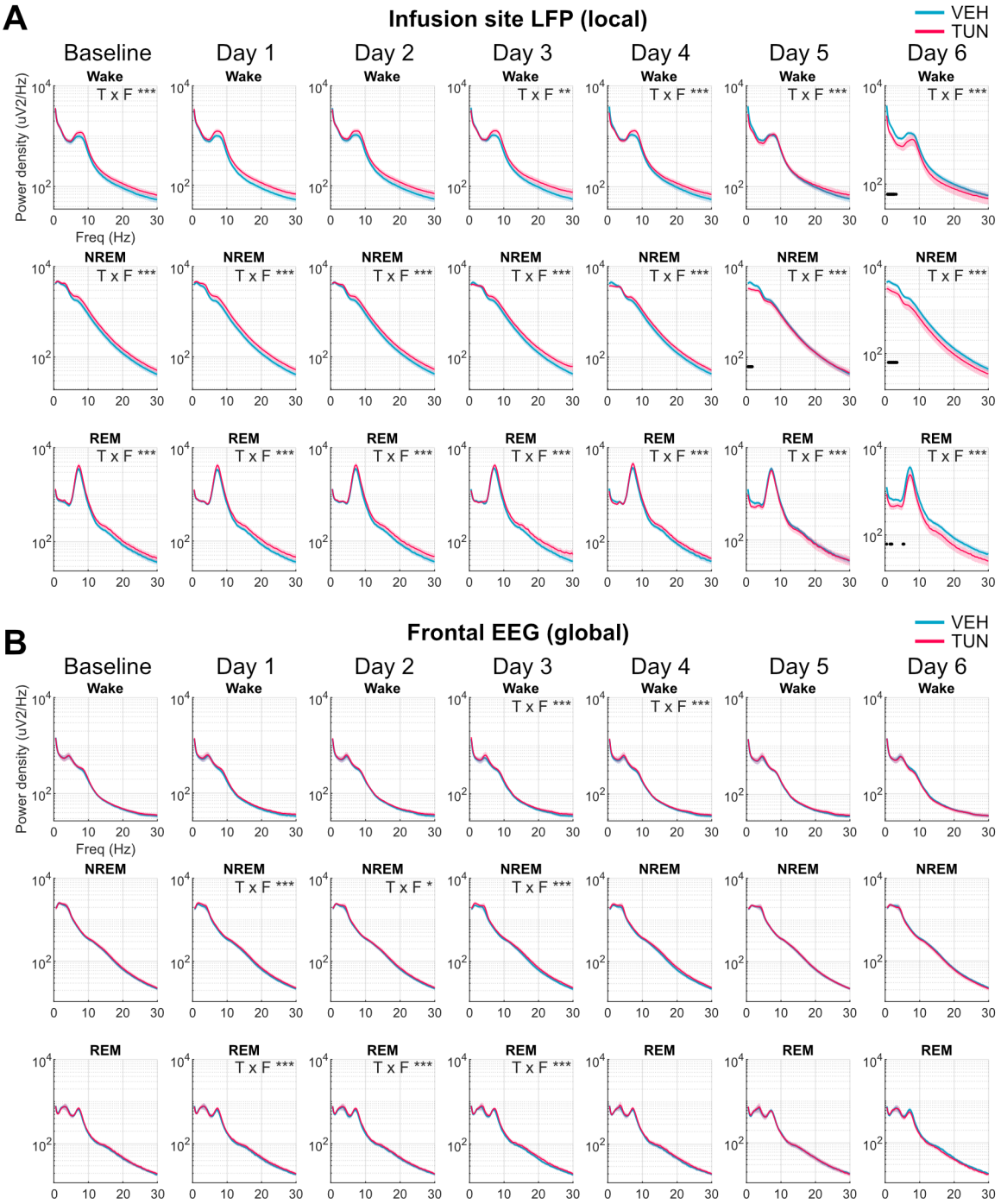

Figure 3.9 Spectral power changes occur locally at the infusion site, but not globally, after several days following TUN infusion (full experimental cohort).

(A) Mean spectral power densities from the infusion site LFP (local) on a 24-hour baseline day and subsequent days following either VEH or TUN infusion, during wake, NREM and REM (n=8 animals). **(B)** Mean spectral power densities from frontal EEG (global; n=7 animals). Data represented as mean ± SEM from all animals in the experimental cohort. Repeated measures 2-way ANOVAs were conducted, and a significant interaction effect between Treatment and Frequency (T x F) is indicated on the top right of individual graphs, with asterisks representing significance levels (see Methods section **3.2.12**). Black dots under curves represent $p<0.05$ from paired *t* tests per 0.25 Hz frequency bin, following a significant T x F interaction.

To better understand how the signals changed as a result of the infusion, all post-infusion power spectra were normalised to the corresponding baseline day's spectra for each individual animal. Upon analysis of the average normalised spectra of the infusion site LFP across the entire experimental cohort, I observed a notable decrease in the delta frequency range power on day 3 post-TUN compared to post-VEH, which was most pronounced during NREM (**Figure 3.10**A). A prominent decrease in delta power then occurred in all vigilance states from days 4 to 6 after TUN infusion. Broadband power was also reduced on days 5-6, which is likely attributable to the experimental subgroup that showed a drop in LFP power on day 5. Interestingly, the frontal EEG spectra relative to baseline also revealed differences between the TUN and VEH treatment conditions (**Figure 3.10**B). On day 2 post-TUN, there was an increase in the low theta range, 4.5 – 5.25 Hz specifically, during REM. On day 3 post-TUN, this increase in REM low theta was accompanied by an increase in the low theta range during NREM, 4 – 4.5 Hz specifically. Since theta primarily originates from the hippocampus, its increase may indicate changes in hippocampal activity. Moreover, a shift from delta to low theta power during NREM may indicate faster slow waves (V. V. Vyazovskiy et al., 2011; V. V. Vyazovskiy & Tobler, 2005). Specific higher frequencies in the frontal EEG were also elevated during NREM and REM on day 3 post-TUN. However, on subsequent days, there were no significant differences between TUN and VEH during NREM. On day 6 post-TUN, there were trends of a decrease in EEG spectral power across several frequency bins during wake, NREM and REM.

Next, I further divided the experimental group into animals that showed a drop in broadband LFP power post-TUN and those that did not. The group of animals that did not show a drop in LFP power post-TUN exhibited a marked and selective decrease in delta power in the infusion site LFP during NREM on day 3 (**Figure 3.11**A). This persisted until day 5 post-TUN and showed a trend of recovery back to baseline on day 6. The wake LFP spectra of these animals also displayed differences between VEH and TUN treatments, with a significant decrease in the delta and theta range and an increase in the high beta range from day 4 post-TUN, which also showed

signs of recovery on day 6. The post-VEH LFP spectra during wake deviated from baseline consistently, which may suggest that the 24-hour baseline used for normalisation was not representative of other days. The LFP spectra during REM showed differences in various frequency bins, which were difficult to interpret. For these animals, the frontal EEG spectra did not show obvious differences at specific frequencies between VEH and TUN treatments (**Figure 3.11**B). In contrast, the group of animals that showed a drop in LFP power post-TUN exhibited different trends. After TUN infusion, the infusion site LFP spectra did not show any marked differences until day 5 (**Figure 3.12**A). On day 5, there was a broadband decrease in power across all vigilance states, without any recovery by day 6. The LFP spectra during NREM and REM showed trends of a selective decrease in delta power on days 3 and 4 post-TUN, but not to the same extent as the first subgroup of animals. Unlike the first subgroup, the frontal EEG of these animals exhibited more obvious trends of differences between the treatment conditions (**Figure 3.12**B). On days 2 and 3 post-TUN, EEG spectra during NREM showed trends of a shift in power from delta to low theta. There was also a noticeable increase in REM low theta power in the EEG from day 2 to day 4 post-TUN compared to post-VEH. By day 6 post-TUN, there was a decrease in the EEG spectral power across several frequencies during NREM and REM, with the wake spectra also showing trends of broadband decrease in power.

The spectral data collectively suggest that all animals exhibited an electrophysiological response to TUN-induced UPR over multiple days post-infusion. While both subgroups of animals exhibited a reduction in NREM delta power as an early effect, there were differences in the global EEG effects observed between the two subgroups. These findings suggest that the effects of TUN-induced UPR on brain activity were heterogenous and state- and location- specific.

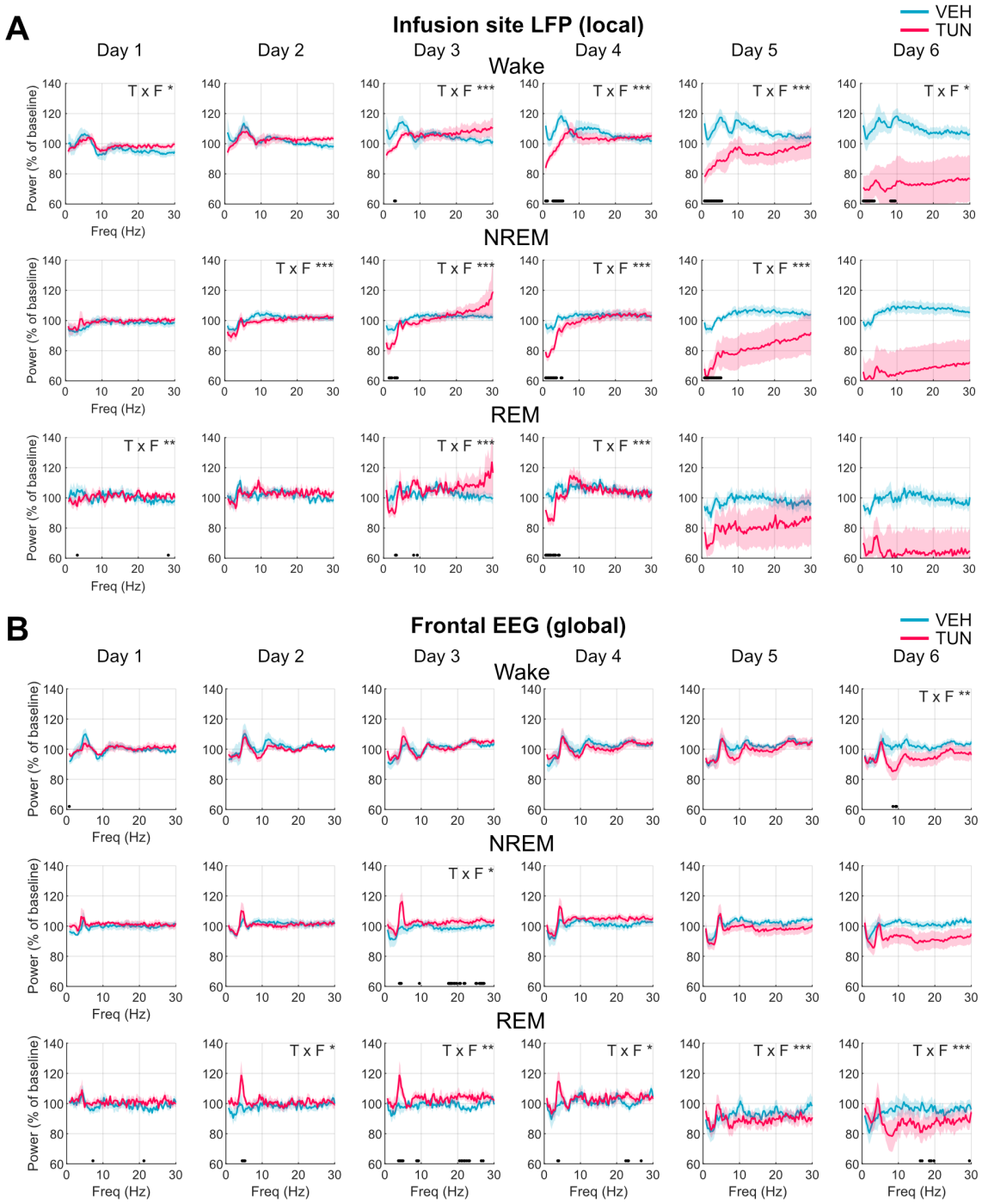

Figure 3.10 Normalised spectra from the infusion site LFP and the frontal EEG from days 1 to 6 after infusion (full experimental cohort).

(A) Infusion site LFP (local) spectral power densities, normalised to 24-hour baseline, on days 1 to 6 following either VEH or TUN infusion (n=8 animals). **(B)** Frontal EEG spectral power densities normalised to baseline (global; n=7 animals). Data represented as mean ± SEM from all animals in the experimental cohort. Repeated measures 2-way ANOVAs were conducted, and a significant interaction effect between Treatment and Frequency (T x F) is indicated on the top right of individual graphs, with asterisks representing significance levels. Black dots under curves represent $p<0.05$ from paired *t* tests per 0.25 Hz frequency bin, following a significant T x F interaction.

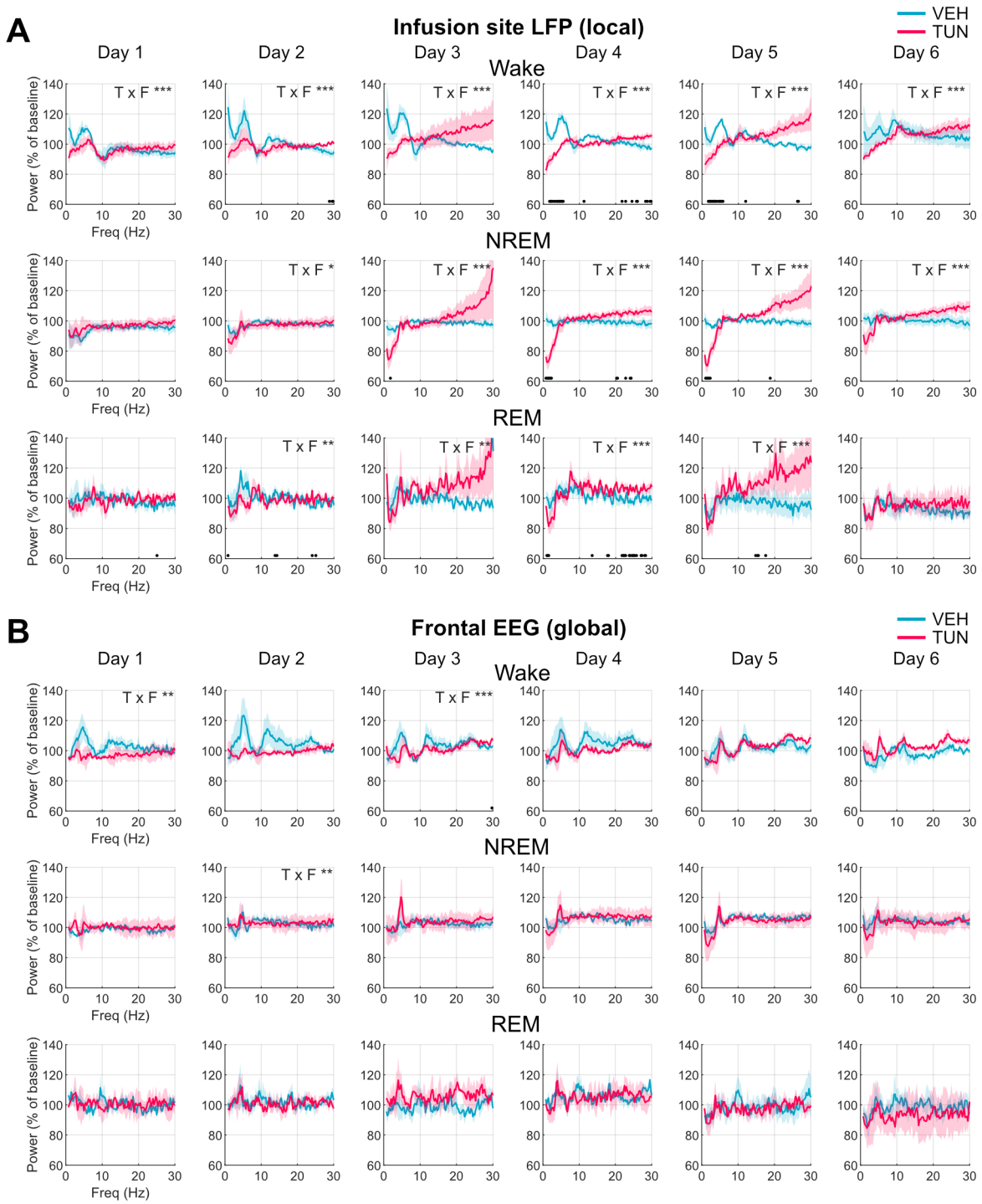

Figure 3.11 Normalised spectra from the infusion site LFP and the frontal EEG from days 1 to 6 after infusion (animals that did <u>not</u> show a drop in LFP power).

(A) Infusion site LFP (local) spectral power densities, normalised to a 24-hour baseline, on days 1 to 6 following either VEH or TUN infusion (n=4 animals). **(B)** Frontal EEG spectral power densities normalised to baseline (global; n=3 animals). Data represented as mean ± SEM from the subgroup of animals that did not show a drop in LFP power. Repeated measures 2-way ANOVAs were conducted, and a significant interaction effect between Treatment and Frequency (T x F) is indicated on the top right of individual graphs, with asterisks representing significance levels. Black dots under curves represent $p<0.05$ from paired *t* tests per 0.25 Hz frequency bin, following a significant T x F interaction.

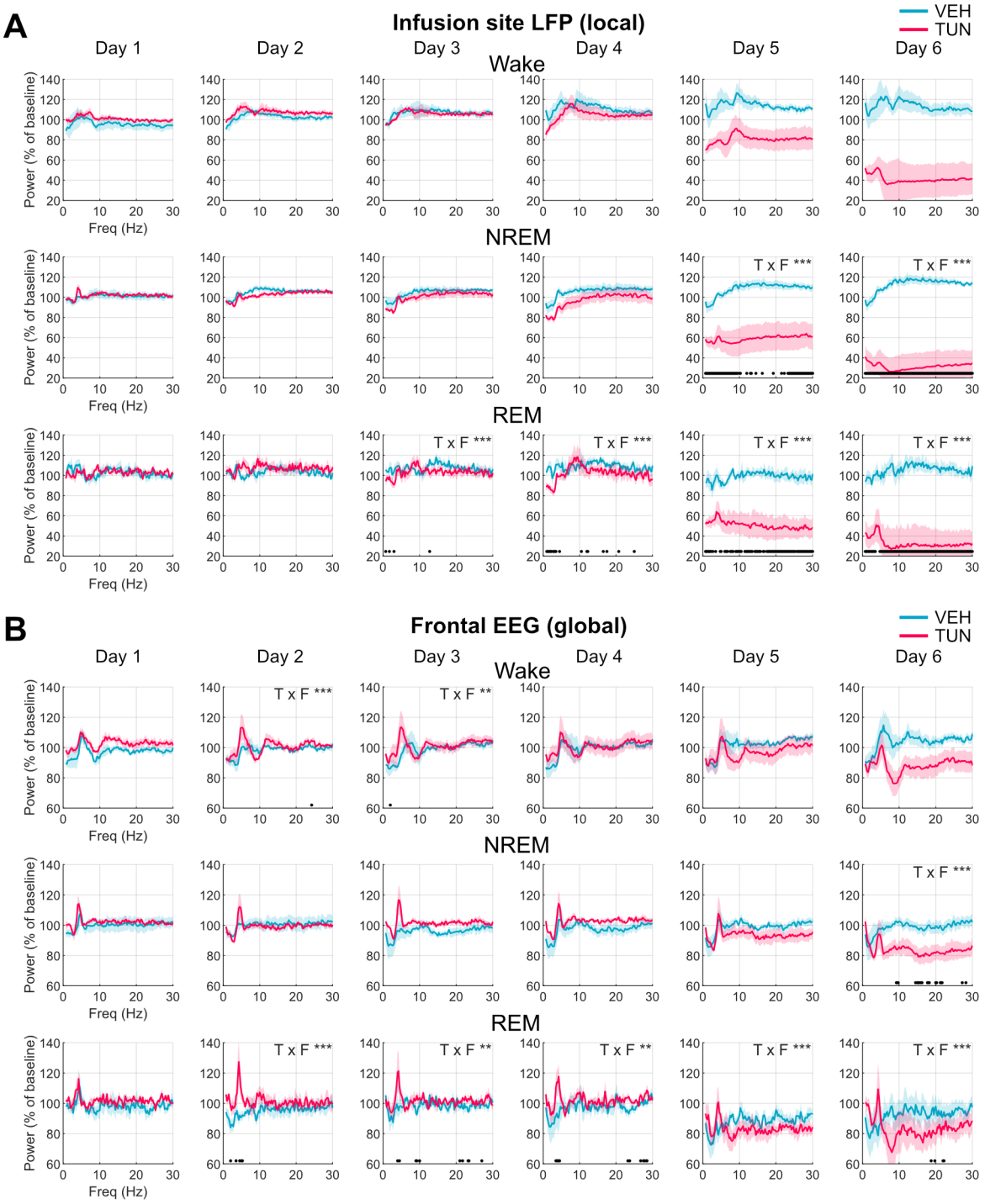

Figure 3.12 Normalised spectra from the infusion site LFP and the frontal EEG from days 1 to 6 after infusion (animals that showed a drop in LFP power).

(A) Infusion site LFP (local) spectral power densities, normalised to a 24-hour baseline, on days 1 to 6 following either VEH or TUN infusion (n=4 animals). **(B)** Frontal EEG spectral power densities normalised to baseline (global; n=4 animals). Data represented as mean ± SEM from the subgroup of animals that showed a drop in LFP power. Repeated measures 2-way ANOVAs were conducted, and a significant interaction effect between Treatment and Frequency (T x F) is indicated on the top right of individual graphs, with asterisks representing significance levels. Black dots under curves represent $p<0.05$ from paired *t* tests per 0.25 Hz frequency bin, following a significant T x F interaction.

3.3.6 Spectral power in the delta frequency band was the first to decrease in the infusion site LFP following Tunicamycin treatment

Brain network oscillations are often classified into specific frequency bands, based on a strong correlation of each band with distinct behavioural states (Destexhe et al., 1999; Steriade et al., 1993). As demonstrated in the previous section, the effects of TUN-induced UPR occur at various frequencies and seem to occur first during NREM sleep. Therefore, to gain a potentially more physiologically relevant understanding of the effects of TUN, I classified the LFP signal from the infusion site into distinct frequency bands: delta [0.5 – 4 Hz], associated with slow wave activity and sleep pressure; theta [6 – 9 Hz], associated with arousal and memory replay; sigma [12 – 15 Hz], associated with sleep spindles; and gamma [35 – 100 Hz], associated with arousal and sensory processing.

The average power in each frequency band was calculated in 24-hour intervals relative to baseline day, and compared between VEH and TUN treatments during 6 days post-infusion. Following TUN infusion, delta power at the infusion site LFP during NREM was the first to exhibit a significant decline relative to VEH (**Figure 3.13**A). This suggests that SWA during NREM may be particularly sensitive to TUN-induced UPR. Subsequently, from day 4 onwards, the decline in delta power post-TUN also manifested across wake and REM. Meanwhile, theta, sigma and gamma frequency bands showed significant interactions between treatment and time, however, there were no pair-wise differences between VEH and TUN at specific timepoints (**Figure 3.13**B-D). Moreover, the decline across all frequency bands on day 5 is attributable to the subgroup of animals that showed a drop in broadband LFP power at the infusion site after TUN infusion. Therefore, once again I divided the experimental cohort into two subgroups: animals that showed a drop in LFP power following TUN infusion and those that did not. The subgroup of animals that did not have a drop in LFP power only showed a significant effect of treatment and time interaction in the delta frequency band power during NREM (**Figure 3.14**A). However, pair-wise comparisons between VEH and TUN did not reveal significant differences at any timepoint. There was a clear trend of

decreased NREM delta power on day 3 post-TUN, which plateaued until day 6. As expected, the subgroup of animals that showed a drop in LFP power on day 5 post-TUN showed a decrease in LFP power across all selected frequency bands on day 5 post-TUN compared to post-VEH (**Figure 3.15**). However, there were changes in delta power earlier than day 5, with a significant decrease in delta power during REM appearing on day 3 post-TUN, and a decrease in delta power during NREM appearing on day 4 post-TUN (**Figure 3.15**A). There were also significant changes in sigma power during REM sleep, however this is difficult to interpret since power in the sigma band is not a signature of REM sleep.

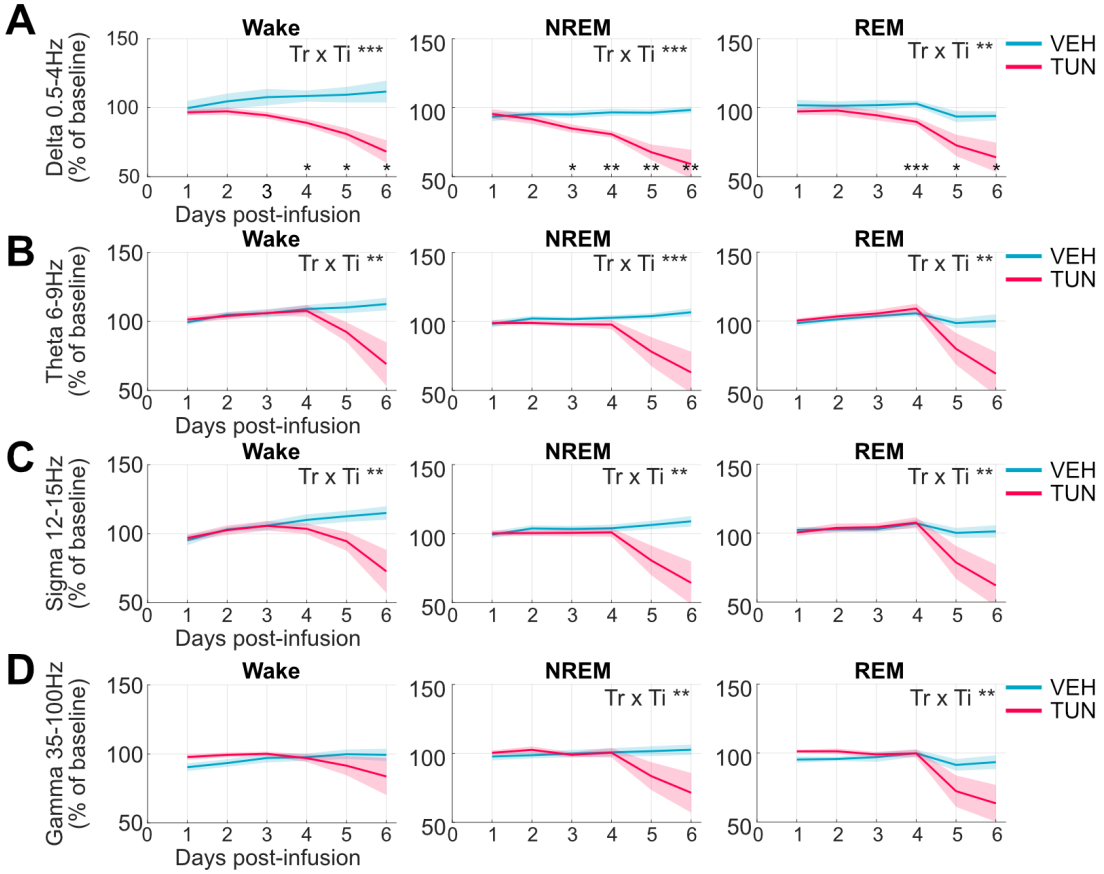

Figure 3.13 Infusion site LFP spectral power in delta, theta, sigma and gamma frequency bands following VEH or TUN infusion (full experimental cohort).

(A) Mean power in the delta frequency range, 0.5 - 4 Hz, during wake, NREM and REM over 6 days post-infusion with VEH or TUN, normalised to a 24-hour baseline (n=8 animals). **(B)** Mean power in the theta frequency range, 6 - 9 Hz (n=8 animals). **(C)** Mean power in the sigma frequency range, 10 - 15 Hz (n=8 animals). **(D)** Mean power in the gamma frequency range, 35 - 100 Hz (n=8 animals). Data represented as mean ± SEM in 1-day intervals, from all animals in the experimental cohort. Repeated measures 2-way ANOVAs were conducted, and a significant interaction effect between Treatment and Time (Tr x Ti) is indicated on the top right of individual graphs, with asterisks representing significance levels. Asterisks under curves represent significance levels from paired *t* tests per 0.25 Hz frequency bin, following a significant Tr x Ti interaction.

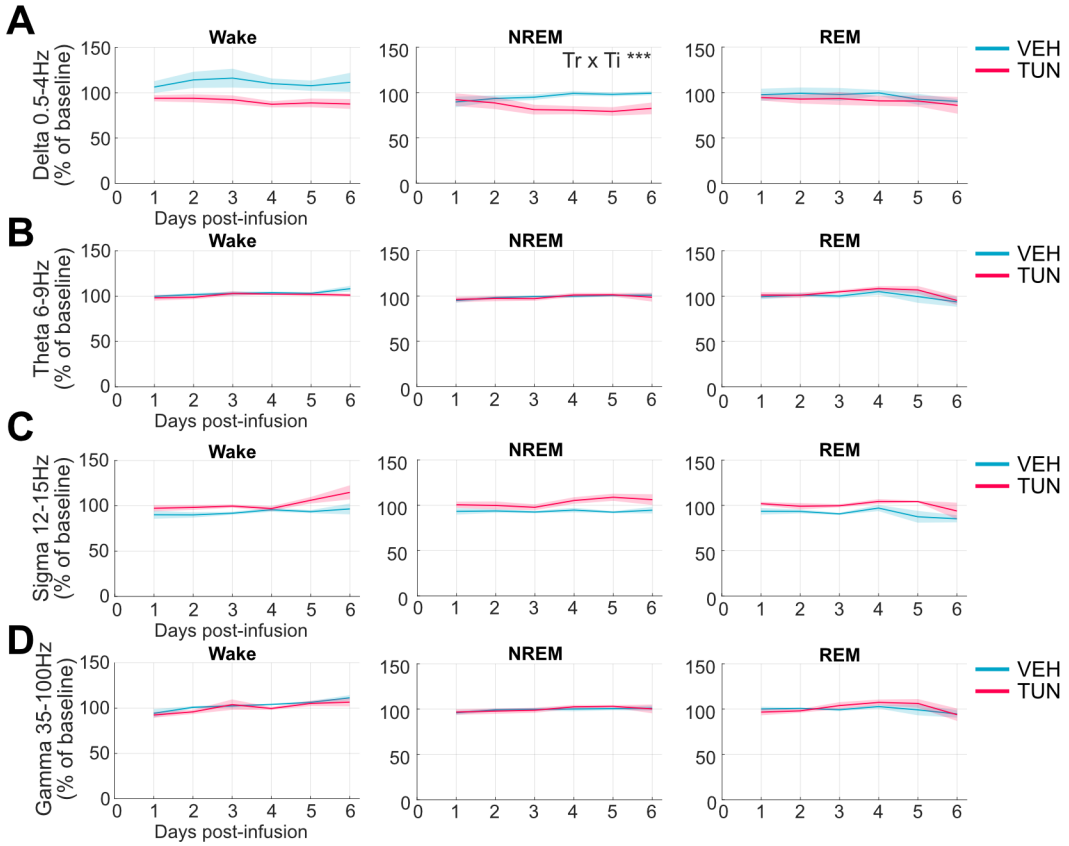

Figure 3.14 Infusion site LFP spectral power in delta, theta, sigma and gamma frequency bands following VEH or TUN infusion (animals that did not show a drop in LFP power).

(A) Mean power in the delta frequency range, 0.5 - 4 Hz, during wake, NREM and REM over 6 days post-infusion with VEH or TUN, normalised to a 24-hour baseline (n=8 animals). **(B)** Mean power in the theta frequency range, 6 - 9 Hz (n=8 animals). **(C)** Mean power in the sigma frequency range, 10 - 15 Hz (n=8 animals). **(D)** Mean power in the gamma frequency range, 35 - 100 Hz (n=8 animals). Data represented as mean ± SEM in 1-day intervals, from the subgroup of animals that did not show a drop in LFP power. Repeated measures 2-way ANOVAs were conducted, and a significant interaction effect between Treatment and Time (Tr x Ti) is indicated on the top right of individual graphs, with asterisks representing significance levels. Asterisks under curves represent significance levels from paired *t* tests per 0.25 Hz frequency bin, following a significant Tr x Ti interaction.

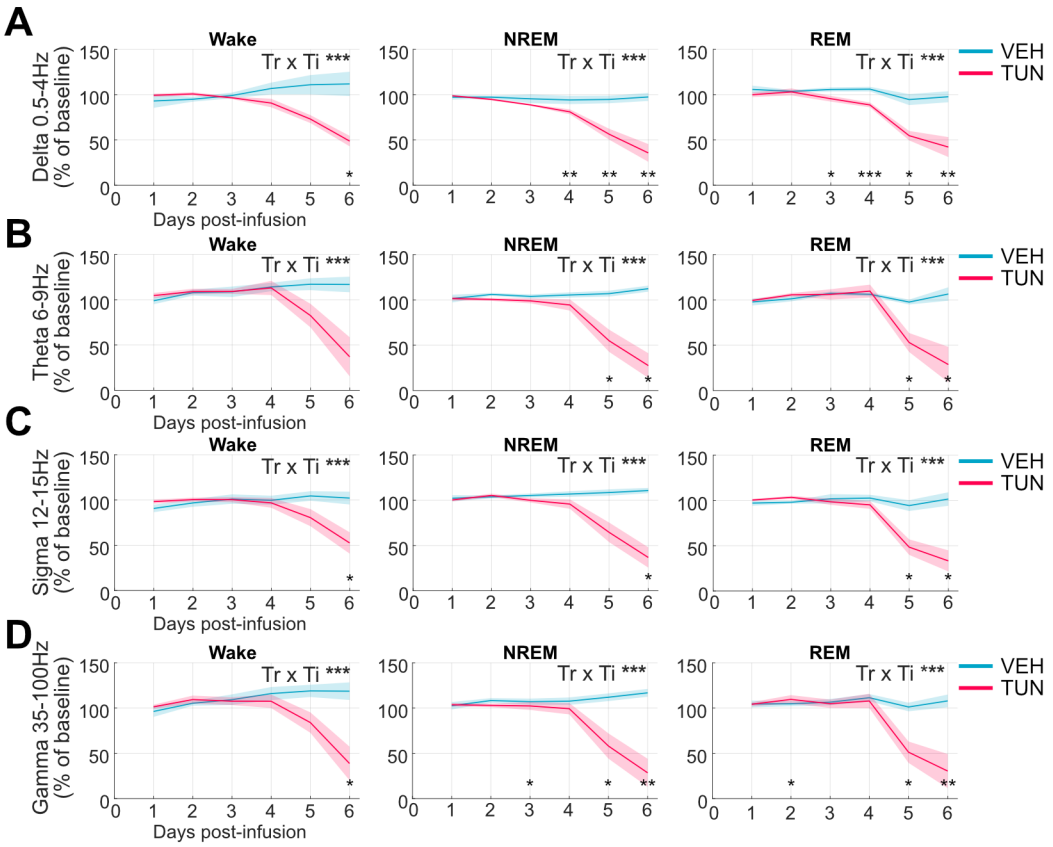

Figure 3.15 Infusion site LFP spectral power in delta, theta, sigma and gamma frequency bands following VEH or TUN infusion (animals that showed a drop in LFP power).

(A) Mean power in the delta frequency range, 0.5 - 4 Hz, during wake, NREM and REM over 6 days post-infusion with VEH or TUN, normalised to a 24-hour baseline (n=8 animals). **(B)** Mean power in the theta frequency range, 6 - 9 Hz (n=8 animals). **(C)** Mean power in the sigma frequency range, 10 - 15 Hz (n=8 animals). **(D)** Mean power in the gamma frequency range, 35 - 100 Hz (n=8 animals). Data represented as mean ± SEM in 1-day intervals, from the subgroup of animals that showed a drop in LFP power. Repeated measures 2-way ANOVAs were conducted, and a significant interaction effect between Treatment and Time (Tr x Ti) is indicated on the top right of individual graphs, with asterisks representing significance levels. Asterisks under curves represent significance levels from paired *t* tests per 0.25 Hz frequency bin, following a significant Tr x Ti interaction.

The decline in delta power at the infusion site LFP was first evident during NREM sleep after 3 days post-TUN (84.9 ± 2.9%) compared to post-VEH (95.1 ± 2.7%)(**Figure 3.16**). The decline in NREM delta on day 3 post-TUN occurred in 6 out of 8 animals, whereas on days 4 and 5 it was evident in all 8 animals (**Figure 3.16**). On days 5 and 6 post-TUN, there was greater variability between animals, with half the cohort showing a further decrease in delta power. In summary, frequency band analysis revealed that NREM delta power was consistently decreased from day 4 onwards post-TUN across all animals, while the decrease in the other frequency bands showed greater variability.

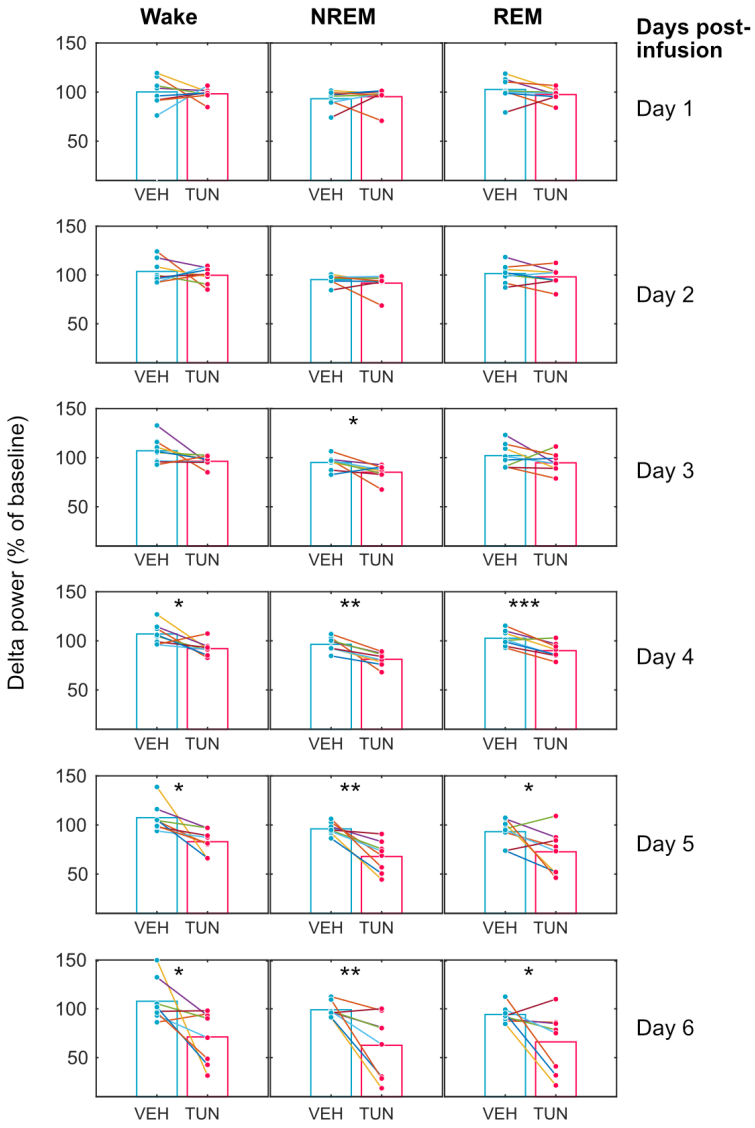

Figure 3.16 NREM slow wave activity in the delta range (0.5 - 4 Hz) is the first to decrease following TUN infusion (full experimental cohort).

Mean power in the delta frequency range (0.5 - 4 Hz) during wake, NREM and REM over six days post-infusion with VEH or TUN as a percentage of a 24-hour baseline (n=8; asterisks represent significance levels following paired *t* tests). Bars represent mean values of the full experimental cohort, and individual datapoints within each bar represent individual animals.

3.3.7 Tunicamycin decreased delta power locally at the infusion site

Having identified delta activity to be particularly vulnerable to TUN-induced UPR, the next objective was to establish whether this vulnerability was localised solely to the infusion site or extended more globally. To achieve this, I calculated the delta band power following TUN infusion as a percentage of delta power post-VEH at the same timepoint, from the infusion site LFP, the contralateral LFP, and the global frontal EEG. Since SWA in the delta range during NREM and wake

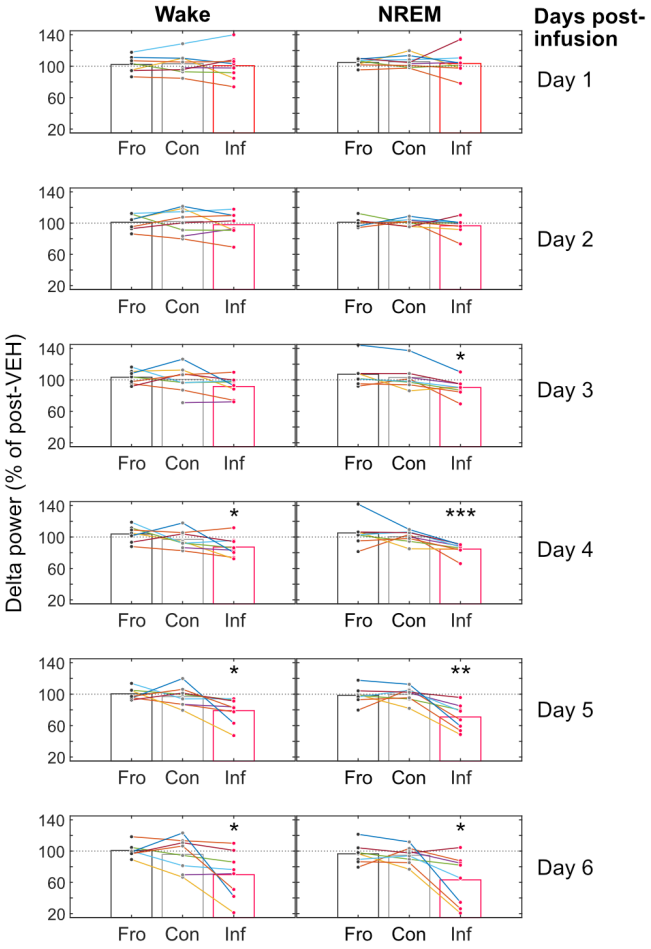

Figure 3.17 Delta band power exhibited a local decrease at the infusion site after TUN infusion, with no effects on the frontal EEG or the contralateral LFP.

Mean power in the delta band post-TUN infusion was calculated as a percentage of post-VEH delta power, and compared across the frontal EEG (Fro), the LFP from hemisphere contralateral to the infusion site (Con) and the LFP at the infusion site (Inf). Delta power during wake showed significant variation between the different sites from day 4 onwards (n=7-8; $p<0.05$, repeated measures 1-way ANOVA), with only the infusion site showing delta power significantly lower than 100% of post-VEH. Delta power during NREM showed significant variation between the sites from day 3 onwards (n=7-8; $p<0.05$, repeated measures 1-way ANOVA), with only the infusion site displaying significantly reduced delta power. Asterisks represent significance levels from one sample *t* tests following significant effect of site in ANOVA.

is a marker of sleep pressure, I focused on these two vigilance states when comparing local and global signals. Delta power showed a selective decrease at the infusion site LFP from days 3 to 6 during NREM and from days 4 to 6 during wake (**Figure 3.17**). This observation confirms that within the timeframe of the experiment, the reduction in delta power due to TUN-induced UPR was restricted to the location of the infusion, and did not affect global network levels of SWA.

3.3.8 TUN infusion resulted in a decrease in amplitude and duration of slow waves during NREM sleep

During NREM sleep, delta activity is mainly characterised by the occurrence of large amplitude slow waves, which result from the synchronised ON and OFF periods of cortical firing (V. V. Vyazovskiy et al., 2009). The magnitude of SWA increase is known to be influenced by prior sleep-wake history and it has been proposed that the level of SWA may reflect its restorative capacity (V. V. Vyazovskiy & Harris, 2013). To investigate whether the observed alterations in delta-frequency activity are associated with specific changes in the morphology of LFP slow waves at the infusion site, the amplitude, duration and number of individual slow waves were compared in 6-hour intervals following VEH or TUN infusions, all normalised to baseline day. Amplitude was determined as the distance to the positive slow wave peak from the zero-crossing (**Figure 3.18**A)**.** Duration was

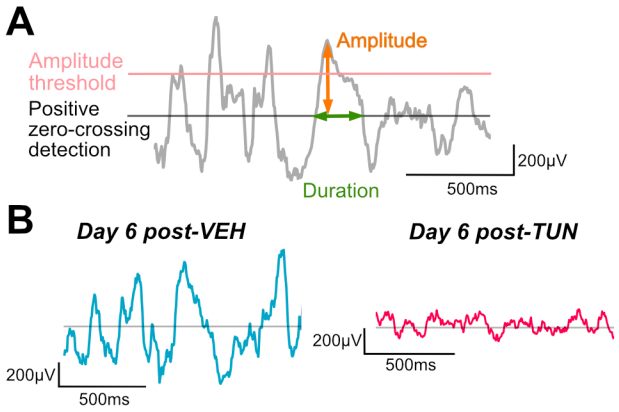

Figure 3.18 The properties of slow waves at the infusion site during NREM sleep showed changes after TUN infusion.

(A) Slow waves were detected from signals after bandpass filtering between 0.5 – 4 Hz. Slow waves were defined as positive deflections in between two consecutive negative deflections below the zero-crossing. Slow wave amplitude, duration and incidence per minute of NREM were measured. Only the top 25th percentile of largest slow waves were considered in subsequent analyses. **(B)** Representative traces of slow waves from an animal that displayed a drop in broadband LFP power on day 5 post-TUN. Slow wave amplitude was significantly diminished on day 6 post-TUN compared to on day 6 post-VEH.

defined as the time between the upward and the downward zero-crossings of the slow waves. The number of bona fide slow waves, which I defined as the top 25th percentile of largest slow waves, were counted per minute of NREM.

The experimental cohort was considered as a whole (**Figure 3.19**A) or divided into subgroups: animals that did not show a drop in broadband LFP power post-TUN (**Figure 3.19**B) and those that did (**Figure 3.19**C). Overall, there were significant interaction effects of treatment and time in the number, amplitude and duration of slow waves in the whole experimental cohort (**Figure 3.19**A). No differences were observed between TUN and VEH conditions immediately after infusion. However, there was a significant decrease in slow wave duration from 78 hours post-TUN, and a decrease in the number and amplitude of slow waves from 90 hours post-TUN. While slow wave amplitude and counts showed a gradual and consistent decline, the duration showed recovery back to post-VEH levels between 120 and 144 hours post-TUN.

Dividing the experimental cohort into subgroups based on a drop in overall LFP power post-TUN, I observed different trends. Animals that did not show a drop in LFP power showed an interaction effect of treatment and time in the number and amplitude of slow waves, but not in the duration (**Figure 3.19**B). While there were no pair-wise differences in slow wave counts between VEH and TUN at specific timepoints, there was a significant reduction in amplitude at 120 hours post-TUN compared to post-VEH. Slow wave duration varied as a function of time and treatment, showing a trend of a gradual decline post-TUN relative to post-VEH. On the other hand, animals that did show a drop in LFP power post-TUN showed a significant and consistent decrease in slow wave counts and amplitude from 120 hours post-TUN (**Figure 3.19**C), which coincided with the timepoint when the overall LFP power decreased. These animals also showed an interaction effect of treatment and time on their slow wave duration, which did not show differences between VEH and TUN until 126 hours, when the duration increased post-TUN compared to post-VEH, possibly indicating pathological tissue damage.

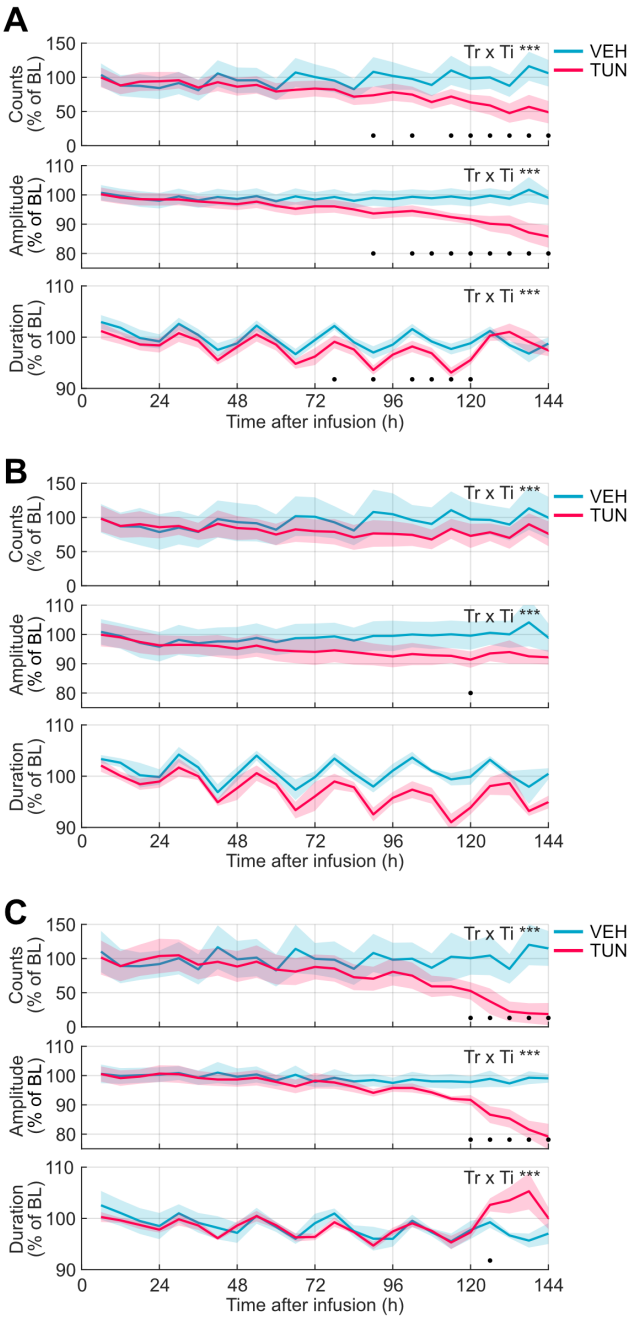

Figure 3.19 Slow waves at the infusion site during NREM show changes in number, amplitude and duration after TUN infusion.

(A) Mean slow wave counts per minute of NREM (top), amplitude (middle) and duration (bottom) from all animals post-infusion with VEH or TUN in 6-hour intervals, normalised to baseline day. Slow wave counts showed an overall effect of treatment and time and their interaction (n=8; Treatment: p=0.0191, Time: p<0.001, Treatment x Time: p<0.001; repeated measures 2-way ANOVA). Amplitude showed an overall effect of treatment and time and their interaction (Treatment: p=0.0095, Time: p<0.001, Treatment x Time: p<0.001). Duration showed an overall effect of time but not treatment, and showed an interaction effect (Treatment: p=0.47, Time: p<0.001, Treatment x Time: p<0.001). **(B)** Mean slow wave counts, amplitude and duration from animals that did not show a collapse in LFP power following TUN. Slow wave counts showed an overall effect of time but not treatment, and showed an interaction effect (n=4; Treatment: p=0.32, Time: p=0.031, Treatment x Time: p<0.001, repeated measures 2-way ANOVA). Amplitude did not show an overall effect of treatment or time, but showed an interaction effect (Treatment: p=0.21, Time: p=0.11, Treatment x Time: p<0.001). Duration showed an overall effect of treatment and time but not their interaction (Treatment: p=0.039, Time: p<0.001, Treatment x Time: p=0.16). **(C)** Mean slow wave counts, amplitude and duration from animals that did show a collapse in signal power following TUN. Slow wave counts showed an overall effect of time and treatment and their interaction (n=4; Treatment: p=0.035, Time: p<0.001, Treatment x Time: p<0.001, repeated measures 2-way ANOVA). Amplitude showed an overall effect of time and treatment and their interaction (Treatment: p=0.007, Time: p<0.001, Treatment x Time: p<0.001). Duration showed an overall effect of time but not treatment, and showed an interaction effect (Treatment: p=0.20, Time: p<0.001, Treatment x Time: p<0.001). Black dots represent p<0.05 from paired *t* tests following significant interaction effect in ANOVA.

In summary, these findings highlight the heterogeneous effects of TUN-induced UPR on slow waves. The decrease in slow wave counts and amplitude is most pronounced in the subgroup of animals that showed a broadband decrease in LFP power post-TUN, which suggests that the decrease in slow wave amplitude in these animals may be due to a pathological loss of neuronal cells in the region of TUN infusion. However, the decrease in slow wave duration was only observed in the subgroup of animals with no drop in LFP power post-TUN, suggesting that this effect may be due to activation of a milder UPR rather than cell death.

3.3.9 Tissue composition at the infusion site corresponds to overall signal composition following TUN infusion

To investigate the cause of the inter-individual differences seen as a result of TUN infusion, at the end of the experiments, animals were sacrificed and their brains were processed for histological examination. Brain sections were immunostained with antibodies against UPR markers, BiP and CHOP, and cell type markers, NeuN and GFAP. **Figure 3.20** depicts representative brain sections from the infusion site and contralateral hemisphere implantation site in an example animal that retained its overall LFP power (**Figure 3.20**A,C), and in an example animal that underwent a decrease in overall LFP power following TUN (**Figure 3.20**B,C). Brain sections from other animals with comparable electrophysiological effects looked similar.

In both subgroups of animals, there was a noticeable increase in KDEL and CHOP immunofluorescence in sections from the infusion site, compared to the contralateral hemisphere, indicating continued activation of the UPR following TUN infusion. In both subgroups, I also observed a greater invasion of GFAP-positive astrocytes in the infusion hemisphere compared to the contralateral hemisphere. However, in the subgroup that displayed an overall loss of LFP power, I found substantial changes in tissue composition at the infusion site. This was characterised by a pronounced loss of NeuN staining in the lower layers of the cortex at the end of the cannula implantation site, often extending into the hippocampus, and indicative of neuronal death. Most of

these animals also showed a dense plaque of GFAP+ astrocytes surrounding the infusion site, suggesting the presence of tissue scarring.

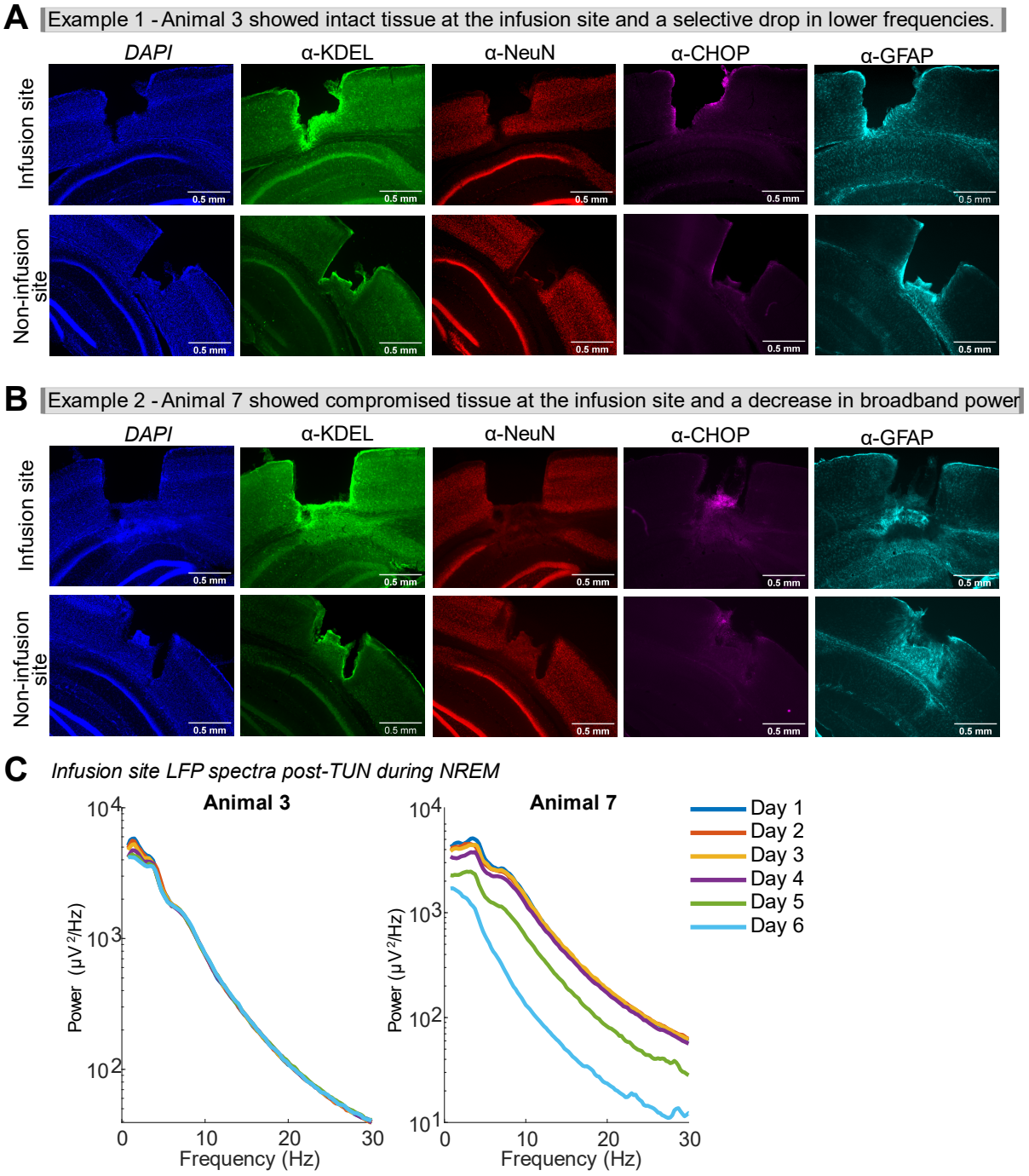

Figure 3.20 Inter-individual differences in tissue composition at the infusion site corresponds to differences in overall LFP power post-TUN infusion.

(A) Histological brain sections showing the infusion site and non-infusion site in an example animal (Animal 3) that did not show a drop in LFP power post-TUN. Brain sections were immunostained with antibodies against UPR markers, KDEL and CHOP and cell-type markers NeuN and GFAP. KDEL and CHOP were increased at the infusion site and there was a greater invasion of GFAP-positive astrocytes in that hemisphere compared to the non-infusion site. There was no noticeable loss of NeuN staining locally.

Legend continued from previous page……

(B) Histological brain sections showing the infusion site and non-infusion site in an example animal (Animal 7) that underwent a decrease in overall LFP power following TUN. Brain sections were immunostained with antibodies against UPR markers, KDEL and CHOP and cell-type markers NeuN and GFAP. KDEL and CHOP were increased at the infusion site compared to the non-infusion site. However, there was also a noticeable loss of NeuN staining locally surrounding the infusion site compared to the non-infusion site, indicating neuronal death. **(C)** NREM power spectra from the infusion site LFP for Animal 3 (shown in '**A**') and Animal 7 (shown in '**B**'), across days 1 to 6 after TUN infusion. Animal 3 showed a selective decrease in the lower frequencies following TUN but no broadband decrease in LFP power. Animal 7 showed a broadband collapse in LFP power on day 5 post-TUN, with an earlier decrease in lower frequencies.

These histological sections provide a snapshot of the tissue at the end timepoint of the experiment, when animals would have received a TUN infusion either 1 week or 2 weeks prior to tissue collection. Therefore, these immunohistological findings reveal that TUN-induced UPR was long-lasting, and that the chronic effects may have ultimately led to cell death in some animals, resulting in the pathophysiological loss of signal power observed at the infusion site.

3.4 Discussion

The overall aim of this chapter was to investigate possible effects of the UPR on sleep-wake regulation and associated neural activity. To address this, the pharmacological ER stress inducer, Tunicamycin (TUN), was used to activate the UPR in a local region of the cortex. Although initial immunohistochemical examination from pilot studies indicated a relatively mild induction of UPR after 24 hours of drug treatment, long-lasting effects were found in the brains of mice in the final experimental cohort. Despite the chronic effects of TUN at the location of infusion, there were no noticeable changes in sleep-wake architecture following drug administration, suggesting that the global regulation of sleep was not altered by local induction of the UPR. TUN infusion resulted in varied effects on neural activity patterns across animals. During the first 24 hours post-infusion, when ER stress was acute and milder, spectral analysis of the local infusion site LFP and the global EEG from the frontal derivation did not reveal significant changes in signal composition in any of the vigilance states. However, from 72 hours post-infusion, there was a consistent decrease specifically in the SWA delta frequency range at the infusion site LFP during NREM sleep. The frontal EEG also displayed subtle changes, specifically an increase in the low theta range, perhaps as a compensatory mechanism following UPR activation in a region of the cortex. During later timepoints, the experimental cohort displayed two distinct outcomes: half of the animals showed a widespread decrease in overall infusion site LFP signal power across all vigilance states, whereas the other half showed a selective decrease in NREM SWA, which showed signs of recovery. The decrease in SWA was localised to the infusion site, and was accompanied by changes in the number, amplitude and duration of slow waves during NREM post-TUN infusion. The subgroup of animals that displayed the greatest decrease in slow wave amplitude and overall LFP signal power were found to have significant neuronal loss at the infusion site when analysed post-mortem. The other subgroup of animals showed intact tissue composition, with continued BiP upregulation at the end of the experimental timeframe. Taken together, these findings suggest that SWA during NREM is particularly vulnerable to chronic ER stress.

Tunicamycin has been previously used as a pharmacological agent to study the effects of the UPR on the brain *in vivo*, and often at higher concentrations than that used in the present study (C.-M. Chen et al., 2012; Cóppola-Segovia et al., 2017; Leaver et al., 1988; L. Lin et al., 2018; Obukuro et al., 2013; Ono et al., 2012; Ozcan et al., 2009; Tong et al., 2017b; Y. Wang et al., 2017, 2018). Wang et al. (2017) reported that 0.15 mg/ml and 1.5 mg/ml of TUN administered intracerebroventricularly activated a benign and moderate ER stress response in the hippocampus by 24 hours. Furthermore, Chen et al. (2012) found 0.1 mg/ml TUN to be the lowest concentration to initiate an upregulation of BiP protein and mRNA after 24 hours of intracerebroventricular administration. Intracerebroventricular drug infusions are delivered into the cerebrospinal fluid, which bathes the entire brain in the further diluted drug solution. However, an infusion directly into the brain tissue may have different diffusion and dilution properties. In a study investigating the effects of TUN on the striatum, 0.2 mg/ml TUN was infused directly into the striatum every day for 7 days consecutively, which resulted in a loss of neurons at the end of the 7-day treatment (Cóppola-Segovia et al., 2017). Meanwhile, a minimum dose of 0.4 mg/ml TUN was required for infusion into the olfactory bulb for a UPR-dependent impairment of LTP (Tong et al., 2017a). Considering these previous findings, a concentration of 0.1 mg/ml TUN was used in the present study in an attempt to achieve a mild induction of the UPR.

Nonetheless, there is a lack of characterisation of the time course and reversibility of TUN-induced UPR. In this chapter, findings reveal that intracortical infusion of 0.1 mg/ml TUN results in chronic effects that persist over multiple days following TUN administration, and in some animals result in neuronal loss. Based on immunohistochemical observations at the 24-hour timepoint, and evidence from previous studies, 0.1 mg/ml TUN is likely to have elicited a mild ER stress in the early timepoints, with a pro-survival and adaptive UPR. However, due to the possibly constant and cumulative activation of ER stress, the UPR may have progressed to activate pro-apoptotic signalling pathways (Hetz, 2012; Ryoo, 2016). Therefore, further work is necessary to characterise the

strength and dynamics of UPR activation to establish a TUN dose that induces a mild and reversible UPR in the cortex.

The effects of TUN on neural activity were slow to manifest. Spectral analysis was conducted in 24-hour intervals because spectra calculated in 2-hour and 6-hour intervals revealed no changes in the first 48 hours post-infusion. This suggests that milder UPR activation in the early timepoints after TUN infusion was not sufficient to impact neural activity patterns. Electrophysiological changes were observed at least 2 days post-TUN infusion, suggesting that longer-term activation of the UPR alters neural activity in the affected region, when there is potentially reduced pro-survival signalling and more pro-apoptotic signalling (Hetz, 2012). Another striking feature of the TUN-induced UPR was the delay in the pathophysiological loss of broadband LFP power that occurred in half of the experimental cohort. This effect was observed consistently on day 5 post-infusion with TUN. In a separate pilot study conducted by Dr Jose Prius Mengual in the Vyazovskiy group, mice injected intraperitoneally with TUN exhibited an identical delay in the appearance of neurological and general symptoms of ill-health (personal communication). The animals in the current study that showed a pathophysiological loss of LFP power and tissue damage at the infusion site did not manifest any obvious neurological symptoms or signs of ill health before or after the drop in LFP power. An early study carefully characterised the cellular pathology of the neurotoxic effect of TUN infusion into the brain of rats (Leaver et al., 1988). In that study, localised TUN infusions resulted in localised lesions near the infusion site, with vascular damage being the predominant feature, accompanied with necrosis of brain cells and spongy degeneration of white matter. The neuronal damage appeared to be the result of secondary anoxia. The overall pattern of the lesions showed a sharp demarcation between damaged and normal tissue resembling an infarct, which I also observed in some of the mice in my experiment. Furthermore, the immunohistochemical observations of the present study revealed that the greatest upregulation of BiP following TUN infusion occurred in non-neuronal cell types. Therefore, one possible explanation for the slow onset of the electrophysiological effects is that the TUN-mediated UPR does not

primarily act on neurons directly. Instead, the UPR may result in dysfunction of non-neuronal cell types, such as vascular cells of brain blood vessels, which may manifest in a later neurological phenotype (Kito et al., 2011; Lenna et al., 2014).

Alternatively, it is possible that the early alterations in neural activity as a result of mild UPR activation were not detectable because the LFP recording was simply not sufficiently sensitive. The LFP reflects the summed signal of excitatory and inhibitory potentials from a large number of neurons near the recording site, as well as volume-conducted signals from distant locations (Herreras, 2016; Kajikawa & Schroeder, 2011). Therefore, alterations in the LFP usually reflect a synchronised response amongst a large network of neurons. However, the UPR acts at the individual neuron level and may produce shifts in subthreshold or firing activity, which may not be synchronous between large numbers of neurons, and would therefore fail to result in a consistent change in the LFP. Greater sensitivity to the effects of mild UPR may be provided by *in vivo* single unit recordings, to detect alterations in firing patterns at the individual neuronal level, and *in vivo* patch-clamp recordings, to detect alterations in both subthreshold and suprathreshold events.

The LFP recordings revealed a selective vulnerability of slow frequencies to TUN-induced UPR before other frequencies were impacted. Activation of the PERK pathway during sleep has been reported to reduce SWA in the delta range (Methippara et al., 2012). The selective reduction in NREM delta after 72 hours post-TUN infusion seen in the present study could be an effect of the PERK arm of the UPR. However, the contributions of the individual arms of the UPR in impacting SWA are as yet unknown. While it is difficult to interpret the initial decrease in SWA, it is likely that the overall loss in LFP power observed in half of the animals was due to neuronal death in the local region, resulting in a weaker LFP signal from more distant neurons. In the other half of the experimental cohort, the reduction in delta power showed trends of recovery by day 6 post-infusion, which may reflect a milder and more reversible TUN-induced UPR in those animals.

The effects of TUN manifested as changes in cortical activity, but did not result in changes to the global sleep-wake architecture. While the amount of time spent in each state may not have shown differences, the sleep macro-architecture can be further dissected in future work by looking at bout lengths of each vigilance state. This would provide information about how fragmented or consolidated those states were. Moreover, while neural activity in the delta range was predominantly affected at the local infusion site, notable changes in spectral properties were also observed at the frontal derivation EEG. These non-local changes included a selective increase in low theta power, which was coincident with the timepoints when delta power showed a reduction at the infusion site. This trend was visible in both subgroups of animals, although it was most prominent in the subgroup that showed a drop in LFP power after TUN infusion. Low theta power has been associated with increased sleep pressure and may reflect faster slow waves (V. V. Vyazovskiy et al., 2011; V. V. Vyazovskiy & Tobler, 2005). It has been found that following extended wakefulness, when homeostatic sleep pressure is high, slow waves increase in frequency (Hubbard et al., 2020). Faster slow waves were more sensitive to prior time spent awake, and therefore sleep pressure, than slower slow waves. Therefore, the trend of increased levels of low theta power in the frontal EEG may reflect increased homeostatic slow wave activity of faster slow waves. Since this effect was observed at the frontal EEG, it suggests that local cortical UPR activation, especially pathological UPR, may result in non-local changes in network activity, perhaps to compensate for the localised loss in neural function at the infusion site.

Some animals also showed histological effects of TUN infusion in the hippocampus, with increased level of BiP expression or neuronal loss. This suggests that the effect of the infusions may not have been purely localised to the neocortex, but also resulted in hippocampal UPR. Therefore, the changes in theta power observed at the frontal EEG, especially during REM sleep, may also reflect changes in hippocampal activity. The visual cortex is a particularly thin region of the neocortex, which means that infusions through a cannula implanted in that region is more likely to reach the hippocampus too. The visual cortex was chosen for the present study to align with a

parallel project, in which visual stimulation was being used to manipulate cortical activity to investigate activity-dependent effects on the UPR and local SWA. Moreover, the visual cortex has lower baseline levels of BiP expression compared to the frontal cortex (**Chapter 2**), thus offering the opportunity to produce a greater fold-induction of the UPR. In future work, the experimental design could be altered to target the frontal cortex, where the cortical thickness is greater and infusions are more likely to result in cortex-specific effects.

In summary, the present study reveals novel insights into the effects of TUN-induced UPR on neural activity patterns during sleep and wake, however, it has its limitations. While pharmacological manipulation of the UPR provides a useful tool to investigate overarching effects of the UPR, it is known to cause pleiotropic effects and is non-physiological (Bergmann & Molinari, 2018). Alternative approaches include more cell-targeted manipulations of the UPR, such as using genetically expressed misfolded proteins in the cell types of interest (Bergmann et al., 2018). The cause of the physiological UPR observed following sleep deprivation has not yet been identified. Therefore, it seems that further investigation is needed to understand the wake-related physiological increase in UPR, in order to be able to manipulate this process in a physiological manner.

Chapter 4 Developing a novel transcriptional reporter of global UPR activity

Contents

4.1 Introduction

The unfolded protein response (UPR) is a highly dynamic and tuneable process and, as I show in **Chapter 3**, it is induced in cortical neurons by physiological stimuli such as sleep deprivation. The past two decades has seen the development of many *in vitro* assays for measuring and monitoring UPR activation and downstream effectors of the UPR (Hiramatsu et al., 2011; Oslowski & Urano, 2011). Immunocytochemistry and western blots, as used in **Chapter 3**, offer methods to measure tissue-wide UPR at a single timepoint. Using such methods at discrete timepoints, it has been shown that UPR levels increase as a function of sleep deprivation duration, and exhibit signs of recovery after subsequent sleep, but still remain high after 24 hours of recovery (Naidoo et al., 2005, 2007b; Terao et al., 2003). However, the precise dynamics of UPR activation and recovery in the brain during sleep, wakefulness and following sleep deprivation have not been thoroughly characterised. To better investigate the bidirectional relationship between sleep and the UPR, a different approach is required for monitoring the UPR's activation and recovery dynamics in individual cells with high sensitivity. Therefore, in this chapter, I aimed to develop a novel tool that can be expressed in live cells, which can report UPR activation at low levels, track UPR recovery and respond to various ER stress stimuli.

The development of genetically encoded fluorescent reporter constructs has paved the way for monitoring the UPR dynamically and in a cell-targeted manner. Most of the available constructs provide readouts of individual arms of the UPR (Clark et al., 2020; Helseth et al., 2021; Iwawaki et al., 2004; F. Walter et al., 2015). One such construct is XBP1-Venus, also known as 'ER-stress activated indicator' (ERAI), a fluorescent reporter specific for the IRE1 arm of the UPR (Iwawaki et al., 2004). This reporter encodes Venus, a variant of green fluorescent protein (GFP), fused to a sequence of XBP1. The XBP1-Venus reporter relies on the unconventional splicing of an intron in the XBP1 mRNA by activated IRE1 under ER stress conditions. This splicing event results in a frame shift in the mRNA, which no longer encodes a stop codon between XBP1 and Venus, allowing the

translation of the XBP1-Venus fusion protein. The XBP1-Venus construct and transgenic reporter mice have since been used to investigate the IRE1 arm of the UPR in a variety of contexts, such as the activation of immune cells (Dong et al., 2019), intercellular ER stress transmission in the liver (Tirosh et al., 2021) and cell type-specific effects of brain injury and ischemia (Fan et al., 2023). Another more recently developed construct, SPOTlight, is a ratiometric fluorescent reporter for the PERK arm of the UPR (Helseth et al., 2021). SPOTlight relies on the differential usage of open reading frames (ORFs) for translation regulation under conditions of ER stress and PERK-mediated phosphorylation of eIF2α. The construct was designed by inserting a red fluorophore, TdTomato, into the ATF4 ORF, which is translated under conditions of high p-eIF2α. In contrast, enhanced GFP (EGFP) was inserted into an upstream ORF, which is translated under conditions of low p-eIF2α. Therefore, SPOTlight produces a scale-like readout of eIF2α phosphorylation downstream of PERK activation. SPOTlight expression in the brain revealed a cell type-specific activation of the PERK pathway in cholinergic neurons in the striatum under baseline conditions (Helseth et al., 2021). The PERK pathway is part of the integrated stress response, and therefore, relying solely on a readout of PERK activity may not reflect UPR levels in a cell (Costa-Mattioli & Walter, 2020).

While the aforementioned tools are useful for detecting the activation of specific arms of the UPR, they may be limited in their overall sensitivity in terms of reporting the global state of UPR activity in a cell. The three UPR arms exhibit distinct sensitivities and kinetics to specific stress inducers (DuRose et al., 2006; Yoshida et al., 2003). However, there is a lack of understanding regarding the specific activation levels and timing of the three UPR arms in response to different stress stimuli, particularly in physiological contexts. Hence, there is a need to develop a means of quantifying activation of the overall UPR, irrespective of specific pathways. Additionally, capturing the activity of all three arms of the UPR could be crucial for achieving a higher cumulative sensitivity to detect low levels of UPR activation in physiological conditions, such as after sleep deprivation. A reliable and sensitive reporter should exhibit a high signal-to-noise ratio, characterised by low baseline expression and a significant increase in expression upon UPR activation. Furthermore, it

should be capable of tracking the ON/OFF dynamics of UPR activation and deactivation. Ultimately, for a reporter to effectively reflect the UPR, it must be capable of detecting its activation by a range of stimuli.

One alternative approach has utilised regions of the rat BiP promoter sequence driving LacZ expression for monitoring BiP activation *in vitro* and *in vivo* (A. S. Lee, 2005; Mao et al., 2006). The BiP promoter sequence is responsive to transcription factors downstream of all three arms of the UPR (ATF4, sXBP1 and ATF6) and therefore offers a possible method to detect global UPR activation (A. S. Lee, 2005; Luo et al., 2003a; Yamamoto et al., 2004). Developments in fluorescent protein engineering provide opportunities to enhance the temporal performance of a reporter, such as by using rapidly maturing and brighter variants of GFP, like mNeonGreen (mNG) (Hostettler et al., 2017; Shaner et al., 2013). Furthermore, protein destabilising elements that encourage quick protein turnover, such as the PEST sequence from mouse ODC (ornithine decarboxylase, a metabolic enzyme), can offer a further improvement in reporter kinetics (Corish & Tyler-Smith, 1999; Kitsera et al., 2007).

AIMS

To facilitate the study of the physiological UPR in the nervous system, my objective was to design a highly sensitive reporter of the global UPR with good kinetics. In this chapter, I describe the development and characterisation of the **s**ensor of **UPR a**ctivity (sUPRa), a fluorescent UPR reporter construct that uses a region of the mouse BiP promoter, where the three arms of the activated UPR converge, to drive expression of mNG. Incorporation of a second, UPR-independent promoter and fluorophore allows for normalisation of reporter copy number and unbiased signal quantification in individual cells. Overall, in this chapter I aimed to:

1. Design and optimise a BiP promoter-based fluorescent sensor of the UPR that is capable of sensitive and dynamic readouts of UPR activation.

2. Characterise the reporter's performance compared to previously established single-arm UPR reporters, in terms of sensitivity and temporal dynamics.
3. Characterise the novel UPR sensor's response to different forms of ER stress stimuli.

4.2 Methods

4.2.1 Constructs and cloning

sUPRa is a dual promoter construct designed to encode the green fluorescent protein, mNG, under the control of BiP mouse promoter fragment and a red fluorescent protein, mScarlet (mSc), under the control of a constitutively expressed nEF promoter. The BiP promoter fragment in sUPRa encompasses -195 to -9 of the mouse gene relative to the transcriptional start site (Tillman et al., 1995). The constructs described in **Figure 4.1**, 500BiP-mNG-PEST and 170BiP-mNG-PEST, encompass promoter fragments -500 to -9 and -170 to -9 respectively. The design of these BiP promoter constructs was informed by the work of Amy S Lee and colleagues using rat promoter reporter constructs (Luo et al., 2003b).

sUPRa was constructed using the vector pAAV-CAG-mNeonGreen as a starting point (Chan et al., 2017). The woodchuck hepatitis virus post-transcriptional regulatory element (WPRE) sequence was removed using a BsrGI/XhoI digest and the mouse ornithine decarboxylase (ODC) PEST sequence (Corish & Tyler-Smith, 1999), encompassing the carboxy-terminal 39 amino acids of ODC (NCBI Reference Sequence: NM_013614.3), was inserted in-frame with the C-terminus of mNG. The PEST sequence was PCR amplified from a mouse brain cDNA library using primers BsrGI_PEST_Fwr and XhoI_PEST_Rev, listed in **Table 4.1.** The CAG promoter was removed using MluI/KpnI and replaced with the -195 BiP mouse promoter fragment, which was amplified from genomic DNA purified from mouse cerebellum, using primers MluI_mBip-195bp_Fwr and KpnI_mBip-8_rev (**Table 4.1**). This generated 195BiP-mNG-PEST, and the constructs 500BiP-mNG-PEST and 170BiP-mNG-PEST were made in the same way using primers listed in **Table 4.1**. All PCR products for cloning were generated using Q5 High Fidelity DNA polymerase (New England Biolabs, USA) and digests were performed using restriction enzymes from New England Biolabs, USA**.** Vectors were dephosphorylated using Antarctic phosphatase (New England Bioloabs, USA), ligations were performed with DNA Ligation Kit Mighty Mix (Takara Bio) and transformations were carried

out using Max Efficiency Stbl2 competent cells (Thermo Fisher Scientific). All constructs were fully sequenced (Source Biosciences).

Gene/Promoter	Primer sequence (5'-3')	Digest
PEST	**Forward primer:** BsRGI_PEST_Fwr GAGAAGCTGTACAAGCATGGCTTCCCGCCGGAGGT	BsRGI/XhoI
	Reverse primer: XhoI_PEST_Rev GAGAAGCTCGAGCTACACATTGATCCTAGCAGAAG	
500bp BiP	**Forward primer**: MluI_mBip_0.5kb_Fwr GATAAGACGCGTATCCGAGAACGTGTGGAGGCT	MluI/KpnI
	Reverse primer: KpnI-mBip-8_Rev GAGTACGGTACCCAGTGTTGTCTCGGCCAGTA	
195bp BiP	**Forward primer**: Mlu_mBip_-195bp_Fwr GAGAACACGCGTTAGCAATGACGTGAGTTGCGGA	MluI/KpnI
	Reverse primer: KpnI-mBip-8_Rev GAGTACGGTACCCAGTGTTGTCTCGGCCAGTA	
170bp BiP	**Forward primer**: Mlu-mBip_-170bp_Fwr GAGAACACGCGTAGGCCGCTTCGAATCGGCAGCA	MluI/KpnI
	Reverse primer: KpnI-mBip-8_Rev GAGTACGGTACCCAGTGTTGTCTCGGCCAGTA	
nEF promoter	**Forward primer**: MluI_nEF_Fwr GAGAACACGCGTAAGGATCTGCGATCG	MluI/SalI
	Reverse primer: SalI_nEF_Rev GAGAACGTCGACGTAGGCGCCGGTCACAGCTTG	
mScarlet-I	**Forward primer:** XhoI_mScarlet-I_Fwr GAGAACCTCGAGGCCACCATGGTGAGCAAGGGCGAGG	XhoI/EcoRI cloned into SalI/EcoRI sites in vector
	Reverse primer: EcoRI_mScar_TdT_Rev GAGAACGAATTCTTACTTGTACAGCTCGTCCATGC	
nEF-mScarlet-I-W3SL cassette	**Forward primer:** PmlI_nEF1_Fwr GAGAACCACGTGAAGGATCTGCGATCGCTCCG	PmlI
	Reverse primer: PmlI W3SL_Rev GACAACCACGTGGCGGCCGCTTTAAAAAACCTC	

Table 4.1 Primers and restriction sites used for cloning all constructs made in this study.

The second step for constructing sUPRa was to combine a constitutively expressed red fluorophore with 195BiP-mNG-PEST. To this end, we constructed the vector pAAV-nEF-mScarlet-W3SL, which consists of the short 'nEF' promoter, which is a constitutively expressed chimeric EF1α/HTLV promoter (Fenno et al., 2014), the fluorophore mScarlet-I (Bindels et al., 2017) and the W3SL sequence, which is a modified and compact combined WPRE and SV40 late polyadenylation signal sequence (Choi et al., 2014). Starting with the vector pAAV-hSyn-DIO {ChETA-mRuby2}on-W3SL (S.-J. Li et al., 2018), the hSyn promoter was removed using MluI/SalI and replaced with the nEF promoter, which was PCR amplified from the construct pAAV-nEF Con/Foff hChR2(H134R)-EYFP

(Fenno et al., 2014) using primers MluI-nEF-Fwr and SalI_nEF_Rev (**Table 4.1**). The insert and LoxP sites were subsequently removed using SalI/EcoRI and replaced with mScarlet-I, amplified from pCytERM-mScarlet-I-G-GECO1.2 using primers XhoI_mScarlet-I_Fwr and EcoRI_mScar_TdT_Rev (**Table 4.1**). To make sUPRa, the nEF-mScarlet-W3SL cassette was amplified using primers PmlI_nEF1_Fwr and PmlI_W3SL_Rev (**Table 4.1**) and inserted into a PmlI site in 195BiP-mNG-PEST. The orientation of the nEF-mScarlet-W3SL cassette was confirmed by restriction digest and sequencing of the entire construct.

4.2.2 Cell culture transfection and treatment

NIH3T3 mouse embryonic fibroblast cells were maintained at 37 °C and 5% CO_2 in Dulbecco's modified Eagle medium (DMEM, Gibco, Thermo Fisher Scientific, UK) with high glucose and pyruvate, supplemented with GlutaMAX and 10% bovine serum (Gibco, Thermo Fisher Scientific, UK) and passaged at 90-95% confluence every 3-4 days. Before experiments, 13 mm glass coverslips were placed in 24-well plates, incubated with poly-D-lysine (0.1 mg/ml in dH_2O) for 1 hour at 37 °C, then washed and air-dried. NIH3T3 cells were trypsinized using 0.05% Trypsin-EDTA and seeded onto the coverslips at a density of $1x10^6$ cells per plate. The following day, at 60-80% confluency, cells were transfected with a mixture of Lipofectamine 2000 (Invitrogen, Thermo Fisher Scientific) and plasmid DNA, as per the manufacturer's instructions. The media was changed after 3 hours and cells were left overnight before further treatment. Tunicamycin (Sigma-Aldrich, UK, Cat #T7765) was prepared as a 5 mg/ml stock in dimethyl sulfoxide (DMSO, Sigma-Aldrich, UK, Cat #D2560) and further diluted in cell culture media. Thapsigargin (Sigma-Aldrich, UK, Cat #T9033) was prepared as a 1 mM stock in DMSO and further diluted in cell culture media. L-Azetidine carboxylic acid (Sigma-Aldrich, UK, Cat #A0760) was prepared as a 50 mg/ml stock in dH_2O and further diluted in cell culture media. Final concentrations of drug solutions and incubation times are indicated where relevant. Following the treatment period, cells were pre-fixed in 2% PFA in PBS for 10 minutes, followed by fixation in 4% PFA for 10 minutes.

4.2.3 Immunocytochemistry

Cells were first incubated in 10% goat serum, 0.3%-TritonX-100 for 1 hour at room temperature before being incubated with primary antibodies (**Table 4.2**) diluted in 5% goat serum in 0.15% TritonX-100 for 1 hour at room temperature. After washing in 0.3% TritonX-100, cells were then incubated with Alexa Fluor-conjugated IgG secondary antibodies diluted in 5% goat serum in 0.15% TritonX-100 for 1 hour at room temperature. After further washes, cells were stained with DAPI (1:10000 in PBS) for 5 minutes. After a final wash, coverslips were mounted onto glass microscope slides using Prolong Diamond Antifade mountant (Invitrogen, Thermo Fisher Scientific).

Primary AB	Catalogue no. and supplier	Dilution
Mouse anti-KDEL (mAb)	10C3, Enzo Life Sciences, ADI-SPA-827	1:500
Rat anti-RFP (mAb)	5F8, Chromotek, lot # 90228002AB	1:300

Table 4.0.2 List of antibodies used for immunocytochemistry in this chapter.

4.2.4 Epifluorescence imaging

Fixed NIH3T3 cells on coverslips were imaged using a 20x objective (Olympus, UPlanFL N 20x/0.5na) on an epifluorescence microscope (Olympus BX40), equipped with a Hamamatsu ORCA-ER camera and HCImage Live software (RFP: 540/40 nm excitation filter, 570 nm dichroic, 600/50 nm emission filter; GFP: 485/20-25 nm excitation filter, 506 nm dichroic, 524/24-25 nm emission filter). Auto Hi-Lo and Contrast settings were turned off. Imaging parameters including exposure times were adjusted per fluorescent construct to avoid saturation, and were kept constant within each experiment. Cells from multiple non-overlapping fields of view (FOVs) were captured from each coverslip, with 2-3 coverslips per experimental repeat. The number of FOVs and experiments used are specified in the figure legends.

4.2.5 Image analysis

Transfected NIH3T3 cells were identified from the UPR-independent fluorescence channel (mScarlet or anti-RFP), using `Cellpose` (Stringer et al., 2020). Segmentation “masks” generated by `Cellpose` were applied on the reporter fluorescence channel to obtain a sum fluorescence value for each cell. An averaged background fluorescence value, which was obtained for each image

by averaging all of the pixels that were excluded from the cell masks, was subtracted from each cell. A threshold was applied such that cells with a background-subtracted fluorescence of zero or below were not included in subsequent analyses.

4.2.6 Statistical analysis

All data were assessed for normality using the Shapiro Wilk test, following which the appropriate parametric or non-parametric statistical tests were applied. Statistical analyses were performed using the `Scipy` and `Statsmodels` packages in Python. Graphs were generated using `Matplotlib` and `Seaborn` packages in Python. Asterisks represent significant p-values following statistical tests (*$p<0.05$, **$p<0.01$ and ***$p<0.001$). The statistical tests and p-values are detailed in the appropriate figure legends.

4.3 Results

4.3.1 Novel fluorescent reporters for monitoring UPR levels

To generate new BiP promoter-based fluorescent reporters, we initially started with a 500 base pair (bp) long portion of the mouse BiP promoter (bases -500 to -9 of the mouse gene relative to the transcriptional start site), which consists of three tandem repeats of the endoplasmic reticulum stress element (ERSE), a cAMP response element (CRE), and several other regulatory response elements (A. S. Lee, 2005) (**Figure 4.1**A). The ERSE portion is sufficient to be activated by transcription factors ATF6 and sXBP1 downstream of the ATF6 and IRE1 arms of the UPR respectively, but is not activated by the PERK arm of the UPR (A. S. Lee, 2005; Y. Wang et al., 2000; Yoshida et al., 2001). The CRE site binds to ATF4, the primary transcription factor upregulated downstream of PERK activation (Luo et al., 2003a). The regulatory elements on the 500bp promoter may be responsible for basal or UPR-independent expression of BiP. A short 170bp portion (bases -170 to -9), which consists of just the ERSEs, should reduce baseline expression but would not capture the PERK arm of the UPR (**Figure 4.1**C). Therefore, we created a novel 195bp promoter portion (bases -195 to -9) by combining the ERSEs and the CRE site to encapsulate all three arms of the UPR (**Figure 4.1**B). The candidate BiP promoters were used to drive expression of the rapidly maturing and brighter variant of GFP, mNeonGreen (Hostettler et al., 2017; Shaner et al., 2013).

In addition to comparing the three variations of the BiP promoter constructs, my objective was to assess whether increasing or decreasing the fluorophore expression stability would yield a more favourable signal-to-noise ratio. To this end, two versions of each construct were created by fusing mNG with either a protein destabilising sequence, proline-glutamate-serine-threonine (PEST) from mouse ornithine decarboxylase (ODC), or WPRE, an mRNA stabilising sequence. PEST targets the fluorescent protein to the proteasome and allows for rapid turnover of mNG to provide a good temporal readout of UPR activation and deactivation in live cells (Corish & Tyler-Smith, 1999; Kitsera et al., 2007). WPRE stabilises fluorophore expression, which allows for a brighter overall mNG signal.

These constructs will hereon be referred to as 500BiP-mNG-PEST, 500BiP-mNG-WPRE, 170BiP-mNG-PEST, 170BiP-mNG-WPRE, 195BiP-mNG-PEST and 195BiP-mNG-WPRE.

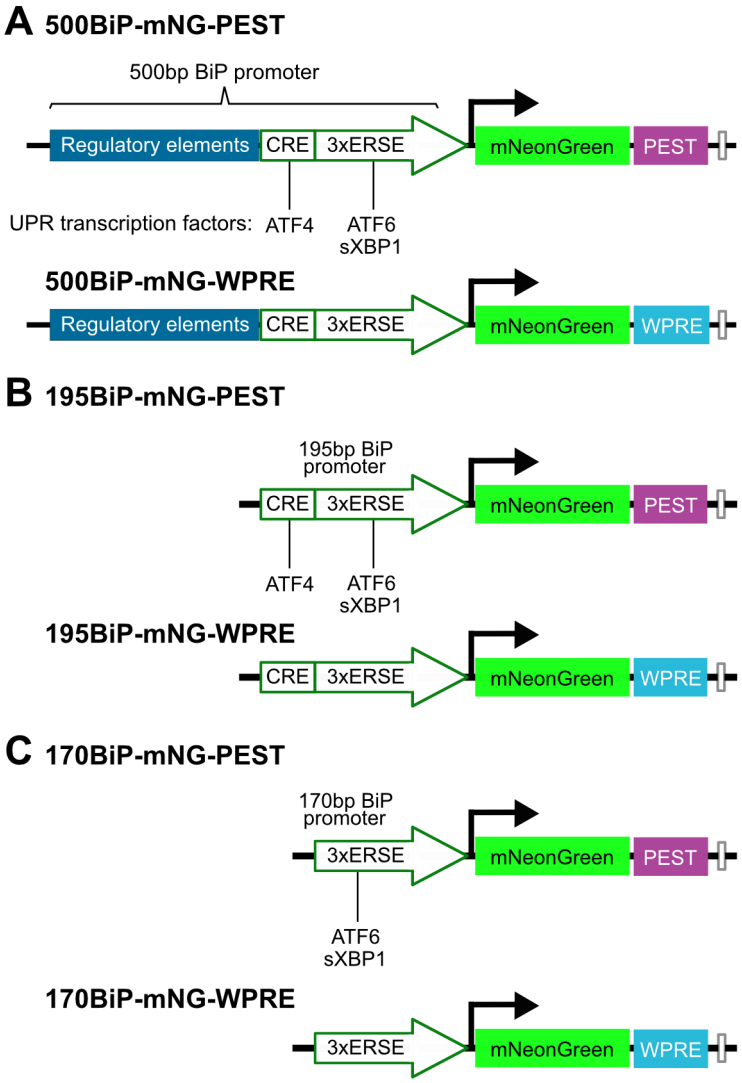

Figure 4.1 Candidate UPR reporter constructs.

(A) Schematic representations of reporter constructs driving expression of mNeonGreen (mNG) using a 500bp portion of the mouse BiP promoter. The ER stress response element (ERSE) binds transcription factors ATF6 and sXBP1, downstream of the ATF6 and IRE1 pathways of the UPR respectively. The CRE element binds transcription factor ATF4, downstream of the PERK pathway of the UPR. The other regulatory elements respond to other transcription factors, likely responsible for non-UPR related expression of BiP. Each construct was developed as a version encoding mNG fused to PEST, a destabilising element (top), and a version encoding mNG fused to WPRE, a stabilising element (bottom). **(B)** Reporter constructs using a 195bp portion of the BiP promoter, which contains specifically the response elements to transcription factors downstream of all three arms of the UPR. **(C)** Reporter constructs using a 170bp portion of the BiP promoter, which contains only the ERSEs.

Treatment with pharmacological inducers of ER stress such as Tunicamycin (TUN), an N-linked glycosylation inhibitor that disrupts protein folding in the ER (Heifetz et al., 1979), have been widely used to elicit and study the UPR. Therefore, to assess the candidate reporters' responses to UPR induction, NIH3T3 mouse fibroblast cells were co-transfected with one of the reporter constructs and a control CAG-mCherry plasmid to enable automatic cell segmentation on an UPR-independent channel for quantification of reporter fluorescence. The cells were then treated with either 1:1000 DMSO vehicle (VEH) or different doses of Tunicamycin (TUN) for 20 hours, after which they were fixed with PFA and imaged to quantify reporter fluorescence (**Figure 4.2**A). Each of the candidate BiP-based reporter constructs showed a dose-related increase in green fluorescence in response to TUN treatment (**Figure 4.2**B). Although the WPRE constructs had higher overall mNG fluorescence levels, the fold-induction was consistently lower compared to the corresponding PEST constructs, due to reduced rates of fluorophore turnover and high baseline expression with VEH treatment (**Figure 4.2**A). Therefore, the WPRE constructs were ruled out for use as sensitive UPR reporters.

Out of the PEST constructs, 500BiP-mNG-PEST showed the lowest fold-induction across all doses of TUN due to a high baseline level of mNG fluorescence with VEH treatment (**Figure 4.2**A top). The responses with 170BiP-mNG-PEST and 195BiP-mNG-PEST showed improved signal-to-noise due to lower baseline mNG fluorescence. While the 170BiP-mNG-PEST response plateaued for the 0.5 µg/ml and 2 µg/ml TUN doses, 195BiP-mNG-PEST was able to capture a difference between the highest two doses (**Figure 4.2**B). Thus, the 195bp BiP promoter segment offered the greatest dynamic range for UPR detection, justifying its selection as the promoter of choice for the final reporter construct.

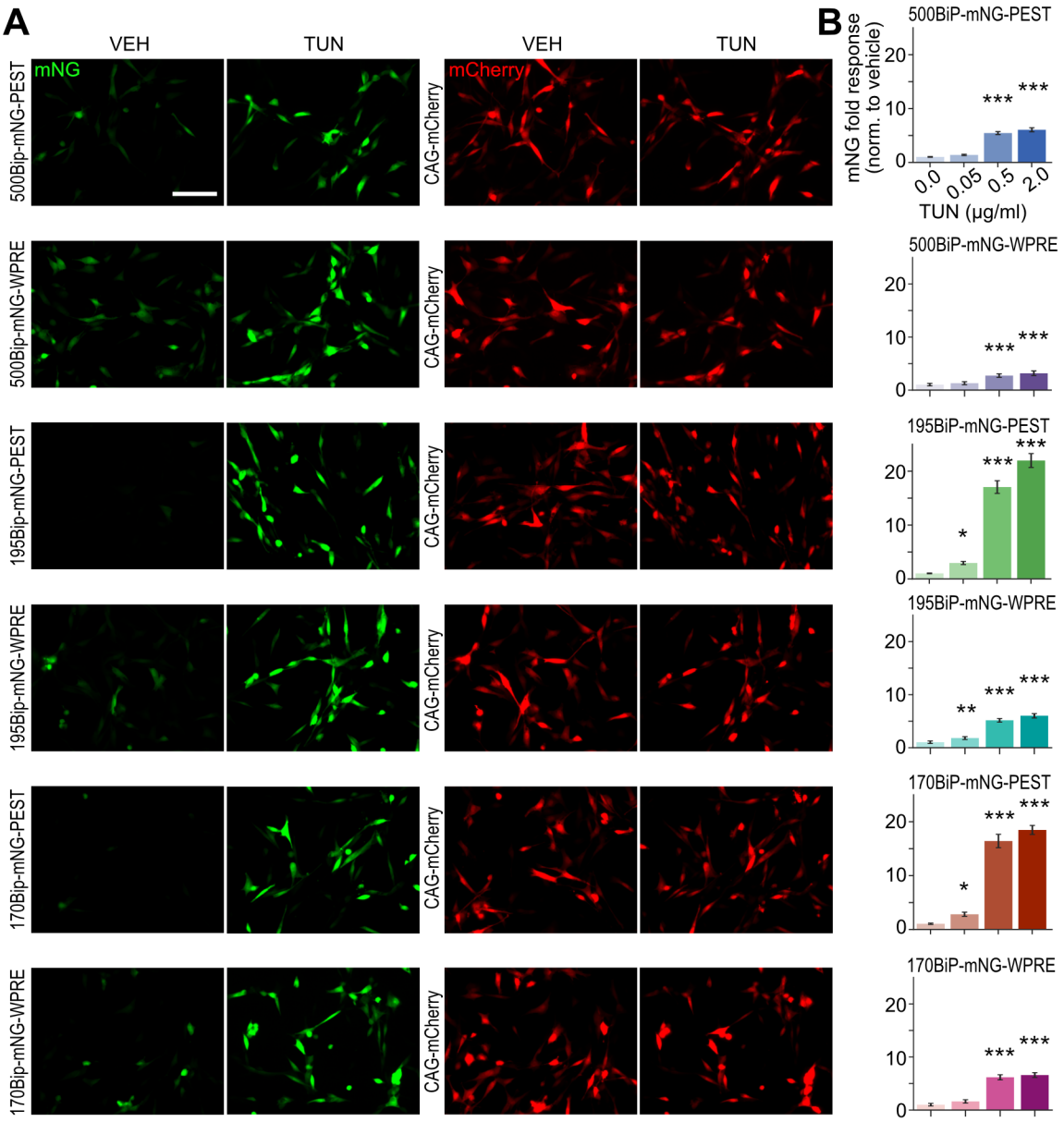

Figure 4.2 A 195bp fragment of the BiP promoter captures the UPR with a large dynamic range.

(A) NIH3T3 cells were co-transfected with one of the candidate BiP promoter constructs and a separate CAG-mCherry plasmid, for cell detection, and treated with DMSO vehicle (1:1000) or a range of Tunicamycin doses for 20 hours. Images show fields of view (FOVs) of cells treated with 2 µg/ml TUN (scalebar 100 µm). **(B)** Mean mNG fluorescence intensity relative to vehicle from cells that were transfected with the respective BiP promoter constructs and treated with VEH or different doses of TUN for 20 hours. mNG expression was induced by 0.5 µg/ml and 2 µg/ml Tunicamycin across all constructs (n=24 FOVs from three experiments; $p<0.001$, Dunn's multiple comparisons tests comparing to vehicle, following significant Kruskal Wallis tests). The WPRE constructs consistently showed smaller responses compared to the PEST constructs. The 195BiP-mNG-PEST showed a difference in response between 0.5 µg/ml and 2 µg/ml TUN (n=24 FOVs from three experiments; $p=0.0033$, Mann Whitney U with Bonferroni correction). However, there was no difference between the responses of the 500BiP-mNG-PEST or 170BiP-mNG-PEST constructs to 0.5 µg/ml and 2 µg/ml TUN ($p=0.2856$ and $p=0.3298$ respectively, Mann Whitney U with Bonferroni correction). The 195BiP-mNG-PEST response to 2 µg/ml TUN was greater than the 500bp construct ($p<0.001$, Mann Whitney U test) and the 170bp construct ($p=0.0173$, Mann Whitney U test).

Next, it was important to confirm that the 195bp BiP promoter did not interfere with endogenous UPR activation mechanisms. To assess this, NIH3T3 cells were transfected with 195BiP-mNG-PEST or a control CAG-GFP-WPRE construct and treated with TUN or VEH. Since endogenous BiP protein levels are also known to be upregulated upon UPR activation, cells were immunostained with an anti-KDEL antibody to detect BiP protein (**Figure 4.3**A; see Chapter 3 section **2.3.2** for antibody selection). The BiP fluorescence was upregulated with TUN relative to VEH, and did not differ between cells expressing sUPRa and the control construct (**Figure 4.3**B). Therefore, the 195bp BiP promoter does not appear to alter endogenous UPR activation processes.

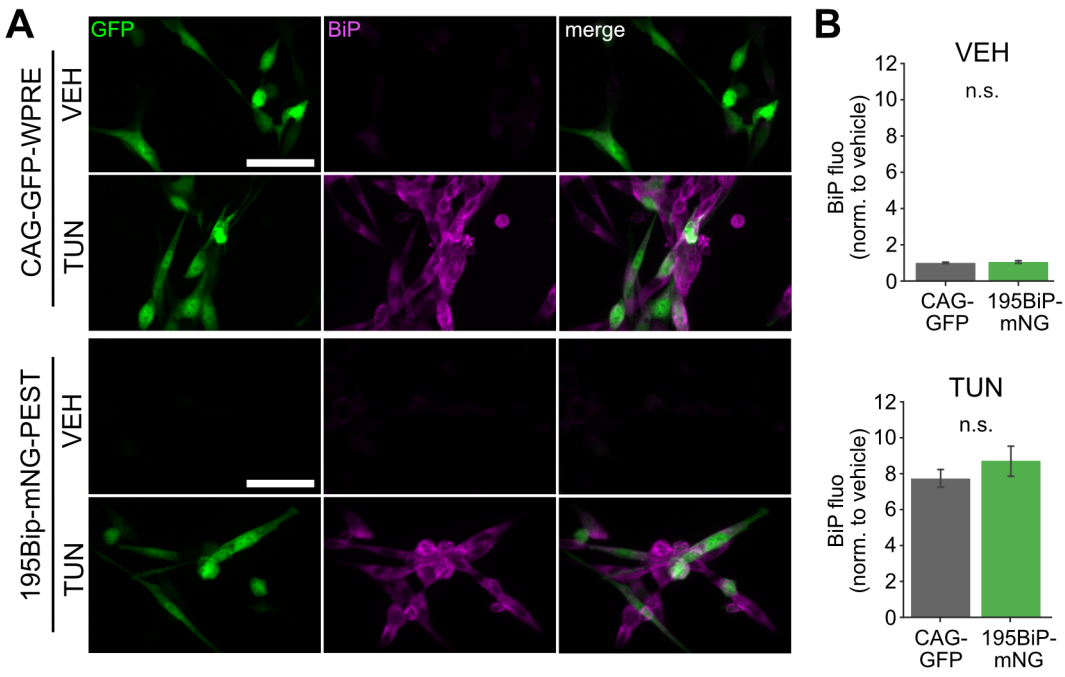

Figure 4.3 BiP promoter construct does not interfere with UPR activation.

(A) NIH3T3 cells were transfected with either 195BiP-mNG-PEST or a control CAG-GFP-WPRE plasmid, and treated with VEH or 2 µg/ml TUN for 20 hours, after which they were immunostained with an anti-KDEL antibody to detect endogenous BiP protein expression (scalebar 50 µm). **(B)** There was no difference in BiP protein level with VEH treatment or with TUN between the two plasmids (n=16-24 FOVs; VEH p=0.5049, TUN p=0.0748, *t* tests).

4.3.2 Designing a dual-colour fluorescent sensor of UPR activity (sUPRa)

Having designed and characterised the UPR-sensing portion of the reporter using a 195bp BiP promoter, the next step was to incorporate a second, red fluorophore into the construct to be driven by a UPR-independent constitutively active promoter. This would provide a stable red signal to which the UPR-dependent green signal could be normalised, in order to control for cell-to-cell variance in DNA copy number and morphology. The red fluorophore would also ensure the unbiased detection of cells expressing the construct, even when green fluorescence is too low to be detected.

We chose mScarlet (mSc) as the second fluorophore, given its good spectral separation from mNG, fast maturation, and superior brightness compared to other RFPs (Fenno et al., 2014). A constitutively active promoter called 'nEF' was selected to drive the expression of mSc. nEF is a chimeric EF1α/HTLV promoter, which has been reported to be well-expressed in the nervous system and is compact enough to fit within the size limitations of the construct's AAV backbone (Fenno et al., 2020). mSc expression was maximised by incorporating the combined WPRE/ SV40 early/late polyadenylation signal sequence, W3SL, to maintain expression stability and minimise alterations in response to cell conditions (Choi et al., 2014). We combined these elements to construct a plasmid encoding mScarlet-W3SL downstream of the nEF promoter (nEF-mSc-W3SL).

Starting with separate plasmids for the BiP promoter construct and the nEF promoter construct (**Figure 4.4**A), we created different versions of a dual promoter construct combining the BiP and nEF components in different configurations (**Figure 4.4**B-E). To compare the performance of the different configurations, NIH3T3 cells were transfected with either the two separate plasmid constructs, 195BiP-mNG-PEST or nEF-mSc-W3SL, or one of the variants of the dual-promoter constructs, and treated with either VEH or TUN (2 µg/ml) for 20 hours. For each individual cell, the mNG fluorescence was normalised to its corresponding mSc fluorescence (mNG:mSc). While all the configurations displayed a mNG response to TUN relative to VEH and no change in mSc expression, they showed varying degrees of fluorophore expression levels both at baseline and with UPR

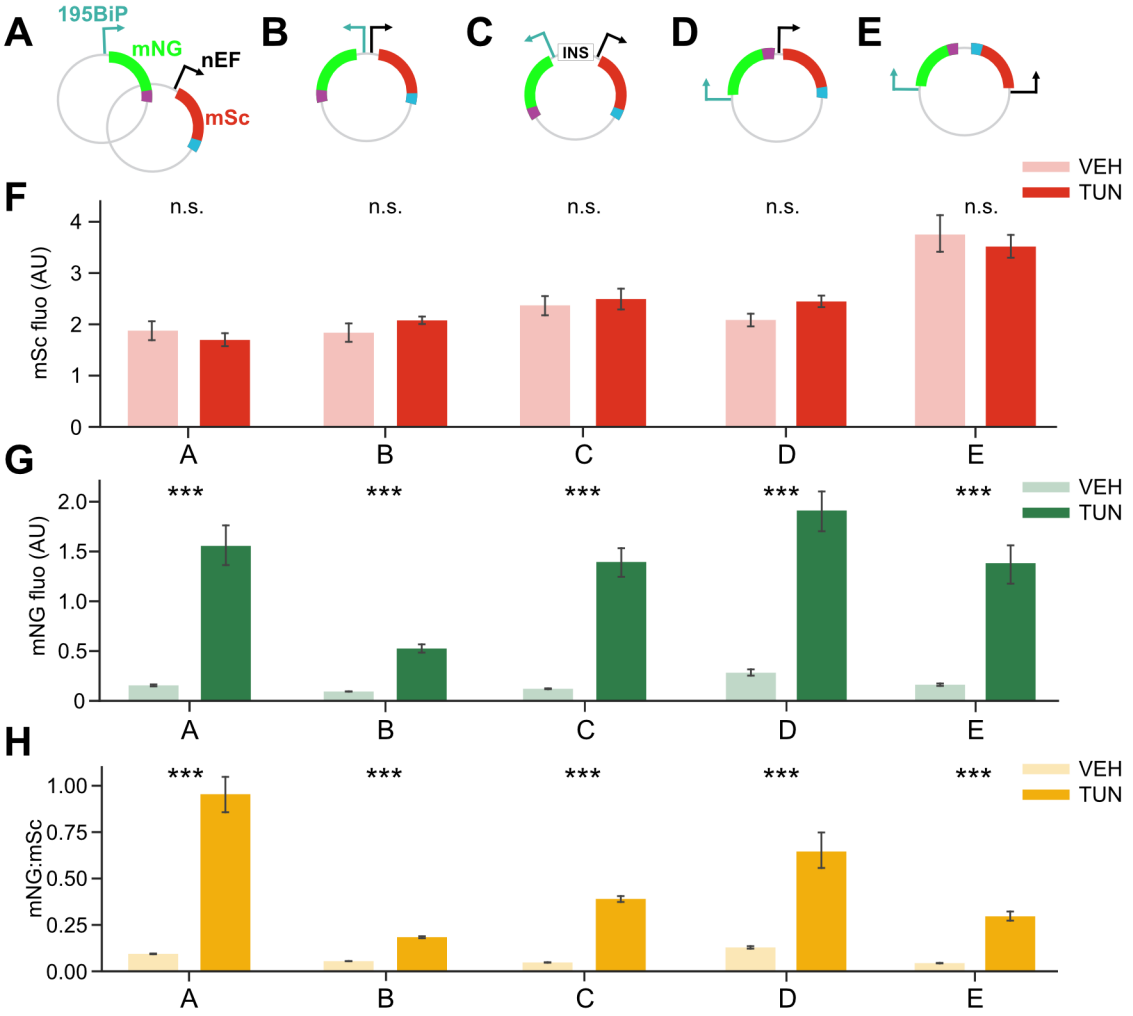

Figure 4.4 Designing a dual colour UPR reporter construct and optimizing the orientation of promoter sequences.

(A) Schematic diagram of two separate plasmid constructs, 195BiP-mNG-PEST and nEF-mSc-W3SL, that were combined to form dual colour constructs. The red fluorescent construct consists of mScarlet, mSc, fused to a W3SL mRNA stabilization sequence, downstream of a nEF promoter, which is a constitutively active EF1α promoter. **(B)** A candidate dual colour construct using a back-to-back promoter configuration. **(C)** A candidate construct using a back-to-back promoter configuration separated by an insulator (INS) sequence. **(D)** A candidate construct with promoters arranged one after the other. **(E)** A candidate construct with promoters facing each other. NIH3T3 cells were transfected with one of the construct variants shown in '**A**' to '**E**' and treated with either VEH or 2 µg/ml TUN for 20 hours, then fixed and imaged. **(F)** mSc fluorescence did not differ significantly between VEH and TUN treatments for all construct variants (n=8 FOVs from one experiment; $p>0.05$, *t* tests). **(G)** mNG fluorescence was significantly increased with TUN for all construct variants (n=8 FOVs from one experiment; $p<0.001$, *t* tests). **(H)** mNG:mSc fluorescence ratio is significantly increased with TUN for all construct variants (n=8 FOVs from one experiment; $p<0.001$, *t* tests).

induction. Among the dual promoter constructs, there was a noticeable trend where configuration D exhibited the most intense mNG fluorescence following TUN treatment (1.9 ± 0.23 AU), and therefore, the highest mNG:mSc ratio (0.64 ± 0.11 AU). A bright reporter is well-suited for expression in dense tissue, such as the brain. Therefore, configuration D was selected as the final dual-colour UPR reporter, and I named it "sUPRa" (sensor of UPR activity).

The mSc fluorescence of sUPRa showed no significant differences in response to a 20-hour treatment with 0.5 µg/ml TUN when compared to the VEH treatment (**Figure 4.5**B,C). In contrast, sUPRa's mNG fluorescence demonstrated an increase with TUN treatment (0.52 ± 0.05 AU) compared to VEH (0.09 ± 0.01 AU; **Figure 4.5**D). The ratio of mNG:mSc was observed to increase by ~400% with TUN (0.29 ± 0.02) compared to VEH (0.07 ± 0.005; **Figure 4.5**E). These findings illustrate that sUPRa's ratio response is a robust measure to quantify UPR activation.

Next, I evaluated whether sUPRa can be considered to be truly ratiometric. If truly ratiometric, sUPRa's expression levels should not have an effect on sUPRa's response to a given dose of TUN (mNG:mSc). To determine this, cells treated with VEH or TUN were categorised by percentiles of mSc fluorescence intensity, which reflects the total DNA load and expression level of sUPRa per cell. It was observed that the level of mSc fluorescence had an impact on the mNG:mSc ratio response of sUPRa with TUN (**Figure 4.5**F). Specifically, higher levels of mSc expression correlated with a greater sUPRa response, suggesting that sUPRa cannot be regarded as truly ratiometric. Nonetheless, the mSc signal plays a significant role in cell identification, and normalising the mNG signal can compensate for certain aspects of cell-to-cell variation in reporter expression levels.

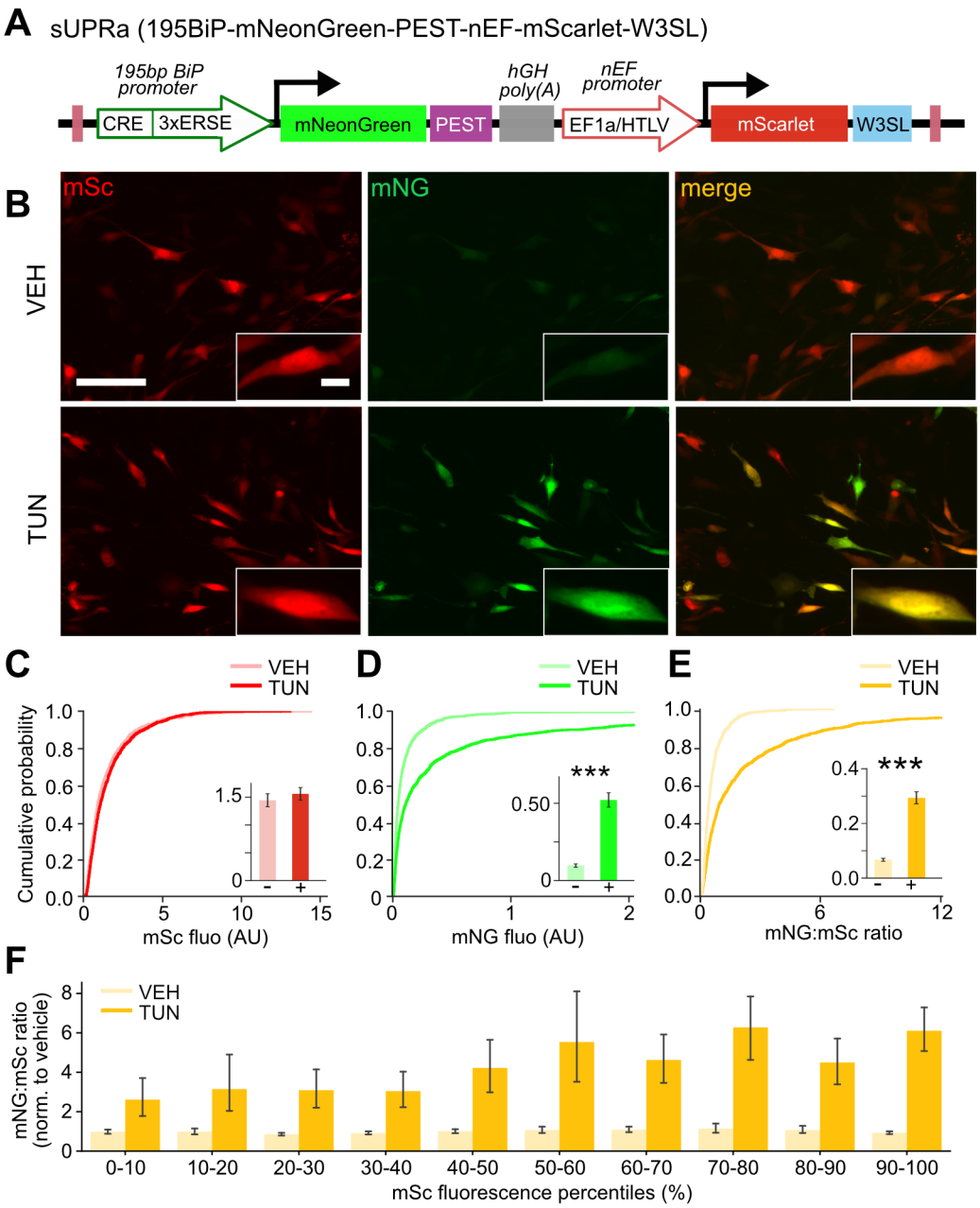

Figure 4.5 sUPRa, a dual colour fluorescent reporter designed to detect global UPR activation.

(A) sUPRa encodes for a bright and rapidly maturing green fluorophore, mNeonGreen (mNG), under the control of a 195bp portion of the BiP promoter. In addition, sUPRa also encodes for a constitutively expressed red fluorophore, mScarlet (mSc), under the control of a Ef1α-based promoter. **(B)** NIH3T3 mouse fibroblasts were transfected with sUPRa and treated with either DMSO vehicle (1:1000) or Tunicamycin (0.5 µg/ml) for 20 hours. Images show representative fields of view of cells (scalebar 100 µm) with an inset of a single cell (scalebar 10 µm). **(C)** Cumulative distribution of mSc fluorescence of all cells. Bar plots (inset) showing mean ± SEM. mSc fluorescence was not altered with 0.5 µg/ml Tunicamycin (TUN) treatment relative to vehicle (VEH)(n=27 FOVs from three experiments; p=0.4833, *t* test). **(D)** Cumulative distribution and bar plot showing that mean mNG fluorescence is increased by 4-fold with TUN relative to VEH (n=27 FOVs from three experiments; p<0.001, Mann-Whitney U test). **(E)** Similarly, mean mNG:mSc ratio also increased by 4-fold with TUN relative to VEH (n=27 FOVs, from three experiments; p<0.001, Mann-Whitney U test). **(F)** All cells from '**E**' grouped by percentiles of mSc fluorescence intensity show an effect of mSc fluorescence on the mNG:mSc ratio response of sUPRa with TUN (p<0.001, Kruskal Wallis test) but not with VEH (p=0.4731, Kruskal Wallis test).

4.3.3 sUPRa response to UPR activation is highly sensitive and dose-related

In order to benchmark sUPRa's ability to detect UPR activation, I compared sUPRa's response sensitivity to previously published fluorescent reporters of single arms of the UPR, XBP1-Venus (pCax-F–XBP1ΔDBD-Venus)(Iwawaki et al., 2004) and SPOTlight (Helseth et al., 2021). XBP1-Venus is specific for the IRE1 arm of the UPR and expresses the green Venus protein under ER stress conditions. Meanwhile, SPOTlight is a ratiometric fluorescent reporter for the PERK arm of the UPR, which expresses higher tdTomato and lower EGFP under ER stress conditions (high phosphorylated eIF2α) (Helseth et al., 2021).

NIH3T3 cells were transfected with either sUPRa, XBP1-Venus or SPOTlight. Since XBP1-Venus provides only a green fluorescence readout, these cells were co-transfected with equal amounts of nEF-mScarlet-W3SL plasmid for automated cell detection. To activate the UPR, cells were treated for 20 hours with different concentrations of TUN (0.05, 0.1, 0.5, 1.0, 1.5, 2.0 μg/ml) or VEH. Consistent with previous work, the tdTomato expression from SPOTlight was low and therefore required amplification with an anti-RFP antibody (Helseth et al., 2021) (**Figure 4.6**A). Subsequently, the fluorescence response of each reporter was quantified. For sUPRa, the response was defined as the ratio of mNG:mSc fluorescence. For XBP1-Venus, the response was defined as the relative change in Venus fluorescence. For SPOTlight, the response was defined as the ratio of tdTomato:EGFP fluorescence. Reporter responses with TUN were normalised to VEH.

All three reporters showed an increase in response with the maximal dose of Tunicamycin, (2 μg/ml) relative to vehicle (**Figure 4.6**A). sUPRa's response (8.51 ± 0.54 AU) was ~two-fold greater than the XBP1-Venus response (4.37 ± 0.25 AU) and more than six-fold greater than the SPOTlight response (1.35 ± 0.08 AU; **Figure 4.6**B). The three reporters showed varying degrees of dose-related responses to Tunicamycin (**Figure 4.6**C). sUPRa had the biggest dynamic range, and displayed the highest responses relative to VEH across all doses compared to XBP1-Venus and SPOTlight. Taken

together, these results suggest that sUPRa provides a superior signal-to-noise ratio in comparison to two of the single-arm UPR reporter constructs.

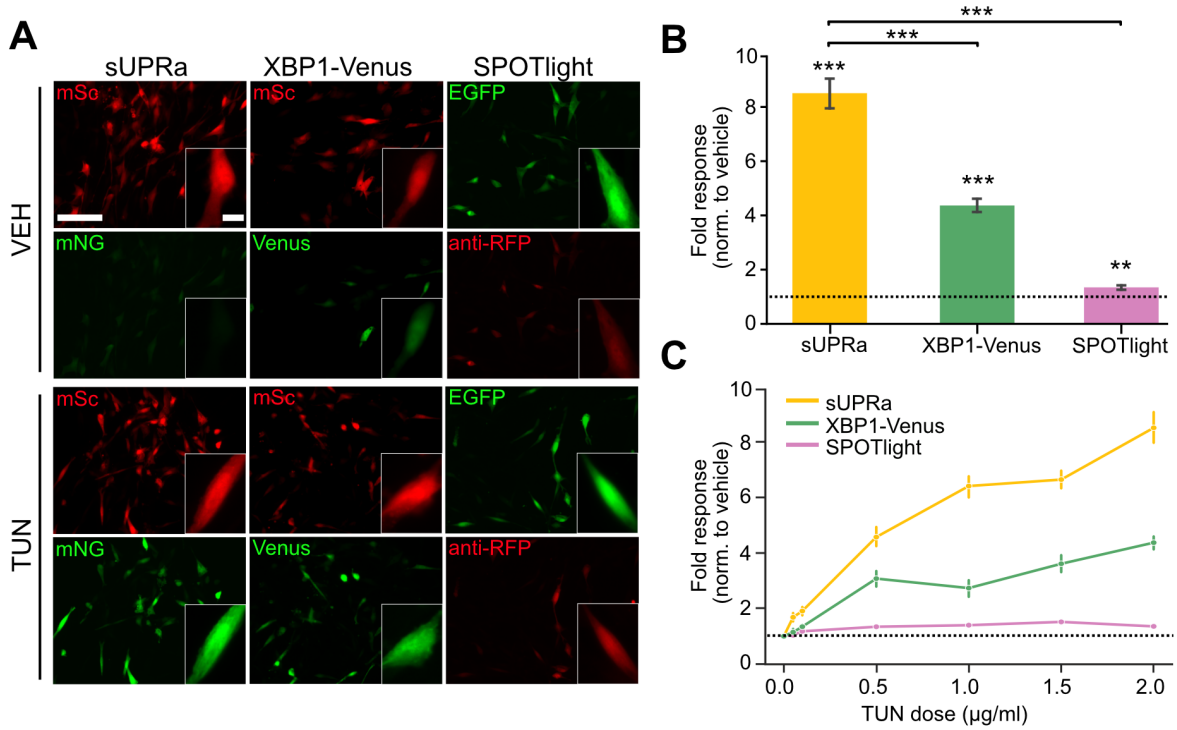

Figure 4.6 sUPRa exhibits dose-related responses and greater sensitivity than single arm UPR reporters.

(A) NIH3T3 cells were transfected with either sUPRa, XBP1-Venus or SPOTlight, and treated with VEH or 2 µg/ml TUN for 20 hours. SPOTlight-expressing cells were immunostained with an anti-RFP antibody to amplify the construct's tdTomato signal. Images show representative fields of view of cells (scalebar 100 µm) with an inset of a single cell (scalebar 10 µm). **(B)** All three reporters showed a response to 2 µg/ml TUN relative to VEH (n=16-24 FOVs from at least two experiments; p<0.001, Mann-Whitney U tests). sUPRa showed the greatest response compared to XBP1-Venus and SPOTlight (n=16-24 FOVs from 2-3 experiments; p<0.001, Mann-Whitney U tests). sUPRa response is the ratio of mNG to mSc fluorescence; XBP1-Venus response is Venus fluorescence; SPOTlight response is the ratio of anti-RFP to EGFP fluorescence. **(C)** Responses induced by a series of different TUN doses (0, 0.05, 0.1, 0.5, 1 and 2µg/ml) relative to VEH for each reporter construct (data represented as mean ± SEM from n=16-24 FOVs from at least two experiments). All reporters showed a dose-related response to the range of Tunicamycin doses (0, 0.05, 0.1, 0.5, 1 and 2µg/ml) relative to vehicle (p<0.001, Kruskal-Wallis test for dose effect). sUPRa exhibits a greater response than XBP1-Venus and SPOTlight at all TUN doses (p<0.05, Mann Whitney U tests with Bonferroni correction).

4.3.4 sUPRa provides a route to monitor UPR temporal dynamics

In addition to reporting UPR activation at a given timepoint, sUPRa also offers an opportunity to monitor the dynamics of UPR activation and recovery. To investigate this, I compared sUPRa and XBP1-Venus in terms of their ability to report induction and recovery from a short UPR activation. Cells were exposed to VEH or 2 µg/ml TUN for a 2-hour period, and then fixed after 0, 2, 6, 12, 24, 48 or 72 hours (**Figure 4.7**A). In response to this transient UPR activation, both sUPRa and

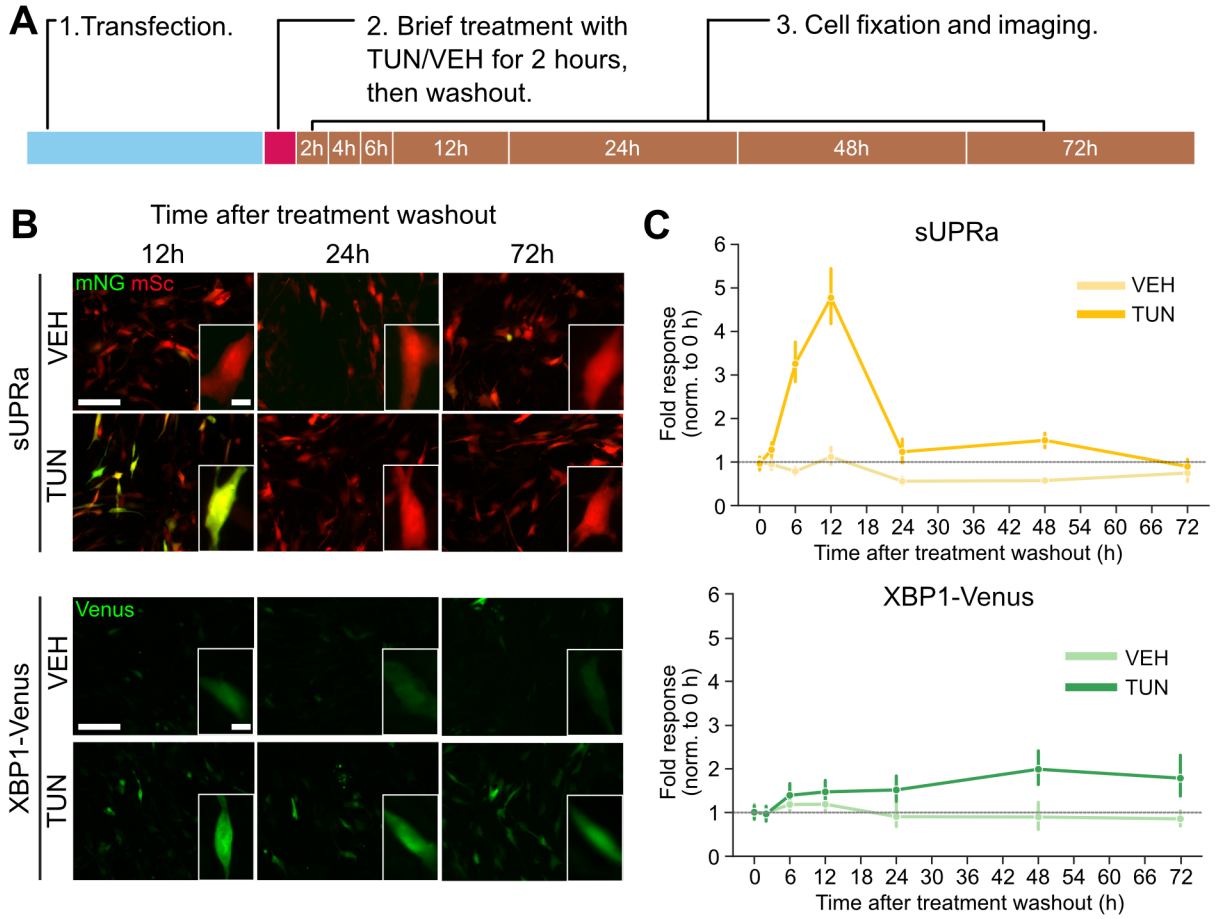

Figure 4.7 sUPRa displays superior ON/OFF dynamics in response to transient ER stress induction.

(A) NIH3T3 cells expressing either sUPRa or XBP1-Venus were treated with VEH or 2 µg/ml TUN for 2 hours. The treatment was then washed out and cells were fixed and imaged at different timepoints after washout. **(B)** Images show representative fields of view of cells (scalebar 100 µm) with an inset of a single cell (scalebar 10 µm) expressing sUPRa (top) and XBP1-Venus (bottom) at 12, 24 and 72 h after treatment washout. **(C)** Response dynamics of sUPRa (top) and XBP1-Venus (bottom) relative to 0h after washout (data represented as mean ± SEM from n=24 FOVs from three experiments per timepoint). sUPRa response to TUN peaked at 12 hours post-washout and returned to baseline by 24 hours post-washout ($p<0.001$, 2-way ANOVA for timepoint and treatment effect; $p<0.001$ comparing 0 h and 12 h and $p=0.9$ comparing 0 h and 24 h, post hoc Tukey HSD). XBP1-Venus response remained high 72 hours after treatment washout ($p<0.001$, 2-way ANOVA for timepoint and treatment effect; $p=0.0135$ comparing 0 h and 72 h, post hoc Tukey HSD). sUPRa exhibited a faster and larger peak response and a faster recovery to baseline than XBP1-Venus.

XBP1-Venus displayed a timepoint and treatment-dependent increase in response (**Figure 4.7**B), suggesting that they are sufficiently sensitive to report the UPR that had been elicited during a period of 2 hours. sUPRa exhibited a faster and larger peak response and a faster recovery to baseline than XBP1-Venus. sUPRa response to TUN peaked at 12 hours post-treatment (4.71 ± 0.26 AU) and returned to baseline by 24 hours post-treatment (1.19 ± 0.09 AU). XBP1-Venus response was slower to peak at 48 hours (1.96 ± 0.11 AU) and remained high 72 hours after treatment. Thus, sUPRa proved to be more effective in providing a readout of the dynamics of UPR onset and offset.

4.3.5 sUPRa responds to UPR induction by other ER stressors, including misfolded proteins

ER stress can be caused by various factors that may elicit the three arms of the UPR differently. Having established that sUPRa reports UPR activation by Tunicamycin, an N-glycosylation inhibitor, I next wanted to confirm that sUPRa can detect UPR activation that is elicited by different stimuli. There are a number of other well-characterised pharmacological inducers of the UPR, such as Thapsigargin (Thaps), an inhibitor of the sarco/endoplasmic reticulum Ca2+ ATPase (SERCA), and L-azetidine-2-carboxylic acid (AZC), a proline analogue known to induce protein aggregation in the ER (Krebs et al., 2015; Roest et al., 2018; Rubenstein, 2000; Thastrup et al., 1990). To investigate whether sUPRa responds to these different ER stress inducers, NIH3T3 cells were transfected with sUPRa and treated with either 25 nM Thaps, 0.5 mM AZC, or the appropriate vehicle for 20 hours (**Figure 4.8**A,C). Both Thaps and AZC treated cells exhibited a ~four-fold sUPRa response relative to vehicle (**Figure 4.8**B,D). These findings demonstrate that sUPRa is capable of responding to UPR activation by a variety of ER stress-inducing agents.

Whilst the aforementioned pharmacological agents have been well-established to induce the UPR indirectly by altering ER function and resulting in misfolded proteins, they are also likely to induce pleiotropic effects. An alternative drug-free approach to directly induce the UPR in a cell-targeted way involves delivering genetic constructs encoding misfolded proteins. Such genetic tools

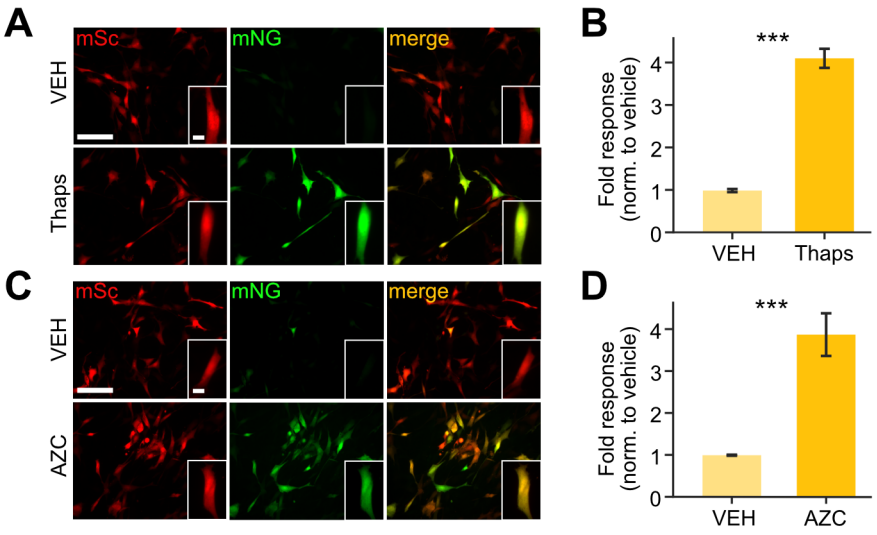

Figure 4.8 sUPRa responds to different forms of pharmacological ER stress induction.

(A) NIH3T3 cells transfected with sUPRa were treated with either Thapsigargin (Thaps), a SERCA pump blocker, or VEH (DMSO 1:1000). **(B)** ER stress induction with Thaps produced more than a 4-fold increase in sUPRa response relative to VEH (n=17 FOVs from two experiments; p<0.001, *t* test). **(C)** Cells expressing sUPRa were treated with either L-Azetidine carboxylic acid (AZC), a proline analogue and inducer of protein misfolding, or VEH (dH_2O). **(D)** ER stress induction with AZC also produced a ~4-fold increase in sUPRa response relative to VEH (n=17 FOVs from two experiments; p<0.001, *t* test).

have been well characterised and shown to induce a physiological and more specific UPR than pharmacological ER stressors (Bakunts et al., 2017; Bergmann et al., 2018). To test whether sUPRa reports UPR induction caused by misfolded proteins, sUPRa-expressing cells were co-transfected with either a misfolded polypeptide construct or a control folded polypeptide construct and fixed 48 hours after transfection. I tested a misfolded variant of pancreatic β-secretase, BACE457, and its soluble variant, BACE457Δ, which are retained in the ER in an immature state (Molinari et al., 2002). The effects were compared directly to control cells expressing a correctly folded serine protease inhibitor, $\alpha1AT_M$, which matures in the ER and is released (Merulla et al., 2015) (**Figure 4.9**A). The polypeptides incorporate an HA-tag sequence, therefore, their expression was confirmed using a HA-tag antibody (**Figure 4.9**B). Compared to $\alpha1AT_M$, sUPRa's ratio response showed a 10.51 ± 1.13 and 16.13 ± 1.56 fold-increase with BACE457 and BACE457Δ, respectively (**Figure 4.9**C). This demonstrates that sUPRa is capable of detecting the UPR caused by a direct accumulation of misfolded proteins in the ER.

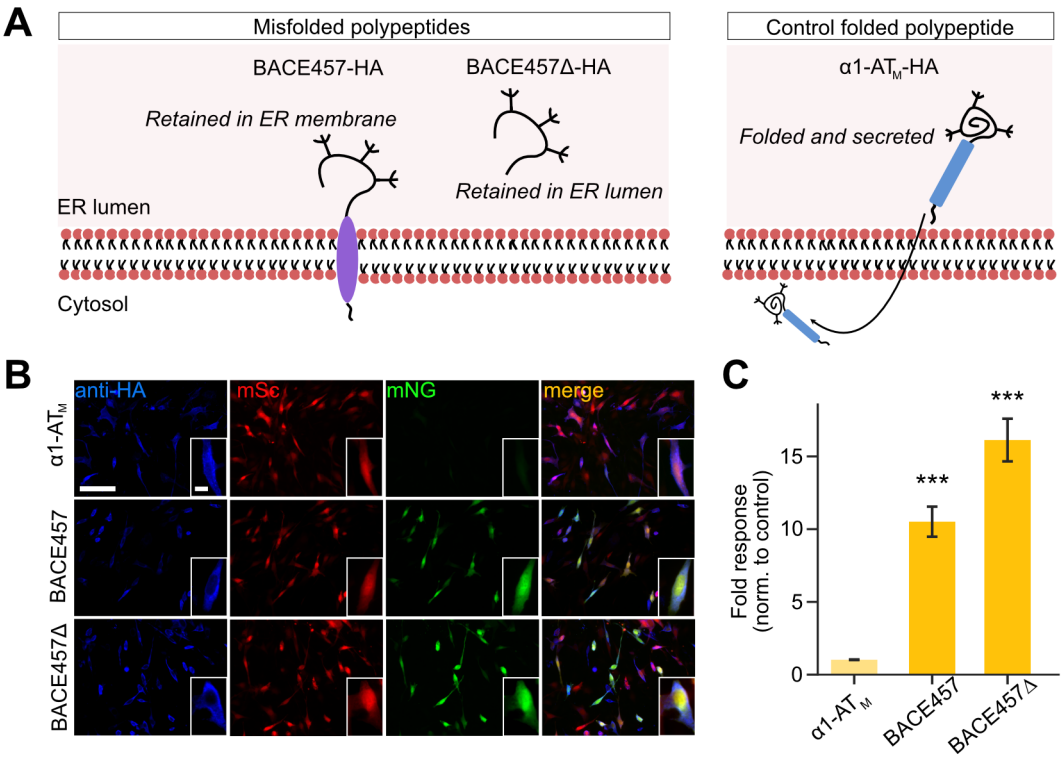

Figure 4.9 sUPRa responds to ER stress induction caused by the expression of misfolded polypeptides retained in the ER.

(A) ER stress and the UPR were induced in NIH3T3 cells by the expression of mutant misfolded polypeptides (left), which are retained in the ER membrane (BACE457) or ER lumen (BACE457Δ). Control cells expressed a folded polypeptide that does not accumulate in the ER (α1-AT_M). Cells were fixed for imaging 48 hours after transfection. **(B)** Images show representative fields of view of cells (scalebar 100 µm) with an inset of a single cell (scalebar 10 µm) co-expressing sUPRa and the polypeptides shown in '**A**'. An anti-HA antibody was used to detect polypeptide expression. **(C)** sUPRa shows more than a 10-fold response to both forms of misfolded polypeptide relative to the control polypeptide, with the ER luminal polypeptide, BACE457Δ, inducing the strongest UPR response (n=24 FOVs from three experiments; $p<0.001$, Mann Whitney U tests).

4.4 Discussion

To better understand the contribution of the UPR in physiological and pathological processes, it is important to be able to detect and monitor the UPR in individual cells with high sensitivity and temporal resolution. In this chapter, I presented a novel dual colour fluorescent reporter, sUPRa, that was designed to detect and quantify the global UPR state of individual cells. I demonstrated that sUPRa provides a sensitive and dose-related readout of UPR activation, exhibiting effective onset and offset kinetics as the UPR initiates and then dissipates. sUPRa responded to the UPR elicited by different forms of ER stress, including disruptions to protein folding by inhibition of N-glycosylation or incorporation of a non-amino acid proline analogue, alterations to calcium homeostasis, or the selective expression of misfolded proteins in the ER.

sUPRa incorporates a novel region of the mouse BiP promoter sequence upstream of the transcriptional start site, encompassing ERSE sequences and a CRE/ATF binding site. This enables the construct to report all three arms of UPR signalling that converge on BiP transcriptional upregulation. This sets it apart from previously described reporters that either detect a single arm of the UPR (Clark et al., 2020; Helseth et al., 2021; Iwawaki et al., 2004; F. Walter et al., 2015) or utilise only the ERSE sequence of the rat BiP promoter (Kudo et al., 2008; Lajoie & Snapp, 2011). The selection of the BiP promoter underpins sUPRa's high sensitivity. To test this, sUPRa's performance was benchmarked against reporters of single arms of the UPR. Compared to a reporter of XBP1 splicing downstream of the IRE1 arm (Iwawaki et al., 2004) and a reporter of the PERK arm (Helseth et al., 2021), sUPRa showed superior response properties across a range of UPR activation levels. This is consistent with the idea that transcriptional activation of the BiP promoter downstream of the three UPR arms allows for a cumulative signal that is larger than any one arm alone (Yoshida et al., 2001). Since sUPRa is designed to capture a cell's global UPR, it can be applied to study whether an UPR is elicited under particular conditions, after which the contribution of the individual UPR pathways could be further dissected using other available tools.

A reporter should ideally match the dynamics of its target (Doupé & Perrimon, 2014). Although there was a delay between UPR initiation and the onset of sUPRa response, sUPRa showed a distinct ON-OFF profile of activation in response to a transient UPR activation, which was not evident with the XBP1-Venus reporter. This difference in performance may be attributable to the different kinetics of BiP transcriptional activation and XBP1 splicing, and/or to the stability of the different reporter fluorophores. sUPRa was designed for good ON kinetics by incorporating the rapidly maturing fluorophore, mNG, which has a maturation speed over five-fold faster than other GFPs (Lambert, 2019; Shaner et al., 2013). sUPRa was also designed for improved OFF kinetics by fusing a PEST degradation sequence to mNG, which decreases the fluorophore half-life by an order of magnitude, from approximately twenty hours to two hours (He et al., 2019; X. Li et al., 1998). The greater turnover also means a lower level of baseline expression, which contributes to a better signal-to-noise ratio. Destabilized reporter fluorophores often suffer from a reduction in signal intensity at any given time. However, mNG is a super bright variant of GFP, and the characterisation of sUPRa confirmed that it can provide a strong signal with mild UPR activation. While mNG turnover was increased, mSc was fused to a mRNA stabilisation sequence, to maintain expression stability and minimise alterations in response to cell conditions, providing a stable normalisation signal (S.-J. Li et al., 2018; Zufferey et al., 1999). The combination of these properties enabled sUPRa to closely track UPR activation and recovery in cells. While I used sUPRa imaging to provide readouts of the UPR at discrete timepoints from different cell populations, further experiments are warranted to track the activation and recovery dynamics of the UPR within individual live cells.

As a dual colour reporter, sUPRa was designed to account for cell-to-cell variability in reporter expression levels than can result from differences in copy number, or reflect differences in cell size and morphology. Incorporating a second, spectrally-separate fluorophore under the control of a constitutive promoter provides a readout of reporter copy number per cell. I confirmed that expression of the red monomeric protein mSc does not vary with UPR activation and thus provides a normalisation signal for the quantification of mNG. Importantly, mSc expression also ensures the

unbiased detection of cells exhibiting both high and low levels of UPR for quantification from representative cell samples. It is worth noting that the sUPRa response was not perfectly ratiometric: the greater the level of mSc expression, the greater also sUPRa's mNG:mSc response. The DNA load per cell may be having a combinatorial effect with the TUN-induced UPR to compound sUPRa's mNG response. However, the constitutively expressed red fluorophore still offers an optimisation to the UPR reporter since a mNG:mSc ratio will partly account for high red expression levels by limiting the ratio readout, whereas, a mNG-only readout would give exaggerated responses.

sUPRa successfully responded to UPR activation by various stimuli, which supports its use as a general reporter of global UPR. However, future work could assess sUPRa's specificity to ER stress-induced UPR, by comparing its response to different types of cell stress, such as oxidative stress, DNA damage and heat stress. It is becoming clearer that many other pathways converge on the UPR in response to other cellular stresses, such as the integrated stress response (Costa-Mattioli & Walter, 2020). Moreover, the cellular conditions for other types of cellular stress are often sufficient to disturb ER homeostasis too. Therefore, it will not be surprising if other forms of cellular stress also elicit a sUPRa response.

In summary, the results in this chapter demonstrate sUPRa's utility as a sensitive reporter of the overall UPR with the potential to track UPR dynamics. Having characterised sUPRa in an immortalised cell line, in the next chapter I test its expression in neuronal tissue to assess its usefulness for addressing the relationship between sleep and the physiological UPR.

Chapter 5 Novel reporter responds to UPR activation in neuronal tissue

Contents

5.1 Introduction

In **Chapter 4**, I described a newly developed dual colour fluorescent reporter of UPR activity, sUPRa, and characterised its performance in non-neuronal mouse cells *in vitro*. In order to monitor the UPR in the brain within the sleep-wake cycle, there is a need for a reporter tool that expresses well in neurons and exhibits high sensitivity to physiological UPR activation. Therefore, in this chapter, I characterise sUPRa's performance in neuronal tissue and its response to sleep deprivation.

While single-arm UPR reporters have been used before to investigate neuronal ER stress within disease models, there is a lack of reporters specifically designed for or tested in brain tissue under physiological conditions. For example, the XBP1-Venus transgenic mouse line (Iwawaki et al., 2004) shows systemic expression of the fluorescent reporter across many organs, and was recently shown to be activated in different cell types in the brain with physical brain injury and ischemia (Fan et al., 2023). However, it has not been shown to detect physiologically induced ER stress in the brain, such as with ageing (Iwawaki et al., 2004). The SPOTlight reporter for the PERK arm of the UPR was the first reporter used to identify physiological activation of the stress response in a class of tonically firing cholinergic neurons in the mouse brain (Helseth et al., 2021). However, the SPOTlight response required amplification with an anti-RFP antibody, which makes it unsuitable for monitoring the UPR in live cells over time. Moreover, as shown in **Chapter 4**, neither the XBP1-Venus nor SPOTlight reporters matched sUPRa's high sensitivity to low levels of UPR activation, and single-arm reporters only depict activation of specific arms of the UPR rather than capturing the overall UPR state of a cell.

Expression of reporter constructs in brain tissue can be achieved by a variety of methods. Transgenic mouse lines are a useful non-invasive strategy for reporter expression in different cell types throughout the animal's lifespan (Gama Sosa et al., 2010; Houdebine, 2002). ER stress reporter transgenic mice, such as ER stress-activated indicator (ERAI) mice encoding XBP1-Venus

(Iwawaki et al., 2004) and CARE-Luciferase mice reporting PERK activation (Chaveroux et al., 2015), have been previously used to investigate UPR activation in the context of ischemia and brain injury (Fan et al., 2023; Louessard et al., 2017). However, transgenic mice are expensive and time-consuming to make and maintain, and do not afford the temporal control of transgene expression. An alternative approach is viral vector mediated transduction of adult mouse brain tissue (S.-H. Chen et al., 2019). Adeno-associated viruses (AAVs) are widely used for gene delivery in the nervous system, and offer long-term expression of the transgene without the risk of genome integration mutations (Penaud-Budloo et al., 2008). AAV serotypes, which are determined by the type of capsid protein on the outer shell of the virus, provide specificity in transduction tropism (Burger et al., 2004; C. Wang et al., 2003; Zincarelli et al., 2008). AAV transduction is reported to induce lower levels of immune response compared to retroviruses and lentiviruses (Daya & Berns, 2008), however, viral infection itself may increase baseline levels of UPR (Balakrishnan et al., 2013). A third approach for expressing reporter constructs in mouse brain tissue is via *in vivo* delivery of plasmid DNA. Specifically, *in utero* electroporation can achieve long-term expression of transgenes in specific neuronal populations, by targeting progenitor cells during development (De Vry et al., 2010; Tabata & Nakajima, 2001). This delivery method is associated with minimal disruption of the tissue and is not expected to elicit an immune response, which may make it more suitable for studying the physiological UPR.

AIMS

In this chapter, I investigate the best approach for expressing sUPRa in neuronal tissue and characterise its performance both *ex vivo* and *in vivo*. Based on my findings, I proceed to test whether sUPRa can effectively detect the sleep deprivation-induced UPR in cortical neurons, which I previously demonstrated using immunohistochemistry (**Chapter 2**). Therefore, I aimed to:

1. Test the expression of sUPRa in neuronal tissue with viral transduction and *in utero* electroporation.
2. Characterise sUPRa's response to neuronal UPR activation *ex vivo.*
3. Characterise sUPRa's response to neuronal UPR activation *in vivo* using expression of misfolded proteins and a sleep deprivation paradigm.

5.2 Methods

5.2.1 Mouse organotypic slice culture

Hippocampal or cerebrocortical organotypic slices from C57BL/6J pups were generated according to (Stoppini et al., 1991) and (Bendfeldt et al., 2007) with slight modifications. Pups at postnatal day 5 (P5) to P8 were rapidly decapitated and the brain was removed into freshly prepared ice-cold dissection media containing Earle's balanced salt solution with calcium chloride and magnesium sulphate supplemented with 25.5 mM Hepes, 36.5 mM D-glucose and 5 mM sodium hydroxide. To make hippocampal slices, the hemispheres were separated, and the individual hippocampi were dissected and immediately sectioned into 400 μm thick slices on a McIlwain tissue chopper. To make cortical slices, the hemispheres were separated and the entire cortex along with subcortical structures was sectioned at 400 μm with a McIlwain Tissue Chopper. Slices were placed onto Millicell cell culture inserts (0.4 μm, 30 mm diameter) and were maintained at an interface between air and feeding media (containing 78.8% v/v Gibco Minimum Essential Media with GlutaMAX, 20% heat inactivated horse serum, 1% B27, 30 mm Hepes, 26 mM D-glucose, 5.8 mM sodium bicarbonate, 1 mM calcium chloride, 2 mM magnesium sulphate, and 1% pen/strep containing 10000 units of Penicillin-G, 10 mg Streptomycin and 25 μg Amphotericin B per ml). Slices were incubated at 35 °C in a 5% CO_2 humidified incubator.

5.2.2 Viral transduction of organotypic slices

After 1-5 days in culture, brain slices were transduced with adeno-associated virus (AAV; serotype 1) containing the sUPRa DNA sequence (University of North Carolina Gene Therapy Center Vector Core and Addgene, USA). Organotypic slices were transduced by injecting the AAV solution (mixed with 1% wt/vol fast-green dye for visualisation) into 5-10 locations per slice. Injection pipettes were pulled from glass capillaries (1.2 mm outer diameter, 0.69 mm inner diameter; Warner Instruments) using a horizontal puller (Sutter P-97, USA). Pipettes were filled with AAV solution, mounted on a manual manipulator (M-152, Narishige, Japan) and monitored under a

dissection scope (Leica S6E, Germany) coupled with an external fibre optic light source (Fiber-Lite MI-150, Dolan-Jenner Industries, USA). A Picospritzer III system (IntraCel, UK) was used to deliver controlled pressure pulses (20 psi of 50 ms pulses) to facilitate gradual diffusion of the viral solution into the tissue. Typical viral titres were $\sim 10^{11}$ GC/ml and injection volumes were ~250 nl per slice. Slices were fed with fresh media every two days thereafter and monitored for expression before being used. After 3-5 days of recovery, slices were treated with either Tunicamycin or vehicle (DMSO). Following treatment, slices were fixed overnight at 4 °C in 4% PFA with 4% sucrose, in 0.01 M PBS and mounted onto glass slides using VectaShield mounting medium (Vector labs) for confocal imaging.

5.2.3 Preparation of sUPRa viral DNA for PCR amplification

Stocks of sUPRa-encoding AAV were diluted 1:1000 into 5% Tween-20 in TE buffer. The diluted AAV solution was incubated with 4 units/ml of Proteinase K (stock at 600 units/ml) at 37 °C for 1 hour. The solution was then heat-treated at 95 °C for 20 minutes to denature capsid proteins and release DNA. The final denatured AAV solution was used as the substrate for PCR amplification alongside control sUPRa plasmid DNA using the primers detailed in **Table 5.1**.

Construct region	Primer sequence (5'-3')
AAV ITR – BiP promoter	**Forward primer:** AAV2_ITR_Fwr TGCGGCCGCACGCGTTAG
	Reverse primer: mNeonGreen_rev1 CACCATGTCAAAGTCCACACC
BiP promoter – PEST	**Forward primer**: BiP-mneongreen_Fwr CAACGAGTAGCGACTTCACCA
	Reverse primer: ODC_PEST_Rev TCTCGAGCTACACATTGATCC
mNG – nEF promoter	**Forward primer**: ODC_PEST_Fwr CTGTACAAGCATGGCTTCCCG
	Reverse primer: nEF_Prom_rev CTTCTCGGGGACTGTGGGCGAT
nEF promoter – mSc	**Forward primer**: nEF_Fwr2 CAACGGGTTTGCCGCCAGAAC
	Reverse primer: mScarlet_Rev GTGGGAGGTGATGTCCAAC
mSc – AAV ITR	**Forward primer**: mScarlet_Fwr GTGCTGAAGGGCGACATTAAG
	Reverse primer: AAV2_ITR_W3SL_Rev TTCCTGCGGCCGCTCGGTC

Table 5.1 Primers used for PCR amplification to verify sUPRa construct in AAV vector.

5.2.4 *In utero* electroporation

In utero electroporation (IUE) was performed using standard procedures (Ellender et al., 2019) by Gemma Gothard and Dr Kashif Mahfooz in the Akerman lab. Briefly, pregnant female C57BL/6J mice were anaesthetised using isoflurane and their uterine horns were exposed by midline laparotomy. A mixture of plasmid DNA (1.5 µg/µl) and 0.03% fast-green dye (Sigma-Aldrich) was injected intraventricularly in each embryo through the uterine wall and amniotic sac with a glass micropipette (World Precision Instruments) pulled using a Flaming/Brown Micropipette Puller (Sutter Instrument Company). Plasmid DNA was prepared using the EndoFree Plasmid Kit (Qiagen, Hilden, Germany). The total volume injected per embryo was ~1 µl. Electroporation was performed by placing the anode of a Tweezertrode (Genetronics) over the dorsal telencephalon outside the uterine muscle. Five pulses (50 ms duration separated by 950 ms) at 42 V (at E14.5 and E15.5), 40 V (at E13.5), or 38 V (at E12.5) were delivered with a BTX ECM 830 pulse generator (Genetronics). The uterus was then lavaged with warmed, sterile Hartmann's solution (Dechra Pharmaceuticals) and replaced into the abdomen. The abdominal muscle and skin incision were closed with Vicryl and Prolene sutures (Ethicon). Dams were allowed to recover in a clean cage and litter down naturally. The day of birth was taken as postnatal day (P) 0.

5.2.5 Sleep deprivation and tissue collection

8 week-old male and female C57BL/6J mice from 2 litters that had been *in utero* electroporated with sUPRa were used for sleep deprivation (SD) experiments. The experiment was carried out 1 week after animals were transferred to the holding facility and habituated to being singly housed. SD was performed for 12 hours starting at light onset as described in (V. V. Vyazovskiy et al., 2002). Mouse behaviour and locomotion were constantly monitored, and upon signs of sleepiness the experimenter provided the animal with novel objects. 4 mice (3 males, 1 female) underwent SD whilst 4 control mice (2 males, 2 females) were allowed to sleep undisturbed. Following the 12-hour SD period, mice were injected with a lethal dose of urethane and transcardially perfused with PBS followed by 4% PFA with 4% sucrose, in 0.01 M PBS (pH 7.4), before

tissue collection. Brains were kept in the 4% PFA/sucrose solution at 4 °C for 24 hours before being transferred for storage in 0.05% sodium azide solution (Sigma Aldrich). Coronal sections (50 μm) were cut from each perfusion-fixed brain using a vibrating microtome (Leica VT1000S), and mounted onto glass microscope slides using VectaShield.

5.2.6 Confocal imaging and image analysis

Fluorescence images from fixed mouse brain slices were captured with a LSM 710 confocal microscope using ZEN software. Z-stack images were taken from each slice at intervals of ~1-5 μm. Exposure times were carefully adjusted such that the fluorescence signals were not saturated, and kept constant across all slices. Other settings such as pinhole aperture, optical zoom, laser intensity and dwell time were also kept constant in each experiment. Tile-scan images were taken from a segment of the slice and stitched together. Neurons expressing sUPRa in brain slices were identified on the red mScarlet (mSc) channel using `Cellpose` (Stringer et al., 2020). The segmentation masks generated by `Cellpose` were applied on the mNeonGreen (mNG) channel to obtain a sum fluorescence value for each cell. An averaged background value surrounding the cell masks was subtracted from each cell. There was a range in the level of mSc expression, likely due to the variable copy numbers of plasmids that were retained in each neuron derived from its parent progenitor. To avoid issues with spectral bleed-through from the red into the green signal, neurons with extremely high red expression, which showed a correlation with the green expression, were thresholded out.

5.2.7 Statistical analysis

All data were assessed for normality using the Shapiro Wilk test, following which the appropriate parametric or non-parametric statistical tests were applied. Statistical analyses were performed using the `Scipy` and `Statsmodels` packages in Python. Graphs were generated using `Matplotlib` and `Seaborn` packages in Python. Asterisks represent significant p-values following statistical tests (*$p<0.05$, **$p<0.01$ and ***$p<0.001$). The statistical tests and p-values are detailed in the appropriate figure legends.

5.3 Results

5.3.1 Testing sUPRa's performance with viral gene delivery

Adenovirus-associated viral vectors (AAVs) provide a useful tool for recombinant gene expression both *ex vivo* and *in vivo* with high transduction efficiencies and high levels of expression (S.-H. Chen et al., 2019). AAVs have been widely used to deliver genes to the brain, with serotype 1 producing widespread expression in neuronal and glial cell types (Burger et al., 2004; C. Wang et al., 2003, p. 1; Zincarelli et al., 2008). Therefore, sUPRa was packaged into an AAV 1 capsid (hereon referred to as AAV_1-sUPRa) to be expressed in brain tissue.

First, I evaluated the performance of AAV_1-sUPRa in mouse neuronal tissue. To do this, I used an *ex vivo* preparation of mouse organotypic hippocampal brain slice cultures. These cultures offer an *ex vivo* model system to examine integrated neuronal functions, such as the UPR (Duff et al., 2002; Lacour et al., 2007; Leggett et al., 2012; Shahani et al., 2006), and are amenable to viral transduction (Keir et al., 1999; Wiegert et al., 2017). Slices remain viable in culture for up to two weeks, allowing for long-term monitoring of gene expression (Humpel, 2015; Stoppini et al., 1991). Organotypic brain slices transduced with AAV_1-sUPRa (1:10) and allowed to recover for five days post-viral transduction to ensure adequate expression levels of sUPRa, as judged by mSc fluorescence intensity. After 5 days, slices were incubated with 10 µg/ml Tunicamycin (TUN), a concentration known to induce ER stress in organotypic brain slices (Lacour et al., 2007), or 1:1000 DMSO vehicle (VEH; **Figure 5.1**A,B). Slices were fixed 24 hours after treatment onset and imaged to quantify sUPRa's response. Upon visual inspection, sUPRa was primarily expressed in neurons, but was also present in putative glial cells. All cells expressing sUPRa were quantified. Cells from TUN-treated slices showed a reduction in mSc fluorescence to 0.70 ± 0.04 fold compared to VEH-treated cells (**Figure 5.1**C, left). On the contrary, sUPRa's mNG expression was 9.06 ± 1.07 fold greater with TUN compared to VEH treatment (**Figure 5.1**C, middle). Therefore, sUPRa's ratio response (mNG:mSc) was 12.63 ± 1.16 fold greater with TUN compared to VEH treatment (**Figure 5.1**C, right).

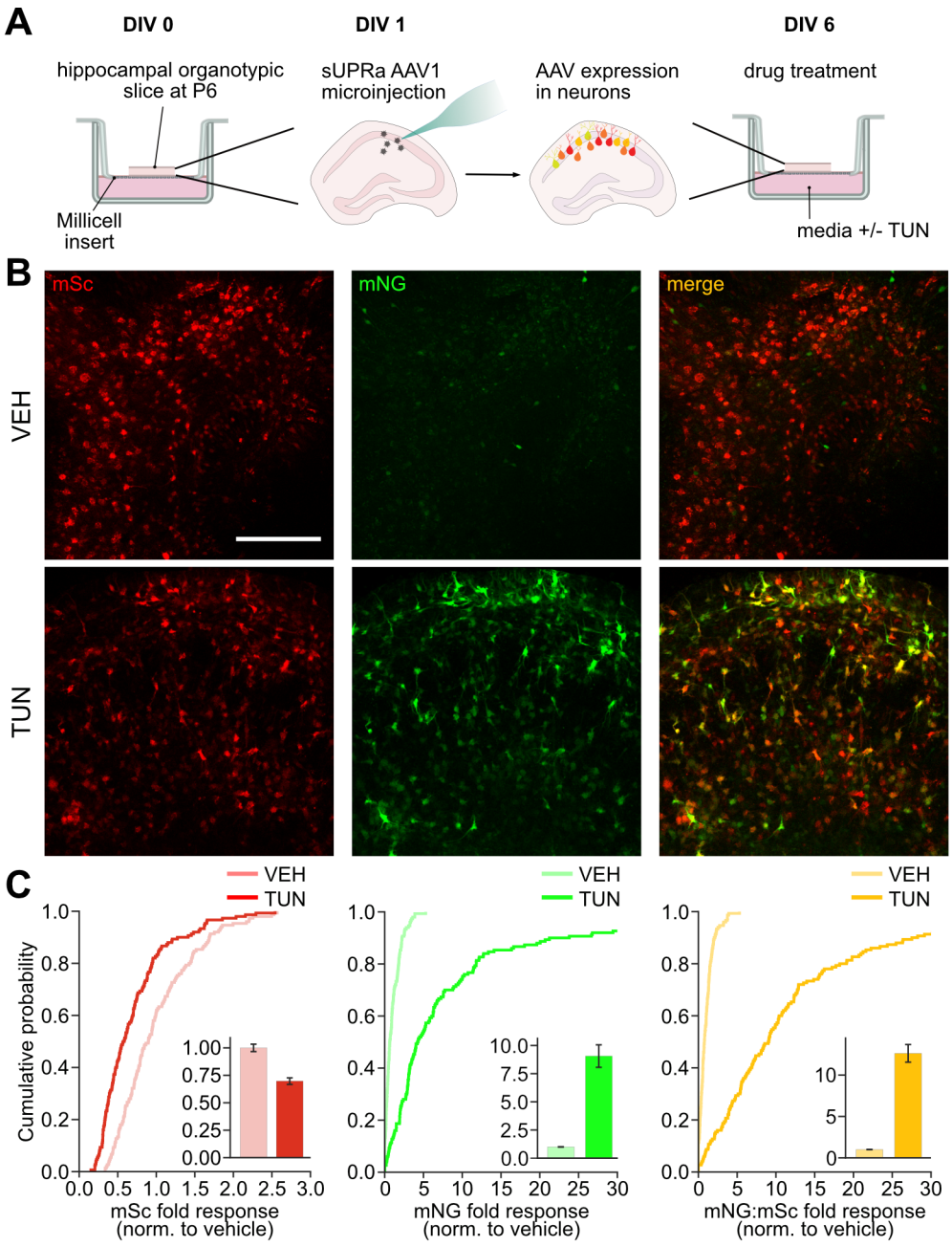

Figure 5.1 Organotypic brain slices transduced with AAV encoding sUPRa exhibit a strong response to UPR activation.

(A) Hippocampal organotypic slices were generated from P6 mouse pups and cultured on day in vitro 0 (DIV 0). Slices were transduced with sUPRa AAVs on DIV 1 and allowed to recover. On DIV 6, slices were treated with either 10 µg/ml TUN or VEH for 24 hours, after which they were fixed and mounted for imaging. **(B)** Representative images of sUPRa expression in hippocampal slices following VEH or TUN treatment (scalebar 250 µm). **(C)** Cumulative distributions of sUPRa's fold response (normalized to VEH) in VEH-treated cells and TUN-treated cells (n=150 cells from 3 slices). Bar plot (inset) shows mean ± SEM values. sUPRa's mSc signal (**left**) in TUN-treated cells was reduced to 0.7-fold relative to VEH-treated cells ($p<0.001$, Mann Whitney U test). The mNG signal (**middle**) was increased by 9-fold with TUN relative to VEH ($p<0.001$, Mann Whitney U test). sUPRa's mNG:mSc ratio response increased 13-fold with TUN relative to VEH ($p<0.001$, Mann Whitney U test).

This was the first time sUPRa had been expressed in neuronal tissue and was found to successfully elicit a response to experimental UPR activation. This came with the caveat that under these experimental conditions, the nEF promoter-driven expression of mSc also showed a modest reduction, which was not something that was observed with mouse fibroblast cells (Chapter 4 **Figure 4.5**). However, this phenomenon made sUPRa's ratio response even more sensitive to UPR activation, with mNG expression increasing and mSc expression decreasing.

Having had initially promising results with AAV_1-sUPRa, I then tested its expression in mouse cortex *in vivo*. In a pilot study, I performed stereotactic cortical injections in 2 mice at 4 weeks of age, with either the high-titre stock preparation of AAV_1-sUPRa (6.2×10^{12} GC/ml; 'neat') or a 1:10 diluted preparation. Since it can take up to 3 to 4 weeks for optimal AAV expression *in vivo,* I harvested the two brains 4 weeks post-injection to assess baseline sUPRa expression (**Figure 5.2**A,B). I observed that the brain transduced with the neat AAV preparation exhibited much lower mSc expression and many more mNG-expressing cells compared to the brain transduced with 1:10 AAV. With the neat AAV preparation, 20% of all sUPRa-expressing cells exclusively expressed mNG with no mSc, while 18% exclusively expressed mSc with no mNG. Meanwhile in the 1:10 AAV brain, 4% of all sUPRa-expressing cells exclusively expressed mNG, while 15% exclusively expressed mSc. sUPRa's mean mSc fluorescence in the 1:10 AAV brain was approximately 3-fold greater than that of the neat AAV brain (**Figure 5.2**C), whereas, sUPRa's mean mNG fluorescence in the 1:10 AAV brain was half of that observed in the neat AAV brain (**Figure 5.2**D). To quantify the mNG:mSc ratio response, all cells that exclusively expressed mNG with no mSc fluorescence were assigned a maximal ratio value, which are not shown in the cumulative distribution plot (**Figure 5.2**E). The mean mNG:mSc ratio for the neat AAV brain was more than 5 times greater than in the 1:10 AAV brain. Therefore, the baseline sUPRa response in neuronal tissue seemed to be dependent on viral titre, suggesting that long-term viral expression itself may elicit a UPR (Balakrishnan et al., 2013).

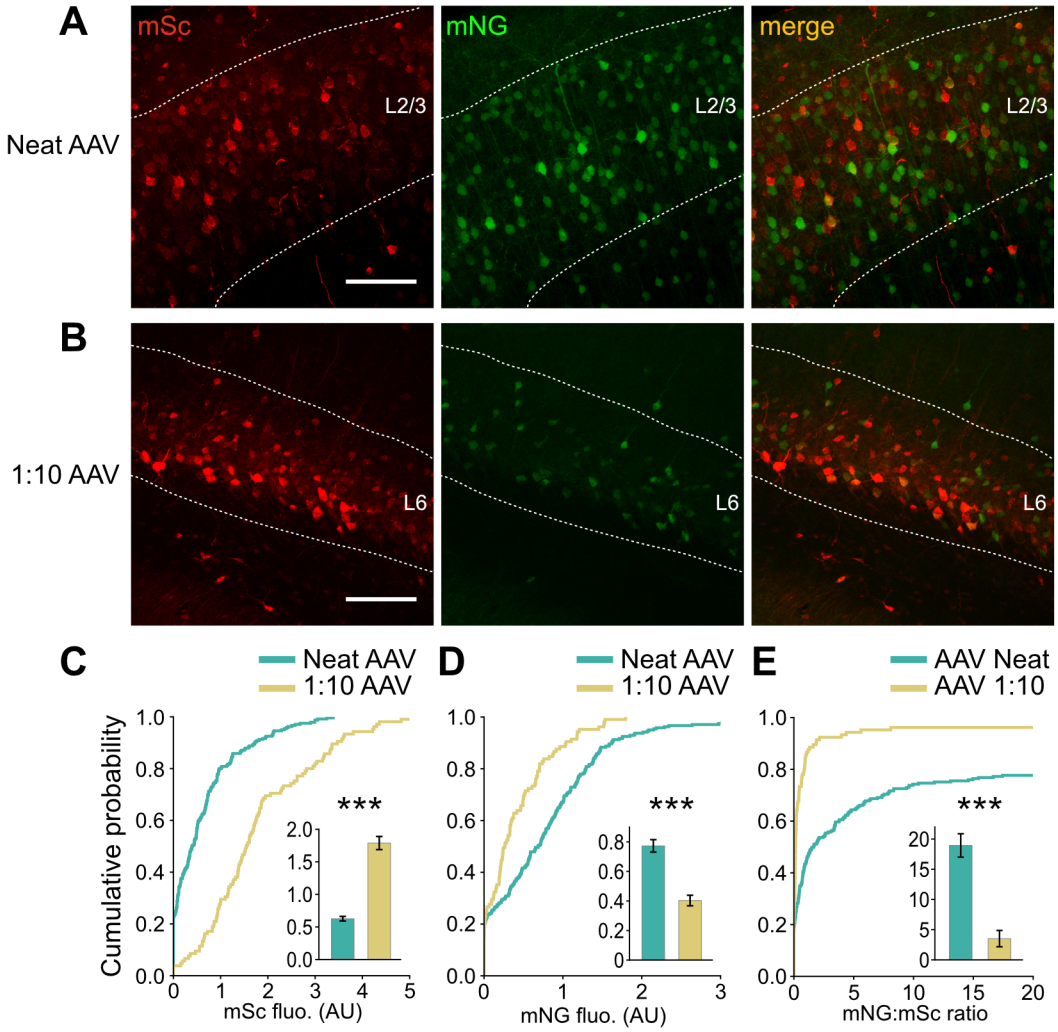

Figure 5.2 sUPRa expression by AAV transduction in mouse cortex varied as a function of viral titre.

(A) Mouse cortical sections showing sUPRa expression 4 weeks following intracortical injection with a $6x10^{12}$ GC/ml titre of AAV_1-sUPRa (neat AAV; 100 µm). Cells showed high mNG expression, where many mNG-expressing cells lacked mSc expression. **(B)** Mouse cortical sections showing sUPRa expression 4 weeks following intracortical injection with a 1:10 dilution of AAV_1-sUPRa (scalebar 100 µm). Some cells showed exclusive mNG expression. **(C)** Cumulative distributions of sUPRa's mSc fluorescence in cortical cells transduced with neat AAV (n=240 cells from 1 animal) or 1:10 AAV (n=105 cells from 1 animal). Bar plot (inset) shows mean ± SEM values. mSc expression was 3 times brighter with 1:10 AAV transduction compared to neat AAV ($p<0.0001$, Mann Whitney U test). **(D)** Cumulative distributions and means of sUPRa's mNG fluorescence with neat or 1:10 AAV transduction. In contrast to mSc expression, mNG expression was two times greater with neat AAV than with 1:10 AAV ($p<0.0001$, Mann Whitney U test). **(E)** Cumulative distributions and means of the mNG:mSc ratio with neat or 1:10 AAV transduction. Cells expressing mNG with no mSc were assigned a maximal ratio value of 80, which results in a long tail in the cumulative distribution plot (clipped). This shows with neat AAV transduction, ~20% of cells expressed mNG without mSc, resulting in a high mean mNG:mSc ratio value of 18.94 ± 2.07. With 1:10 AAV transduction, ~4% of cells expressed mNG without mSc, resulting in a mean mNG:mSc ratio of 3.52 ± 1.48 ($p<0.0001$, Mann-Whitney U test).

The mutually exclusive expression of mNG and mSc was unexpected, since I had not observed this phenomenon in the virally transduced organotypic slices at DIV 6 (**Figure 5.1**) or in any of the heterologous cell experiments in **Chapter 4**. However, in the organotypic slices, mSc expression showed a suppression following UPR activation by TUN. Therefore, I wondered whether UPR activation caused by viral infection may gradually act to suppress the nEF promoter activity over time. If this is the case, one might expect to observe fewer mNG-only cells at earlier timepoints after viral transduction, and more mNG-only cells at later timepoints. To test this idea, I qualitatively assessed sUPRa's baseline expression in organotypic slices transduced with AAV_1-sUPRa and fixed for imaging at different timepoints post-transduction (**Figure 5.3**).

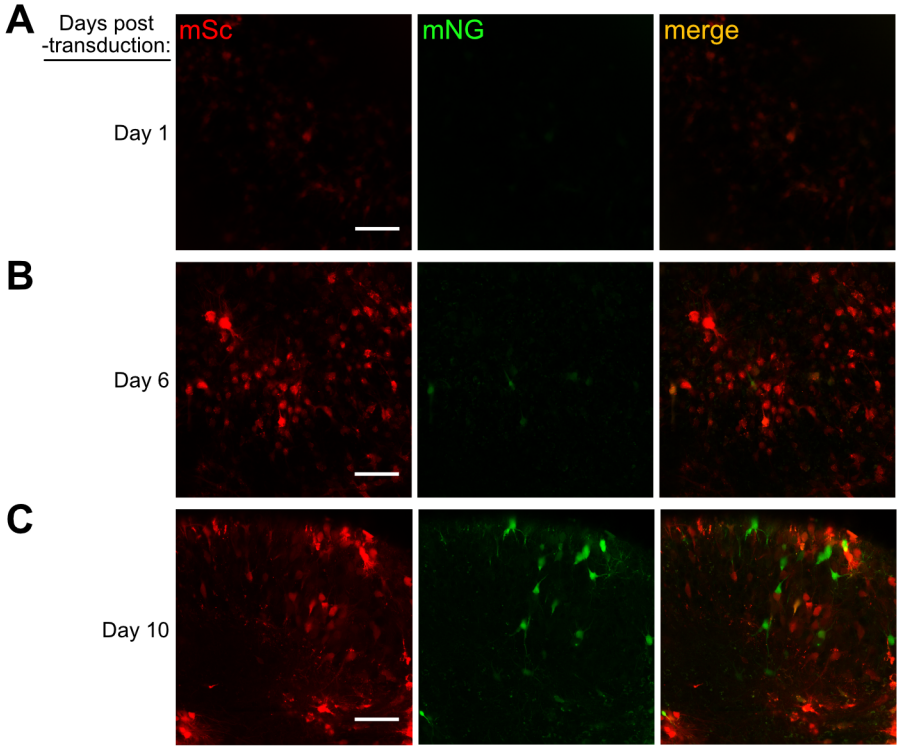

Figure 5.3 Organotypic slices imaged at different timepoints after AAV_1-sUPRa infection show the onset of baseline mNG expression.

(A) Hippocampal organotypic slices transduced with AAV_1-sUPRa (1:10 dilution) and imaged on Day 1 post-transduction (scalebar 100 µm). At this timepoint, cells had low overall expression levels of mSc and no baseline mNG expression. **(B)** Slices transduced with AAV_1-sUPRa and imaged on Day 6 post-transduction (scalebar 100 µm). Cells showed higher levels of mSc expression, and low baseline mNG. **(C)** Slices transduced with AAV_1-sUPRa and imaged on Day 10 post-transduction (scalebar 100 µm). Cells showed similar levels of mSc expression as Day 6, but higher levels of baseline mNG. Most mNG-expressing cells showed little to no mSc expression. Some mSc-expressing cells also express mNG.

On day 1 post-transduction (**Figure 5.3**A), cells showed very low levels of sUPRa mSc expression and no mNG expression. On day 6, mSc expression levels increased and some mSc-expressing cells also expressing low levels of mNG, while some cells displayed mNG expression without mSc (**Figure 5.3**B). On day 10, mSc expression levels were comparable to day 6. However, there was an increase in the number of cells that only expressed mNG on day 10 compared to day 6. Additionally, these mNG-only cells on day 10 exhibited higher levels of mNG than on day 6 (**Figure 5.3**C).

These observations over time still do not explain the stochastic nature of some virally infected cells expressing mNG without mSc, and other cells expressing mSc without mNG with long-term viral expression *in vivo*. Recombinant AAVs are often susceptible to recombination of the DNA arrangement during production. Therefore, I verified AAV_1-sUPRa's sequence to confirm that all of the components of sUPRa are present in the correct positions and orientations (**Figure 5.4**A). To do this, I designed primer pairs (**Table 5.1**) to amplify the regions across each major component of sUPRa (**Figure 5.4**B), and performed PCR on the AAV_1-sUPRa DNA and control sUPRa plasmid DNA. The PCR confirmed that all the components were present in AAV_1-sUPRa, same as in the plasmid DNA (**Figure 5.4**C), suggesting that there was no DNA recombination during AAV production.

In summary, while AAV gene delivery initially seemed like a convenient method for expressing sUPRa in mouse cortex, its performance was not reliable. AAV_1-sUPRa's high baseline response and stochastic behaviour would not be well-suited for detecting low levels of physiological UPR, such as following periods of sleep deprivation.

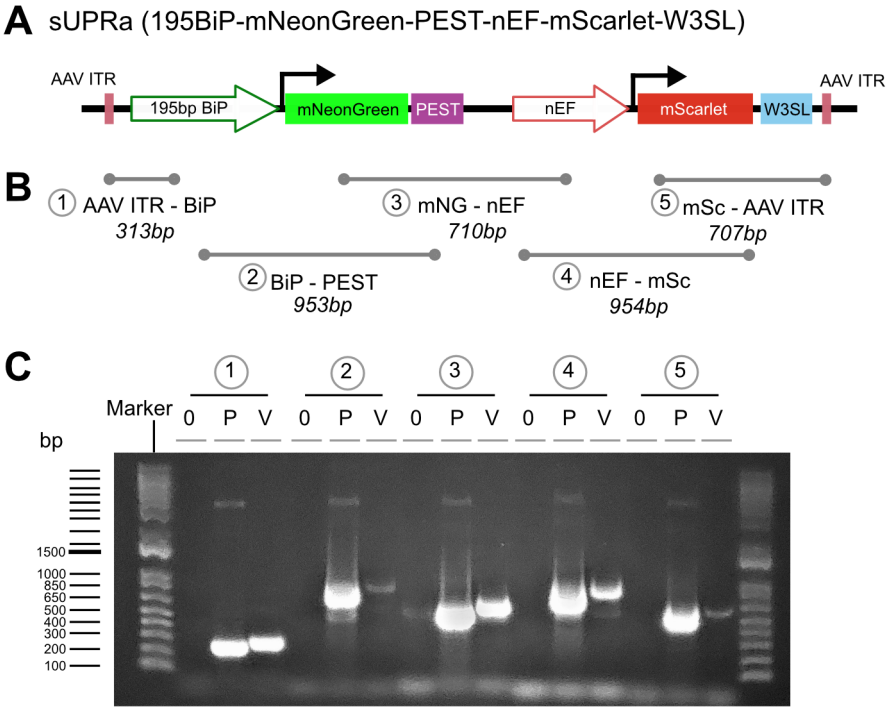

Figure 5.4 PCR amplification of different regions of sUPRa in the AAV vector confirms the presence of all expected components of the construct.

(A) Schematic diagram of sUPRa's construct composition. **(B)** Five primer pairs were designed to detect the presence of each component of the sUPRa construct in the correct orientation. **(C)** PCR products using the primer pairs 1 to 5 shown in '**B**' were separated on a 1% agarose gel. Each primer pair has a lane from a no template control (0), sUPRa's plasmid construct (P) and sUPRa's AAV construct (V). All primer pairs detected the same PCR products in sUPRa's plasmid and AAV construct.

5.3.2 sUPRa expression in cortical neuronal subpopulations via *in utero* electroporation

In utero electroporation (IUE) offers an alternative approach for targeting sUPRa expression to a defined population of cortical neurons *in vivo*. This involves delivering sUPRa plasmid DNA to a population of dividing progenitor cells in the ventricular zone of mouse embryos, when cortical excitatory neurons are being born (Greig et al., 2013; Langevin et al., 2007). Given the Akerman lab's expertise in this technique and the willingness of my colleagues to help, I validated the use of IUE for sUPRa expression and response to UPR activation in mouse cortical neurons. Mouse embryos were electroporated at embryonic gestation day 15 (E15), when cortical L2/3 excitatory neurons are being born (**Figure 5.5**A). I then harvested and imaged the IUE brains at age P7 and 8 weeks, which was 2 weeks and 9 weeks from the time of sUPRa electroporation, respectively (**Figure**

5.5B,C). Both brains showed high levels of mSc expression and low levels of mNG expression, with no cells expressing mNG exclusively. The few cells that showed low baseline mNG expression also showed high mSc expression, which may be resulting from the effect of DNA load as seen in **Chapter 4** (**Figure 4.5**F). However, the level of mNG fluorescence was the same as background autofluorescence in most mSc-expressing cells at P7 and 8 weeks. Therefore, this suggested that cortical delivery of sUPRa using *in utero* electroporation is a viable option for long-term expression.

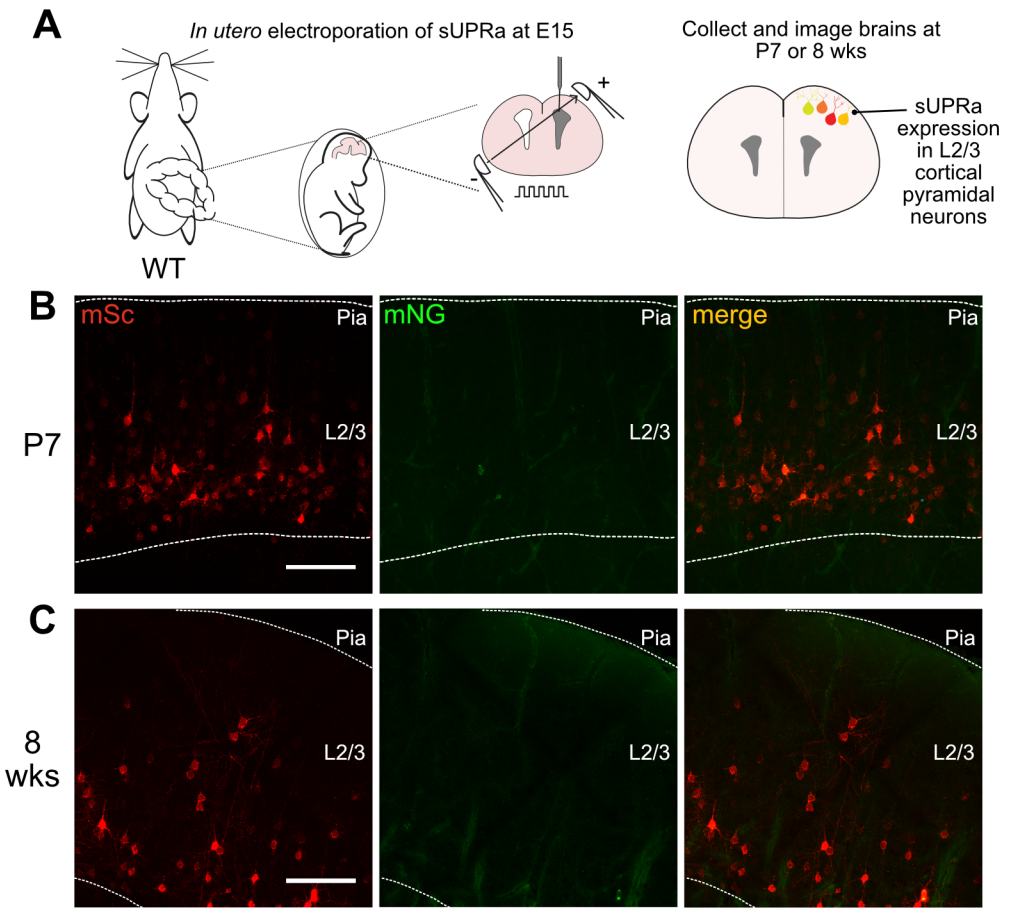

Figure 5.5 In utero electroporation as a route to express sUPRa in cortical layer 2/3 pyramidal neurons with low baseline expression.

(A) sUPRa expression was targeted to L2/3 pyramidal neurons in mouse cortex by performing *in utero* electroporation on mouse embryos at embryonic day 15 (E15) using plasmid DNA. Expression of sUPRa in cortical neurons was assessed in postnatal day 7 (P7) and 8 week-old mice. **(B)** Representative images of sUPRa expression in cortical L2/3 pyramidal neurons from a P7 mouse (scalebar 100 µm). **(C)** Representative images of sUPRa expression in cortical L2/3 pyramidal neurons from an 8 week-old mouse (scalebar 100 µm). There was low baseline mNG expression at both short-term and long-term expression timepoints.

Next, I tested whether sUPRa, when expressed in cortical L2/3 pyramidal neurons through IUE, is able to report pharmacologically induced UPR. To do this, I prepared organotypic cortical brain slices from electroporated mice at P7. Slices were treated with either 5 μg/ml TUN or VEH for 6 hours and fixed with PFA a further 18 hours later (**Figure 5.6**A). sUPRa showed good expression in L2/3 pyramidal neurons (**Figure 5.6**B) and exhibited a robust response to UPR activation with TUN (**Figure 5.6**C). Neurons in slices treated with TUN showed a 0.80 ± 0.07 fold mSc expression relative to VEH (**Figure 5.6**D left), which was similar to the reduction in mSc expression seen in cells transduced with AAV_1-sUPRa (**Figure 5.1**C left). Meanwhile, mNG expression in neurons from slices treated with TUN showed a 4.06 ± 0.55 fold increase relative to VEH (**Figure 5.6**D middle). Neurons in slices treated with TUN showed a 5.65 ± 0.79 fold increase in sUPRa's mNG:mSc ratio response relative to VEH (**Figure 5.6**D right), thereby supporting the use of IUE to express sUPRa for detection of the UPR in neuronal populations.

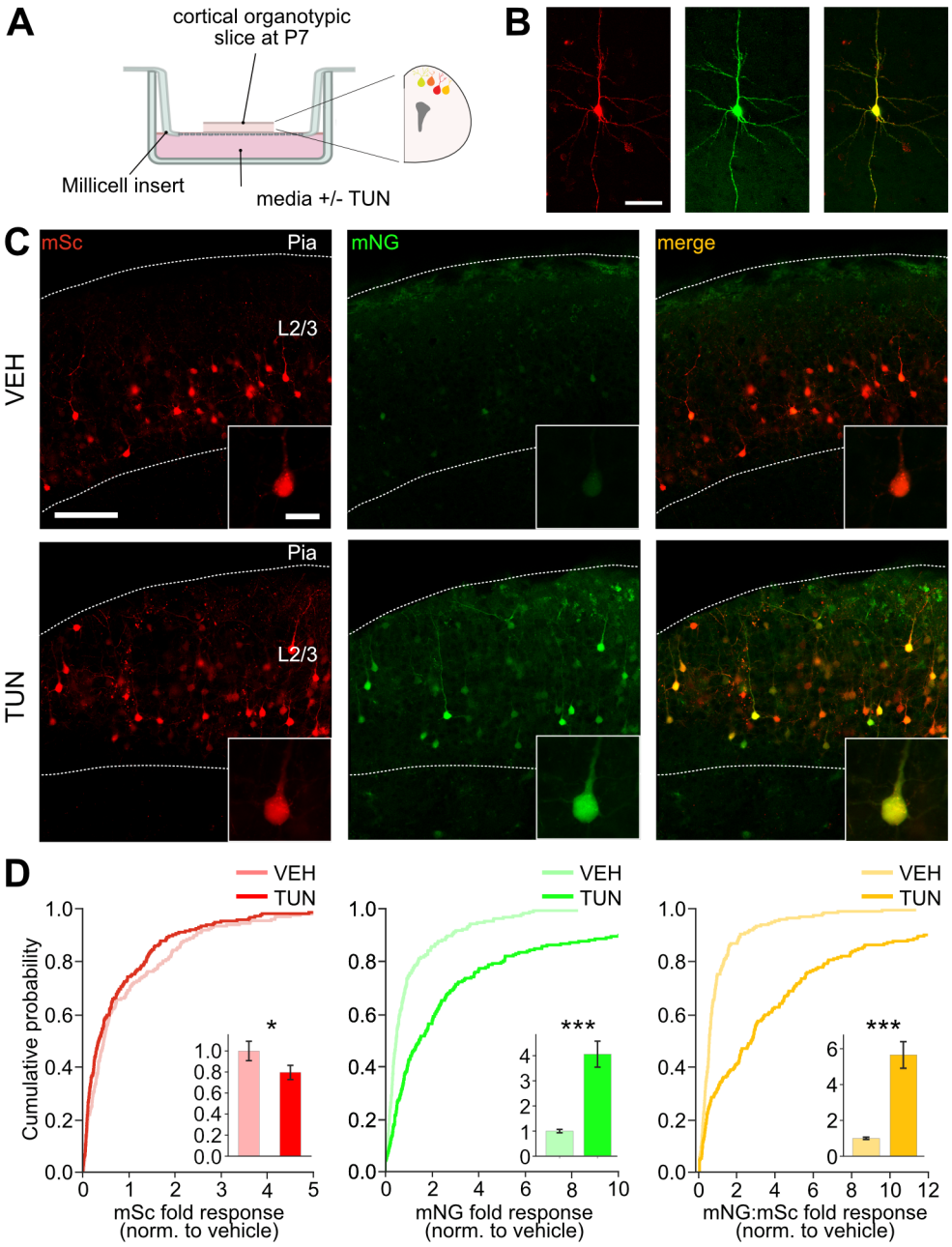

Figure 5.6 sUPRa responds to Tunicamycin-induced UPR in mouse cortical neurons.

(A) Cortical organotypic slices were generated at P7 from mouse pups that had been electroporated with sUPRa at E15. Slices were treated with either 5 µg/ml TUN or VEH for 6 hours and fixed a further 18 hours later. **(B)** A L2/3 cortical pyramidal expressing sUPRa at P7 (scalebar 50 µm). **(C)** Representative images of sUPRa expression in L2/3 pyramidal neurons following VEH or TUN treatment. Low power image shows L2/3 of an organotypic slice (scalebar 100 µm), and inset shows individual pyramidal neuron (scalebar 20 µm). **(D)** Cumulative distributions of sUPRa's fold response in VEH-treated cells (n=197 cells from 3 slices) and TUN-treated cells (n=211 cells from 3 slices). Bar plot (inset) shows mean ± SEM values. sUPRa's mSc expression (**left**) with TUN treatment was 0.8-fold of VEH ($p=0.0357$, Mann Whitney U test). sUPRa's mNG expression (**middle**) was increased by 4-fold with TUN relative to VEH ($p<0.001$, Mann Whitney U test). sUPRa's mNG:mSc ratio response (**right**) was 6-fold greater in L2/3 pyramidal neurons treated with TUN relative to VEH ($p<0.001$, Mann Whitney U test).

5.3.3 sUPRa reveals a sleep deprivation-induced UPR in L2/3 cortical pyramidal neurons

Having established sUPRa's high sensitivity to a range of stress-inducing factors in **Chapter 4**, here I investigated whether sUPRa could report UPR activation associated with *in vivo* physiological processes in a defined cell population. Biochemical methods have previously shown a tissue-wide increase in UPR in mouse cerebral cortex following sleep deprivation (SD) (Cirelli & Tononi, 2000b; Naidoo et al., 2005; Terao et al., 2003). In **Chapter 2**, I further demonstrated that cortical neurons contribute to the sleep deprivation-induced UPR in the cortex. However, as a genetic construct, sUPRa offers a further methodological refinement that can be used to provide novel insights into cell type-specific UPR activation *in vivo* in live cells. To test its usefulness for studying the physiological UPR in a neuronal subpopulation in adult mice, I used IUE to express sUPRa in L2/3 cortical pyramidal neurons followed by sleep deprivation (SD) to activate the UPR (**Figure 5.7**A). 8 week-old male and female mice, that had been electroporated with sUPRa at E15, were either allowed to sleep undisturbed or kept awake with novel objects for 12 hours from light onset, when they would naturally be sleeping. At the end of the sleep deprivation period, brains were harvested and prepared for imaging. Firstly, sUPRa showed successful expression in L2/3 cortical neurons in these adult 8 week-old mice that were electroporated at E15. There were indications of altered intracellular distribution of the fluorescent proteins in mice at this age. Neurons displayed possible patterns of aggregated fluorophore expression rather than the evenly dispersed cytosolic expression observed in neurons with shorter-term expression (**Figure 5.6**). Nevertheless, sUPRa response displayed a SD-induced increase in cortical pyramidal neurons. Following SD, sUPRa's mNG expression was increased to 1.67 ± 0.06 fold in mice compared to the rested control mice (**Figure 5.7**C middle). mSc expression in neurons from SD mice was 0.87 ± 0.03 fold of control mice (**Figure 5.7**C left). Hence, sUPRa's mNG:mSc ratio response increased to 1.88 ± 0.27 fold in mice following the 12 hours of SD compared to control conditions (**Figure 5.7**C right). These experiments confirm that sUPRa is compatible with stable long-term neuronal expression *in*

vivo. Importantly, the results demonstrate the ability of sUPRa to monitor physiologically relevant UPR activity in an intact *in vivo* system.

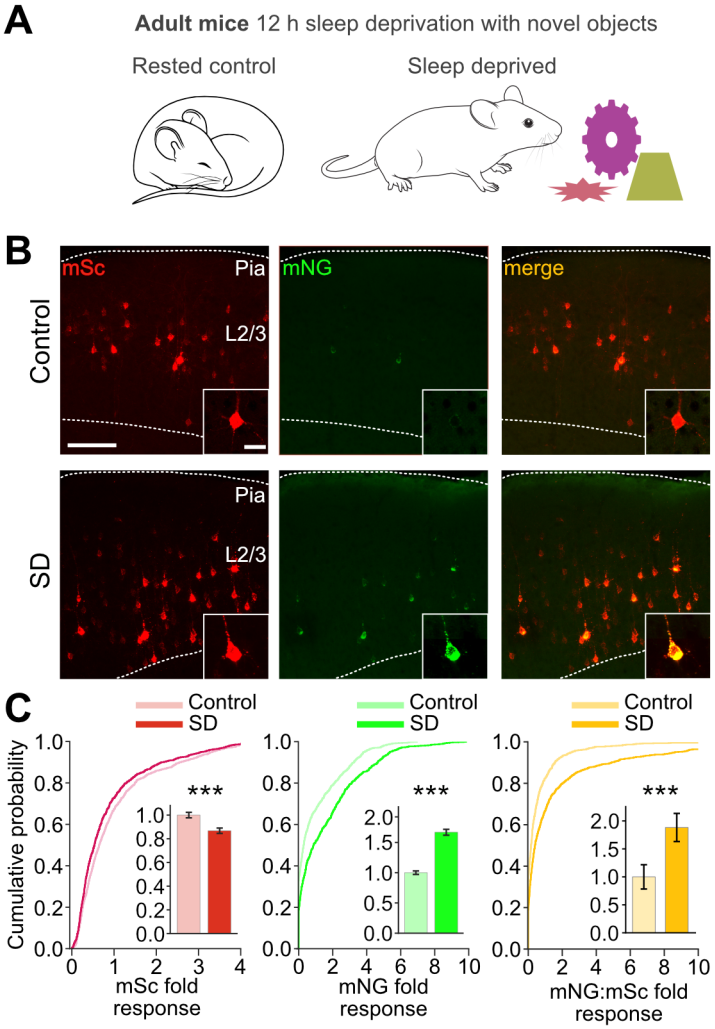

Figure 5.7 sUPRa reveals a sleep deprivation-induced UPR in L2/3 cortical pyramidal neurons.

(A) At postnatal age 8 weeks, sUPRa expressing mice were either allowed to sleep undisturbed or sleep deprived (SD) for 12 hours from light onset. **(B)** Representative images of sUPRa expression in L2/3 pyramidal neurons in rested control or sleep-deprived mice. Low power image shows L2/3 in an organotypic slice (scalebar 100 µm), and inset shows an individual pyramidal neuron (scalebar 20 µm). **(C)** Cumulative distributions of sUPRa's fold response in control mice (n=1080 cells from 4 animals) and SD mice (n=980 cells from 4 animals). Bar plot (inset) shows mean ± SEM values. With SD, sUPRa's mSc expression was reduced to 0.87-fold of the control ($p<0.001$, Mann Whitney U test). sUPRa's mNG expression was increased 1.67-fold with SD relative to control ($p<0.001$, Mann Whitney U test). sUPRa's mNG:mSc ratio response in neurons from SD mice was increased by 1.88-fold relative to control ($p<0.001$, Mann Whitney U test).

5.4 Discussion

In order to investigate the relationship between the sleep-wake cycle and ER stress, we need tools with high sensitivity to be able to track mild UPR activation in neurons *in vivo.* I have aimed to develop such a tool in the form of sUPRa, which provides a sensitive readout of low levels of UPR activation and shows improved ON-OFF kinetics, as shown in **Chapter 4**. In the present chapter, I tested sUPRa's usefulness for detecting UPR activation in neuronal systems and under physiological conditions. First, I established the most amenable method for the delivery of sUPRa into neuronal tissue. I found that neurons transduced with sUPRa packaged into an adeno-associated virus (AAV) capsid (AAV_1-sUPRa) exhibited an increase in sUPRa's mNG:mSc ratio response to TUN-induced ER stress. However, AAV_1-sUPRa infected neurons also showed a high level of baseline sUPRa response, with many cells expressing either mNG or mSc in a stochastic and mutually exclusive manner. In contrast, I found that *in utero* electroporation (IUE) of sUPRa into a subset of cortical pyramidal neurons produced low baseline mNG responses, with mSc displaying stable long-term ubiquitous expression. Furthermore, electroporated neurons displayed a strong sUPRa response to TUN treatment. Therefore, IUE was the method of choice for expressing sUPRa in neurons to be able to capture physiological UPR activation. Indeed, sUPRa was able to detect UPR upregulation in cortical pyramidal neurons of mice that had been sleep deprived compared to mice that received undisturbed sleep. Hence, sUPRa presents an opportunity to monitor UPR activation in neurons with physiologically relevant processes *in vivo,* such as across the sleep-wake cycle.

Molecular genetic reporter tools are useful for providing a cell-specific readout of their target. In order to provide a readout, the reporter DNA first needs to be introduced into living cells. The method of delivery of a molecular genetic construct into live cells can itself interfere with intrinsic cellular processes that may mask the readout of the UPR. Therefore, it is important to have a low baseline reporter readout in conditions known to not elicit the UPR. Recombinant viruses

have been instrumental in neuroscience for highly efficient gene delivery *in vivo* (S.-H. Chen et al., 2019). However, viral transduction has been reported to elicit all three arms of the UPR, as well as upregulation of BiP transcript levels (Balakrishnan et al., 2013; Sen et al., 2014; L. Zhang & Wang, 2012). Therefore, the high level of baseline sUPRa expression *in vivo* in mouse brains transduced with AAV_1-sUPRa may be attributed to viral infection itself driving UPR activation. More unexpectedly, 4 weeks post-transduction, many neurons expressing mNG showed no detectable mSc expression, and vice versa. The onset of mNG expression seems to be time-dependent after initial viral transduction, as indicated by the observations in organotypic slices transduced with AAV_1-sUPRa. Moreover, mSc expression was found to show a modest reduction following UPR activation, which may suggest that cells exhibiting high levels of viral load, and therefore high levels of UPR, may show further suppression of nEF driven mSc expression. The nEF promoter (EF1α/HTLV hybrid) has been previously reported to show long-lasting ubiquitous activity in neurons (Fenno et al., 2014, 2020; Sylwestrak et al., 2022), and there is no known effect of ER stress on suppressing the nEF promoter activity. To examine whether higher levels of UPR activation are associated with reduced nEF promoter activity, I quantified BiP protein levels in AAV-transduced cells from fixed brain sections, and saw no apparent differences in between cells that were only mNG-positive compared to cells that were only mSc-positive (data not shown). I also ruled out the possibility of DNA rearrangements within AAV_1-sUPRa by comparing PCR products across all the major construct components between the viral DNA and control plasmid DNA. There is a possibility that the design of the construct packaged into viral particles caused some unknown interactions between the two promoters, whereby activation of one may have led to suppression of the other (Curtin et al., 2008). For the purposes of this thesis, I chose not to troubleshoot the issues with AAV_1-sUPRa any further, as it did not present a practical method for expressing sUPRa to detect physiological UPR in neurons.

Given the local expertise with *in utero* electroporation (IUE), it was an attractive alternative for expressing sUPRa in neuronal populations. Unlike AAV transduction, IUE of ventricular zone progenitors is able to target excitatory pyramidal neurons in the mouse cortex at specific stages of development. This offers more cell type specificity than the AAV_1, which has a tropism for expression across all neuronal and glial cell types (Burger et al., 2004; C. Wang et al., 2003). The cortex is the main region of interest to monitor the relationship between neuronal UPR and slow wave activity during sleep homeostasis (V. V. Vyazovskiy & Harris, 2013). Therefore, by targeting pyramidal neurons in specific layers of the cortex using IUE, it is possible to elucidate the interactions between sleep-wake and the UPR in cortical neurons. Furthermore, refinements to the electroporation technique allow for the targeted delivery of constructs to a wider range of cell populations within the adult brain, extending beyond the restriction of only targeting pyramidal neurons in the developing brain (Nomura et al., 2016). Importantly, with IUE, sUPRa-expressing cells showed low baseline mNG expression, and there were no cells expressing mNG without mSc. Additionally, IUE neurons expressing sUPRa displayed a robust response to TUN. Therefore, IUE of sUPRa into cortical neurons offers a better opportunity than AAVs for detecting low levels of physiological UPR.

Similar to the AAV transduced neurons, IUE neurons showed a modest reduction in mSc expression alongside the strong increase in mNG expression following TUN-induced ER stress. I did not observe this in mouse fibroblast cells in **Chapter 4**, therefore, the suppression of the nEF promoter driven mSc expression upon ER stress could be a neuronal cell type-specific effect. Upon ER stress, PERK activation results in an increase in p-eIF2α, which results in global translation suppression of genes that do not have an uORF (Harding et al., 2002; Jaud et al., 2020; P. D. Lu et al., 2004). Therefore, it could be that both mSc and mNG expression of sUPRa is suppressed to some degree because they do not contain uORFs, but mNG still displays an increase due the relative upregulation of its mRNA levels. On the other hand, it could be that greater BiP promoter activity interferes with nEF promoter activity in neurons, resulting in divergent mNG and mSc expression

levels (Curtin et al., 2008). Nevertheless, sUPRa's mNG:mSc ratio response was larger as a result of the decrease in mSc and the increase in mNG, which makes the ratio a robust measure of UPR activation.

The successful expression of sUPRa in cortical neurons generates the opportunity to investigate the intrinsic activation of the UPR under physiologically relevant conditions. In **Chapter 2**, I used immunohistochemistry to show that sleep deprivation upregulated BiP protein levels in cortical neurons. However, immunohistochemistry involves sacrificing an animal to measure UPR activation at a single timepoint. Instead, sUPRa offers the potential to track UPR activation in the same population of neurons in the same animal over a period of time. This capability makes it especially valuable for monitoring UPR levels in neurons across the sleep-wake cycle. By targeting expression to layer 2/3 excitatory pyramidal neurons using IUE, sUPRa was able to reveal a sleep deprivation-induced UPR in this neuronal subpopulation for the first time. While mSc expression decreased following sleep deprivation, mNG expression increased, consistent with the effect seen with TUN treatment in neurons. The net effect was an increase in sUPRa response following sleep deprivation. This proof-of-principle establishes the basis for future work that could capitalise on sUPRa's favourable dynamics in order to track cell-specific UPR over time, for example using 2-photon imaging in head-fixed mice, or fibre photometry in freely behaving mice. sUPRa can also be used to determine how distinct cell populations differ in their sleep-wake related UPR. Considering the rapid onset of expression following gene delivery and viable long-term expression, sUPRa also lends itself to monitoring the UPR in models of development or ageing.

In summary, sUPRa offers a powerful resource to quantify and monitor global UPR activity with cellular resolution. sUPRa can be an important tool for understanding ER stress and the UPR in a variety of contexts, including physiological prophylactic functions that preserve cell viability, such as during sleep, and pathological functions in disease models and ageing.

Chapter 6 General Discussion

Contents

The UPR is a highly conserved essential cellular maintenance programme for all cells in the body. Far from being just a pathological state, the UPR constitutes a sophisticated and adaptive process under physiological conditions. One physiological state in which it becomes apparent is extended wakefulness or sleep deprivation. The UPR is tightly intertwined with sleep-wake history and the homeostatic regulation of sleep, whereby the need for sleep accumulates with wakefulness and dissipates during subsequent sleep. The UPR in the brain mirrors the pattern of increase and decrease in sleep need. Despite substantial characterisation of the UPR and its discrete signalling pathways, there is a considerable lack of understanding of its role in basal cellular physiology. Therefore, to address this gap in knowledge, this thesis aimed to contribute towards characterising the UPR in the context of the universal physiological phenomenon of sleep. Specifically, the objectives of the thesis were three-fold:

1. Investigate whether sleep deprivation results in a heterogeneous activation of the UPR across cortical regions and cell types.
2. Investigate whether local ER stress induction in the cortex results in altered sleep and associated changes in neural activity patterns.
3. Develop a molecular genetic tool to effectively quantify the overall UPR in the nervous system for future applications.

In this chapter, I will first summarise the key findings from Chapters 2 to 5 of this thesis and discuss important methodological limitations and constraints. I will then explore the implications of my findings within the broader field and speculate on their meaning in the context of other research. Specifically, I will discuss evidence for the heterogeneity of the UPR across the cortex and cortical cell types as well as the impact of the UPR on brain activity patterns. I will provide recommendations for potential future directions of this research and its applications, and consider alternative approaches for monitoring and manipulating the physiological UPR. Finally, I will conclude by addressing what I perceive to be a major outstanding question in the field: what causes

UPR activation during sleep deprivation? This will include a discussion of potential underlying causes of UPR activation and what they imply about the functions of sleep.

6.1 Summary of findings

Seminal research has demonstrated that cortical activation of UPR-related components, including molecular chaperones downstream of the UPR, is a reliable molecular indicator of sleep deprivation (Cirelli et al., 2004; Mackiewicz et al., 2007; Naidoo et al., 2005; Terao et al., 2003, 2006). The cerebral cortex is highly diverse, both in terms of anatomical regions and transcriptionally defined cell types. However, to date, there have been limited efforts to study the effects of sleep deprivation, a physiological stressor, on the cortical UPR in a region- and cell-specific manner. In **Chapter 2**, I reproduced previous findings of the effects of sleep deprivation on UPR levels in mouse cortex, while also exploring the differences in effects across cortical regions and cell types. Results showed an upregulation of BiP protein and transcript levels, as well as sXBP1 transcript levels, in the frontal cortex after sleep deprivation. In addition, there were differences in BiP protein levels among different cortical regions, with no increase in somatosensory or visual cortical tissue following sleep deprivation. Immunohistochemical quantification of BiP levels revealed that cortical neurons in particular display a sleep deprivation-induced BiP upregulation in a region-specific manner, similar to that observed at the tissue level. Furthermore, different neuronal subtypes exhibited variations in baseline BiP expression levels, with no observable sleep deprivation-induced upregulation in PV+ and SST+ inhibitory interneuron populations. These results suggest that the UPR may play distinct roles across different regions of the cortex and in different cell types under physiological conditions.

Having demonstrated that disrupted sleep results in increased UPR activation in the cortex, in **Chapter 3** I investigated the opposite relationship: how does the UPR affect *in vivo* cortical activity and sleep regulation? While previous research has suggested that sleep is important for restoring the UPR after wakefulness, there has not yet been compelling evidence directly linking the UPR,

resulting from ER stress, to the need for sleep. To address this, the pharmacological ER stress inducer, Tunicamycin (TUN), was used to activate the UPR in a local region of mouse cortex. Despite TUN infusion inducing an UPR within 24 hours of drug treatment, there were no noticeable changes in sleep-wake architecture following drug administration. This suggested that global regulation of sleep was not affected by local activation of the UPR. However, TUN infusion did result in varied effects on neuronal activity patterns across all animals. During the first 24 hours post-infusion, there were no significant changes in signal composition in any of the vigilance states. However, from 72 hours post-infusion, there was a consistent decrease in the SWA delta frequency range recorded local to the infusion site during NREM sleep, which was accompanied by a reduction in the amplitude of slow waves. A subgroup of animals that displayed the greatest decrease in slow wave amplitude and overall LFP signal power were found to have neuronal damage at the infusion site when analysed post-mortem. These findings suggest that TUN is prone to inducing an UPR that is more pathological than physiological, which results in greater cellular damage than restoration. Beyond this, these findings highlight the particular vulnerability of sleep SWA to prolonged ER stress, which could have implications for various neurodegenerative disorders or ageing, both of which are associated with chronic UPR activation.

The UPR is a highly dynamic and tuneable process with different timeframes of activation and deactivation depending on the stimulus context. Several *in vitro* assays have been developed for monitoring UPR activation and its downstream effectors. Western blotting, qPCR, and immunocytochemistry allow for the measurement of UPR levels at a specific timepoint in tissue samples. However, to better understand the physiological roles of the UPR, such as the interplay between sleep and the UPR, it is necessary to detect and monitor the UPR with high sensitivity and temporal precision. There is a shortage of suitable tools in the field to achieve this. A major contribution of this thesis is the development of a novel tool that can be applied to study the UPR in a variety of contexts. In **Chapter 4** I presented the development and characterisation of sUPRa, a novel reporter capable of detecting global UPR activity with high sensitivity. The sUPRa response to

UPR activation was shown to be dose-related and displayed good recovery kinetics as the UPR subsided. sUPRa was responsive to the UPR elicited by various forms of ER stress, including pharmacological disruption of protein folding, disruption of ER calcium homeostasis, and the expression of misfolded proteins in the ER. Finally in **Chapter 5**, I tested sUPRa's usefulness for detecting UPR activation in neuronal systems and under physiological conditions. While studying the proteostatic mechanisms of cells, it is important to be mindful of the method of expression of the reporter construct, since it may interfere with endogenous levels of stress responses. *In utero* electroporation presented an effective method for sUPRa expression in the nervous system, as neurons expressing sUPRa displayed low levels of baseline UPR activation and a strong response to UPR activated by TUN treatment. Furthermore, sUPRa was able to detect the physiologically activated UPR in cortical pyramidal neurons of mice that had been sleep deprived. Thus, sUPRa provides an opportunity to track UPR activation in neurons undergoing physiologically relevant processes *in vivo,* including those occurring throughout the sleep-wake cycle.

6.2 Methodological limitations

In this section of the General Discussion, I will reflect on some of the methodological limitations of this thesis, in an attempt to critically assess the findings and identify areas for future development. In **Chapter 2**, the principal method used to investigate the heterogeneity of the UPR across the cerebral cortex was immunohistochemistry. As a method, immunohistochemistry offers better spatial resolution than tissue-wide assays such as western blotting and RT-PCR. However, the quantitative immunohistochemistry pipeline developed in **Chapter 2** focused on a somatic readout of BiP immunostaining, which therefore ignored cellular compartments such as neuronal processes. Axonal and dendritic processes have a different transcriptome and proteome than the soma, with local protein synthesis occurring in these cellular sub-compartments (Giandomenico et al., 2022; Middleton et al., 2019; Perez et al., 2021). The localisation of BiP immunofluorescence was mainly observed in neuronal soma, with diffuse background signal likely to have come from neuronal

processes and other cell types. Therefore, the measurement of somatic BiP levels is likely to provide a useful measure of the cell's global UPR state. Nevertheless, this raises the question of how to accurately capture UPR effects in different parts of a neuron. Alternative methods could be utilised to capture different sub-compartments of neuronal cells, such as super-resolution imaging and image reconstruction to track axons and dendrites (G. Wang et al., 2020).

Immunohistochemistry is also limited by the high variability in staining intensity observed between samples, which makes it challenging to statistically detect small changes that may occur under physiological conditions. To address this issue, I minimised variability in my samples by conducting all immunostaining in batches, in which all brain sections per batch were treated as identically as possible, where sleep and sleep deprived brains were counter-balanced throughout the process. Additionally, fluorescence measurements were normalised within each batch of immunostaining to ensure comparability. Another source of variability in immunohistochemistry studies is the antibodies. As illustrated in **Chapter 2**, most antibodies tested for the detection of UPR proteins failed to either detect the correct protein, or to produce any detectable changes following UPR activation. Antibodies can vary between manufacturers and between batches from the same manufacturer, which warrants caution when using them without first characterising exactly what they are detecting. An anti-KDEL antibody was used throughout the thesis to provide a readout of BiP protein levels in intact cells. However, as seen in the western blots, the anti-KDEL antibody is not strictly BiP-specific, as it also binds to Grp94. Both BiP and Grp94 are ER-resident chaperones and are upregulated by ER stress downstream of the UPR. However, the high expression levels of BiP in baseline conditions limited the signal-to-noise of the anti-KDEL antibody. For the purposes of this thesis, this antibody was sufficient to detect the adaptive outcomes of the UPR in terms of chaperone upregulation. However, in future work, more antibodies could be tested to identify a protein with low baseline expression that is specifically upregulated downstream of the UPR, ideally by multiple arms of the UPR. This would improve signal-to-noise and enable the detection of small changes in the physiological UPR.

In **Chapter 3**, a pharmacological approach was used to activate the UPR in mouse cortex in order to investigate how the UPR may affect neural activity patterns during sleep and wake. Unlike genetic methods for manipulating molecular components of the UPR, pharmacological stressors manipulate the UPR by inducing changes to ER load directly. Tunicamycin was used because it leads to the accumulation of unfolded proteins, which triggers the UPR as a result of the cell's proteostatic needs. However, even at relatively low doses, Tunicamycin can have pleiotropic effects that are much broader than the physiological UPR (Bergmann et al., 2018). Therefore, Tunicamycin's dose needs to be carefully titrated and the method of administration optimised further to elicit a moderate and acute UPR.

Combining intracortical infusions of Tunicamycin with LFP recordings required the chronic implantation of metallic cannulas and electrodes directly into the cortex. This inherently alters cellular physiology locally and may change the susceptibility of the tissue to ER stress (Grill, 2008; Obrenovitch et al., 1993; Whittle et al., 1998). Chronic implantation in the brain is known to induce a foreign body response that results in inflammation, immune activation and formation of scar tissue (Gretzer et al., 2006). In a separate study conducted by Dr Jose Prius Mengual and Dr Lewis Taylor, the relative change in BiP transcript levels was reduced when sleep deprived and control animals were implanted with EEG screws (personal communication). This highlights the need for care when designing experiments and interpreting results from chronically implanted animals. Human studies have tended to pay more attention to the biomechanical compatibility of implant materials to minimise disruption to the implanted tissue (Guo et al., 2018; Khodagholy et al., 2013). Further technological advances in biomaterials are therefore likely to aid the study of the brain in animal models. Nonetheless, with proper experimental considerations, current approaches combining drug infusions and electrophysiological recordings provide valuable insight. Suitable controls using sham implantation and vehicle administration make it possible to explore specific effects of the drug on cellular physiology. Continuous and long-term electrophysiological recordings provide internal temporal controls to compare changes in neural activity patterns within the same

animal. While implantation is currently unavoidable to record brain activity from mice, alternative non-invasive approaches to manipulate the UPR do exist, such as molecular-genetic methods to overexpress misfolded proteins or UPR-related proteins (Bergmann et al., 2018; Shoulders et al., 2013). Recombinant genetic constructs or transgenic mouse models can also be utilised to target specific cell types in the brain using the Cre recombinase system (Utomo et al., 1999) or cell type-specific promoters (Walther & Stein, 1996). These approaches could be further combined with inducible expression systems for greater temporal control of UPR activation (Jaisser, 2000).

The fluorescent reporter described in **Chapter 4**, sUPRa, provides a novel tool for quantifying the global UPR with cellular resolution. The design of the reporter used a fragment of the BiP promoter to detect the downstream effects of the ATF6, IRE1 and PERK arms of the UPR. This thesis has not characterised the degree to which each individual arm of the UPR contributes to sUPRa's readout. However, as a starting point in research questions that are initially agnostic in terms of the individual UPR pathways, the BiP transcriptional reporter would provide a robust readout of the adaptive effects of the UPR. One limitation is that the onset of sUPRa's signal shows a lag due to its transcriptional nature, with delays between the onset of ER stress, UPR signalling, transcriptional activation and ultimately translation of the fluorescent protein. Despite the delay, the reporter provides a useful readout of the cell's recent ER stress and UPR history. Further characterisation of the ON/OFF dynamics could be conducted to determine the temporal limitations and better contextualise sUPRa's readout of UPR activity. Although sUPRa was designed to be used in live cells, this thesis used microscope imaging of fixed cells at discrete timepoints to monitor reporter responses. An alternative approach would be to use high-throughput flow cytometry to measure sUPRa fluorescence from live cells. Moreover, live cell imaging to monitor sUPRa's responses over time within the same cell populations would also provide further information on the kinetics of the reporter signal.

In **Chapter 5**, I considered methods for long-term neuronal expression of reporter constructs for studying the physiological UPR in the mouse brain. Certain recombinant gene expression methods are likely to inherently alter cellular physiology because of the exogenous introduction of DNA and expression of fluorophores. *In utero* electroporation of sUPRa plasmid DNA was found to cause a lower baseline reporter response than viral transduction, making electroporation better suited to studying physiological UPR, at least in cortex. However, one of the limitations of IUE is the range of cell types that can be easily targeted: excitatory neurons in specific cortical layers. Transgenic reporter mouse lines offer a solution for long-term expression of the reporter in more varied cell types, across different brain regions, and with a potentially low impact on baseline UPR levels.

While using mice as a model organism allowed the investigation of the UPR within an intact brain, one of the limitations within this thesis was the selective use of male mice in **Chapter 2** and **Chapter 3**. This limitation arises from the common practice in biomedical research to predominantly use male mice, due to the variability that arises from using female mice at different stages of the oestrous cycle. Gonadal sex and sex chromosomes have a substantial impact at all levels of the central nervous system, from gene expression to behaviour (Cahill, 2006; Hajali et al., 2019; Jazin & Cahill, 2010). Sleep-wake regulation has been found to differ between males and females, and within females, at different stages of the oestrous cycle (Dib et al., 2021; Ehlen et al., 2013; Koehl et al., 2003; Schwierin et al., 1998). Therefore, the cellular effects of sleep deprivation and the brain network effects of the UPR are also likely to be different in females at different stages of the oestrous cycle compared to males. In **Chapter 5**, both male and female mice were used to assess sUPRa's response in cortical neurons after sleep deprivation. However, the difference in effect between males and females was not addressed. When using female mice in an experiment, it is arguably more challenging to account for the variability in the stages of their oestrous cycles. This would require careful statistical power analysis to determine the number of female mice required

to detect the expected effect. Needless to say, incorporating female mice in research is crucial for a comprehensive understanding of fundamental biological processes, such as the UPR and sleep.

Having considered some of the methodological limitations of the experimental work, I will use the next sections of this General Discussion to further discuss the implications of my findings in relation to the broader field. I will also reflect on how we might hope to make progress in addressing some of the outstanding questions in the future.

6.3 Heterogeneity of the UPR

The brain is the most heterogenous organ of the body, with the cortex alone comprising of at least 133 distinct cell types (Tasic et al., 2018). Brain tissue is made of a variety of neuronal, glial, endothelial, epithelial, vascular and immune cell types arranged into functionally distinct regions. Since the histological and morphological classification of neurons by Santiago Ramon y Cajal and Camillo Golgi in the late 1800s, neuronal cell types have continued to be classified based on their electrical properties, connectivity and gene expression. Over the last decade, high throughput technologies have allowed significant advances in revealing the entire transcriptome of these cell types (Hrvatin et al., 2018; Jha et al., 2022; Longo et al., 2021; Tasic et al., 2018). While these technologies require highly specialised and expensive resources, more accessible methods using immunohistochemistry or *in situ* hybridisation can also be important for probing specific proteins or transcripts of interest within unique cell types.

Most seminal research studies that indicated that sleep deprivation causes UPR activation in the cerebral cortex used bulk tissue methods to measure transcript or protein levels (Cirelli et al., 2004; Naidoo et al., 2005; Terao et al., 2003). The frontal cortex was shown to express greater levels of BiP protein following sleep deprivation (Naidoo et al., 2005). However, a systematic comparison of UPR activation across spatially distinct regions and distinct cell types was missing. In **Chapter 2**, I began to address this gap by assessing whether different regions of the cortex display the same levels of UPR activation after sleep deprivation. The finding that BiP protein levels vary across

cortical regions, at baseline and in their response to sleep deprivation, highlights spatial heterogeneity within the cortex across the antero-posterior axis (Chapter 2 **Figure 2.3**). This variation in BiP expression aligns with the variation observed in slow wave activity (SWA) following sleep deprivation, which is particularly prominent in the frontal cortex (Chapter 2 **Figure 2.1**). This raises the question of whether the observed spatial correlation between UPR activation and SWA rebound following sleep deprivation may have a causal relationship. I explored this question in **Chapter 3**. However, the pharmacological approach used to activate the UPR resulted in non-physiological levels of the UPR, due to which it was difficult to draw definitive conclusions. Nevertheless, in future experiments, employing more refined strategies to manipulate the UPR (refer to section **6.6**) can contribute to a better understanding of the causal relationship between the UPR and SWA.

To date, there has been no investigation into whether neurons in particular contribute to the observed increase in BiP levels in the frontal cortex after sleep deprivation. In **Chapter 2**, I was able to confirm that neurons in the frontal cortex showed an increased expression of BiP (Chapter 2 **Figure 2.5**). Future immunohistochemical experiments could use markers of other cell types in the brain, for example glial fibrillary acidic protein (GFAP) to identify astrocytes or ionising calcium-binding adaptor molecule 1 (Iba1) to identify microglia and macrophages, to quantify their BiP expression levels. Alternatively, novel scRNAseq and cell type proteomics datasets from the brains of sleep deprived and control mice could be probed to identify UPR-related transcripts and proteins in specific cell types (Jha et al., 2022).

In the cortex, 15-20% of neuronal cells are GABAergic inhibitory interneurons, out of which approximately 40% are PV+ and 30% are SST+ (Keller et al., 2018; Rodarie et al., 2021). The majority of the non-inhibitory cells in the cortex are excitatory pyramidal neurons (Keller et al., 2018). Given that the general neuronal population exhibits a BiP upregulation following sleep deprivation, I next probed this effect in the largest pools of inhibitory interneurons, PV+ and SST+ interneurons.

Interestingly, both of these neuronal subpopulations had lower expression of BiP compared to a neighbouring neuron regardless of sleep history (Chapter 2 **Figure 2.6**). Given the densities of inhibitory and excitatory cell types in the cortex, it is likely therefore, that the neighbouring non-interneuron cell types were excitatory pyramidal neurons. Additionally, neither of the two interneuron types exhibited a significant upregulation of BiP following sleep deprivation, although PV+ interneurons showed a trend (Chapter 2 **Figure 2.7**). This highlights the cell type-specific heterogeneity of UPR activation. Furthermore, this indicates that the observed increase in BiP within the overall neuronal population may primarily originate from putative excitatory neurons. This could be confirmed in future experiments by using a glutamatergic cell marker, for example vesicular glutamate transporter 1 or 2 (vGluT1 or vGluT2), to identify pyramidal neurons in the cortex. If it is indeed the case that excitatory neurons are primarily affected by the response to sleep deprivation, this would be consistent with previous findings showing that the translational profile of excitatory neurons is more susceptible to alterations caused by sleep deprivation compared to interneurons (Puentes-Mestril & Aton, 2017). Furthermore, the lower susceptibility of interneurons to sleep deprivation induced BiP upregulation may be due to their lower activity levels compared to excitatory neurons during wakefulness (Niethard et al., 2016). I further explore the possibility of activity-dependent UPR activation in section **6.7** of this chapter.

Neurons in the cortex also exhibit functional diversity across different layers, and each layer gives rise to distinct network activity patterns. A recent study has shown that different cortical layers also exhibit differences in their transcriptional response to sleep deprivation (Vanrobaeys et al., 2023). In **Chapter 2**, I showed that NeuN+ neurons in L5 exhibited the greatest BiP expression level compared to other layers in the frontal cortex (Chapter 2 **Figure 2.8**). L5 neurons in the frontal cortex have been implicated in sleep regulation, whereby mice with a subset of neurons functionally silenced in L5 showed increased wakefulness and decreased homeostatic rebound in SWA after sleep deprivation (Krone et al., 2021). In addition, slow wave amplitude is significantly greater in L5 compared to L2/3. Thus, there is a correlation between the level of SWA and BiP expression in

cortical layers, similar to that observed in cortical regions along the antero-posterior axis. In future experiments it would be interesting to identify specific cell types within L5, such as excitatory pyramidal neurons and inhibitory interneurons, to investigate the distinct effects of sleep deprivation within this layer.

While immunohistochemistry is a valuable means to identify the diversity in the physiological UPR across regions and cell types in the cortex, additional methods could be utilised to further investigate the dynamics and the cause of UPR activation. In the upcoming section, I will explore some of these alternative approaches to monitoring the UPR.

6.4 How to monitor the UPR

The first stage in studying the UPR involved detecting and quantifying it. There are a range of methods for assessing ER homeostasis and the state of the UPR in mammalian systems, including immunological, chemical and genetic approaches (Sicari et al., 2020). One of the major hurdles in detecting low levels of the physiological UPR is a lack of tools with sufficient sensitivity. As evident from the current thesis and other studies, deciphering the UPR under physiological conditions is extremely challenging due to small effect sizes. Given that the UPR pathways result in highly diverse activation patterns depending on specific stimuli, another challenge lies in knowing which specific aspect of the UPR is associated with a particular physiological process. Although many studies examining the UPR typically concentrate on characterising individual UPR pathways, such as detecting XBP1 splicing or levels of p-eIF2α, this approach may fail to capture the overall effect on the UPR.

In **Chapter 4**, I attempted to develop a highly sensitive fluorescent reporter of the UPR, sUPRa, by incorporating a region of the BiP promoter that encapsulates activity of all three UPR pathways cumulatively, and displays low levels of baseline expression to maximise the reporter's signal-to-noise (Chapter 4 section **4.3.2**). sUPRa was found to display greater responses than a reporter of IRE1 activity (Iwawaki et al., 2004) and a reporter of PERK/p-eIF2α signalling (Helseth et

al., 2021) with experimental UPR activation (Chapter 4 section **4.3.3**). In a previous study, a transcriptional reporter of BiP was found to only respond to overexpression of activated ATF6, but not to sXBP1 or ATF4 (Origel Marmolejo et al., 2020). However, that reporter used a ~1kb BiP promoter, which is likely to have a high degree of baseline expression and fail to detect activation by sXBP1 or ATF4. Moreover, the ~1kb BiP promoter-based reporter resulted in a 2-fold fluorescence increase with 1 µg/ml Tunicamycin, whereas sUPRa showed a ~7-fold increase with the same treatment. This supports the finding that sUPRa's promoter design allows for greater sensitivity to UPR activation. Future experiments should aim to determine the extent to which sUPRa captures each of the three UPR arms, by measuring its response to overexpression of the main transcription factors downstream of each arm: ATF6, sXBP1 and ATF4.

sUPRa was capable of detecting physiological UPR activation with 12 hours of sleep deprivation in a neuronal subpopulation (Chapter 5 section **5.3.3**). However, in **Chapter 5** I measured sUPRa expression at a terminal timepoint at the end of the 12-hour sleep deprivation, which may not be the optimal timepoint for sUPRa's peak response. By employing methods such as *in vivo* 2-photon imaging or fibre photometry, it will be possible to continuously monitor the levels of sUPRa fluorescence at a finer temporal resolution. This would allow us to optimally detect the peak UPR activation during and following a period of sleep deprivation. Furthermore, it would help us understand the temporal patterns of UPR activation caused by sleep deprivation. The 12-hour sleep deprivation paradigm used in Chapter 5 is arguably non-physiological and may not occur naturally. UPR activation under sleep deprivation may also have different characteristics to UPR activation under normal sleep and wake behaviours. To this end, future experiments could examine how sUPRa responds during spontaneous wakefulness, sleep and sleep deprivation. This could be achieved by either harvesting tissue samples at specific timepoints or utilising continuous fibre photometric recordings of sUPRa fluorescence *in vivo.*

Tracking the UPR with high sensitivity over time will also help to address whether and how sleep may act to restore the UPR or protein homeostasis. BiP levels have been found to remain elevated after a recovery period following acute sleep deprivation, even after 24 hours (Naidoo et al., 2007a; Terao et al., 2003), which might indicate that the adaptive UPR remains active for protein homeostasis during recovery sleep. On the other hand, a study showed that cortical BiP transcript levels are not elevated to the same extent following chronic sleep deprivation (8 days) compared to acute sleep deprivation (8 hours) (Cirelli et al., 2006). It seems possible that undergoing chronic sleep deprivation leads to prolonged UPR activation, which can result in the adaptive UPR being inhibited, similar to what is observed in aged animals (Naidoo et al., 2008). To further explore the induction and recovery dynamics of the UPR, transgenic mice could be used for widespread and strong expression of sUPRa in the brain, and combined with *in vivo* fibre photometry or 2-photon imaging. sUPRa imaging could help provide better temporal resolution of the UPR's dynamics following different durations and paradigms of sleep deprivation. Moreover, since sUPRa is amenable to long-term expression in neurons, it could also be used to track the effects of sleep disruption on the UPR in models of ageing and neurodegeneration.

Genetic reporters are useful tools for obtaining cell-specific readouts of UPR activation either at the transcriptional or protein level. While sUPRa is a genetic reporter that detects the transcriptional activity of BiP, other genetic reporter tools can be used to detect the protein level or activity of a protein of interest. For example, fusion fluorescent reporters that tag the protein of interest can be used to provide a readout of protein abundance to assess the downstream effects of UPR activation. However, it is important to consider that using fluorescent protein tags may interfere with protein function. Moreover, many protein components are extremely long-lived and persist long after inactivation of the UPR, making them suboptimal for monitoring the kinetics of the UPR (Lajoie et al., 2014). Therefore, alternative approaches using cleavage of tagged fluorescent proteins or a readout of transcriptional activation of a gene of interest may be preferable. Considering that BiP protein like other proteins exists in multiple states, for example due to post-

translational modifications or re-localisation to other cellular compartments (Preissler et al., 2017; Sun et al., 2006; Y. Zhang et al., 2010), fluorescent biosensors that track its post-translational modifications using fluorescence resonance energy transfer (FRET) could also be useful (Aye-Han et al., 2009). The optimisation of new and improved, highly sensitive genetic reporters is essential for studying physiological processes. Strategies such as increasing fluorophore turnover within the cell are being increasingly utilised to improve kinetic properties of genetic reporters (Lajoie et al., 2014). Moreover, improvements in the properties of fluorescent proteins, for example optimising their structure to increase their brightness (Pédelacq et al., 2006), could contribute to enhancing reporter sensitivity. Alternative methods using non-organic luminescent nanomaterials may further improve our ability to sensitively detect physiological UPR levels, which highlights the need for interdisciplinary collaboration (Q. Liu et al., 2011; Veeramani et al., 2019).

An alternative approach to studying the UPR under physiological conditions is to visualise and quantify changes in the ER unfolded protein burden or the ER environment. Fluorescence recovery after photobleaching (FRAP) can be used to assess the diffusional mobility of fluorescently tagged chaperones, such as BiP, to indicate their interactions with unfolded proteins in the ER lumen (Costantini & Snapp, 2013; Lai et al., 2010). This approach can detect early changes in the ER protein burden that cannot be detected by classical UPR assays (Lai et al., 2010). Alternatively, the level of protein unfolding or misfolding in a cell can be detected by staining with Thioflavin T, a small molecule that exhibits increased fluorescence when bound to protein aggregates (Beriault & Werstuck, 2013). While Thioflavin T has been used to detect the presence of pathological protein aggregates, such as amyloid beta and alpha synuclein (Manning-Bog et al., 2002; Rajamohamedsait & Sigurdsson, 2012), there is a lack of evidence for its ability to detect low levels of unfolded proteins within the ER, which may not cause aggregation. Other approaches include spectroscopy-based methods to detect deviations in the protein states within live cells (Hosoda et al., 2011; Karunanithy et al., 2019; Wheeler et al., 2019). These methods hold great potential for investigating the protein burden within live cells as they do not require the unnatural expression of reporters or

tags. However, these methods are limited by their lack of specificity for detecting increased protein load within the ER, since deviations in spectral readouts may correspond to more general changes in the structural state of proteins within the cell. For greater specificity, the folding state of individual candidate proteins could also be investigated by site-specific labelling or small molecule probes that bind to specific folded forms of specific proteins (Hsieh et al., 2014; Y. Liu et al., 2014). In addition to ER protein load, reporters have been developed to detect perturbations to the ER environment, specifically, calcium homeostasis and redox balance within the ER (Henderson et al., 2014; Merksamer et al., 2008; Xia et al., 2020). Together, these strategies could provide a useful indication of the factors leading to physiological UPR activation.

Advances in methods to detect ER protein burden and environment will be extremely helpful in understanding the functional relevance of UPR signalling, and to study physiological conditions more fundamentally in terms of their protein homeostasis. Although the physiological UPR is known to be activated under conditions such as sleep deprivation, it remains to be determined whether this is due to an upstream imbalance in the ER protein load and ER capacity. While disturbances in the ER load and folding capacity are thought to be the primary stimulus for the UPR, there are also other stimuli, such as oestrogen and epidermal growth factor, that may activate an anticipatory UPR independent of ER stress (Andruska et al., 2015; Shapiro et al., 2016; Yu et al., 2016). Therefore, in any new research question investigating the UPR in particular physiological processes, it will be important to first identify and characterise UPR activity using UPR-sensing reporters. To begin with, it may be helpful to use a reporter of global UPR activity to identify kinetics of the response. This could then be followed by dissecting individual UPR pathways using single-arm reporters or a multiplexed approach (Adamson et al., 2016; Nougarède et al., 2018). Ultimately, the causes of UPR activation could be further examined through measurements of environmental perturbations in the ER and ER protein burden.

6.5 UPR and brain activity

While sleep deprivation is a physiological condition that triggers UPR activation in cortical neurons, the impact of the UPR on cortical activity, and therefore the regulation of sleep, is poorly understood. In **Chapter 3**, I characterised the effects of UPR activation on brain activity and sleep regulation. I activated the UPR locally in a region of the cortex and measured brain activity directly from the affected region, as well as from a distant region. Although the effects on brain activity may be obscured by the toxic effects of Tunicamycin in some animals a few days after drug infusion, we should consider the possibility that the early stages of UPR activation were not toxic. Local UPR activation did not result in acute effects on brain activity in either the local or the distant regions during the first 2 days. This is consistent with the findings in Nosyreva & Kavalali (2010), where no alterations in synaptic activity was observed within the first 2 days of UPR induction in cultured neurons. Therefore, it appears that the early UPR does not directly regulate population activity but rather may help to restore other cellular factors for maintaining normal neuronal activity. Since LFP activity is more likely to reflect population level fluctuations in synaptic membrane potential as opposed to spiking rates (Einevoll et al., 2013; Lindén et al., 2011), mild alterations in the spiking activity of single neurons that are caused by the early UPR (D.-C. Liu et al., 2019) may not be detectable in the LFP. In future experiments, techniques such as *in vivo* patch clamping could be used to directly measure the electrical activity of individual neurons within the intact brain after UPR activation. This approach may offer higher resolution and potentially greater sensitivity to detect the effects of UPR activation in its early stages.

Unlike a localised UPR activation, studies that have manipulated the UPR across the whole brain via intracerebroventricular or intraperitoneal drug administration (Crider et al., 2018; Methippara et al., 2009, 2012) have found early changes in brain activity. Specifically, enforced activation of PERK/p-eIF2α signalling during sleep deprivation has been reported to increase slow frequencies during subsequent NREM sleep, whereas, PERK/p-eIF2α activation during sleep

decreases slow frequencies in brain EEG recordings (Methippara et al., 2012). This also suggests that the timing of UPR activation in relation to sleep-wake history has an impact on its subsequent effects upon neural activity. Specifically, local UPR activation during sleep deprivation may have a greater impact on subsequent neural activity than UPR activation prior to spontaneous wakefulness, which was the strategy used in **Chapter 3**. This could be tested by activating the UPR in a local region of the cortex during a period of sleep deprivation, after which SWA during recovery sleep could be measured to assess potential local effects on homeostatic SWA regulation.

While *in vivo* experiments are directly relevant to understanding the UPR's role in normal physiology and pathology, simplified *in vitro* systems are also valuable for characterising certain properties of neural activity. A previous study has demonstrated that pharmacological activation of the UPR in neuronal cultures with Tunicamycin and Thapsigargin for over 48 hours leads to an increase in spontaneous excitatory neurotransmission (Nosyreva & Kavalali, 2010). Earlier timepoints were not shown to alter synaptic transmission, suggesting that chronic, potentially pro-apoptotic, UPR activation alters synaptic transmission. In a separate study, pharmacological UPR activation in neuronal cultures suppressed neuronal spiking within the first hour of Thapsigargin treatment (D.-C. Liu et al., 2019). Therefore, the early adaptive UPR might act to downregulate further excitatory signalling as part of a homeostatic process to prevent over-excitation and neuronal damage (Kezuka et al., 2016). However, when UPR activation persists for longer periods, it may fail to mount a sufficient homeostatic response and may lead to excessive excitation and neuronal damage.

Although in Chapter 3 there were no immediate effects of the UPR on brain activity, the longer term effects, such as the selective decrease in slow frequencies during NREM sleep (Chapter 3 section **3.3.6**), may reflect the pre-pathological or pathological state resulting from sustained UPR activation. The UPR is primarily an adaptive process that aims to restore protein homeostasis within a cell. Early adaptive UPR responses act to attenuate ER protein load and increase folding capacity

by (1) inhibiting translation and translocation of proteins into the ER, (2) autophagy and degradation of damaged proteins in the ER, and (3) upregulation of folding chaperones. However, unresolved ER stress and the chronic activation of the UPR can result in undesirable effects that limit cellular function or exacerbate dysfunction and ultimately may result in cell death (Tabas & Ron, 2011). Therefore, in order to study the causal role of the physiological UPR in regulating brain activity and sleep, it is important to employ methods that result in mild and reversible UPR activation. In the next section, I will explore some of these alternative approaches for manipulating the UPR.

6.6 How to manipulate the UPR

To fully understand the effects of the UPR in regulating physiology or pathophysiology, it is necessary to employ systems and models to manipulate the UPR. This in itself poses a challenge since most experimental methods of manipulation are non-physiological. Pharmacological methods to induce ER stress rely on the gross impairment of protein folding in the ER, and can also have pleiotropic effects causing a much broader pathological phenotype than physiological stress (Bergmann et al., 2018). However, for the experimental investigation of the UPR, a "sledgehammer" approach is typically used for manipulating the UPR with high concentrations of drugs to exacerbate an ER stress phenotype. It has been shown that carefully titrating the concentration of ER stress-inducing drugs can better mimic a physiological stress, in terms of the transcriptional profile of UPR activation (Bergmann et al., 2018; Bergmann & Molinari, 2018). Therefore, further work needs to be done to identify the concentration-dependent intensity and profile of UPR activation using pharmacological approaches.

In addition to pharmacological approaches, more sophisticated tools are needed to manipulate the UPR with greater spatial and temporal resolution. One such approach is the direct genetically targeted overexpression of misfolded proteins in the ER, which has been shown to elicit an UPR-specific transcriptional profile, rather than eliciting non-specific effects (Bakunts et al., 2017; Bergmann et al., 2018). This approach could be tailored for different cell types by expressing

misfolded variants of proteins that are specifically expressed in the cell types of interest. For example, in neurons, transmembrane proteins that are processed through the ER, such as NMDA receptors or potassium channels (D. Ma et al., 2001; Mu et al., 2003), could be mutated to be retained in the ER and activate an UPR. The genetic expression of such constructs could be inducible, using a Tet-ON system, and targeted to specific cell types, using the Cre-LoxP system, for a high degree of temporal and spatial control (Jaisser, 2000; Utomo et al., 1999).

To investigate the UPR independently of ER protein burden, genetic tools and transgenic models can be used for the specific manipulation of transcription factors and effectors of the UPR. A caveat with this approach is that exogenous transgene expression in a cell may itself perturb the physiological conditions and interfere with the UPR. Therefore, for this method to be used successfully, it is first necessary to establish that the transgene expression system or model is not inherently altering the UPR. Moreover, even after careful optimisation, constitutive expression of target genes produce non-physiological levels of expression and significant off-target effects. A promising refinement to this approach is the use of chemical genetic tools that enable the tuneable and orthogonal activation of UPR pathways to physiological levels in the absence of stress. Using small molecules to activate the expression of genetically encoded sXBP1 and/or ATF6 to physiologically relevant levels has been shown to influence the handling of faulty proteins in the ER, without affecting the global endogenous proteome (Shoulders et al., 2013).

In addition to direct manipulation of the UPR, more physiological perturbations to the cellular environment could be probed to tune a physiologically relevant UPR. Several studies have demonstrated that the profile of UPR activation and its downstream effects are finely tuned to the form of ER stress stimulus, and can display unique temporal dynamics (Acosta-Alvear et al., 2007; DuRose et al., 2006; J. H. Lin et al., 2007; Rutkowski & Kaufman, 2007; F. Walter et al., 2015). Consequently, when manipulating the UPR to study its physiological roles, it is preferable to first determine the profile of the physiological UPR and the form of ER stress that triggers its activation,

and then attempt to closely match that stimulus using exogenous agents or genetic manipulations. For instance, the UPR is known to respond to glucose availability, redox balance and calcium homeostasis, but the response may vary in the context of the functions of the specific cell type. Pancreatic beta cells modulate the UPR in response to plasma glucose levels in preparation for insulin production (Elouil et al., 2007; Kaufman et al., 2002). Therefore, to study the physiological processes of beta cells, the UPR could be indirectly modulated by altering glucose concentration, which is a physiologically relevant variable for that cell type. Similarly, physiological stimuli for UPR activation in neurons could first be identified and then manipulated to modulate the UPR. For example, since excitatory neurotransmission is found to activate the physiological UPR (Saito et al., 2018), modulating excitatory transmission could be used as a strategy to indirectly manipulate the UPR. However, this approach for physiologically manipulating the UPR requires caution because it retains the complexity of physiological systems, whereby the outcomes of the manipulation may not be UPR-specific. Taken together, it is likely that a combination of multiple approaches and manipulation strategies will be required to understand the diverse roles of the UPR in normal physiology and pathophysiology.

6.7 What causes UPR activation during sleep deprivation?

In this section, I will consider a major outstanding question in the field, and discuss potential approaches to address it in future work. I showed in **Chapter 2** that cortical neurons display elevated levels of adaptive UPR as a result of extended wakefulness. However, the underlying cause of the neuronal UPR during sleep deprivation is not clear. The UPR is an adaptive mechanism that serves to match the levels of ER protein folding capacity with ER unfolded protein load, in order to maintain proteostasis. Under normal physiological conditions, ER load can fluctuate due to changing protein synthesis demands and a change in the level of protein flux through the ER. Conversely, ER protein folding capacity may be altered due to perturbations in the cellular and ER environment. This results

in finely-tuned alterations in the physiological UPR to maintain the cell's proteostatic balance. So what mechanisms are responsible for the activation of the UPR in neurons during sleep deprivation?

One possibility is that the neuronal UPR is activity-dependent. The neuronal proteome has been shown to vary during wake and sleep (Cirelli et al., 2009; Jha et al., 2022; Noya et al., 2019), and is known to be activity-dependent (Di Liegro et al., 2014; Ehlers, 2003; Madabhushi & Kim, 2018). Neuronal firing is generally higher during wake compared to sleep, with sleep deprivation causing a further elevation in cortical firing rates (Cirelli, 2017; McKillop et al., 2018b; V. V. Vyazovskiy et al., 2009). Interestingly, this observed increase in neuronal firing is region- and cell type-specific (Hengen et al., 2013; Steriade et al., 2001). Therefore, the increase in UPR levels observed with sleep deprivation, which I have shown are also region- and cell type-specific, may be a reflection of neuronal activity levels. The newly developed fluorescent reporter, sUPRa, could be used to study the underlying mechanism of UPR elevation in the cerebral cortex as a result of sleep deprivation. To investigate whether sleep deprivation-induced UPR is activity-dependent, *in vitro* brain slice systems could be used for live cell sUPRa imaging to monitor the dynamics of UPR activation in neuronal populations under different activity levels. Neuronal activity could be manipulated using optogenetic or electrophysiological strategies. This could be extended to *in vivo* systems using sUPRa-expressing transgenic mice for fibre photometric recordings of sUPRa responses to optogenetic or sensory stimulation of neuronal populations. sUPRa could be further optimised to be expressed in specific cell populations in a Cre-dependent manner, to identify cell type-specific effects of synaptic activity on the UPR.

Neuronal activity patterns also determine synaptic plasticity processes, which rely on *de novo* protein synthesis of synaptic components and their trafficking through the ER (Cajigas et al., 2010; Lüscher et al., 2000; Martínez et al., 2018; Mu et al., 2003). There is molecular, ultrastructural and electrophysiological evidence suggesting that wakefulness is associated with a net increase in synaptic strength (Bellesi & de Vivo, 2020; Z.-W. Liu et al., 2010; V. V. Vyazovskiy et al., 2008). The

demands associated with synaptic plasticity may therefore be another putative cause for increased ER load and the onset of adaptive UPR during wakefulness. However, extended wakefulness or sleep deprivation, which causes greater UPR activation than normal wakefulness, has been shown to impair LTP and related protein synthesis (Havekes et al., 2012; Lyons et al., 2023b; Tudor et al., 2016; Vecsey et al., 2009). This impairment in LTP may reflect homeostatic plasticity mechanisms, whereby the cumulative potentiation of synapses during prior normal wakefulness results in an increase in net synaptic strength towards saturation, thereby raising the threshold for further potentiation during sleep deprivation (Kuhn et al., 2016; J. Li et al., 2019). This is the basis of the influential synaptic homeostasis hypothesis (SHY) of sleep, which proposes that increases in synaptic strengths during waking are downscaled during sleep to restore the ability of neurons to undergo potentiation (Tononi & Cirelli, 2003, 2006). Currently, the relationship between synaptic potentiation and the UPR across the sleep-wake cycle remains unexplored. However, future investigation into the interplay between synaptic plasticity, protein synthesis and the UPR could provide valuable insights into the mechanisms underlying the physiological UPR activated by sleep deprivation.

Both the UPR and synaptic plasticity have been hypothesised to play a role in accumulating sleep pressure. The potential interactions between the UPR and synaptic plasticity could be explored using simplified systems such as *in vitro* organotypic brain slices. Firstly, standard long-term potentiation (LTP) protocols could be combined with sUPRa imaging to determine whether synaptic plasticity triggers UPR activation. Secondly, the UPR could be induced using pharmacological or molecular genetic approaches, followed by LTP induction, to assess if ER stress affects a neuron's capacity for synaptic plasticity. In parallel to these *in vitro* studies, the roles of the UPR, synaptic plasticity, and sleep drive could be investigated *in vivo*: a sensory stimulation paradigm that is known to induce synaptic plasticity could be used along with pharmacological or genetic techniques to block plasticity. This would enable the assessment of whether synaptic

activity leads to UPR activation, and whether this UPR can enhance sleep drive independent of synaptic plasticity.

The UPR has been previously shown to modulate sleep drive, although the mechanism underlying this is not understood (Ly et al., 2020; Methippara et al., 2009, 2012; Naidoo et al., 2007a). The UPR has a reciprocal relationship with protein synthesis. When there is a surge in protein synthesis and increased protein flux through the ER, the UPR's quality control mechanisms are activated to ensure proper folding and processing of proteins. In turn, the UPR acts as a negative feedback loop, dampening protein synthesis to prevent excessive ER stress and maintain cellular homeostasis. Slow wave sleep (NREM) is associated with higher rates of protein synthesis in the brain compared to either wake or REM sleep (Nakanishi et al., 1997; Ramm & Smith, 1990). On the contrary, sleep deprivation is associated with an inhibition of protein synthesis, indicated by the increase in PERK/p-eIF2α signalling and changes in the ribosomal profile (Naidoo et al., 2005). The macromolecule biosynthesis hypothesis proposes that sleep, perhaps slow wave sleep in particular, functions to restore cellular stresses in order to relieve the inhibition of protein synthesis (Mackiewicz et al., 2007). This poses a conceptual difficulty. Since the physiological UPR is an adaptive process to restore protein homeostasis, why does sleep not promote it further? And if the rates of protein synthesis are highest during slow wave sleep, why does that not result in higher levels of UPR activation?

Gene expression and protein synthesis profiles are known to be very different during wake and sleep (Cirelli et al., 2004, 2009). Sleep-wake processes are thought to be a major regulator of the synaptic proteome, whereas the transcriptome is thought to be under greater circadian control (Noya et al., 2019). Wakefulness is associated with the upregulation of cellular components involved in synaptic plasticity and glutamatergic neurotransmission, which require processing through the ER (Cirelli et al., 2004). Therefore, it could be that during waking activity a high proportion of protein synthesis requires ER processing, which cumulatively results in a mild adaptive UPR. During

subsequent sleep, perhaps ER load is further suppressed to deactivate the UPR, or perhaps the UPR is somehow suppressed directly, to allow ER-independent protein synthesis to occur (**Figure *6.1***). To date, there is no direct evidence suggesting that the ER protein load does increase during wakefulness. Therefore, the wakefulness-associated UPR may be unrelated to wakefulness-associated protein synthesis, and may instead be due to environmental perturbations in the ER. In this case, sleep may act to restore the cellular and ER environment to attenuate the UPR and its translational block. Therefore, increased homeostatic sleep pressure may reflect a higher demand for brain protein synthesis following a translational block (Ly et al., 2020; Methippara et al., 2009). To address these speculations, a series of experiments would need to be conducted to identify whether ER protein load and ER environment vary between sleep and sleep deprivation. Techniques for monitoring ER protein load, such as *in vivo* fibre photometry or 2-photon imaging for FRET measurements of BiP-GFP (Lajoie & Snapp, 2011), could be used to investigate whether sleep

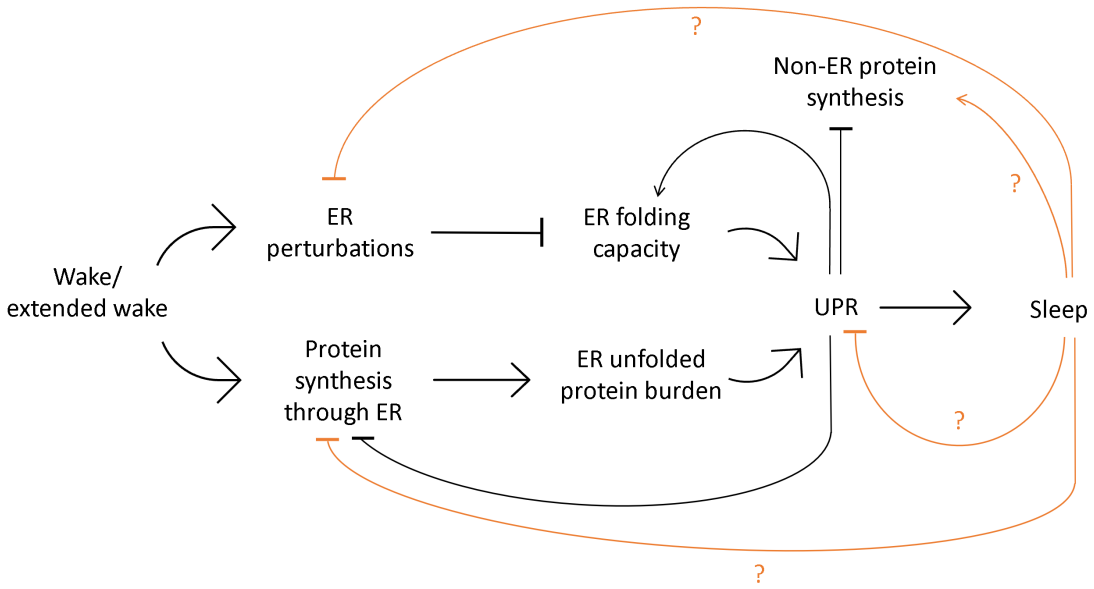

Figure 6.1 Schematic of possible interactions between protein synthesis, the UPR and sleep.

During waking activity, there may be an increase in ER protein processing, due to increased synthesis of proteins related to synaptic transmission and plasticity, which cumulatively results in a mild adaptive UPR. During subsequent sleep, ER load may be further suppressed to deactivate the UPR, or perhaps the UPR is somehow suppressed directly, to allow ER-independent protein synthesis to occur. Alternatively, the wakefulness-associated UPR may be unrelated to wakefulness-associated protein synthesis, and may instead be due to environmental perturbations in the ER, such as calcium fluctuations arising from synaptic activity. In this case, sleep may act to restore the cellular and ER environment, which attenuates the UPR and its translational block.

deprivation leads to an increased ER protein load compared to periods of sleep. Additionally, *in vivo* monitoring of the ER environment, with tools such as SERcAMP (Henderson et al., 2014), could be used to investigate potential differences in ER calcium homeostasis during sleep and sleep deprivation.

Overall, sleep does seem to play a restorative role in protein homeostasis. It is critical for proper cognitive functioning associated with learning and memory, which relies on protein synthesis-dependent plasticity (Grønli et al., 2014; Seibt et al., 2012). Moreover, there are associations between disrupted NREM sleep and increased levels of amyloid beta in the brains of older adults and patients in the early stages of Alzheimer's disease (Lucey et al., 2019; Mander et al., 2013; Winer et al., 2019). Sleep has also been associated with increased glymphatic clearance of amyloid beta and other metabolites (Eide et al., 2021; Ju et al., 2017; Xie et al., 2013), which may serve a function in removing dysfunctional proteins and restoring protein homeostasis in the brain. Therefore, sleep, and SWA in particular, may have therapeutic benefits in proteinopathies and related disorders as well as for healthy ageing (Y. F. Lee et al., 2020). There is a strong case, therefore, for further research into the underlying mechanisms of how sleep helps to restore protein homeostasis in the brain.

6.8 Conclusion

This thesis has contributed to the growing body of research investigating the intricate relationship between the UPR and sleep. Protein homeostasis, including protein synthesis, trafficking and turnover represents a fundamental process in all cells, including neurons in the brain. Moreover, sleep disruption is associated with disturbances to protein homeostasis, which may have implications for disease pathogenesis. Therefore, understanding the fundamental properties of sleep and sleep loss is of immense importance in advancing our understanding of cellular health and disease.

This thesis specifically investigated the UPR's correlation with the physiological challenge posed by sleep deprivation. The research findings presented in this thesis demonstrate that the UPR is associated with prolonged wakefulness, further supporting previous findings. Moreover, the thesis uncovered region- and cell type-specific effects of sleep deprivation on the UPR in mouse cortex, mirroring the spatial patterns observed in homeostatic slow wave activity during NREM sleep. These findings provide insights into the localised and heterogeneous impact of sleep deprivation on cellular stress responses. Furthermore, this thesis revealed that localised pharmacological activation of the UPR does not result in global alterations in sleep regulation. Continuous and long-term monitoring of brain activity following UPR activation also revealed potentially deleterious effects of the pharmacological approach on tissue health, highlighting the need for more nuanced interventions of the physiological UPR in future studies. Finally, this thesis introduced a novel dual colour fluorescent reporter of the UPR, sUPRa, which offers enhanced sensitivity and temporal dynamics for quantifying physiologically relevant levels of the UPR. This innovative tool will facilitate future research to better understand the dynamic relationship between the physiological UPR and sleep.

Bibliography

Abdullahi, A., Stanojcic, M., Parousis, A., Patsouris, D., & Jeschke, M. G. (2017). Modeling Acute ER stress in vivo and in vitro. *Shock (Augusta, Ga.)*, *47*(4), 506–513. https://doi.org/10.1097/SHK.0000000000000759

Abisambra, J. F., Jinwal, U. K., Blair, L. J., O'Leary, J. C., Li, Q., Brady, S., Wang, L., Guidi, C. E., Zhang, B., Nordhues, B. A., Cockman, M., Suntharalingham, A., Li, P., Jin, Y., Atkins, C. A., & Dickey, C. A. (2013). Tau Accumulation Activates the Unfolded Protein Response by Impairing Endoplasmic Reticulum-Associated Degradation. *Journal of Neuroscience*, *33*(22), 9498–9507. https://doi.org/10.1523/JNEUROSCI.5397-12.2013

Aboufares El Alaoui, A., Buhl, E., Galizia, S., Hodge, J. J. L., de Vivo, L., & Bellesi, M. (2023). Increased interaction between endoplasmic reticulum and mitochondria following sleep deprivation. *BMC Biology*, *21*(1), 1. https://doi.org/10.1186/s12915-022-01498-7

Achermann, P., & Borbély, A. A. (1998). Coherence analysis of the human sleep electroencephalogram. *Neuroscience*, *85*(4), 1195–1208. https://doi.org/10.1016/S0306-4522(97)00692-1

Acosta-Alvear, D., Karagöz, G. E., Fröhlich, F., Li, H., Walther, T. C., & Walter, P. (2018). The unfolded protein response and endoplasmic reticulum protein targeting machineries converge on the stress sensor IRE1. *ELife*, *7*, e43036. https://doi.org/10.7554/eLife.43036

Acosta-Alvear, D., Zhou, Y., Blais, A., Tsikitis, M., Lents, N. H., Arias, C., Lennon, C. J., Kluger, Y., & Dynlacht, B. D. (2007). XBP1 Controls Diverse Cell Type- and Condition-Specific Transcriptional Regulatory Networks. *Molecular Cell*, *27*(1), 53–66. https://doi.org/10.1016/j.molcel.2007.06.011

Adamantidis, A. R., Gutierrez Herrera, C., & Gent, T. C. (2019). Oscillating circuitries in the sleeping brain. *Nature Reviews Neuroscience*, *20*(12), Article 12. https://doi.org/10.1038/s41583-019-0223-4

Adamson, B., Norman, T. M., Jost, M., Cho, M. Y., Nuñez, J. K., Chen, Y., Villalta, J. E., Gilbert, L. A., Horlbeck, M. A., Hein, M. Y., Pak, R. A., Gray, A. N., Gross, C. A., Dixit, A., Parnas, O., Regev, A., & Weissman, J. S. (2016). A Multiplexed Single-Cell CRISPR Screening Platform Enables Systematic Dissection of the Unfolded Protein Response. *Cell*, *167*(7), 1867-1882.e21. https://doi.org/10.1016/j.cell.2016.11.048

Adesnik, H., & Naka, A. (2018). Cracking the Function of Layers in the Sensory Cortex. *Neuron*, *100*(5), 1028–1043. https://doi.org/10.1016/j.neuron.2018.10.032

Alfonsa, H., Burman, R. J., Brodersen, P. J. N., Newey, S. E., Mahfooz, K., Yamagata, T., Panayi, M. C., Bannerman, D. M., Vyazovskiy, V. V., & Akerman, C. J. (2023). Intracellular chloride regulation mediates local sleep pressure in the cortex. *Nature Neuroscience*, *26*(1), Article 1. https://doi.org/10.1038/s41593-022-01214-2

Alreja, A., Nemenman, I., & Rozell, C. J. (2022). Constrained brain volume in an efficient coding model explains the fraction of excitatory and inhibitory neurons in sensory cortices. *PLOS Computational Biology*, *18*(1), e1009642. https://doi.org/10.1371/journal.pcbi.1009642

Ameri, K., & Harris, A. L. (2008). Activating transcription factor 4. *The International Journal of Biochemistry & Cell Biology*, *40*(1), 14–21. https://doi.org/10.1016/j.biocel.2007.01.020

Amzica, F., & Steriade, M. (1995). Short- and long-range neuronal synchronization of the slow (< 1 Hz) cortical oscillation. *Journal of Neurophysiology*, *73*(1), 20–38. https://doi.org/10.1152/jn.1995.73.1.20

Anafi, R. C., Kayser, M. S., & Raizen, D. M. (2019). Exploring phylogeny to find the function of sleep. *Nature Reviews Neuroscience*, *20*(2), Article 2. https://doi.org/10.1038/s41583-018-0098-9

Andruska, N., Zheng, X., Yang, X., Helferich, W. G., & Shapiro, D. J. (2015). Anticipatory estrogen activation of the unfolded protein response is linked to cell proliferation and poor survival in estrogen receptor α-positive breast cancer. *Oncogene*, *34*(29), Article 29. https://doi.org/10.1038/onc.2014.292

Anken, E. van, Romijn, E. P., Maggioni, C., Mezghrani, A., Sitia, R., Braakman, I., & Heck, A. J. R. (2003). Sequential Waves of Functionally Related Proteins Are Expressed When B Cells Prepare for Antibody Secretion. *Immunity*, *18*(2), 243–253. https://doi.org/10.1016/S1074-7613(03)00024-4

Aserinsky, E., & Kleitman, N. (1953). Regularly Occurring Periods of Eye Motility, and Concomitant Phenomena, During Sleep. *Science*, *118*(3062), 273–274. https://doi.org/10.1126/science.118.3062.273

Ashery, U., Bielopolski, N., Lavi, A., Barak, B., Michaeli, L., Ben-Simon, Y., Sheinin, A., Bar-On, D., Shapira, Z., & Gottfried, I. (2014). Chapter Two - The Molecular Mechanisms Underlying Synaptic Transmission: A View of the Presynaptic Terminal. In V. Pickel & M. Segal (Eds.), *The Synapse* (pp. 21–109). Academic Press. https://doi.org/10.1016/B978-0-12-418675-0.00002-X

Ashraf, G. M., Greig, N. H., Khan, T. A., Hassan, I., Tabrez, S., Shakil, S., Sheikh, I. A., Zaidi, S. K., Wali, M. A., Jabir, N. R., Firoz, C. K., Naeem, A., Alhazza, I. M., Damanhouri, G. A., & Kamal, M. A. (2014). Protein misfolding and aggregation in Alzheimer's disease and Type 2 Diabetes Mellitus. *CNS & Neurological Disorders Drug Targets*, *13*(7), 1280–1293.

Aye-Han, N.-N., Ni, Q., & Zhang, J. (2009). Fluorescent Biosensors for Real-time Tracking of Post-translational Modification Dynamics. *Current Opinion in Chemical Biology*, *13*(4), 392–397. https://doi.org/10.1016/j.cbpa.2009.07.009

Bahar, E., Kim, H., & Yoon, H. (2016). ER Stress-Mediated Signaling: Action Potential and Ca2+ as Key Players. *International Journal of Molecular Sciences*, *17*(9). https://doi.org/10.3390/ijms17091558

Bakunts, A., Orsi, A., Vitale, M., Cattaneo, A., Lari, F., Tadè, L., Sitia, R., Raimondi, A., Bachi, A., & van Anken, E. (2017). Ratiometric sensing of BiP-client versus BiP levels by the unfolded protein response determines its signaling amplitude. *ELife*, *6*, e27518. https://doi.org/10.7554/eLife.27518

Balakrishnan, B., Sen, D., Hareendran, S., Roshini, V., David, S., Srivastava, A., & Jayandharan, G. R. (2013). Activation of the Cellular Unfolded Protein Response by Recombinant Adeno-Associated Virus Vectors. *PLOS ONE*, *8*(1), e53845. https://doi.org/10.1371/journal.pone.0053845

Bardo, S., Cavazzini, M. G., & Emptage, N. (2006). The role of the endoplasmic reticulum Ca2+ store in the plasticity of central neurons. *Trends in Pharmacological Sciences*, *27*(2), 78–84. https://doi.org/10.1016/j.tips.2005.12.008

Basheer, R., Brown, R., Ramesh, V., Begum, S., & McCarley, R. W. (2005). Sleep deprivation-induced protein changes in basal forebrain: Implications for synaptic plasticity. *Journal of Neuroscience Research*, *82*(5), 650–658. https://doi.org/10.1002/jnr.20675

Bellesi, M., & de Vivo, L. (2020). Structural synaptic plasticity across sleep and wake. *Current Opinion in Physiology*, *15*, 74–81. https://doi.org/10.1016/j.cophys.2019.12.007

Bell-Pedersen, D., Cassone, V. M., Earnest, D. J., Golden, S. S., Hardin, P. E., Thomas, T. L., & Zoran, M. J. (2005). Circadian rhythms from multiple oscillators: Lessons from diverse organisms. *Nature Reviews Genetics*, *6*(7), Article 7. https://doi.org/10.1038/nrg1633

Beltramo, R., D'Urso, G., Dal Maschio, M., Farisello, P., Bovetti, S., Clovis, Y., Lassi, G., Tucci, V., De Pietri Tonelli, D., & Fellin, T. (2013). Layer-specific excitatory circuits differentially control recurrent network dynamics in the neocortex. *Nature Neuroscience*, *16*(2), 227–234. https://doi.org/10.1038/nn.3306

Bendfeldt, K., Radojevic, V., Kapfhammer, J., & Nitsch, C. (2007). Basic Fibroblast Growth Factor Modulates Density of Blood Vessels and Preserves Tight Junctions in Organotypic Cortical Cultures of Mice: A New In Vitro Model of the Blood–Brain Barrier. *Journal of Neuroscience*, *27*(12), 3260–3267. https://doi.org/10.1523/JNEUROSCI.4033-06.2007

Benington, J. H. (2000). Sleep Homeostasis and the Function of Sleep. *Sleep*, *23*(7), 1–8. https://doi.org/10.1093/sleep/23.7.1j

Benington, J. H., & Craig Heller, H. (1995). Restoration of brain energy metabolism as the function of sleep. *Progress in Neurobiology*, *45*(4), 347–360. https://doi.org/10.1016/0301-0082(94)00057-O

Benington, J. H., Kodali, S. K., & Heller, H. C. (1995). Stimulation of A1 adenosine receptors mimics the electroencephalographic effects of sleep deprivation. *Brain Research*, *692*(1), 79–85. https://doi.org/10.1016/0006-8993(95)00590-M

Bergmann, T. J., Fregno, I., Fumagalli, F., Rinaldi, A., Bertoni, F., Boersema, P. J., Picotti, P., & Molinari, M. (2018). Chemical stresses fail to mimic the unfolded protein response resulting from luminal load with unfolded polypeptides. *Journal of Biological Chemistry*, *293*(15), 5600–5612. https://doi.org/10.1074/jbc.RA117.001484

Bergmann, T. J., & Molinari, M. (2018). Three branches to rule them all? UPR signalling in response to chemically versus misfolded proteins-induced ER stress. *Biology of the Cell*, *110*(9), 197–204. https://doi.org/10.1111/boc.201800029

Beriault, D. R., & Werstuck, G. H. (2013). Detection and quantification of endoplasmic reticulum stress in living cells using the fluorescent compound, Thioflavin T. *Biochimica et Biophysica Acta (BBA) - Molecular Cell Research*, *1833*(10), 2293–2301. https://doi.org/10.1016/j.bbamcr.2013.05.020

Bernardi, G., Siclari, F., Handjaras, G., Riedner, B. A., & Tononi, G. (2018). Local and Widespread Slow Waves in Stable NREM Sleep: Evidence for Distinct Regulation Mechanisms. *Frontiers in Human Neuroscience*, *12*. https://www.frontiersin.org/articles/10.3389/fnhum.2018.00248

Berridge, M. J. (1998). Neuronal calcium signaling. *Neuron*, *21*(1), 13–26. https://doi.org/10.1016/s0896-6273(00)80510-3

Bertolotti, A., Zhang, Y., Hendershot, L. M., Harding, H. P., & Ron, D. (2000). Dynamic interaction of BiP and ER stress transducers in the unfolded-protein response. *Nature Cell Biology*, *2*(6), Article 6. https://doi.org/10.1038/35014014

Bindels, D. S., Haarbosch, L., van Weeren, L., Postma, M., Wiese, K. E., Mastop, M., Aumonier, S., Gotthard, G., Royant, A., Hink, M. A., & Gadella, T. W. J. (2017). mScarlet: A bright monomeric red fluorescent protein for cellular imaging. *Nature Methods*, *14*(1), Article 1. https://doi.org/10.1038/nmeth.4074

Borbély, A. A., Baumann, F., Brandeis, D., Strauch, I., & Lehmann, D. (1981). Sleep deprivation: Effect on sleep stages and EEG power density in man. *Electroencephalography and Clinical Neurophysiology*, *51*(5), 483–493. https://doi.org/10.1016/0013-4694(81)90225-X

Borbély, A. A., Daan, S., Wirz-Justice, A., & Deboer, T. (2016). The two-process model of sleep regulation: A reappraisal. *Journal of Sleep Research*, *25*(2), 131–143. https://doi.org/10.1111/jsr.12371

Borbély, A. A., Tobler, I., & Hanagasioglu, M. (1984). Effect of sleep deprivation on sleep and EEG power spectra in the rat. *Behavioural Brain Research*, *14*(3), 171–182. https://doi.org/10.1016/0166-4328(84)90186-4

Bos, H., Diesmann, M., & Helias, M. (2016). Identifying Anatomical Origins of Coexisting Oscillations in the Cortical Microcircuit. *PLOS Computational Biology*, *12*(10), e1005132. https://doi.org/10.1371/journal.pcbi.1005132

Braun, A. R., Balkin, T. J., Wesenten, N. J., Carson, R. E., Varga, M., Baldwin, P., Selbie, S., Belenky, G., & Herscovitch, P. (1997). Regional cerebral blood flow throughout the sleep-wake cycle. An H2(15)O PET study. *Brain*, *120*(7), 1173–1197. https://doi.org/10.1093/brain/120.7.1173

Broadwell, R. D., & Cataldo, A. M. (1983). The neuronal endoplasmic reticulum: Its cytochemistry and contribution to the endomembrane system. I. Cell bodies and dendrites. *The Journal of Histochemistry and Cytochemistry*, *31*(9), 1077–1088. https://doi.org/10.1177/31.9.6309951

Brodersen, P. J. N., Alfonsa, H., Krone, L. B., Duque, C. B., Fisk, A. S., Flaherty, S. J., Guillaumin, M. C. C., Huang, Y.-G., Kahn, M. C., McKillop, L. E., Milinski, L., Taylor, L., Thomas, C. W., Yamagata, T., Vyazovskiy, V. V., & Akerman, C. J. (2021). *Somnotate: A robust automated sleep stage classifier that exceeds human performance and identifies ambiguous states in mice* (p. 2021.10.06.463356). bioRxiv. https://doi.org/10.1101/2021.10.06.463356

Brown, L. A., Hasan, S., Foster, R. G., & Peirson, S. N. (2016). COMPASS: Continuous Open Mouse Phenotyping of Activity and Sleep Status. *Wellcome Open Research*, *1*, 2. https://doi.org/10.12688/wellcomeopenres.9892.1

Buchsbaum, M. S., Gillin, J. C., Wu, J., Hazlett, E., Sicotte, N., Dupont, R. M., & Bunney, W. E. (1989). Regional cerebral glucose metabolic rate in human sleep assessed by positron emission tomography. *Life Sciences*, *45*(15), 1349–1356. https://doi.org/10.1016/0024-3205(89)90021-0

Burger, C., Gorbatyuk, O. S., Velardo, M. J., Peden, C. S., Williams, P., Zolotukhin, S., Reier, P. J., Mandel, R. J., & Muzyczka, N. (2004). Recombinant AAV Viral Vectors Pseudotyped with Viral Capsids from Serotypes 1, 2, and 5 Display Differential Efficiency and Cell Tropism after Delivery to Different Regions of the Central Nervous System. *Molecular Therapy*, *10*(2), 302–317. https://doi.org/10.1016/j.ymthe.2004.05.024

Buzsáki, G., Anastassiou, C. A., & Koch, C. (2012). The origin of extracellular fields and currents—EEG, ECoG, LFP and spikes. *Nature Reviews. Neuroscience*, *13*(6), 407–420. https://doi.org/10.1038/nrn3241

Cahill, L. (2006). Why sex matters for neuroscience. *Nature Reviews Neuroscience*, *7*(6), Article 6. https://doi.org/10.1038/nrn1909

Cajigas, I. J., Will, T., & Schuman, E. M. (2010). Protein homeostasis and synaptic plasticity. *The EMBO Journal*, *29*(16), 2746–2752. https://doi.org/10.1038/emboj.2010.173

Cajochen, C., Foy, R., & Dijk, D.-J. (1999). Frontal predominance of a relative increase in sleep delta and theta EEG activity after sleep loss in humans. *Sleep Research Online : SRO*, *2*, 65–69.

Călin, A., Waseem, T., Raimondo, J. V., Newey, S. E., & Akerman, C. J. (2023). A genetically targeted ion sensor reveals distinct seizure-related chloride and pH dynamics in GABAergic interneuron populations. *IScience*, *26*(4), 106363. https://doi.org/10.1016/j.isci.2023.106363

Carskadon, M. A., & Dement, W. C. (1979). Effects of Total Sleep Loss on Sleep Tendency. *Perceptual and Motor Skills*, *48*(2), 495–506. https://doi.org/10.2466/pms.1979.48.2.495

Chan, K. Y., Jang, M. J., Yoo, B. B., Greenbaum, A., Ravi, N., Wu, W.-L., Sánchez-Guardado, L., Lois, C., Mazmanian, S. K., Deverman, B. E., & Gradinaru, V. (2017). Engineered AAVs for efficient noninvasive gene delivery to the central and peripheral nervous systems. *Nature Neuroscience*, *20*(8), 1172–1179. https://doi.org/10.1038/nn.4593

Chanaday, N. L., & Kavalali, E. T. (2022). Role of the endoplasmic reticulum in synaptic transmission. *Current Opinion in Neurobiology*, *73*, 102538. https://doi.org/10.1016/j.conb.2022.102538

Chauvette, S., Crochet, S., Volgushev, M., & Timofeev, I. (2011). Properties of Slow Oscillation during Slow-Wave Sleep and Anesthesia in Cats. *Journal of Neuroscience*, *31*(42), 14998–15008. https://doi.org/10.1523/JNEUROSCI.2339-11.2011

Chauvette, S., Volgushev, M., & Timofeev, I. (2010). Origin of Active States in Local Neocortical Networks during Slow Sleep Oscillation. *Cerebral Cortex (New York, NY)*, *20*(11), 2660–2674. https://doi.org/10.1093/cercor/bhq009

Chaveroux, C., Carraro, V., Canaple, L., Averous, J., Maurin, A.-C., Jousse, C., Muranishi, Y., Parry, L., Mesclon, F., Gatti, E., Mallet, J., Ravassard, P., Pierre, P., Fafournoux, P., & Bruhat, A. (2015). In vivo imaging of the spatiotemporal activity of the eIF2α-ATF4 signaling pathway: Insights into stress and related disorders. *Science Signaling*, *8*(374), rs5–rs5. https://doi.org/10.1126/scisignal.aaa0549

Chen, C.-M., Wu, C.-T., Chiang, C.-K., Liao, B.-W., & Liu, S.-H. (2012). C/EBP Homologous Protein (CHOP) Deficiency Aggravates Hippocampal Cell Apoptosis and Impairs Memory Performance. *PLoS ONE*, *7*(7). https://doi.org/10.1371/journal.pone.0040801

Chen, S.-H., Haam, J., Walker, M., Scappini, E., Naughton, J., & Martin, N. P. (2019). Recombinant Viral Vectors as Neuroscience Tools. *Current Protocols in Neuroscience*, *87*(1), e67. https://doi.org/10.1002/cpns.67

Cheng, Z., Teo, G., Krueger, S., Rock, T. M., Koh, H. W., Choi, H., & Vogel, C. (2016). Differential dynamics of the mammalian mRNA and protein expression response to misfolding stress. *Molecular Systems Biology*, *12*(1), 855. https://doi.org/10.15252/msb.20156423

Choi, J.-H., Yu, N.-K., Baek, G.-C., Bakes, J., Seo, D., Nam, H. J., Baek, S. H., Lim, C.-S., Lee, Y.-S., & Kaang, B.-K. (2014). Optimization of AAV expression cassettes to improve packaging capacity and transgene expression in neurons. *Molecular Brain*, *7*(1), 17. https://doi.org/10.1186/1756-6606-7-17

Christianson, J. C., & Carvalho, P. (2022). Order through destruction: How ER-associated protein degradation contributes to organelle homeostasis. *The EMBO Journal*, *41*(6), e109845. https://doi.org/10.15252/embj.2021109845

Cirelli, C. (2006). Cellular consequences of sleep deprivation in the brain. *Sleep Medicine Reviews*, *10*(5), 307–321. https://doi.org/10.1016/j.smrv.2006.04.001

Cirelli, C. (2017). Sleep, synaptic homeostasis and neuronal firing rates. *Current Opinion in Neurobiology*, *44*, 72–79. https://doi.org/10.1016/j.conb.2017.03.016

Cirelli, C., Faraguna, U., & Tononi, G. (2006). Changes in brain gene expression after long-term sleep deprivation. *Journal of Neurochemistry*, *98*(5), 1632–1645. https://doi.org/10.1111/j.1471-4159.2006.04058.x

Cirelli, C., Gutierrez, C. M., & Tononi, G. (2004). Extensive and Divergent Effects of Sleep and Wakefulness on Brain Gene Expression. *Neuron*, *41*(1), 35–43. https://doi.org/10.1016/S0896-6273(03)00814-6

Cirelli, C., LaVaute, T. M., & Tononi, G. (2005). Sleep and wakefulness modulate gene expression in Drosophila. *Journal of Neurochemistry*, *94*(5), 1411–1419. https://doi.org/10.1111/j.1471-4159.2005.03291.x

Cirelli, C., Pfister-Genskow, M., McCarthy, D., Woodbury, R., & Tononi, G. (2009). Proteomic profiling of the rat cerebral cortex in sleep and waking. *Archives Italiennes de Biologie*, *147*(3), 59–68.

Cirelli, C., & Tononi, G. (2000a). Differential Expression of Plasticity-Related Genes in Waking and Sleep and Their Regulation by the Noradrenergic System. *Journal of Neuroscience*, *20*(24), 9187–9194. https://doi.org/10.1523/JNEUROSCI.20-24-09187.2000

Cirelli, C., & Tononi, G. (2000b). Gene expression in the brain across the sleep–waking cycle. *Brain Research*, *885*(2), 303–321. https://doi.org/10.1016/S0006-8993(00)03008-0

Cirelli, C., & Tononi, G. (2008). Is Sleep Essential? *PLOS Biology*, *6*(8), e216. https://doi.org/10.1371/journal.pbio.0060216

Clark, E. M., Nonarath, H. J. T., Bostrom, J. R., & Link, B. A. (2020). Establishment and validation of an endoplasmic reticulum stress reporter to monitor zebrafish ATF6 activity in development and disease. *Disease Models & Mechanisms*, *13*(1), dmm041426. https://doi.org/10.1242/dmm.041426

Colavito, V., Fabene, P., Grassi Zucconi, G., Pifferi, F., Lamberty, Y., Bentivoglio, M., & Bertini, G. (2013). Experimental sleep deprivation as a tool to test memory deficits in rodents. *Frontiers in Systems Neuroscience*, *7*. https://www.frontiersin.org/articles/10.3389/fnsys.2013.00106

Cóppola-Segovia, V., Cavarsan, C., Maia, F. G., Ferraz, A. C., Nakao, L. S., Lima, M. M., & Zanata, S. M. (2017). ER Stress Induced by Tunicamycin Triggers α-Synuclein Oligomerization, Dopaminergic Neurons Death and Locomotor Impairment: A New Model of Parkinson's Disease. *Molecular Neurobiology*, *54*(8), 5798–5806. https://doi.org/10.1007/s12035-016-0114-x

Corish, P., & Tyler-Smith, C. (1999). Attenuation of green fluorescent protein half-life in mammalian cells. *Protein Engineering*, *12*(12), 1035–1040. https://doi.org/10.1093/protein/12.12.1035

Costa-Mattioli, M., & Walter, P. (2020). The integrated stress response: From mechanism to disease. *Science*, *368*(6489). https://doi.org/10.1126/science.aat5314

Costantini, L., & Snapp, E. (2013). Probing Endoplasmic Reticulum Dynamics using Fluorescence Imaging and Photobleaching Techniques. *Current Protocols in Cell Biology / Editorial Board, Juan S. Bonifacino ... [et Al.]*, *60*, 21.7.1-21.7.29. https://doi.org/10.1002/0471143030.cb2107s60

Creighton, T. E. (1997). Protein folding coupled to disulphide bond formation. *Biological Chemistry*, *378*(8), 731–744. https://doi.org/10.1515/bchm.1997.378.8.731

Cretenet, G., Le Clech, M., & Gachon, F. (2010). Circadian Clock-Coordinated 12 Hr Period Rhythmic Activation of the IRE1α Pathway Controls Lipid Metabolism in Mouse Liver. *Cell Metabolism*, *11*(1), 47–57. https://doi.org/10.1016/j.cmet.2009.11.002

Crider, A., Nelson, T., Davis, T., Fagan, K., Vaibhav, K., Luo, M., Kamalasanan, S., Terry, A. V., & Pillai, A. (2018). Estrogen Receptor β Agonist Attenuates Endoplasmic Reticulum Stress-Induced Changes in Social Behavior and Brain Connectivity in Mice. *Molecular Neurobiology*, *55*(9), 7606–7618. https://doi.org/10.1007/s12035-018-0929-8

Csala, M., Bánhegyi, G., & Benedetti, A. (2006). Endoplasmic reticulum: A metabolic compartment. *FEBS Letters*, *580*(9), 2160–2165. https://doi.org/10.1016/j.febslet.2006.03.050

Csercsa, R., Dombovári, B., Fabó, D., Wittner, L., Erőss, L., Entz, L., Sólyom, A., Rásonyi, G., Szűcs, A., Kelemen, A., Jakus, R., Juhos, V., Grand, L., Magony, A., Halász, P., Freund, T. F., Maglóczky, Z., Cash, S. S., Papp, L., … Ulbert, I. (2010). Laminar analysis of slow wave activity in humans. *Brain*, *133*(9), 2814–2829. https://doi.org/10.1093/brain/awq169

Curtin, J. A., Dane, A. P., Swanson, A., Alexander, I. E., & Ginn, S. L. (2008). Bidirectional promoter interference between two widely used internal heterologous promoters in a late-generation lentiviral construct. *Gene Therapy*, *15*(5), Article 5. https://doi.org/10.1038/sj.gt.3303105

Daya, S., & Berns, K. I. (2008). Gene Therapy Using Adeno-Associated Virus Vectors. *Clinical Microbiology Reviews*, *21*(4), 583–593. https://doi.org/10.1128/CMR.00008-08

De Vry, J., Martínez-Martínez, P., Losen, M., Temel, Y., Steckler, T., Steinbusch, H. W. M., De Baets, M. H., & Prickaerts, J. (2010). In vivo electroporation of the central nervous system: A non-viral approach for targeted gene delivery. *Progress in Neurobiology*, *92*(3), 227–244. https://doi.org/10.1016/j.pneurobio.2010.10.001

DeFelipe, J., López-Cruz, P. L., Benavides-Piccione, R., Bielza, C., Larrañaga, P., Anderson, S., Burkhalter, A., Cauli, B., Fairén, A., Feldmeyer, D., Fishell, G., Fitzpatrick, D., Freund, T. F., González-Burgos, G., Hestrin, S., Hill, S., Hof, P. R., Huang, J., Jones, E. G., … Ascoli, G. A. (2013). New insights into the classification and nomenclature of cortical GABAergic interneurons. *Nature Reviews Neuroscience*, *14*(3), Article 3. https://doi.org/10.1038/nrn3444

Destexhe, A., Contreras, D., & Steriade, M. (1999). Spatiotemporal Analysis of Local Field Potentials and Unit Discharges in Cat Cerebral Cortex during Natural Wake and Sleep States. *The Journal of Neuroscience*, *19*(11), 4595–4608. https://doi.org/10.1523/JNEUROSCI.19-11-04595.1999

Di Liegro, C. M., Schiera, G., & Di Liegro, I. (2014). Regulation of mRNA transport, localization and translation in the nervous system of mammals (Review). *International Journal of Molecular Medicine*, *33*(4), 747–762. https://doi.org/10.3892/ijmm.2014.1629

Dib, R., Gervais, N. J., & Mongrain, V. (2021). A review of the current state of knowledge on sex differences in sleep and circadian phenotypes in rodents. *Neurobiology of Sleep and Circadian Rhythms*, *11*, 100068. https://doi.org/10.1016/j.nbscr.2021.100068

DiNuzzo, M., & Nedergaard, M. (2017). Brain Energetics During the Sleep-Wake Cycle. *Current Opinion in Neurobiology*, *47*, 65–72. https://doi.org/10.1016/j.conb.2017.09.010

Dong, H., Adams, N. M., Xu, Y., Cao, J., Allan, D. S. J., Carlyle, J. R., Chen, X., Sun, J. C., & Glimcher, L. H. (2019). The IRE1 endoplasmic reticulum stress sensor activates natural killer cell immunity in part by regulating c-Myc. *Nature Immunology*, *20*(7), Article 7. https://doi.org/10.1038/s41590-019-0388-z

Doupé, D. P., & Perrimon, N. (2014). Visualizing and Manipulating Temporal Signaling Dynamics with Fluorescence-Based Tools. *Science Signaling*, *7*(319), re1–re1. https://doi.org/10.1126/scisignal.2005077

Duff, K., Noble, W., Gaynor, K., & Matsuoka, Y. (2002). Organotypic slice cultures from transgenic mice as disease model systems. *Journal of Molecular Neuroscience*, *19*(3), 317–320. https://doi.org/10.1385/JMN:19:3:317

Duran-Aniotz, C., Cornejo, V. H., Espinoza, S., Ardiles, Á. O., Medinas, D. B., Salazar, C., Foley, A., Gajardo, I., Thielen, P., Iwawaki, T., Scheper, W., Soto, C., Palacios, A. G., Hoozemans, J. J. M., & Hetz, C. (2017). IRE1 signaling exacerbates Alzheimer's disease pathogenesis. *Acta Neuropathologica*, *134*(3), 489–506. https://doi.org/10.1007/s00401-017-1694-x

DuRose, J. B., Tam, A. B., & Niwa, M. (2006). Intrinsic Capacities of Molecular Sensors of the Unfolded Protein Response to Sense Alternate Forms of Endoplasmic Reticulum Stress. *Molecular Biology of the Cell*, *17*(7), 3095–3107. https://doi.org/10.1091/mbc.E06-01-0055

Ehlen, J. C., Hesse, S., Pinckney, L., & Paul, K. N. (2013). Sex Chromosomes Regulate Nighttime Sleep Propensity during Recovery from Sleep Loss in Mice. *PLOS ONE*, *8*(5), e62205. https://doi.org/10.1371/journal.pone.0062205

Ehlers, M. D. (2003). Activity level controls postsynaptic composition and signaling via the ubiquitin-proteasome system. *Nature Neuroscience*, *6*(3), Article 3. https://doi.org/10.1038/nn1013

Eide, P. K., Vinje, V., Pripp, A. H., Mardal, K.-A., & Ringstad, G. (2021). Sleep deprivation impairs molecular clearance from the human brain. *Brain*, *144*(3), 863–874. https://doi.org/10.1093/brain/awaa443

Einevoll, G. T., Kayser, C., Logothetis, N. K., & Panzeri, S. (2013). Modelling and analysis of local field potentials for studying the function of cortical circuits. *Nature Reviews Neuroscience*, *14*(11), Article 11. https://doi.org/10.1038/nrn3599

Ellender, T. J., Avery, S. V., Mahfooz, K., Scaber, J., von Klemperer, A., Nixon, S. L., Buchan, M. J., van Rheede, J. J., Gatti, A., Waites, C., Pavlou, H. J., Sims, D., Newey, S. E., & Akerman, C. J. (2019). Embryonic progenitor pools generate diversity in fine-scale excitatory cortical subnetworks. *Nature Communications*, *10*(1), Article 1. https://doi.org/10.1038/s41467-019-13206-1

Ellgaard, L., & Helenius, A. (2003). Quality control in the endoplasmic reticulum. *Nature Reviews Molecular Cell Biology*, *4*(3), 181–191. https://doi.org/10.1038/nrm1052

Elliott, A. S., Huber, J. D., O'Callaghan, J. P., Rosen, C. L., & Miller, D. B. (2014). A review of sleep deprivation studies evaluating the brain transcriptome. *SpringerPlus*, *3*(1), 728. https://doi.org/10.1186/2193-1801-3-728

Elouil, H., Bensellam, M., Guiot, Y., Vander Mierde, D., Pascal, S. M. A., Schuit, F. C., & Jonas, J. C. (2007). Acute nutrient regulation of the unfolded protein response and integrated stress response in cultured rat pancreatic islets. *Diabetologia*, *50*(7), 1442–1452. https://doi.org/10.1007/s00125-007-0674-4

Fan, Q., Takarada-Iemata, M., Okitani, N., Tamatani, T., Ishii, H., Hattori, T., Kiryu-Seo, S., Kiyama, H., & Hori, O. (2023). Brain injury triggers cell-type-specific and time-dependent endoplasmic reticulum stress responses. *Glia*, *71*(3), 667–681. https://doi.org/10.1002/glia.24303

Fellows, L. K., Boutelle, M. G., & Fillenz, M. (1992). Extracellular Brain Glucose Levels Reflect Local Neuronal Activity: A Microdialysis Study in Awake, Freely Moving Rats. *Journal of Neurochemistry*, *59*(6), 2141–2147. https://doi.org/10.1111/j.1471-4159.1992.tb10105.x

Fenno, L. E., Mattis, J., Ramakrishnan, C., Hyun, M., Lee, S. Y., He, M., Tucciarone, J., Selimbeyoglu, A., Berndt, A., Grosenick, L., Zalocusky, K. A., Bernstein, H., Swanson, H., Perry, C., Diester, I., Boyce, F. M., Bass, C. E., Neve, R., Huang, Z. J., & Deisseroth, K. (2014). Targeting cells with single vectors using multiple-feature Boolean logic. *Nature Methods*, *11*(7), Article 7. https://doi.org/10.1038/nmeth.2996

Fenno, L. E., Ramakrishnan, C., Kim, Y. S., Evans, K. E., Lo, M., Vesuna, S., Inoue, M., Cheung, K. Y. M., Yuen, E., Pichamoorthy, N., Hong, A. S. O., & Deisseroth, K. (2020). Comprehensive Dual- and Triple-Feature Intersectional Single-Vector Delivery of Diverse Functional Payloads to Cells of Behaving Mammals. *Neuron*, *107*(5), 836-853.e11. https://doi.org/10.1016/j.neuron.2020.06.003

Fernandez, L. M. J., & Lüthi, A. (2020). Sleep Spindles: Mechanisms and Functions. *Physiological Reviews*, *100*(2), 805–868. https://doi.org/10.1152/physrev.00042.2018

Fiáth, R., Kerekes, B. P., Wittner, L., Tóth, K., Beregszászi, P., Horváth, D., & Ulbert, I. (2016). Laminar analysis of the slow wave activity in the somatosensory cortex of anesthetized rats. *European Journal of Neuroscience*, *44*(3), 1935–1951. https://doi.org/10.1111/ejn.13274

Finelli, L. A., Baumann, H., Borbély, A. A., & Achermann, P. (2000). Dual electroencephalogram markers of human sleep homeostasis: Correlation between theta activity in waking and slow-wave activity in sleep. *Neuroscience*, *101*(3), 523–529. https://doi.org/10.1016/S0306-4522(00)00409-7

Funk, C. M., Peelman, K., Bellesi, M., Marshall, W., Cirelli, C., & Tononi, G. (2017). Role of Somatostatin-Positive Cortical Interneurons in the Generation of Sleep Slow Waves. *Journal of Neuroscience*, *37*(38), 9132–9148. https://doi.org/10.1523/JNEUROSCI.1303-17.2017

Gama Sosa, M. A., De Gasperi, R., & Elder, G. A. (2010). Animal transgenesis: An overview. *Brain Structure and Function*, *214*(2), 91–109. https://doi.org/10.1007/s00429-009-0230-8

Gao, L., Liu, S., Gou, L., Hu, Y., Liu, Y., Deng, L., Ma, D., Wang, H., Yang, Q., Chen, Z., Liu, D., Qiu, S., Wang, X., Wang, D., Wang, X., Ren, B., Liu, Q., Chen, T., Shi, X., … Yan, J. (2022). Single-neuron projectome of mouse prefrontal cortex. *Nature Neuroscience*, *25*(4), Article 4. https://doi.org/10.1038/s41593-022-01041-5

Gass, J. N., Gifford, N. M., & Brewer, J. W. (2002). Activation of an Unfolded Protein Response during Differentiation of Antibody-secreting B Cells *. *Journal of Biological Chemistry*, *277*(50), 49047–49054. https://doi.org/10.1074/jbc.M205011200

Gerakis, Y., & Hetz, C. (2018). Emerging roles of ER stress in the etiology and pathogenesis of Alzheimer's disease. *The FEBS Journal*, *285*(6), 995–1011. https://doi.org/10.1111/febs.14332

Gething, M.-J., & Sambrook, J. (1992). Protein folding in the cell. *Nature*, *355*(6355), Article 6355. https://doi.org/10.1038/355033a0

Giandomenico, S. L., Alvarez-Castelao, B., & Schuman, E. M. (2022). Proteostatic regulation in neuronal compartments. *Trends in Neurosciences*, *45*(1), 41–52. https://doi.org/10.1016/j.tins.2021.08.002

Gidalevitz, T., Stevens, F., & Argon, Y. (2013). Orchestration of secretory protein folding by ER chaperones. *Biochimica et Biophysica Acta*, *1833*(11), 2410–2424. https://doi.org/10.1016/j.bbamcr.2013.03.007

Girardeau, G., & Lopes-dos-Santos, V. (2021). Brain neural patterns and the memory function of sleep. *Science*, *374*(6567), 560–564. https://doi.org/10.1126/science.abi8370

Gloor, P., Ball, G., & Schaul, N. (1977). Brain lesions that produce delta waves in the EEG. *Neurology*, *27*(4), 326–326. https://doi.org/10.1212/WNL.27.4.326

Gomez, E., Powell, M. L., Bevington, A., & Herbert, T. P. (2008). A decrease in cellular energy status stimulates PERK-dependent eIF2α phosphorylation and regulates protein synthesis in pancreatic β-cells. *Biochemical Journal*, *410*(3), 485–493. https://doi.org/10.1042/BJ20071367

Gonzalez-Teuber, V., Albert-Gasco, H., Auyeung, V. C., Papa, F. R., Mallucci, G. R., & Hetz, C. (2019). Small Molecules to Improve ER Proteostasis in Disease. *Trends in Pharmacological Sciences*, *40*(9), 684–695. https://doi.org/10.1016/j.tips.2019.07.003

Goodman, R. H., Aron, D. C., & Roos, B. A. (1983). Rat pre-prosomatostatin. Structure and processing by microsomal membranes. *Journal of Biological Chemistry*, *258*(9), 5570–5573. https://doi.org/10.1016/S0021-9258(20)81928-0

Greig, L. C., Woodworth, M. B., Galazo, M. J., Padmanabhan, H., & Macklis, J. D. (2013). Molecular logic of neocortical projection neuron specification, development and diversity. *Nature Reviews Neuroscience*, *14*(11), Article 11. https://doi.org/10.1038/nrn3586

Gretzer, C., Emanuelsson, L., Liljensten, E., & Thomsen, P. (2006). The inflammatory cell influx and cytokines changes during transition from acute inflammation to fibrous repair around implanted materials. *Journal of Biomaterials Science, Polymer Edition*, *17*(6), 669–687. https://doi.org/10.1163/156856206777346340

Grill, W. M. (2008). Signal Considerations for Chronically Implanted Electrodes for Brain Interfacing. In W. M. Reichert (Ed.), *Indwelling Neural Implants: Strategies for Contending with the In Vivo Environment*. CRC Press/Taylor & Francis. http://www.ncbi.nlm.nih.gov/books/NBK3931/

Grønli, J., Soulé, J., & Bramham, C. R. (2014). Sleep and protein synthesis-dependent synaptic plasticity: Impacts of sleep loss and stress. *Frontiers in Behavioral Neuroscience*, *7*. https://doi.org/10.3389/fnbeh.2013.00224

Gross, D. W., & Gotman, J. (1999). Correlation of high-frequency oscillations with the sleep–wake cycle and cognitive activity in humans. *Neuroscience*, *94*(4), 1005–1018. https://doi.org/10.1016/S0306-4522(99)00343-7

Gülow, K., Bienert, D., & Haas, I. G. (2002). BiP is feed-back regulated by control of protein translation efficiency. *Journal of Cell Science*, *115*(11), 2443–2452.

Guo, Y., Fang, Z., Du, M., Yang, L., Shao, L., Zhang, X., Li, L., Shi, J., Tao, J., Wang, J., Li, H., & Fang, Y. (2018). Flexible and biocompatible nanopaper-based electrode arrays for neural activity recording. *Nano Research*, *11*(10), 5604–5614. https://doi.org/10.1007/s12274-018-2005-0

Haas, I. G., & Wabl, M. (1983). Immunoglobulin heavy chain binding protein. *Nature*, *306*(5941), Article 5941. https://doi.org/10.1038/306387a0

Hafner, A.-S., Donlin-Asp, P. G., Leitch, B., Herzog, E., & Schuman, E. M. (2018). Local protein synthesis in axon terminals and dendritic spines differentiates plasticity contexts. *BioRxiv*, 363184. https://doi.org/10.1101/363184

Hajali, V., Andersen, M. L., Negah, S. S., & Sheibani, V. (2019). Sex differences in sleep and sleep loss-induced cognitive deficits: The influence of gonadal hormones. *Hormones and Behavior*, *108*, 50–61. https://doi.org/10.1016/j.yhbeh.2018.12.013

Hakim, F., Wang, Y., Carreras, A., Hirotsu, C., Zhang, J., Peris, E., & Gozal, D. (2015). Chronic Sleep Fragmentation During the Sleep Period Induces Hypothalamic Endoplasmic Reticulum Stress and PTP1b-Mediated Leptin Resistance in Male Mice. *Sleep*, *38*(1), 31–40. https://doi.org/10.5665/sleep.4320

Halliday, M., Radford, H., Zents, K. A. M., Molloy, C., Moreno, J. A., Verity, N. C., Smith, E., Ortori, C. A., Barrett, D. A., Bushell, M., & Mallucci, G. R. (2017). Repurposed drugs targeting eIF2α-P-mediated translational repression prevent neurodegeneration in mice. *Brain*, *140*(6), 1768–1783. https://doi.org/10.1093/brain/awx074

Halperin, L., Jung, J., & Michalak, M. (2014). The many functions of the endoplasmic reticulum chaperones and folding enzymes. *IUBMB Life*, *66*(5), 318–326. https://doi.org/10.1002/iub.1272

Hanslick, J. L., Lau, K., Noguchi, K. K., Olney, J. W., Zorumski, C. F., Mennerick, S., & Farber, N. B. (2009). Dimethyl sulfoxide (DMSO) produces widespread apoptosis in the developing central nervous system. *Neurobiology of Disease*, *34*(1), 1–10. https://doi.org/10.1016/j.nbd.2008.11.006

Harding, H. P., Calfon, M., Urano, F., Novoa, I., & Ron, D. (2002). Transcriptional and Translational Control in the Mammalian Unfolded Protein Response. *Annual Review of Cell and Developmental Biology*, *18*(1), 575–599. https://doi.org/10.1146/annurev.cellbio.18.011402.160624

Harding, H. P., Zhang, Y., & Ron, D. (1999). Protein translation and folding are coupled by an endoplasmic-reticulum-resident kinase. *Nature*, *397*(6716), Article 6716. https://doi.org/10.1038/16729

Havekes, R., Vecsey, C. G., & Abel, T. (2012). The impact of sleep deprivation on neuronal and glial signaling pathways important for memory and synaptic plasticity. *Cellular Signalling*, *24*(6), 1251–1260. https://doi.org/10.1016/j.cellsig.2012.02.010

Hawkins, R. A., Mans, A. M., Davis, D. W., Hibbard, L. S., & Lu, D. M. (1983). Glucose Availability to Individual Cerebral Structures Is Correlated to Glucose Metabolism. *Journal of Neurochemistry*, *40*(4), 1013–1018. https://doi.org/10.1111/j.1471-4159.1983.tb08086.x

Haze, K., Yoshida, H., Yanagi, H., Yura, T., & Mori, K. (1999). Mammalian Transcription Factor ATF6 Is Synthesized as a Transmembrane Protein and Activated by Proteolysis in Response to Endoplasmic Reticulum Stress. *Molecular Biology of the Cell*, *10*(11), 3787–3799.

He, L., Binari, R., Huang, J., Falo-Sanjuan, J., & Perrimon, N. (2019). In vivo study of gene expression with an enhanced dual-color fluorescent transcriptional timer. *ELife*, *8*, e46181. https://doi.org/10.7554/eLife.46181

Heifetz, A., Keenan, R. W., & Elbein, A. D. (1979). Mechanism of action of tunicamycin on the UDP-GlcNAc:dolichyl-phosphate GlcNAc-1-phosphate transferase. *Biochemistry*, *18*(11), 2186–2192. https://doi.org/10.1021/bi00578a008

Heiss, W.-D., Pawlik, G., Herholz, K., Wagner, R., & Wienhard, K. (1985). Regional cerebral glucose metabolism in man during wakefulness, sleep, and dreaming. *Brain Research*, *327*(1), 362–366. https://doi.org/10.1016/0006-8993(85)91537-9

Helseth, A. R., Hernandez-Martinez, R., Hall, V. L., Oliver, M. L., Turner, B. D., Caffall, Z. F., Rittiner, J. E., Shipman, M. K., King, C. S., Gradinaru, V., Gerfen, C., Costa-Mattioli, M., & Calakos, N. (2021). Cholinergic neurons constitutively engage the ISR for dopamine modulation and skill learning in mice. *Science*, *372*(6540), eabe1931. https://doi.org/10.1126/science.abe1931

Henderson, M. J., Wires, E. S., Trychta, K. A., Richie, C. T., & Harvey, B. K. (2014). SERCaMP: A carboxy-terminal protein modification that enables monitoring of ER calcium homeostasis. *Molecular Biology of the Cell*, *25*(18), 2828–2839. https://doi.org/10.1091/mbc.e14-06-1141

Hengen, K. B., Lambo, M. E., Van Hooser, S. D., Katz, D. B., & Turrigiano, G. G. (2013). Firing Rate Homeostasis in Visual Cortex of Freely Behaving Rodents. *Neuron*, *80*(2), 335–342. https://doi.org/10.1016/j.neuron.2013.08.038

Herreras, O. (2016). Local Field Potentials: Myths and Misunderstandings. *Frontiers in Neural Circuits*, *10*. https://www.frontiersin.org/articles/10.3389/fncir.2016.00101

Hetz, C. (2012). The unfolded protein response: Controlling cell fate decisions under ER stress and beyond. *Nature Reviews Molecular Cell Biology*, *13*(2), 89–102. https://doi.org/10.1038/nrm3270

Hetz, C. (2021). Adapting the proteostasis capacity to sustain brain healthspan. *Cell*, *184*(6), 1545–1560. https://doi.org/10.1016/j.cell.2021.02.007

Hetz, C., Axten, J. M., & Patterson, J. B. (2019). Pharmacological targeting of the unfolded protein response for disease intervention. *Nature Chemical Biology*, *15*(8), Article 8. https://doi.org/10.1038/s41589-019-0326-2

Hetz, C., & Saxena, S. (2017). ER stress and the unfolded protein response in neurodegeneration. *Nature Reviews Neurology*, *13*(8), Article 8. https://doi.org/10.1038/nrneurol.2017.99

Hill, A. J., Mansfield, R., Lopez, J. M., Raizen, D. M., & Van, C. B. (2014). Cellular stress induces a protective sleep-like state in C. elegans. *Current Biology : CB*, *24*(20), 2399–2405. https://doi.org/10.1016/j.cub.2014.08.040

Hill, V. M., O'Connor, R. M., Sissoko, G. B., Irobunda, I. S., Leong, S., Canman, J. C., Stavropoulos, N., & Shirasu-Hiza, M. (2018). A bidirectional relationship between sleep and oxidative stress in Drosophila. *PLOS Biology*, *16*(7), e2005206. https://doi.org/10.1371/journal.pbio.2005206

Hiramatsu, N., Joseph, V. T., & Lin, J. H. (2011). Chapter eleven—Monitoring and Manipulating Mammalian Unfolded Protein Response. In P. M. Conn (Ed.), *Methods in Enzymology* (Vol. 491, pp. 183–198). Academic Press. https://doi.org/10.1016/B978-0-12-385928-0.00011-0

Hobson, J. A. (2005). Sleep is of the brain, by the brain and for the brain. *Nature*, *437*(7063), Article 7063. https://doi.org/10.1038/nature04283

Hollien, J. (2013). Evolution of the unfolded protein response. *Biochimica et Biophysica Acta (BBA) - Molecular Cell Research*, *1833*(11), 2458–2463. https://doi.org/10.1016/j.bbamcr.2013.01.016

Hollien, J., Lin, J. H., Li, H., Stevens, N., Walter, P., & Weissman, J. S. (2009). Regulated Ire1-dependent decay of messenger RNAs in mammalian cells. *Journal of Cell Biology*, *186*(3), 323–331. https://doi.org/10.1083/jcb.200903014

Hollien, J., & Weissman, J. S. (2006). Decay of Endoplasmic Reticulum-Localized mRNAs During the Unfolded Protein Response. *Science*, *313*(5783), 104–107. https://doi.org/10.1126/science.1129631

Hosoda, A., Maruyama, A., Oikawa, D., Oshima, Y., Komachi, Y., Kanai, G., Sato, H., & Iwawaki, T. (2011). Detection of ER stress in vivo by Raman spectroscopy. *Biochemical and Biophysical Research Communications*, *405*(1), 37–41. https://doi.org/10.1016/j.bbrc.2010.12.112

Hostettler, L., Grundy, L., Käser-Pébernard, S., Wicky, C., Schafer, W. R., & Glauser, D. A. (2017). The Bright Fluorescent Protein mNeonGreen Facilitates Protein Expression Analysis In Vivo. *G3: Genes, Genomes, Genetics*, *7*(2), 607–615. https://doi.org/10.1534/g3.116.038133

Houdebine, L.-M. (2002). The methods to generate transgenic animals and to control transgene expression. *Journal of Biotechnology*, *98*(2), 145–160. https://doi.org/10.1016/S0168-1656(02)00129-3

Hrvatin, S., Hochbaum, D. R., Nagy, M. A., Cicconet, M., Robertson, K., Cheadle, L., Zilionis, R., Ratner, A., Borges-Monroy, R., Klein, A. M., Sabatini, B. L., & Greenberg, M. E. (2018). Single-cell analysis of experience-dependent transcriptomic states in the mouse visual cortex. *Nature Neuroscience*, *21*(1), 120–129. https://doi.org/10.1038/s41593-017-0029-5

Hsieh, T., Nillegoda, N. B., Tyedmers, J., Bukau, B., Mogk, A., & Kramer, G. (2014). Monitoring Protein Misfolding by Site-Specific Labeling of Proteins In Vivo. *PLOS ONE*, *9*(6), e99395. https://doi.org/10.1371/journal.pone.0099395

Hubbard, J., Gent, T. C., Hoekstra, M. M. B., Emmenegger, Y., Mongrain, V., Landolt, H.-P., Adamantidis, A. R., & Franken, P. (2020). Rapid fast-delta decay following prolonged wakefulness marks a phase of wake-inertia in NREM sleep. *Nature Communications*, *11*(1), Article 1. https://doi.org/10.1038/s41467-020-16915-0

Huber, R., Deboer, T., & Tobler, I. (2000). Topography of EEG Dynamics After Sleep Deprivation in Mice. *Journal of Neurophysiology*, *84*(4), 1888–1893. https://doi.org/10.1152/jn.2000.84.4.1888

Huber, R., Ghilardi, M. F., Massimini, M., Ferrarelli, F., Riedner, B. A., Peterson, M. J., & Tononi, G. (2006). Arm immobilization causes cortical plastic changes and locally decreases sleep slow wave activity. *Nature Neuroscience*, *9*(9), Article 9. https://doi.org/10.1038/nn1758

Humpel, C. (2015). Organotypic brain slice cultures: A review. *Neuroscience*, *305*, 86–98. https://doi.org/10.1016/j.neuroscience.2015.07.086

Iurlaro, R., & Muñoz-Pinedo, C. (2016). Cell death induced by endoplasmic reticulum stress. *The FEBS Journal*, *283*(14), 2640–2652. https://doi.org/10.1111/febs.13598

Iwawaki, T., Akai, R., Kohno, K., & Miura, M. (2004). A transgenic mouse model for monitoring endoplasmic reticulum stress. *Nature Medicine*, *10*(1), 98–102. https://doi.org/10.1038/nm970

Jaisser, F. (2000). Inducible Gene Expression and Gene Modification in Transgenic Mice. *Journal of the American Society of Nephrology*, *11*(suppl 2), S95–S100.

Jaud, M., Philippe, C., Di Bella, D., Tang, W., Pyronnet, S., Laurell, H., Mazzolini, L., Rouault-Pierre, K., & Touriol, C. (2020). Translational Regulations in Response to Endoplasmic Reticulum Stress in Cancers. *Cells*, *9*(3), 540. https://doi.org/10.3390/cells9030540

Jazin, E., & Cahill, L. (2010). Sex differences in molecular neuroscience: From fruit flies to humans. *Nature Reviews Neuroscience*, *11*(1), Article 1. https://doi.org/10.1038/nrn2754

Jha, P. K., Valekunja, U. K., Ray, S., Nollet, M., & Reddy, A. B. (2022). Single-cell transcriptomics and cell-specific proteomics reveals molecular signatures of sleep. *Communications Biology*, *5*, 846. https://doi.org/10.1038/s42003-022-03800-3

Jin, M. L., Park, S. Y., Kim, Y. H., Oh, J.-I., Lee, S. J., & Park, G. (2014). The neuroprotective effects of cordycepin inhibit glutamate-induced oxidative and ER stress-associated apoptosis in hippocampal HT22 cells. *NeuroToxicology*, *41*, 102–111. https://doi.org/10.1016/j.neuro.2014.01.005

Jones, S., Pfister-Genskow, M., Benca, R. M., & Cirelli, C. (2008). Molecular correlates of sleep and wakefulness in the brain of the white-crowned sparrow. *Journal of Neurochemistry*, *105*(1), 46–62. https://doi.org/10.1111/j.1471-4159.2007.05089.x

Ju, Y.-E. S., Ooms, S. J., Sutphen, C., Macauley, S. L., Zangrilli, M. A., Jerome, G., Fagan, A. M., Mignot, E., Zempel, J. M., Claassen, J. A. H. R., & Holtzman, D. M. (2017). Slow wave sleep disruption increases cerebrospinal fluid amyloid-β levels. *Brain*, *140*(8), 2104–2111. https://doi.org/10.1093/brain/awx148

Kajikawa, Y., & Schroeder, C. E. (2011). How local is the local field potential? *Neuron*, *72*(5), 847–858. https://doi.org/10.1016/j.neuron.2011.09.029

Karnovsky, M. L., Reich, P., Anchors, J. M., & Burrows, B. L. (1983). Changes in Brain Glycogen During Slow-Wave Sleep in the Rat. *Journal of Neurochemistry*, *41*(5), 1498–1501. https://doi.org/10.1111/j.1471-4159.1983.tb00853.x

Karunanithy, G., Wheeler, R. J., Tear, L. R., Farrer, N. J., Faulkner, S., & Baldwin, A. J. (2019). INDIANA: An in-cell diffusion method to characterize the size, abundance and permeability of cells. *Journal of Magnetic Resonance (San Diego, Calif.: 1997)*, *302*, 1–13. https://doi.org/10.1016/j.jmr.2018.12.001

Kastanenka, K. V., Calvo-Rodriguez, M., Hou, S. S., Zhou, H., Takeda, S., Arbel-Ornath, M., Lariviere, A., Lee, Y. F., Kim, A., Hawkes, J. M., Logan, R., Feng, D., Chen, X., Gomperts, S. N., & Bacskai, B. J. (2019). Frequency-dependent exacerbation of Alzheimer's disease neuropathophysiology. *Scientific Reports*, *9*(1), Article 1. https://doi.org/10.1038/s41598-019-44964-z

Katayama, T., Imaizumi, K., Sato, N., Miyoshi, K., Kudo, T., Hitomi, J., Morihara, T., Yoneda, T., Gomi, F., Mori, Y., Nakano, Y., Takeda, J., Tsuda, T., Itoyama, Y., Murayama, O., Takashima, A., St George-Hyslop, P., Takeda, M., & Tohyama, M. (1999). Presenilin-1 mutations downregulate the signalling pathway of the unfolded-protein response. *Nature Cell Biology*, *1*(8), Article 8. https://doi.org/10.1038/70265

Kaufman, R. J., Scheuner, D., Schröder, M., Shen, X., Lee, K., Liu, C. Y., & Arnold, S. M. (2002). The unfolded protein response in nutrient sensing and differentiation. *Nature Reviews Molecular Cell Biology*, *3*(6), Article 6. https://doi.org/10.1038/nrm829

Kawaguchi, Y. (2017). Pyramidal Cell Subtypes and Their Synaptic Connections in Layer 5 of Rat Frontal Cortex. *Cerebral Cortex*, *27*(12), 5755–5771. https://doi.org/10.1093/cercor/bhx252

Keir, S. D., House, S. B., Li, J., Xiao, X., & Gainer, H. (1999). Gene Transfer into Hypothalamic Organotypic Cultures Using an Adeno-Associated Virus Vector. *Experimental Neurology*, *160*(2), 313–316. https://doi.org/10.1006/exnr.1999.7236

Keller, D., Erö, C., & Markram, H. (2018). Cell Densities in the Mouse Brain: A Systematic Review. *Frontiers in Neuroanatomy*, *12*. https://www.frontiersin.org/articles/10.3389/fnana.2018.00083

Kennedy, C., Gillin, J. C., Mendelson, W., Suda, S., Miyaoka, M., Ito, M., Nakamura, R. K., Storch, F. I., Peetigrew, K., Mishkin, M., & Sokoloff, L. (1982). Local cerebral glucose utilization in non-rapid eye movement sleep. *Nature*, *297*(5864), Article 5864. https://doi.org/10.1038/297325a0

Kezuka, D., Tkarada-Iemata, M., Hattori, T., Mori, K., Takahashi, R., Kitao, Y., & Hori, O. (2016). Deletion of Atf6α enhances kainate-induced neuronal death in mice. *Neurochemistry International*, *92*, 67–74. https://doi.org/10.1016/j.neuint.2015.12.009

Khodagholy, D., Doublet, T., Quilichini, P., Gurfinkel, M., Leleux, P., Ghestem, A., Ismailova, E., Hervé, T., Sanaur, S., Bernard, C., & Malliaras, G. G. (2013). In vivo recordings of brain activity using organic transistors. *Nature Communications*, *4*(1), Article 1. https://doi.org/10.1038/ncomms2573

Kim, R., Emi, M., Tanabe, K., & Murakami, S. (2006). Role of the unfolded protein response in cell death. *Apoptosis*, *11*(1), 5–13. https://doi.org/10.1007/s10495-005-3088-0

Kito, H., Yamazaki, D., Ohya, S., Yamamura, H., Asai, K., & Imaizumi, Y. (2011). Up-regulation of Kir2.1 by ER stress facilitates cell death of brain capillary endothelial cells. *Biochemical and Biophysical Research Communications*, *411*(2), 293–298. https://doi.org/10.1016/j.bbrc.2011.06.128

Kitsera, N., Khobta, A., & Epe, B. (2007). Destabilized green fluorescent protein detects rapid removal of transcription blocks after genotoxic exposure. *BioTechniques*, *43*(2), 222–227. https://doi.org/10.2144/000112479

Koehl, M., Battle, S. E., & Turek, F. W. (2003). Sleep in Female Mice: A Strain Comparison Across the Estrous Cycle. *Sleep*, *26*(3), 267–272. https://doi.org/10.1093/sleep/26.3.267

Kohno, K. (2010). Stress-sensing mechanisms in the unfolded protein response: Similarities and differences between yeast and mammals. *The Journal of Biochemistry*, *147*(1), 27–33. https://doi.org/10.1093/jb/mvp196

Kopp, C., Longordo, F., Nicholson, J. R., & Lüthi, A. (2006). Insufficient Sleep Reversibly Alters Bidirectional Synaptic Plasticity and NMDA Receptor Function. *Journal of Neuroscience*, *26*(48), 12456–12465. https://doi.org/10.1523/JNEUROSCI.2702-06.2006

Korennykh, A. V., Egea, P. F., Korostelev, A. A., Finer-Moore, J., Zhang, C., Shokat, K. M., Stroud, R. M., & Walter, P. (2009). The unfolded protein response signals through high-order assembly of Ire1. *Nature*, *457*(7230), Article 7230. https://doi.org/10.1038/nature07661

Krebs, J., Agellon, L. B., & Michalak, M. (2015). Ca2+ homeostasis and endoplasmic reticulum (ER) stress: An integrated view of calcium signaling. *Biochemical and Biophysical Research Communications*, *460*(1), 114–121. https://doi.org/10.1016/j.bbrc.2015.02.004

Krone, L. B., Yamagata, T., Blanco-Duque, C., Guillaumin, M. C. C., Kahn, M. C., van der Vinne, V., McKillop, L. E., Tam, S. K. E., Peirson, S. N., Akerman, C. J., Hoerder-Suabedissen, A., Molnár, Z., & Vyazovskiy, V. V. (2021). A role for the cortex in sleep–wake regulation. *Nature Neuroscience*, *24*(9), Article 9. https://doi.org/10.1038/s41593-021-00894-6

Krueger, J. M., Nguyen, J. T., Dykstra-Aiello, C. J., & Taishi, P. (2019). Local sleep. *Sleep Medicine Reviews*, *43*, 14–21. https://doi.org/10.1016/j.smrv.2018.10.001

Krueger, J. M., & Obäl Jr., F. (1993). A neuronal group theory of sleep function. *Journal of Sleep Research*, *2*(2), 63–69. https://doi.org/10.1111/j.1365-2869.1993.tb00064.x

Kudo, T., Kanemoto, S., Hara, H., Morimoto, N., Morihara, T., Kimura, R., Tabira, T., Imaizumi, K., & Takeda, M. (2008). A molecular chaperone inducer protects neurons from ER stress. *Cell Death & Differentiation*, *15*(2), Article 2. https://doi.org/10.1038/sj.cdd.4402276

Kuhn, M., Wolf, E., Maier, J. G., Mainberger, F., Feige, B., Schmid, H., Bürklin, J., Maywald, S., Mall, V., Jung, N. H., Reis, J., Spiegelhalder, K., Klöppel, S., Sterr, A., Eckert, A., Riemann, D., Normann, C., & Nissen, C. (2016). Sleep recalibrates homeostatic and associative synaptic plasticity in the human cortex. *Nature Communications*, *7*(1), Article 1. https://doi.org/10.1038/ncomms12455

Lacour, P., Heimrich, B., & Pröls, F. (2007). Induction of cellular stress and chaperone activation in organotypic slice cultures of hippocampus. *Journal of Neuroscience Methods*, *166*(1), 24–31. https://doi.org/10.1016/j.jneumeth.2007.06.019

Lai, C. W., Aronson, D. E., & Snapp, E. L. (2010). BiP Availability Distinguishes States of Homeostasis and Stress in the Endoplasmic Reticulum of Living Cells. *Molecular Biology of the Cell*, *21*(12), 1909–1921. https://doi.org/10.1091/mbc.e09-12-1066

Lajoie, P., Fazio, E. N., & Snapp, E. L. (2014). Approaches to imaging unfolded secretory protein stress in living cells. *Endoplasmic Reticulum Stress in Diseases*, *1*(1), 27–39. https://doi.org/10.2478/ersc-2014-0002

Lajoie, P., & Snapp, E. L. (2011). Changes in BiP availability reveal hypersensitivity to acute endoplasmic reticulum stress in cells expressing mutant huntingtin. *Journal of Cell Science*, *124*(19), 3332–3343. https://doi.org/10.1242/jcs.087510

Lambert, T. J. (2019). FPbase: A community-editable fluorescent protein database. *Nature Methods*, *16*(4), Article 4. https://doi.org/10.1038/s41592-019-0352-8

Langevin, L. M., Mattar, P., Scardigli, R., Roussigné, M., Logan, C., Blader, P., & Schuurmans, C. (2007). Validating in utero electroporation for the rapid analysis of gene regulatory elements in the murine telencephalon. *Developmental Dynamics*, *236*(5), 1273–1286. https://doi.org/10.1002/dvdy.21126

Lazar, A. S., Panin, F., Goodman, A. O. G., Lazic, S. E., Lazar, Z. I., Mason, S. L., Rogers, L., Murgatroyd, P. R., Watson, L. P. E., Singh, P., Borowsky, B., Shneerson, J. M., & Barker, R. A. (2015). Sleep deficits but no metabolic deficits in premanifest Huntington's disease. *Annals of Neurology*, *78*(4), 630–648. https://doi.org/10.1002/ana.24495

Le Bon, O., Popa, D., Streel, E., Alexandre, C., Lena, C., Linkowski, P., & Adrien, J. (2007). Ultradian cycles in mice: Definitions and links with REMS and NREMS. *Journal of Comparative Physiology A*, *193*(10), 1021–1032. https://doi.org/10.1007/s00359-007-0253-7

Leaver, D. D., Schneider, K. M., Rand, M. J., McD. Anderson, R., Gage, P. W., & Malbon, R. (1988). The neurotoxicity of tunicamycin. *Toxicology*, *49*(1), 179–187. https://doi.org/10.1016/0300-483X(88)90191-6

Lee, A. S. (2005). The ER chaperone and signaling regulator GRP78/BiP as a monitor of endoplasmic reticulum stress. *Methods*, *35*(4), 373–381. https://doi.org/10.1016/j.ymeth.2004.10.010

Lee, Y. F., Gerashchenko, D., Timofeev, I., Bacskai, B. J., & Kastanenka, K. V. (2020). Slow Wave Sleep Is a Promising Intervention Target for Alzheimer's Disease. *Frontiers in Neuroscience*, *14*. https://www.frontiersin.org/articles/10.3389/fnins.2020.00705

Leggett, C., McGehee, D. S., Mastrianni, J., Yang, W., Bai, T., & Brorson, J. R. (2012). Tunicamycin produces TDP-43 cytoplasmic inclusions in cultured brain organotypic slices. *Journal of the Neurological Sciences*, *317*(1), 66–73. https://doi.org/10.1016/j.jns.2012.02.027

Lenna, S., Han, R., & Trojanowska, M. (2014). Endoplasmic reticulum stress and endothelial dysfunction. *IUBMB Life*, *66*(8), 530–537. https://doi.org/10.1002/iub.1292

Li, J., Park, E., Zhong, L. R., & Chen, L. (2019). Homeostatic synaptic plasticity as a metaplasticity mechanism—A molecular and cellular perspective. *Current Opinion in Neurobiology*, *54*, 44–53. https://doi.org/10.1016/j.conb.2018.08.010

Li, S.-J., Vaughan, A., Sturgill, J. F., & Kepecs, A. (2018). A Viral Receptor Complementation Strategy to Overcome CAV-2 Tropism for Efficient Retrograde Targeting of Neurons. *Neuron*, *98*(5), 905-917.e5. https://doi.org/10.1016/j.neuron.2018.05.028

Li, X., Zhao, X., Fang, Y., Jiang, X., Duong, T., Fan, C., Huang, C. C., & Kain, S. R. (1998). Generation of destabilized green fluorescent protein as a transcription reporter. *The Journal of Biological Chemistry*, *273*(52), 34970–34975. https://doi.org/10.1074/jbc.273.52.34970

Lim, A. S. P., Kowgier, M., Yu, L., Buchman, A. S., & Bennett, D. A. (2013). Sleep Fragmentation and the Risk of Incident Alzheimer's Disease and Cognitive Decline in Older Persons. *Sleep*, *36*(7), 1027–1032. https://doi.org/10.5665/sleep.2802

Lin, J. H., Li, H., Yasumura, D., Cohen, H. R., Zhang, C., Panning, B., Shokat, K. M., LaVail, M. M., & Walter, P. (2007). IRE1 Signaling Affects Cell Fate During the Unfolded Protein Response. *Science (New York, N.Y.)*, *318*(5852), 944–949. https://doi.org/10.1126/science.1146361

Lin, L., Cao, J., Yang, S., Fu, Z., Zeng, P., Chu, J., Ning, L., Zhang, T., Shi, Y., Tian, Q., Zhou, X., & Wang, J. (2018). Endoplasmic reticulum stress induces spatial memory deficits by activating GSK-3. *Journal of Cellular and Molecular Medicine*, *22*(7), 3489–3502. https://doi.org/10.1111/jcmm.13626

Lindén, H., Tetzlaff, T., Potjans, T. C., Pettersen, K. H., Grün, S., Diesmann, M., & Einevoll, G. T. (2011). Modeling the Spatial Reach of the LFP. *Neuron*, *72*(5), 859–872. https://doi.org/10.1016/j.neuron.2011.11.006

Liu, D., & Dan, Y. (2019). A Motor Theory of Sleep-Wake Control: Arousal-Action Circuit. *Annual Review of Neuroscience*, *42*(1), 27–46. https://doi.org/10.1146/annurev-neuro-080317-061813

Liu, D.-C., Eagleman, D. E., & Tsai, N.-P. (2019). Novel roles of ER stress in repressing neural activity and seizures through Mdm2- and p53-dependent protein translation. *PLOS Genetics*, *15*(9), e1008364. https://doi.org/10.1371/journal.pgen.1008364

Liu, Q., Sun, Y., Yang, T., Feng, W., Li, C., & Li, F. (2011). Sub-10 nm Hexagonal Lanthanide-Doped NaLuF4 Upconversion Nanocrystals for Sensitive Bioimaging in Vivo. *Journal of the American Chemical Society*, *133*(43), 17122–17125. https://doi.org/10.1021/ja207078s

Liu, Y., Beyer, A., & Aebersold, R. (2016a). On the Dependency of Cellular Protein Levels on mRNA Abundance. *Cell*, *165*(3), 535–550. https://doi.org/10.1016/j.cell.2016.03.014

Liu, Y., Beyer, A., & Aebersold, R. (2016b). On the Dependency of Cellular Protein Levels on mRNA Abundance. *Cell*, *165*(3), 535–550. https://doi.org/10.1016/j.cell.2016.03.014

Liu, Y., Tan, Y. L., Zhang, X., Bhabha, G., Ekiert, D. C., Genereux, J. C., Cho, Y., Kipnis, Y., Bjelic, S., Baker, D., & Kelly, J. W. (2014). Small molecule probes to quantify the functional fraction of a specific protein in a cell with minimal folding equilibrium shifts. *Proceedings of the National Academy of Sciences of the United States of America*, *111*(12), 4449–4454. https://doi.org/10.1073/pnas.1323268111

Liu, Z.-W., Faraguna, U., Cirelli, C., Tononi, G., & Gao, X.-B. (2010). Direct evidence for wake-related increases and sleep-related decreases in synaptic strength in rodent cortex. *The Journal of Neuroscience : The Official Journal of the Society for Neuroscience*, *30*(25), 8671–8675. https://doi.org/10.1523/JNEUROSCI.1409-10.2010

Logothetis, N. K., Pauls, J., Augath, M., Trinath, T., & Oeltermann, A. (2001). Neurophysiological investigation of the basis of the fMRI signal. *Nature*, *412*(6843), Article 6843. https://doi.org/10.1038/35084005

Longo, S. K., Guo, M. G., Ji, A. L., & Khavari, P. A. (2021). Integrating single-cell and spatial transcriptomics to elucidate intercellular tissue dynamics. *Nature Reviews Genetics*, *22*(10), Article 10. https://doi.org/10.1038/s41576-021-00370-8

Longordo, F., Fan, J., Steimer, T., Kopp, C., & Lüthi, A. (2011). Do Mice Habituate to "Gentle Handling?" A Comparison of Resting Behavior, Corticosterone Levels and Synaptic Function in Handled and Undisturbed C57BL/6J Mice. *Sleep*, *34*(5), 679–681.

Louessard, M., Bardou, I., Lemarchand, E., Thiebaut, A. M., Parcq, J., Leprince, J., Terrisse, A., Carraro, V., Fafournoux, P., Bruhat, A., Orset, C., Vivien, D., Ali, C., & Roussel, B. D. (2017). Activation of cell surface GRP78 decreases endoplasmic reticulum stress and neuronal death. *Cell Death & Differentiation*, *24*(9), 1518–1529. https://doi.org/10.1038/cdd.2017.35

Lu, P. D., Harding, H. P., & Ron, D. (2004). Translation reinitiation at alternative open reading frames regulates gene expression in an integrated stress response. *The Journal of Cell Biology*, *167*(1), 27–33. https://doi.org/10.1083/jcb.200408003

Lu, W., & Roche, K. W. (2012). Posttranslational regulation of AMPA receptor trafficking and function. *Current Opinion in Neurobiology*, *22*(3), 470–479. https://doi.org/10.1016/j.conb.2011.09.008

Lucey, B. P., McCullough, A., Landsness, E. C., Toedebusch, C. D., McLeland, J. S., Zaza, A. M., Fagan, A. M., McCue, L., Xiong, C., Morris, J. C., Benzinger, T. L. S., & Holtzman, D. M. (2019). Reduced non–rapid eye movement sleep is associated with tau pathology in early Alzheimer's disease. *Science Translational Medicine*, *11*(474), eaau6550. https://doi.org/10.1126/scitranslmed.aau6550

Luo, S., Baumeister, P., Yang, S., Abcouwer, S. F., & Lee, A. S. (2003a). Induction of Grp78/BiP by Translational Block ACTIVATION OF THE Grp78 PROMOTER BY ATF4 THROUGH AN UPSTREAM ATF/CRE SITE INDEPENDENT OF THE ENDOPLASMIC RETICULUM STRESS ELEMENTS. *Journal of Biological Chemistry*, *278*(39), 37375–37385. https://doi.org/10.1074/jbc.M303619200

Luo, S., Baumeister, P., Yang, S., Abcouwer, S. F., & Lee, A. S. (2003b). Induction of Grp78/BiP by Translational Block: ACTIVATION OF THE Grp78 PROMOTER BY ATF4 THROUGH AN UPSTREAM ATF/CRE SITE INDEPENDENT OF THE ENDOPLASMIC RETICULUM STRESS ELEMENTS *. *Journal of Biological Chemistry*, *278*(39), 37375–37385. https://doi.org/10.1074/jbc.M303619200

Lüscher, C., Nicoll, R. A., Malenka, R. C., & Muller, D. (2000). Synaptic plasticity and dynamic modulation of the postsynaptic membrane. *Nature Neuroscience*, *3*(6), 545–550. https://doi.org/10.1038/75714

Ly, S., Lee, D. A., Strus, E., Prober, D. A., & Naidoo, N. (2020). Evolutionarily Conserved Regulation of Sleep by the Protein Translational Regulator PERK. *Current Biology*, *30*(9), 1639-1648.e3. https://doi.org/10.1016/j.cub.2020.02.030

Lyons, L. C., Vanrobaeys, Y., & Abel, T. (2023a). Sleep and memory: The impact of sleep deprivation on transcription, translational control, and protein synthesis in the brain. *Journal of Neurochemistry*, *n/a*(n/a). https://doi.org/10.1111/jnc.15787

Lyons, L. C., Vanrobaeys, Y., & Abel, T. (2023b). Sleep and memory: The impact of sleep deprivation on transcription, translational control, and protein synthesis in the brain. *Journal of Neurochemistry*. https://doi.org/10.1111/jnc.15787

Ma, D., Zerangue, N., Lin, Y.-F., Collins, A., Yu, M., Jan, Y. N., & Jan, L. Y. (2001). Role of ER Export Signals in Controlling Surface Potassium Channel Numbers. *Science*, *291*(5502), 316–319. https://doi.org/10.1126/science.291.5502.316

Ma, Y., & Hendershot, L. M. (2001). The Unfolding Tale of the Unfolded Protein Response. *Cell*, *107*(7), 827–830. https://doi.org/10.1016/S0092-8674(01)00623-7

Ma, Y., & Hendershot, L. M. (2004). ER chaperone functions during normal and stress conditions. *Journal of Chemical Neuroanatomy*, *28*(1), 51–65. https://doi.org/10.1016/j.jchemneu.2003.08.007

Mackiewicz, M., Naidoo, N., Zimmerman, J. E., & Pack, A. I. (2008). Molecular Mechanisms of Sleep and Wakefulness. *Annals of the New York Academy of Sciences*, *1129*(1), 335–349. https://doi.org/10.1196/annals.1417.030

Mackiewicz, M., Shockley, K. R., Romer, M. A., Galante, R. J., Zimmerman, J. E., Naidoo, N., Baldwin, D. A., Jensen, S. T., Churchill, G. A., & Pack, A. I. (2007). Macromolecule biosynthesis: A key function of sleep. *Physiological Genomics*, *31*(3), 441–457. https://doi.org/10.1152/physiolgenomics.00275.2006

Madabhushi, R., & Kim, T.-K. (2018). Emerging themes in neuronal activity-dependent gene expression. *Molecular and Cellular Neuroscience*, *87*, 27–34. https://doi.org/10.1016/j.mcn.2017.11.009

Madisen, L., Zwingman, T. A., Sunkin, S. M., Oh, S. W., Zariwala, H. A., Gu, H., Ng, L. L., Palmiter, R. D., Hawrylycz, M. J., Jones, A. R., Lein, E. S., & Zeng, H. (2010). A robust and high-throughput Cre reporting and characterization system for the whole mouse brain. *Nature Neuroscience*, *13*(1), 133–140. https://doi.org/10.1038/nn.2467

Maiuolo, J., Bulotta, S., Verderio, C., Benfante, R., & Borgese, N. (2011). Selective activation of the transcription factor ATF6 mediates endoplasmic reticulum proliferation triggered by a membrane protein. *Proceedings of the National Academy of Sciences*, *108*(19), 7832–7837. https://doi.org/10.1073/pnas.1101379108

Malhotra, J. D., & Kaufman, R. J. (2007). The Endoplasmic Reticulum and the Unfolded Protein Response. *Seminars in Cell & Developmental Biology*, *18*(6), 716–731. https://doi.org/10.1016/j.semcdb.2007.09.003

Maloney, K. J., Cape, E. G., Gotman, J., & Jones, B. E. (1997). High-frequency γ electroencephalogram activity in association with sleep-wake states and spontaneous behaviors in the rat. *Neuroscience*, *76*(2), 541–555. https://doi.org/10.1016/S0306-4522(96)00298-9

Mander, B. A., Rao, V., Lu, B., Saletin, J. M., Lindquist, J. R., Ancoli-Israel, S., Jagust, W., & Walker, M. P. (2013). Prefrontal atrophy, disrupted NREM slow waves and impaired hippocampal-dependent memory in aging. *Nature Neuroscience*, *16*(3), Article 3. https://doi.org/10.1038/nn.3324

Manning-Bog, A. B., McCormack, A. L., Li, J., Uversky, V. N., Fink, A. L., & Monte, D. A. D. (2002). The Herbicide Paraquat Causes Up-regulation and Aggregation of α-Synuclein in Mice: PARAQUAT AND α-SYNUCLEIN *. *Journal of Biological Chemistry*, *277*(3), 1641–1644. https://doi.org/10.1074/jbc.C100560200

Mao, C., Tai, W.-C., Bai, Y., Poizat, C., & Lee, A. S. (2006). In Vivo Regulation of Grp78/BiP Transcription in the Embryonic Heart ROLE OF THE ENDOPLASMIC RETICULUM STRESS RESPONSE ELEMENT AND GATA-4. *Journal of Biological Chemistry*, *281*(13), 8877–8887. https://doi.org/10.1074/jbc.M505784200

Maret, S., Dorsaz, S., Gurcel, L., Pradervand, S., Petit, B., Pfister, C., Hagenbuchle, O., O'Hara, B. F., Franken, P., & Tafti, M. (2007). Homer1a is a core brain molecular correlate of sleep loss. *Proceedings of the National Academy of Sciences of the United States of America*, *104*(50), 20090–20095. https://doi.org/10.1073/pnas.0710131104

Martayan, A., Sibilio, L., Setini, A., Monaco, E. L., Tremante, E., Fruci, D., Colonna, M., & Giacomini, P. (2008). N-Linked Glycosylation Selectively Regulates the Generic Folding of HLA-Cw1 *. *Journal of Biological Chemistry*, *283*(24), 16469–16476. https://doi.org/10.1074/jbc.M709175200

Martínez, G., Khatiwada, S., Costa-Mattioli, M., & Hetz, C. (2018). ER Proteostasis Control of Neuronal Physiology and Synaptic Function. *Trends in Neurosciences*, *41*(9), 610–624. https://doi.org/10.1016/j.tins.2018.05.009

Masland, R. H. (2004). Neuronal cell types. *Current Biology*, *14*(13), R497–R500. https://doi.org/10.1016/j.cub.2004.06.035

Mattia, M., & Sanchez-Vives, M. V. (2012). Exploring the spectrum of dynamical regimes and timescales in spontaneous cortical activity. *Cognitive Neurodynamics*, *6*(3), 239–250. https://doi.org/10.1007/s11571-011-9179-4

McKillop, L. E., Fisher, S. P., Cui, N., Peirson, S. N., Foster, R. G., Wafford, K. A., & Vyazovskiy, V. V. (2018a). Effects of Aging on Cortical Neural Dynamics and Local Sleep Homeostasis in Mice. *Journal of Neuroscience*, *38*(16), 3911–3928. https://doi.org/10.1523/JNEUROSCI.2513-17.2018

McKillop, L. E., Fisher, S. P., Cui, N., Peirson, S. N., Foster, R. G., Wafford, K. A., & Vyazovskiy, V. V. (2018b). Effects of Aging on Cortical Neural Dynamics and Local Sleep Homeostasis in Mice. *Journal of Neuroscience*, *38*(16), 3911–3928. https://doi.org/10.1523/JNEUROSCI.2513-17.2018

Merksamer, P. I., Trusina, A., & Papa, F. R. (2008). Real-Time Redox Measurements during Endoplasmic Reticulum Stress Reveal Interlinked Protein Folding Functions. *Cell*, *135*(5), 933–947. https://doi.org/10.1016/j.cell.2008.10.011

Merulla, J., Soldà, T., & Molinari, M. (2015). A novel UGGT1 and p97-dependent checkpoint for native ectodomains with ionizable intramembrane residue. *Molecular Biology of the Cell*, *26*(8), 1532–1542. https://doi.org/10.1091/mbc.E14-12-1615

Methippara, M., Bashir, T., Kumar, S., Alam, N., Szymusiak, R., & McGinty, D. (2009). Salubrinal, an inhibitor of protein synthesis, promotes deep slow wave sleep. *American Journal of Physiology - Regulatory, Integrative and Comparative Physiology*, *296*(1), R178–R184. https://doi.org/10.1152/ajpregu.90765.2008

Methippara, M., Mitrani, B., Schrader, F. X., Szymusiak, R., & McGinty, D. (2012). Salubrinal, an endoplasmic reticulum stress blocker, modulates sleep homeostasis and activation of sleep- and wake-regulatory neurons. *Neuroscience*, *209*, 108–118. https://doi.org/10.1016/j.neuroscience.2012.02.016

Michalak, M., Robert Parker, J. M., & Opas, M. (2002). Ca2+ signaling and calcium binding chaperones of the endoplasmic reticulum. *Cell Calcium*, *32*(5), 269–278. https://doi.org/10.1016/S0143416002001884

Middleton, S. A., Eberwine, J., & Kim, J. (2019). Comprehensive catalog of dendritically localized mRNA isoforms from sub-cellular sequencing of single mouse neurons. *BMC Biology*, *17*(1), 5. https://doi.org/10.1186/s12915-019-0630-z

Mignot, E. (2008). Why We Sleep: The Temporal Organization of Recovery. *PLoS Biology*, *6*(4), e106. https://doi.org/10.1371/journal.pbio.0060106

Mistlberger, R. E. (2005). Circadian regulation of sleep in mammals: Role of the suprachiasmatic nucleus. *Brain Research Reviews*, *49*(3), 429–454. https://doi.org/10.1016/j.brainresrev.2005.01.005

Molinari, M., Galli, C., Piccaluga, V., Pieren, M., & Paganetti, P. (2002). Sequential assistance of molecular chaperones and transient formation of covalent complexes during protein degradation from the ER. *The Journal of Cell Biology*, *158*(2), 247–257. https://doi.org/10.1083/jcb.200204122

Moreno, J. A., Radford, H., Peretti, D., Steinert, J. R., Verity, N., Martin, M. G., Halliday, M., Morgan, J., Dinsdale, D., Ortori, C. A., Barrett, D. A., Tsaytler, P., Bertolotti, A., Willis, A. E., Bushell, M., & Mallucci, G. R. (2012). Sustained translational repression by eIF2α-P mediates prion neurodegeneration. *Nature*, *485*(7399), Article 7399. https://doi.org/10.1038/nature11058

Mu, Y., Otsuka, T., Horton, A. C., Scott, D. B., & Ehlers, M. D. (2003). Activity-Dependent mRNA Splicing Controls ER Export and Synaptic Delivery of NMDA Receptors. *Neuron*, *40*(3), 581–594. https://doi.org/10.1016/S0896-6273(03)00676-7

Munro, S., & Pelham, H. R. B. (1986). An hsp70-like protein in the ER: Identity with the 78 kd glucose-regulated protein and immunoglobulin heavy chain binding protein. *Cell*, *46*(2), 291–300. https://doi.org/10.1016/0092-8674(86)90746-4

Myers, R. D. (1966). Injection of solutions into cerebral tissue: Relation between volume and diffusion. *Physiology & Behavior*, *1*(2), 171-IN9. https://doi.org/10.1016/0031-9384(66)90064-3

Naidoo, N., & Brown, M. (2012). The endoplasmic reticulum stress response in aging and age-related diseases. *Frontiers in Physiology*, *3*. https://doi.org/10.3389/fphys.2012.00263

Naidoo, N., Casiano, V., Cater, J., Zimmerman, J., & Pack, A. I. (2007a). A Role for the Molecular Chaperone Protein BiP/GRP78 in Drosophila Sleep Homeostasis. *Sleep*, *30*(5), 557–565. https://doi.org/10.1093/sleep/30.5.557

Naidoo, N., Casiano, V., Cater, J., Zimmerman, J., & Pack, A. I. (2007b). A Role for the Molecular Chaperone Protein BiP/GRP78 in Drosophila Sleep Homeostasis. *Sleep*, *30*(5), 557–565. https://doi.org/10.1093/sleep/30.5.557

Naidoo, N., Ferber, M., Master, M., Zhu, Y., & Pack, A. I. (2008). Aging Impairs the Unfolded Protein Response to Sleep Deprivation and Leads to Proapoptotic Signaling. *Journal of Neuroscience*, *28*(26), 6539–6548. https://doi.org/10.1523/JNEUROSCI.5685-07.2008

Naidoo, N., Giang, W., Galante, R. J., & Pack, A. I. (2005). Sleep deprivation induces the unfolded protein response in mouse cerebral cortex. *Journal of Neurochemistry*, *92*(5), 1150–1157. https://doi.org/10.1111/j.1471-4159.2004.02952.x

Nakanishi, H., Sun, Y., Nakamura, R. K., Mori, K., Ito, M., Suda, S., Namba, H., Storch, F. I., Dang, T. P., Mendelson, W., Mishkin, M., Kennedy, C., Gillin, J. C., Smith, C. B., & Sokoloff, L. (1997). Positive Correlations Between Cerebral Protein Synthesis Rates and Deep Sleep in Macaca mulatta. *European Journal of Neuroscience*, *9*(2), 271–279. https://doi.org/10.1111/j.1460-9568.1997.tb01397.x

Nedeltcheva, A. V., & Scheer, F. A. J. L. (2014). Metabolic effects of sleep disruption, links to obesity and diabetes. *Current Opinion in Endocrinology, Diabetes, and Obesity*, *21*(4), 293–298. https://doi.org/10.1097/MED.0000000000000082

Neske, G. T. (2016). The Slow Oscillation in Cortical and Thalamic Networks: Mechanisms and Functions. *Frontiers in Neural Circuits*, *9*. https://doi.org/10.3389/fncir.2015.00088

Neske, G. T., & Connors, B. W. (2016). Distinct Roles of SOM and VIP Interneurons during Cortical Up States. *Frontiers in Neural Circuits*, *10*. https://doi.org/10.3389/fncir.2016.00052

Ng, L., Bernard, A., Lau, C., Overly, C. C., Dong, H.-W., Kuan, C., Pathak, S., Sunkin, S. M., Dang, C., Bohland, J. W., Bokil, H., Mitra, P. P., Puelles, L., Hohmann, J., Anderson, D. J., Lein, E. S., Jones, A. R., & Hawrylycz, M. (2009). An anatomic gene expression atlas of the adult mouse brain. *Nature Neuroscience*, *12*(3), Article 3. https://doi.org/10.1038/nn.2281

Ngo, H.-V. V., Claassen, J., & Dresler, M. (2020). Sleep: Slow Wave Activity Predicts Amyloid-β Accumulation. *Current Biology*, *30*(22), R1371–R1373. https://doi.org/10.1016/j.cub.2020.09.058

Niethard, N., Hasegawa, M., Itokazu, T., Oyanedel, C. N., Born, J., & Sato, T. R. (2016). Sleep-Stage-Specific Regulation of Cortical Excitation and Inhibition. *Current Biology*, *26*(20), 2739–2749. https://doi.org/10.1016/j.cub.2016.08.035

Nir, Y., Andrillon, T., Marmelshtein, A., Suthana, N., Cirelli, C., Tononi, G., & Fried, I. (2017). Selective neuronal lapses precede human cognitive lapses following sleep deprivation. *Nature Medicine*, *23*(12), Article 12. https://doi.org/10.1038/nm.4433

Nir, Y., & de Lecea, L. (2023). Sleep and vigilance states: Embracing spatiotemporal dynamics. *Neuron*, S0896-6273(23)00297-0. https://doi.org/10.1016/j.neuron.2023.04.012

Nir, Y., Staba, R. J., Andrillon, T., Vyazovskiy, V. V., Cirelli, C., Fried, I., & Tononi, G. (2011). Regional Slow Waves and Spindles in Human Sleep. *Neuron*, *70*(1), 153–169. https://doi.org/10.1016/j.neuron.2011.02.043

Nomura, T., Nishimura, Y., Gotoh, H., & Ono, K. (2016). Rapid and efficient gene delivery into the adult mouse brain via focal electroporation. *Scientific Reports*, *6*(1), Article 1. https://doi.org/10.1038/srep29817

Nosyreva, E., & Kavalali, E. T. (2010). Activity-Dependent Augmentation of Spontaneous Neurotransmission during Endoplasmic Reticulum Stress. *The Journal of Neuroscience*, *30*(21), 7358–7368. https://doi.org/10.1523/JNEUROSCI.5358-09.2010

Nougarède, A., Tesnière, C., Ylanko, J., Rimokh, R., Gillet, G., & Andrews, D. W. (2018). Improved IRE1 and PERK Pathway Sensors for Multiplex Endoplasmic Reticulum Stress Assay Reveal Stress Response to Nuclear Dyes Used for Image Segmentation. *ASSAY and Drug Development Technologies*, *16*(6), 350–360. https://doi.org/10.1089/adt.2018.862

Noya, S. B., Colameo, D., Brüning, F., Spinnler, A., Mircsof, D., Opitz, L., Mann, M., Tyagarajan, S. K., Robles, M. S., & Brown, S. A. (2019). The forebrain synaptic transcriptome is organized by clocks but its proteome is driven by sleep. *Science*, *366*(6462). https://doi.org/10.1126/science.aav2642

Obrenovitch, T. P., Richards, D. A., Sarna, G. S., & Symon, L. (1993). Combined intracerebral microdialysis and electrophysiological recording: Methodology and applications. *Journal of Neuroscience Methods*, *47*(1), 139–145. https://doi.org/10.1016/0165-0270(93)90030-U

Obukuro, K., Nobunaga, M., Takigawa, M., Morioka, H., Hisatsune, A., Isohama, Y., Shimokawa, H., Tsutsui, M., & Katsuki, H. (2013). Nitric Oxide Mediates Selective Degeneration of Hypothalamic Orexin Neurons through Dysfunction of Protein Disulfide Isomerase. *Journal of Neuroscience*, *33*(31), 12557–12568. https://doi.org/10.1523/JNEUROSCI.0595-13.2013

Ono, Y., Shimazawa, M., Ishisaka, M., Oyagi, A., Tsuruma, K., & Hara, H. (2012). Imipramine protects mouse hippocampus against tunicamycin-induced cell death. *European Journal of Pharmacology*, *696*(1), 83–88. https://doi.org/10.1016/j.ejphar.2012.09.037

Origel Marmolejo, C. A., Bachhav, B., Patibandla, S. D., Yang, A. L., & Segatori, L. (2020). A gene signal amplifier platform for monitoring the unfolded protein response. *Nature Chemical Biology*, *16*(5), Article 5. https://doi.org/10.1038/s41589-020-0497-x

Oslowski, C. M., & Urano, F. (2011). Chapter Four—Measuring ER Stress and the Unfolded Protein Response Using Mammalian Tissue Culture System. In P. M. Conn (Ed.), *Methods in Enzymology* (Vol. 490, pp. 71–92). Academic Press. https://doi.org/10.1016/B978-0-12-385114-7.00004-0

Oyadomari, S., & Mori, M. (2004). Roles of CHOP/GADD153 in endoplasmic reticulum stress. *Cell Death & Differentiation*, *11*(4), Article 4. https://doi.org/10.1038/sj.cdd.4401373

Ozcan, L., Ergin, A. S., Lu, A., Chung, J., Sarkar, S., Nie, D., Myers, M. G., & Ozcan, U. (2009). Endoplasmic Reticulum Stress Plays a Central Role in Development of Leptin Resistance. *Cell Metabolism*, *9*(1), 35–51. https://doi.org/10.1016/j.cmet.2008.12.004

Öztürk, Z., O'Kane, C. J., & Pérez-Moreno, J. J. (2020). Axonal Endoplasmic Reticulum Dynamics and Its Roles in Neurodegeneration. *Frontiers in Neuroscience*, *14*. https://doi.org/10.3389/fnins.2020.00048

Parham, P. (1996). Functions forMHC class I carbohydrates inside and outside the cell. *Trends in Biochemical Sciences*, *21*(11), 427–433. https://doi.org/10.1016/S0968-0004(96)10053-0

Paul, A., Crow, M., Raudales, R., He, M., Gillis, J., & Huang, Z. J. (2017). Transcriptional Architecture of Synaptic Communication Delineates GABAergic Neuron Identity. *Cell*, *171*(3), 522-539.e20. https://doi.org/10.1016/j.cell.2017.08.032

Pédelacq, J.-D., Cabantous, S., Tran, T., Terwilliger, T. C., & Waldo, G. S. (2006). Engineering and characterization of a superfolder green fluorescent protein. *Nature Biotechnology*, *24*(1), Article 1. https://doi.org/10.1038/nbt1172

Penaud-Budloo, M., Le Guiner, C., Nowrouzi, A., Toromanoff, A., Chérel, Y., Chenuaud, P., Schmidt, M., von Kalle, C., Rolling, F., Moullier, P., & Snyder, R. O. (2008). Adeno-Associated Virus Vector Genomes Persist as Episomal Chromatin in Primate Muscle. *Journal of Virology*, *82*(16), 7875–7885. https://doi.org/10.1128/JVI.00649-08

Perez, J. D., Fusco, C. M., & Schuman, E. M. (2021). A Functional Dissection of the mRNA and Locally Synthesized Protein Population in Neuronal Dendrites and Axons. *Annual Review of Genetics*, *55*(1), 183–207. https://doi.org/10.1146/annurev-genet-030321-054851

Pick, J. E., & Ziff, E. B. (2018). Regulation of AMPA receptor trafficking and exit from the endoplasmic reticulum. *Molecular and Cellular Neuroscience*, *91*, 3–9. https://doi.org/10.1016/j.mcn.2018.03.004

Pincus, D., Chevalier, M. W., Aragón, T., Anken, E. van, Vidal, S. E., El-Samad, H., & Walter, P. (2010). BiP Binding to the ER-Stress Sensor Ire1 Tunes the Homeostatic Behavior of the Unfolded Protein Response. *PLOS Biology*, *8*(7), e1000415. https://doi.org/10.1371/journal.pbio.1000415

Poulet, J. F. A., & Petersen, C. C. H. (2008). Internal brain state regulates membrane potential synchrony in barrel cortex of behaving mice. *Nature*, *454*(7206), Article 7206. https://doi.org/10.1038/nature07150

Preissler, S., Rohland, L., Yan, Y., Chen, R., Read, R. J., & Ron, D. (2017). AMPylation targets the rate-limiting step of BiP's ATPase cycle for its functional inactivation. *ELife*, *6*, e29428. https://doi.org/10.7554/eLife.29428

Puentes-Mestril, C., & Aton, S. J. (2017). Linking Network Activity to Synaptic Plasticity during Sleep: Hypotheses and Recent Data. *Frontiers in Neural Circuits*, *11*. https://doi.org/10.3389/fncir.2017.00061

Puentes-Mestril, C., Delorme, J., Wang, L., Donnelly, M., Popke, D., Jiang, S., & Aton, S. J. (2021). Sleep Loss Drives Brain Region-Specific and Cell Type-Specific Alterations in Ribosome-Associated Transcripts Involved in Synaptic Plasticity and Cellular Timekeeping. *Journal of Neuroscience*, *41*(25), 5386–5398. https://doi.org/10.1523/JNEUROSCI.1883-20.2021

Raizen, D. M., Zimmerman, J. E., Maycock, M. H., Ta, U. D., You, Y., Sundaram, M. V., & Pack, A. I. (2008). Lethargus is a Caenorhabditis elegans sleep-like state. *Nature*, *451*(7178), Article 7178. https://doi.org/10.1038/nature06535

Rajamohamedsait, H. B., & Sigurdsson, E. M. (2012). Histological Staining of Amyloid and Pre-Amyloid Peptides and Proteins in Mouse Tissue. *Methods in Molecular Biology (Clifton, N.J.)*, *849*, 10.1007/978-1-61779-551-0_28. https://doi.org/10.1007/978-1-61779-551-0_28

Ramm, P., & Smith, C. T. (1990). Rates of cerebral protein synthesis are linked to slow wave sleep in the rat. *Physiology & Behavior*, *48*(5), 749–753. https://doi.org/10.1016/0031-9384(90)90220-X

Read, A., & Schröder, M. (2021). The Unfolded Protein Response: An Overview. *Biology*, *10*(5), Article 5. https://doi.org/10.3390/biology10050384

Rechtschaffen, A. (1998). Current Perspectives on the Function of Sleep. *Perspectives in Biology and Medicine*, *41*(3), 359–390. https://doi.org/10.1353/pbm.1998.0051

Ren, J., Zhang, M.-J., Li, T.-M., Zhang, J., Lin, R., Chen, S., Luo, M., & Dong, M.-Q. (2016). Quantitative Proteomics of Sleep-Deprived Mouse Brains Reveals Global Changes in Mitochondrial Proteins. *PLOS ONE*, *11*(9), e0163500. https://doi.org/10.1371/journal.pone.0163500

Rodarie, D., Verasztó, C., Roussel, Y., Reimann, M., Keller, D., Ramaswamy, S., Gewaltig, M.-O., & Markram, H. (2021). *Atlas of Inhibitory Neurons in the Mouse Brain* (p. 2021.11.20.469384). bioRxiv. https://doi.org/10.1101/2021.11.20.469384

Roest, G., Hesemans, E., Welkenhuyzen, K., Luyten, T., Engedal, N., Bultynck, G., & Parys, J. B. (2018). The ER Stress Inducer l-Azetidine-2-Carboxylic Acid Elevates the Levels of Phospho-eIF2α and of LC3-II in a Ca2+-Dependent Manner. *Cells*, *7*(12), 239. https://doi.org/10.3390/cells7120239

Roussel, B. D., Kruppa, A. J., Miranda, E., Crowther, D. C., Lomas, D. A., & Marciniak, S. J. (2013). Endoplasmic reticulum dysfunction in neurological disease. *The Lancet Neurology*, *12*(1), 105–118. https://doi.org/10.1016/S1474-4422(12)70238-7

Rubenstein, E. (2000). Biologic Effects of and Clinical Disorders Caused by Nonprotein Amino Acids. *Medicine*, *79*(2), 80.

Rutkowski, D. T., & Hegde, R. S. (2010). Regulation of basal cellular physiology by the homeostatic unfolded protein response. *The Journal of Cell Biology*, *189*(5), 783–794. https://doi.org/10.1083/jcb.201003138

Rutkowski, D. T., & Kaufman, R. J. (2007). That which does not kill me makes me stronger: Adapting to chronic ER stress. *Trends in Biochemical Sciences*, *32*(10), 469–476. https://doi.org/10.1016/j.tibs.2007.09.003

Ryoo, H. D. (2016). Long and short (timeframe) of endoplasmic reticulum stress-induced cell death. *The FEBS Journal*, *283*(20), 3718–3722. https://doi.org/10.1111/febs.13755

Saito, A., Cai, L., Matsuhisa, K., Ohtake, Y., Kaneko, M., Kanemoto, S., Asada, R., & Imaizumi, K. (2018). Neuronal activity-dependent local activation of dendritic unfolded protein response promotes expression of brain-derived neurotrophic factor in cell soma. *Journal of Neurochemistry*, *144*(1), 35–49. https://doi.org/10.1111/jnc.14221

Sanchez-Vives, M. V., & McCormick, D. A. (2000). Cellular and network mechanisms of rhythmic recurrent activity in neocortex. *Nature Neuroscience*, *3*(10), Article 10. https://doi.org/10.1038/79848

Scheuner, D., & Kaufman, R. J. (2008). The Unfolded Protein Response: A Pathway That Links Insulin Demand with β-Cell Failure and Diabetes. *Endocrine Reviews*, *29*(3), 317–333. https://doi.org/10.1210/er.2007-0039

Schröder, M., & Kaufman, R. J. (2005). The Mammalian Unfolded Protein Response. *Annual Review of Biochemistry*, *74*(1), 739–789. https://doi.org/10.1146/annurev.biochem.73.011303.074134

Schwierin, B., Achermann, P., Deboer, T., Oleksenko, A., Borbély, A. A., & Tobler, I. (1999). Regional differences in the dynamics of the cortical EEG in the rat after sleep deprivation. *Clinical Neurophysiology*, *110*(5), 869–875. https://doi.org/10.1016/S1388-2457(99)00020-6

Schwierin, B., Borbély, A. A., & Tobler, I. (1998). Sleep homeostasis in the female rat during the estrous cycle. *Brain Research*, *811*(1), 96–104. https://doi.org/10.1016/S0006-8993(98)00991-3

Seibt, J., Dumoulin, M. C., Aton, S. J., Coleman, T., Watson, A., Naidoo, N., & Frank, M. G. (2012). Protein Synthesis during Sleep Consolidates Cortical Plasticity In Vivo. *Current Biology*, *22*(8), 676–682. https://doi.org/10.1016/j.cub.2012.02.016

Sen, D., Balakrishnan, B., & Jayandharan, G. R. (2014). Cellular unfolded protein response against viruses used in gene therapy. *Frontiers in Microbiology*, *5*. https://www.frontiersin.org/articles/10.3389/fmicb.2014.00250

Shahani, N., Subramaniam, S., Wolf, T., Tackenberg, C., & Brandt, R. (2006). Tau Aggregation and Progressive Neuronal Degeneration in the Absence of Changes in Spine Density and Morphology after Targeted Expression of Alzheimer's Disease-Relevant Tau Constructs in Organotypic Hippocampal Slices. *Journal of Neuroscience*, *26*(22), 6103–6114. https://doi.org/10.1523/JNEUROSCI.4245-05.2006

Shaner, N. C., Lambert, G. G., Chammas, A., Ni, Y., Cranfill, P. J., Baird, M. A., Sell, B. R., Allen, J. R., Day, R. N., Israelsson, M., Davidson, M. W., & Wang, J. (2013). A bright monomeric green fluorescent protein derived from *Branchiostoma lanceolatum*. *Nature Methods*, *10*(5), 407–409. https://doi.org/10.1038/nmeth.2413

Shapiro, D. J., Livezey, M., Yu, L., Zheng, X., & Andruska, N. (2016). Anticipatory UPR Activation: A Protective Pathway and Target in Cancer. *Trends in Endocrinology & Metabolism*, *27*(10), 731–741. https://doi.org/10.1016/j.tem.2016.06.002

Shaw, P. J., Cirelli, C., Greenspan, R. J., & Tononi, G. (2000). Correlates of Sleep and Waking in Drosophila melanogaster. *Science*, *287*(5459), 1834–1837. https://doi.org/10.1126/science.287.5459.1834

Shen, J., Chen, X., Hendershot, L., & Prywes, R. (2002). ER Stress Regulation of ATF6 Localization by Dissociation of BiP/GRP78 Binding and Unmasking of Golgi Localization Signals. *Developmental Cell*, *3*(1), 99–111. https://doi.org/10.1016/S1534-5807(02)00203-4

Shiu, R. P., Pouyssegur, J., & Pastan, I. (1977). Glucose depletion accounts for the induction of two transformation-sensitive membrane proteinsin Rous sarcoma virus-transformed chick embryo fibroblasts. *Proceedings of the National Academy of Sciences*, *74*(9), 3840–3844. https://doi.org/10.1073/pnas.74.9.3840

Shoulders, M. D., Ryno, L. M., Genereux, J. C., Moresco, J. J., Tu, P. G., Wu, C., Yates, J. R., Su, A. I., Kelly, J. W., & Wiseman, R. L. (2013). Stress-Independent Activation of XBP1s and/or ATF6 Reveals Three Functionally Diverse ER Proteostasis Environments. *Cell Reports*, *3*(4), 1279–1292. https://doi.org/10.1016/j.celrep.2013.03.024

Sicari, D., Delaunay-Moisan, A., Combettes, L., Chevet, E., & Igbaria, A. (2020). A guide to assessing endoplasmic reticulum homeostasis and stress in mammalian systems. *The FEBS Journal*, 27–42. https://doi.org/10.1111/febs.15107@10.1111/(ISSN)1742-4658.a-guide-to

Siclari, F., & Tononi, G. (2017). Local aspects of sleep and wakefulness. *Current Opinion in Neurobiology*, *44*, 222–227. https://doi.org/10.1016/j.conb.2017.05.008

Sirota, A., & Buzsaki, G. (2005). Interaction between neocortical and hippocampal networks via slow oscillations. *Thalamus & Related Systems*, *3*(4), 245–259. https://doi.org/10.1017/S1472928807000258

Sree, S., Parkkinen, I., Their, A., Airavaara, M., & Jokitalo, E. (2021). Morphological Heterogeneity of the Endoplasmic Reticulum within Neurons and Its Implications in Neurodegeneration. *Cells*, *10*(5), Article 5. https://doi.org/10.3390/cells10050970

Steriade, M., McCormick, D. A., & Sejnowski, T. J. (1993). Thalamocortical Oscillations in the Sleeping and Aroused Brain. *Science*, *262*(5134), 679–685. https://doi.org/10.1126/science.8235588

Steriade, M., Timofeev, I., & Grenier, F. (2001). Natural Waking and Sleep States: A View From Inside Neocortical Neurons. *Journal of Neurophysiology*, *85*(5), 1969–1985. https://doi.org/10.1152/jn.2001.85.5.1969

Stoppini, L., Buchs, P.-A., & Muller, D. (1991). A simple method for organotypic cultures of nervous tissue. *Journal of Neuroscience Methods*, *37*(2), 173–182. https://doi.org/10.1016/0165-0270(91)90128-M

Stringer, C., Michaelos, M., & Pachitariu, M. (2020). Cellpose: A generalist algorithm for cellular segmentation. *BioRxiv*, 2020.02.02.931238. https://doi.org/10.1101/2020.02.02.931238

Sun, F.-C., Wei, S., Li, C.-W., Chang, Y.-S., Chao, C.-C., & Lai, Y.-K. (2006). Localization of GRP78 to mitochondria under the unfolded protein response. *Biochemical Journal*, *396*(1), 31–39. https://doi.org/10.1042/BJ20051916

Sylwestrak, E. L., Jo, Y., Vesuna, S., Wang, X., Holcomb, B., Tien, R. H., Kim, D. K., Fenno, L., Ramakrishnan, C., Allen, W. E., Chen, R., Shenoy, K. V., Sussillo, D., & Deisseroth, K. (2022). Cell-type-specific population dynamics of diverse reward computations. *Cell*, *185*(19), 3568-3587.e27. https://doi.org/10.1016/j.cell.2022.08.019

Tabas, I., & Ron, D. (2011). Integrating the mechanisms of apoptosis induced by endoplasmic reticulum stress. *Nature Cell Biology*, *13*(3), 184–190. https://doi.org/10.1038/ncb0311-184

Tabata, H., & Nakajima, K. (2001). Efficient in utero gene transfer system to the developing mouse brain using electroporation: Visualization of neuronal migration in the developing cortex. *Neuroscience*, *103*(4), 865–872. https://doi.org/10.1016/S0306-4522(01)00016-1

Taniguchi, H., He, M., Wu, P., Kim, S., Paik, R., Sugino, K., Kvitsani, D., Fu, Y., Lu, J., Lin, Y., Miyoshi, G., Shima, Y., Fishell, G., Nelson, S. B., & Huang, Z. J. (2011). A Resource of Cre Driver Lines for Genetic Targeting of GABAergic Neurons in Cerebral Cortex. *Neuron*, *71*(6), 995–1013. https://doi.org/10.1016/j.neuron.2011.07.026

Tasic, B., Yao, Z., Graybuck, L. T., Smith, K. A., Nguyen, T. N., Bertagnolli, D., Goldy, J., Garren, E., Economo, M. N., Viswanathan, S., Penn, O., Bakken, T., Menon, V., Miller, J., Fong, O., Hirokawa, K. E., Lathia, K., Rimorin, C., Tieu, M., … Zeng, H. (2018). Shared and distinct transcriptomic cell types across neocortical areas. *Nature*, *563*(7729), Article 7729. https://doi.org/10.1038/s41586-018-0654-5

Terao, A., Steininger, T. L., Hyder, K., Apte-Deshpande, A., Ding, J., Rishipathak, D., Davis, R. W., Heller, H. C., & Kilduff, T. S. (2003). Differential increase in the expression of heat shock protein family members during sleep deprivation and during sleep. *Neuroscience*, *116*(1), 187–200. https://doi.org/10.1016/S0306-4522(02)00695-4

Terao, A., Wisor, J. P., Peyron, C., Apte-Deshpande, A., Wurts, S. W., Edgar, D. M., & Kilduff, T. S. (2006). Gene Expression in the Rat Brain during Sleep Deprivation and Recovery Sleep: An Affymetrix GeneChip® Study. *Neuroscience*, *137*(2), 593–605. https://doi.org/10.1016/j.neuroscience.2005.08.059

Thastrup, O., Cullen, P. J., Drøbak, B. K., Hanley, M. R., & Dawson, A. P. (1990). Thapsigargin, a tumor promoter, discharges intracellular Ca2+ stores by specific inhibition of the endoplasmic reticulum Ca2(+)-ATPase. *Proceedings of the National Academy of Sciences*, *87*(7), 2466–2470.

Thomas, C. W., Guillaumin, M. C., McKillop, L. E., Achermann, P., & Vyazovskiy, V. V. (2020). Global sleep homeostasis reflects temporally and spatially integrated local cortical neuronal activity. *ELife*, *9*, e54148. https://doi.org/10.7554/eLife.54148

Thompson, C. L., Wisor, J. P., Lee, C.-K., Pathak, S. D., Gerashchenko, D., Smith, K. A., Fischer, S. R., Kuan, C. L., Sunkin, S. M., Ng, L. L., Lau, C., Hawrylycz, M., Jones, A. R., Kilduff, T., & Lein, E. S. (2010). Molecular and Anatomical Signatures of Sleep Deprivation in the Mouse Brain. *Frontiers in Neuroscience*, *4*. https://doi.org/10.3389/fnins.2010.00165

Tillman, J. B., Mote, P. L., Walford, R. L., & Spindler, S. R. (1995). Structure and regulation of the mouse GRP78 (BiP) promoter by glucose and calcium ionophore. *Gene*, *158*(2), 225–229. https://doi.org/10.1016/0378-1119(95)00083-I

Timofeev, I., & Steriade, M. (1996). Low-frequency rhythms in the thalamus of intact-cortex and decorticated cats. *Journal of Neurophysiology*, *76*(6), 4152–4168. https://doi.org/10.1152/jn.1996.76.6.4152

Tirosh, A., Tuncman, G., Calay, E. S., Rathaus, M., Ron, I., Tirosh, A., Yalcin, A., Lee, Y. G., Livne, R., Ron, S., Minsky, N., Arruda, A. P., & Hotamisligil, G. S. (2021). Intercellular Transmission of Hepatic ER Stress in Obesity Disrupts Systemic Metabolism. *Cell Metabolism*, *33*(2), 319-333.e6. https://doi.org/10.1016/j.cmet.2020.11.009

Tobler, I., & Borbély, A. A. (1986). Sleep EEG in the rat as a function of prior waking. *Electroencephalography and Clinical Neurophysiology*, *64*(1), 74–76. https://doi.org/10.1016/0013-4694(86)90044-1

Tomoda, T., Sumitomo, A., Newton, D., & Sibille, E. (2022). Molecular origin of somatostatin-positive neuron vulnerability. *Molecular Psychiatry*, *27*(4), 2304–2314. https://doi.org/10.1038/s41380-022-01463-4

Tong, J., Okutani, F., Murata, Y., Taniguchi, M., Namba, T., Wang, Y.-J., & Kaba, H. (2017a). Tunicamycin impairs olfactory learning and synaptic plasticity in the olfactory bulb. *Neuroscience*, *344*, 371–379. https://doi.org/10.1016/j.neuroscience.2017.01.001

Tong, J., Okutani, F., Murata, Y., Taniguchi, M., Namba, T., Wang, Y.-J., & Kaba, H. (2017b). Tunicamycin impairs olfactory learning and synaptic plasticity in the olfactory bulb. *Neuroscience*, *344*, 371–379. https://doi.org/10.1016/j.neuroscience.2017.01.001

Tononi, G., & Cirelli, C. (2003). Sleep and synaptic homeostasis: A hypothesis. *Brain Research Bulletin*, *62*(2), 143–150.

Tononi, G., & Cirelli, C. (2006). Sleep function and synaptic homeostasis. *Sleep Medicine Reviews*, *10*(1), 49–62. https://doi.org/10.1016/j.smrv.2005.05.002

Tossell, K., Yu, X., Soto, B. A., Vicente, M., Miracca, G., Giannos, P., Miao, A., Hsieh, B., Ma, Y., Yustos, R., Vyssotski, A. L., Constandinou, T., Franks, N. P., & Wisden, W. (2020). Sleep deprivation triggers somatostatin neurons in prefrontal cortex to initiate nesting and sleep via the preoptic and lateral hypothalamus. *BioRxiv*, 2020.07.01.179671. https://doi.org/10.1101/2020.07.01.179671

Tremblay, R., Lee, S., & Rudy, B. (2016). GABAergic Interneurons in the Neocortex: From Cellular Properties to Circuits. *Neuron*, *91*(2), 260–292. https://doi.org/10.1016/j.neuron.2016.06.033

Tudor, J. C., Davis, E. J., Peixoto, L., Wimmer, M. E., van Tilborg, E., Park, A. J., Poplawski, S. G., Chung, C. W., Havekes, R., Huang, J., Gatti, E., Pierre, P., & Abel, T. (2016). Sleep deprivation impairs memory by attenuating mTORC1-dependent protein synthesis. *Science Signaling*, *9*(425), ra41–ra41. https://doi.org/10.1126/scisignal.aad4949

Uddin, Md. S., Tewari, D., Sharma, G., Kabir, Md. T., Barreto, G. E., Bin-Jumah, M. N., Perveen, A., Abdel-Daim, M. M., & Ashraf, G. M. (2020). Molecular Mechanisms of ER Stress and UPR in the Pathogenesis of Alzheimer's Disease. *Molecular Neurobiology*, *57*(7), 2902–2919. https://doi.org/10.1007/s12035-020-01929-y

Uhlén, M., Fagerberg, L., Hallström, B. M., Lindskog, C., Oksvold, P., Mardinoglu, A., Sivertsson, Å., Kampf, C., Sjöstedt, E., Asplund, A., Olsson, I., Edlund, K., Lundberg, E., Navani, S., Szigyarto, C. A.-K., Odeberg, J., Djureinovic, D., Takanen, J. O., Hober, S., … Pontén, F. (2015). Tissue-based map of the human proteome. *Science*, *347*(6220), 1260419. https://doi.org/10.1126/science.1260419

Uhlen, M., Oksvold, P., Fagerberg, L., Lundberg, E., Jonasson, K., Forsberg, M., Zwahlen, M., Kampf, C., Wester, K., Hober, S., Wernerus, H., Björling, L., & Ponten, F. (2010). Towards a knowledge-based Human Protein Atlas. *Nature Biotechnology*, *28*(12), Article 12. https://doi.org/10.1038/nbt1210-1248

Ushimaru, M., & Kawaguchi, Y. (2015). Temporal Structure of Neuronal Activity among Cortical Neuron Subtypes during Slow Oscillations in Anesthetized Rats. *Journal of Neuroscience*, *35*(34), 11988–12001. https://doi.org/10.1523/JNEUROSCI.5074-14.2015

Utomo, A. R. H., Nikitin, A. Y., & Lee, W.-H. (1999). Temporal, spatial, and cell type–specific control of Cre-mediated DNA recombination in transgenic mice. *Nature Biotechnology*, *17*(11), Article 11. https://doi.org/10.1038/15073

Vanrobaeys, Y., Peterson, Z. J., Walsh, E. N., Chatterjee, S., Lin, L.-C., Lyons, L. C., Nickl-Jockschat, T., & Abel, T. (2023). *Spatial transcriptomics reveals unique gene expression changes in different brain regions after sleep deprivation* (p. 2023.01.18.524406). bioRxiv. https://doi.org/10.1101/2023.01.18.524406

Vecsey, C. G., Baillie, G. S., Jaganath, D., Havekes, R., Daniels, A., Wimmer, M., Huang, T., Brown, K. M., Li, X.-Y., Descalzi, G., Kim, S. S., Chen, T., Shang, Y.-Z., Zhuo, M., Houslay, M. D., & Abel, T. (2009). Sleep deprivation impairs cAMP signalling in the hippocampus. *Nature*, *461*(7267), Article 7267. https://doi.org/10.1038/nature08488

Veeramani, V., Bao, Z., Chan, M.-H., Wang, H.-C., Jena, A., Chang, H., Hu, S.-F., & Liu, R.-S. (2019). Quantum dots for light conversion, therapeutic and energy storage applications. *Journal of Solid State Chemistry*, *270*, 71–84. https://doi.org/10.1016/j.jssc.2018.11.002

Voeltz, G. K., Rolls, M. M., & Rapoport, T. A. (2002). Structural organization of the endoplasmic reticulum. *EMBO Reports*, *3*(10), 944–950. https://doi.org/10.1093/embo-reports/kvf202

Vyazovskiy, V., Borbély, A. A., & Tobler, I. (2000). Fast track:Unilateral vibrissae stimulation during waking induces interhemispheric EEG asymmetry during subsequent sleep in the rat. *Journal of Sleep Research*, *9*(4), 367–371. https://doi.org/10.1046/j.1365-2869.2000.00230.x

Vyazovskiy, V. V., Borbély, A. A., & Tobler, I. (2002). Interhemispheric Sleep EEG Asymmetry in the Rat is Enhanced by Sleep Deprivation. *Journal of Neurophysiology*, *88*(5), 2280–2286. https://doi.org/10.1152/jn.00304.2002

Vyazovskiy, V. V., Cirelli, C., Pfister-Genskow, M., Faraguna, U., & Tononi, G. (2008). Molecular and electrophysiological evidence for net synaptic potentiation in wake and depression in sleep. *Nature Neuroscience*, *11*(2), 200–208. https://doi.org/10.1038/nn2035

Vyazovskiy, V. V., & Harris, K. D. (2013). Sleep and the single neuron: The role of global slow oscillations in individual cell rest. *Nature Reviews Neuroscience*, *14*(6), 443–451. https://doi.org/10.1038/nrn3494

Vyazovskiy, V. V., Olcese, U., Hanlon, E. C., Nir, Y., Cirelli, C., & Tononi, G. (2011). Local sleep in awake rats. *Nature*, *472*(7344), 443–447. https://doi.org/10.1038/nature10009

Vyazovskiy, V. V., Olcese, U., Lazimy, Y. M., Faraguna, U., Esser, S. K., Williams, J. C., Cirelli, C., & Tononi, G. (2009). Cortical Firing and Sleep Homeostasis. *Neuron*, *63*(6), 865–878. https://doi.org/10.1016/j.neuron.2009.08.024

Vyazovskiy, V. V., Riedner, B. A., Cirelli, C., & Tononi, G. (2007). Sleep Homeostasis and Cortical Synchronization: II. A Local Field Potential Study of Sleep Slow Waves in the Rat. *Sleep*, *30*(12), 1631–1642. https://doi.org/10.1093/sleep/30.12.1631

Vyazovskiy, V. V., & Tobler, I. (2005). Theta activity in the waking EEG is a marker of sleep propensity in the rat. *Brain Research*, *1050*(1), 64–71. https://doi.org/10.1016/j.brainres.2005.05.022

Walter, F., Schmid, J., Düssmann, H., Concannon, C. G., & Prehn, J. H. M. (2015). Imaging of single cell responses to ER stress indicates that the relative dynamics of IRE1/XBP1 and PERK/ATF4 signalling rather than a switch between signalling branches determine cell survival. *Cell Death & Differentiation*, *22*(9), 1502–1516. https://doi.org/10.1038/cdd.2014.241

Walter, P., & Ron, D. (2011). The Unfolded Protein Response: From Stress Pathway to Homeostatic Regulation. *Science*, *334*(6059), 1081–1086. https://doi.org/10.1126/science.1209038

Walther, W., & Stein, U. (1996). Cell type specific and inducible promoters for vectors in gene therapy as an approach for cell targeting. *Journal of Molecular Medicine*, *74*(7), 379–392. https://doi.org/10.1007/BF00210632

Wang, C., Wang, C.-M., Clark, K. R., & Sferra, T. J. (2003). Recombinant AAV serotype 1 transduction efficiency and tropism in the murine brain. *Gene Therapy*, *10*(17), Article 17. https://doi.org/10.1038/sj.gt.3302011

Wang, G., Ang, C.-E., Fan, J., Wang, A., Moffitt, J. R., & Zhuang, X. (2020). *Spatial organization of the transcriptome in individual neurons* (p. 2020.12.07.414060). bioRxiv. https://doi.org/10.1101/2020.12.07.414060

Wang, Y., Chen, Y., Zhou, Q., Xu, J., Qian, Q., Ni, P., & Qian, Y. (2018). Mild Endoplasmic Reticulum Stress Protects Against Lipopolysaccharide-Induced Astrocytic Activation and Blood-Brain Barrier Hyperpermeability. *Frontiers in Cellular Neuroscience*, *12*. https://doi.org/10.3389/fncel.2018.00222

Wang, Y., Shen, J., Arenzana, N., Tirasophon, W., Kaufman, R. J., & Prywes, R. (2000). Activation of ATF6 and an ATF6 DNA binding site by the ER stress response. *Journal of Biological Chemistry*. https://doi.org/10.1074/jbc.M003322200

Wang, Y., Zhou, Q., Zhang, X., Qian, Q., Xu, J., Ni, P., & Qian, Y. (2017). Mild endoplasmic reticulum stress ameliorates lipopolysaccharide-induced neuroinflammation and cognitive impairment via regulation of microglial polarization. *Journal of Neuroinflammation*, *14*(1), 233. https://doi.org/10.1186/s12974-017-1002-7

Watson, B. O., Levenstein, D., Greene, J. P., Gelinas, J. N., & Buzsáki, G. (2016). Network Homeostasis and State Dynamics of Neocortical Sleep. *Neuron*, *90*(4), 839–852. https://doi.org/10.1016/j.neuron.2016.03.036

Werth, E., Achermann, P., & Borbély, A. A. (1996). Brain topography of the human sleep EEG: Antero-posterior shifts of spectral power. *NeuroReport*, *8*(1), 123.

Wester, J. C., & Contreras, D. (2012). Columnar Interactions Determine Horizontal Propagation of Recurrent Network Activity in Neocortex. *Journal of Neuroscience*, *32*(16), 5454–5471. https://doi.org/10.1523/JNEUROSCI.5006-11.2012

Wheeler, R. J., Lee, H. O., Poser, I., Pal, A., Doeleman, T., Kishigami, S., Kour, S., Anderson, E. N., Marrone, L., Murthy, A. C., Jahnel, M., Zhang, X., Boczek, E., Fritsch, A., Fawzi, N. L., Sterneckert, J., Pandey, U., David, D. C., Davis, B. G., … Hyman, A. A. (2019). *Small molecules for modulating protein driven liquid-liquid phase separation in treating neurodegenerative disease* (p. 721001). bioRxiv. https://doi.org/10.1101/721001

Whittle, I. R., Glasby, M., Lammie, A., Bell, H., & Ungerstedt, U. (1998). Neuropathological findings after intracerebral implantation of microdialysis catheters. *NeuroReport*, *9*(12), 2821.

Wiegert, J. S., Gee, C. E., & Oertner, T. G. (2017). Viral Vector-Based Transduction of Slice Cultures. *Cold Spring Harbor Protocols*, *2017*(2), pdb.prot094896. https://doi.org/10.1101/pdb.prot094896

Winer, J. R., Mander, B. A., Helfrich, R. F., Maass, A., Harrison, T. M., Baker, S. L., Knight, R. T., Jagust, W. J., & Walker, M. P. (2019). Sleep as a Potential Biomarker of Tau and β-Amyloid Burden in the Human Brain. *The Journal of Neuroscience*, *39*(32), 6315–6324. https://doi.org/10.1523/JNEUROSCI.0503-19.2019

Wortel, I. M. N., van der Meer, L. T., Kilberg, M. S., & van Leeuwen, F. N. (2017). Surviving Stress: Modulation of ATF4-Mediated Stress Responses in Normal and Malignant Cells. *Trends in Endocrinology and Metabolism: TEM*, *28*(11), 794–806. https://doi.org/10.1016/j.tem.2017.07.003

Wu, Y., Whiteus, C., Xu, C. S., Hayworth, K. J., Weinberg, R. J., Hess, H. F., & De Camilli, P. (2017). Contacts between the endoplasmic reticulum and other membranes in neurons. *Proceedings of the National Academy of Sciences*, *114*(24), E4859–E4867. https://doi.org/10.1073/pnas.1701078114

Wulff, K., Gatti, S., Wettstein, J. G., & Foster, R. G. (2010). Sleep and circadian rhythm disruption in psychiatric and neurodegenerative disease. *Nature Reviews Neuroscience*, *11*(8), 589–599. https://doi.org/10.1038/nrn2868

Xia, Q., Wang, X., Liu, Y., Shen, Z., Ge, Z., Huang, H., Li, X., & Wang, Y. (2020). An endoplasmic reticulum-targeted two-photon fluorescent probe for bioimaging of HClO generated during sleep deprivation. *Spectrochimica Acta Part A: Molecular and Biomolecular Spectroscopy*, *229*, 117992. https://doi.org/10.1016/j.saa.2019.117992

Xie, L., Kang, H., Xu, Q., Chen, M. J., Liao, Y., Thiyagarajan, M., O'Donnell, J., Christensen, D. J., Nicholson, C., Iliff, J. J., Takano, T., Deane, R., & Nedergaard, M. (2013). Sleep Drives Metabolite Clearance from the Adult Brain. *Science*, *342*(6156), 373–377. https://doi.org/10.1126/science.1241224

Yamamoto, K., Sato, T., Matsui, T., Sato, M., Okada, T., Yoshida, H., Harada, A., & Mori, K. (2007). Transcriptional Induction of Mammalian ER Quality Control Proteins Is Mediated by Single or Combined Action of ATF6α and XBP1. *Developmental Cell*, *13*(3), 365–376. https://doi.org/10.1016/j.devcel.2007.07.018

Yamamoto, K., Yoshida, H., Kokame, K., Kaufman, R. J., & Mori, K. (2004). Differential contributions of ATF6 and XBP1 to the activation of endoplasmic reticulum stress-responsive cis-acting elements ERSE, UPRE and ERSE-II. *Journal of Biochemistry*, *136*(3), 343–350. https://doi.org/10.1093/jb/mvh122

Yan, X.-H., Guo, X.-Y., Jiao, F.-Y., Liu, X., & Liu, Y. (2015). Activation of large-conductance Ca2+-activated K+ channels inhibits glutamate-induced oxidative stress through attenuating ER stress and mitochondrial dysfunction. *Neurochemistry International*, *90*, 28–35. https://doi.org/10.1016/j.neuint.2015.07.004

Yokogawa, T., Marin, W., Faraco, J., Pézeron, G., Appelbaum, L., Zhang, J., Rosa, F., Mourrain, P., & Mignot, E. (2007). Characterization of Sleep in Zebrafish and Insomnia in Hypocretin Receptor Mutants. *PLOS Biology*, *5*(10), e277. https://doi.org/10.1371/journal.pbio.0050277

Yoshida, H., Haze, K., Yanagi, H., Yura, T., & Mori, K. (1998). Identification of the cis-Acting Endoplasmic Reticulum Stress Response Element Responsible for Transcriptional Induction of Mammalian Glucose-regulated Proteins INVOLVEMENT OF BASIC LEUCINE ZIPPER TRANSCRIPTION FACTORS. *Journal of Biological Chemistry*, *273*(50), 33741–33749. https://doi.org/10.1074/jbc.273.50.33741

Yoshida, H., Matsui, T., Hosokawa, N., Kaufman, R. J., Nagata, K., & Mori, K. (2003). A Time-Dependent Phase Shift in the Mammalian Unfolded Protein Response. *Developmental Cell*, *4*(2), 265–271. https://doi.org/10.1016/S1534-5807(03)00022-4

Yoshida, H., Matsui, T., Yamamoto, A., Okada, T., & Mori, K. (2001). XBP1 mRNA Is Induced by ATF6 and Spliced by IRE1 in Response to ER Stress to Produce a Highly Active Transcription Factor. *Cell*, *107*(7), 881–891. https://doi.org/10.1016/S0092-8674(01)00611-0

Yu, L., Andruska, N., Zheng, X., & Shapiro, D. J. (2016). Anticipatory activation of the unfolded protein response by epidermal growth factor is required for immediate early gene expression and cell proliferation. *Molecular and Cellular Endocrinology*, *422*, 31–41. https://doi.org/10.1016/j.mce.2015.11.005

Zavada, A., Strijkstra, A. M., Boerema, A. S., Daan, S., & Beersma, D. G. M. (2009). Evidence for differential human slow-wave activity regulation across the brain. *Journal of Sleep Research*, *18*(1), 3–10. https://doi.org/10.1111/j.1365-2869.2008.00696.x

Zhang, C., Deng, Y., Dai, H., Zhou, W., Tian, J., Bing, G., & Zhao, L. (2017). Effects of dimethyl sulfoxide on the morphology and viability of primary cultured neurons and astrocytes. *Brain Research Bulletin*, *128*, 34–39. https://doi.org/10.1016/j.brainresbull.2016.11.004

Zhang, L., & Wang, A. (2012). Virus-induced ER stress and the unfolded protein response. *Frontiers in Plant Science*, *3*, 293. https://doi.org/10.3389/fpls.2012.00293

Zhang, S., Xu, M., Chang, W.-C., Ma, C., Hoang Do, J. P., Jeong, D., Lei, T., Fan, J. L., & Dan, Y. (2016). Organization of long-range inputs and outputs of frontal cortex for top-down control. *Nature Neuroscience*, *19*(12), 1733–1742. https://doi.org/10.1038/nn.4417

Zhang, Y., Liu, R., Ni, M., Gill, P., & Lee, A. S. (2010). Cell Surface Relocalization of the Endoplasmic Reticulum Chaperone and Unfolded Protein Response Regulator GRP78/BiP. *Journal of Biological Chemistry*, *285*(20), 15065–15075. https://doi.org/10.1074/jbc.M109.087445

Zhao, L., Longo-Guess, C., Harris, B. S., Lee, J.-W., & Ackerman, S. L. (2005). Protein accumulation and neurodegeneration in the woozy mutant mouse is caused by disruption of SIL1, a cochaperone of BiP. *Nature Genetics*, *37*(9), Article 9. https://doi.org/10.1038/ng1620

Zimmerman, J. E., Rizzo, W., Shockley, K. R., Raizen, D. M., Naidoo, N., Mackiewicz, M., Churchill, G. A., & Pack, A. I. (2006). Multiple mechanisms limit the duration of wakefulness in Drosophila brain. *Physiological Genomics*, *27*(3), 337–350. https://doi.org/10.1152/physiolgenomics.00030.2006

Zincarelli, C., Soltys, S., Rengo, G., & Rabinowitz, J. E. (2008). Analysis of AAV Serotypes 1–9 Mediated Gene Expression and Tropism in Mice After Systemic Injection. *Molecular Therapy*, *16*(6), 1073–1080. https://doi.org/10.1038/mt.2008.76

Zinszner, H., Kuroda, M., Wang, X., Batchvarova, N., Lightfoot, R. T., Remotti, H., Stevens, J. L., & Ron, D. (1998). CHOP is implicated in programmed cell death in response to impaired function of the endoplasmic reticulum. *Genes & Development*, *12*(7), 982–995.

Zucca, S., D'Urso, G., Pasquale, V., Vecchia, D., Pica, G., Bovetti, S., Moretti, C., Varani, S., Molano-Mazón, M., Chiappalone, M., Panzeri, S., & Fellin, T. (2017). An inhibitory gate for state transition in cortex. *ELife*, *6*, e26177. https://doi.org/10.7554/eLife.26177

Zufferey, R., Donello, J. E., Trono, D., & Hope, T. J. (1999). Woodchuck Hepatitis Virus Posttranscriptional Regulatory Element Enhances Expression of Transgenes Delivered by Retroviral Vectors. *Journal of Virology*, *73*(4), 2886–2892.